Antoine Pasternak

Dimers, Orientifolds, and Dynamical Supersymmetry Breaking

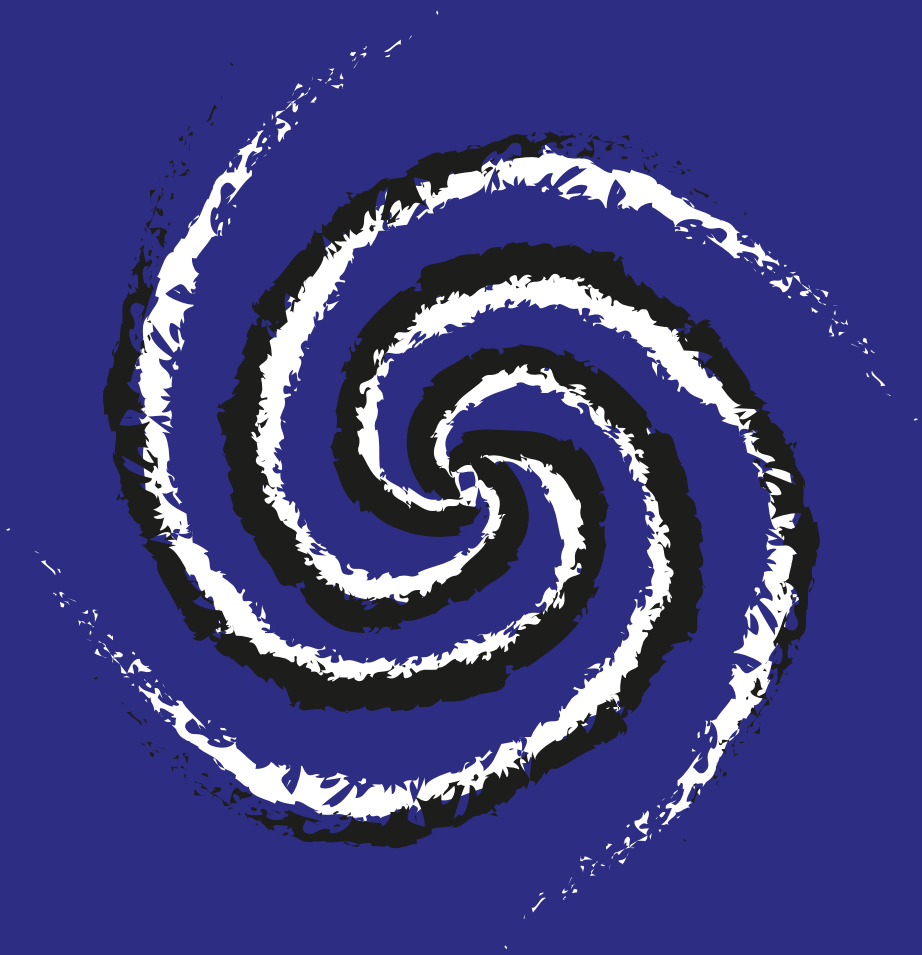

ULB FACULTÉ DES SCIENCES

UNIVERSITÉ LIBRE DE BRUXELLES

Dimers, Orientifolds, and Dynamical Supersymmetry Breaking

Thesis presented by Antoine PASTERNAK

in fulfilment of the requirements of the PhD Degree in Science,
"Docteur en Sciences" at Université Libre de Bruxelles

Academic year 2020-2021

Supervisor : Professor Riccardo ARGURIO
Physique Théorique et Mathématique
International Solvay Institutes

Thesis jury :
Riccardo ARGURIO (Université Libre de Bruxelles)
Glenn BARNICH (Université Libre de Bruxelles, Chair)
Andrés COLLINUCCI (Université Libre de Bruxelles, Secretary)
Iñaki GARCÍA ETXEBARRIA (Durham University)
Amihay HANANY (Imperial College London)

fnrs LA LIBERTÉ DE CHERCHER

Abstract

This thesis is devoted to the study of orientifolds and dynamical supersymmetry breaking in configurations of D-branes placed at the tip of toric Calabi-Yau singularities, through the lens of dimer models. It is divided into three parts, with the last two presenting the original material.

In the first part, we review the basic ingredients that led to the formulation of gauge/gravity dualities in terms of dimer models and relevant toric geometry tools. Elementary notions of supersymmetric gauge theories, as well as two models that break supersymmetry dynamically, are first presented. Secondly, we recall important aspects of string theory and the first realization of a gauge/gravity duality: the AdS/CFT correspondence. We discuss geometric notions of Calabi-Yau and toric varieties, and then move on to introduce important physical features of fractional branes. This part concludes with the use of dimer models, and related ideas, in string theory.

The second part focuses on orientifolds. After reviewing important properties of orientifold planes, we study in detail the anomaly cancellation conditions for non-abelian gauge symmetries in supersymmetric theories arising on D-branes at orientifold singularities. In particular, with the help of techniques that are unique to dimer models, we provide geometric necessary criteria to determine whether an orientifold projection can be safely performed, that is, without introducing uncanceled anomalies. We also find a new type of orientifold projection, without fixed loci, in dimer models and expand on its physical features. The latter allows for superconformal field theories on orientifolds, as well as gauge theories whose renormalization group flow realizes a cascade of Seiberg dualities. Finally, we argue that we exhausted the list of possible orientifold projections in dimer models.

In the last part of this thesis, we investigate dynamical supersymmetry breaking vacua in string theory and their typical instability along $\mathcal{N} = 2$ Coulomb branches. We extend the list of $SU(5)$ models living in dimer models and find unprecedented cases of $3 - 2$ models too. This leads us

to formulate a no-go theorem against their stability based on geometrical features of the singularity, and then to establish a precise way to circumvent it. The latter relies on the elaboration of a variant of the $SU(5)$ model. As a result, we eventually single out the first instance of stable vacuum in string theory that realizes dynamical supersymmetry breaking constructed with D-branes on a particular toric Calabi-Yau singularity, which we refer to as the Octagon.

Conclusions and perspectives for forthcoming research are presented at the end of the chapters related to the original contributions.

Résumé

Cette thèse est vouée à l'étude d'orientifolds et de la brisure dynamique de supersymétrie dans des configurations de D-branes placées sur des singularités toriques de type Calabi-Yau, via les modèles de dimères. Elle est divisée en trois parties, dont les deux dernières présentent mes contributions originales.

Nous passons d'abord en revue les ingrédients essentiels de théorie des cordes qui ont amené à la formulation de dualités jauge/gravité en termes de dimères. Des notions élémentaires de théories de jauge supersymétries, ainsi que des modèles connus pour briser de manière dynamique la supersymétrie sont présentés. Ensuite, nous passons en revue des aspects importants de théorie des cordes et de la première réalisation d'une dualité jauge/gravité : la correspondance AdS/CFT. Nous discutons de notions de géométries de Calabi-Yau et torique pour ensuite introduire quelques aspects physiques importants sur les branes fractionnaires. Cette première partie introductive se conclut sur l'usage de modèles de dimères en théorie des cordes.

La deuxième partie de la thèse se concentre sur les orientifolds. Après avoir passé en revue quelques résultats connus sur ces objets, nous étudions en détail les conditions d'annulation d'anomalies non abéliennes pour les théories de jauge supersymétriques émergeant sur les D-branes. En particulier, et à l'aide de techniques propres aux modèles de dimères, nous établissons des critères nécessaires et géométriques pour déterminer si une projection de type orientifold peut être réalisée sans générer d'anomalies. Nous trouvons également un nouveau type de projection par un orientifold, sans points fixes, dans les modèles de dimères et discutons de ses caractéristiques physiques. Ces derniers permettent d'introduire sur des orientifolds des théories superconformes, ainsi que des théories de jauge dont le flot du groupe de renormalisation peut prendre la forme d'une cascade de dualités de Seiberg. Nous montrons également avoir fait le tour des possibilités de projection de type orientifold dans les modèles de dimères.

Dans la dernière partie de la thèse, nous nous concentrons sur les vides qui réalisent une brisure dynamique de supersymétrie et leur instabilité habituelle sur des branches de Coulomb $\mathcal{N} = 2$. Nous rallongeons la liste d'exemples de modèles $SU(5)$ trouvés dans les modèles de dimères, et trouvons de nouvelles réalisations de modèles $3 - 2$. Le constat de leur instabilité nous amène à formuler un théorème d'impossibilité contre leur stabilité basé sur les caractéristiques géométriques de la singularité associée. Nous trouvons ensuite une manière bien précise de le contourner sur base de la construction d'une variante du modèle $SU(5)$. Suite à cela, nous trouvons finalement un premier exemple de vide stable réalisant une brisure dynamique de supersymétrie en théorie des cordes sur base de D-branes sur une singularité torique de type Calabi-Yau, nommée l'Octogone.

Des conclusions et perspectives pour une recherche future sont présentées en fin de parties ou chapitres de thèse basés sur mes contributions originales.

Acknowledgments

The past four years were exciting at many distinct levels. I have learned a lot from a scientific point of view, but I also quickly realized that such a journey takes its full meaning once shared. For this reason, I am thankful to the many different people I have met and worked with within the course of my PhD program. Let me apologize in advance to those I may have forgotten in the present acknowledgments.

First, I would like to express my warmest thanks to my supervisor, Riccardo, for guiding me in the fascinating subjects of symmetry breaking and string theory for more than five years now. In addition to the considerable amount of knowledge he communicated to me, his approach to physics is and will remain an important source of inspiration for me. Moreover, Riccardo has always been available at crucial times and repeatedly showed himself to be reassuring as well as very patient when dealing with my flaws. I could not think of a better supervisor and will miss his advice in the future.

I feel honored that Glenn, Andrés, Iñaki, and Amihay accepted to be part of my PhD jury. I have benefited a lot from their interesting questions. I am looking forward to pursuing these discussions on any occasion.

I wish to thank all my collaborators (and friends): Matteo, Seba, Edu, Shani, and Valdo, not forgetting Daniel for his implication in my first project. I have learned a lot from their passion and dedication. I would like to emphasize that the original material presented in this thesis is heavily based on their insights and is really the product of these multiple exciting discussions we had all together. My only wish is to keep interacting with them as often as possible.

I would not be writing these lines if I did not benefit from the significant help, countless times, of my friends from the NO building. I met Bilal, Jérôme, Laurent, and Tanguy ten years ago and they never failed to support me at every step towards the Bachelor, Master, and eventually PhD graduation. Pierluigi came to the rescue at this later stage and managed to

answer positively to every call for help (there were many). I owe them so much that I fear never being able to compensate... But I am not resigned yet!

On a lighter note, I would like to thank all the people that shared with me these great moments that I consider to be so many cornerstones of my PhD experience. I was glad to attend the Solvay doctoral school for its relaxed atmosphere and meeting incredible people. I acknowledge, in particular, our fantastic duo with Adrien, and our mystical quatuor with Pablo, Pierluigi, and Valdo. Many thanks to all the participants of the Modave summer school (including Le Baratin), with a special mention to Marine for her skills in organizing it. I will also keep strong memories of our exploration trips with Shani in Brussels, Trieste, and Madrid.

Thanks to everyone at ULB for making such a lively environment. I felt very quickly inserted into the PTM group, mostly due to the kindness of Arash, Céline, Guillaume, Paolo, Roberto, Victor, and all the friendly postdocs that were there at the time. More recently, I took a lot of pleasure gathering with our (almost fully) Italian team: Alessio, Edu, Francesco, Luca, Lorenzo, and Pierluigi. I will miss for sure our semi-autarky at the second floor with Daniel, Pierluigi, Roberto, and Yan, and of course lunches at VUB with Adrien, Bilal, Colin, Daniel, Jérôme, Laurent, Martin, Quentin, Romain, and Tanguy. Many thanks also to Adrien, Bilal, Daniel, Diego, Isabelle, Louis, and Nicolas for helping me with teaching duties.

Je remercie également mes amies et amis au-delà de l'horizon de la physique pour avoir toujours réussi à me changer les idées. Mention spéciale pour les louves et loups qui ont animé notre maison et contribué à en faire un lieu de vie si chaleureux ! J'ai également une pensée pour celles et ceux, qui je pense se reconnaîtront, que je n'ai pas eu l'occasion de voir assez souvent durant ces quatre années, mais qui n'ont jamais pour autant cessé de me manquer et de m'inspirer dans mon quotidien.

Un énorme merci à toute ma famille, et en particulier ma Maman et mon Papa, pour m'avoir soutenu dans ce choix particulier de faire une thèse et de toujours avoir été là quand j'en avais besoin.

Finalement, j'aimerais remercier Béa, qui a trop souvent fait passer son temps après le mien. Son soutien indéfectible et sa présence au quotidien auront donné toutes leurs couleurs à ces quatre années de thèse.

List of publications

During the course of my PhD program, I have written with my collaborators several original contributions, which are presented below. They are listed in chronological order of appearance on the platform `ArXiv`.

[1] R. Argurio, D. Naegels, and A. Pasternak, *Are there Goldstone bosons in $d \leqslant z+1$?*, Phys. Rev. D **100** (2019), no. 6 066002.

[2] R. Argurio, M. Bertolini, S. Meynet, and A. Pasternak, *On supersymmetry breaking vacua from D-branes at orientifold singularities*, JHEP **12** (2019) 145.

[3] R. Argurio, M. Bertolini, S. Franco, E. García-Valdecasas, S. Meynet, A. Pasternak, and V. Tatitscheff, *The Octagon and the Non-Supersymmetric Landscape*, Phys. Lett. B **815** (2021) 136153.

[4] R. Argurio, M. Bertolini, S. Franco, E. García-Valdecasas, S. Meynet, A. Pasternak, and V. Tatitscheff, *Dimers, Orientifolds and Stability of Supersymmetry Breaking Vacua*, JHEP **01** (2021) 061.

[5] R. Argurio, M. Bertolini, S. Franco, E. García-Valdecasas, S. Meynet, A. Pasternak, and V. Tatitscheff, *Dimers, Orientifolds and Anomalies*, JHEP **02** (2021) 153.

[6] E. García-Valdecasas, S. Meynet, A. Pasternak, and V. Tatitscheff, *Dimers in a Bottle*, JHEP **04** (2021) 274.

Although [1] relies partially on an application of the gauge/gravity duality, which is the main theme of this thesis, it will not be presented here since it is not directly connected to the other pieces of work.

Contents

Chapter 1

Introduction

In the past century, a major breakthrough in theoretical physics came with the advent of quantum field theory (QFT). It has been initiated by Dirac in the 1920s, with his first attempt of quantizing the electromagnetic field. Since then, this framework constitutes a real success story, as it is at the origin of many fundamental discoveries on matter and its interactions at a microscopic level. Indeed, it describes a variety of quantum phenomena with very high precision compared to experimental observations. For instance, the Standard Model, as an example of gauge theory in QFT, established in the 1970s, and its subsequent extensions are now the reference tools to understand electro-weak and strong nuclear interactions among the particles that have been observed at the accelerators, at the smallest length scales ever probed in science. QFT also plays an important role at larger scales, in condensed matter, in the effective description of materials, and phase transitions.

Despite its successes, our understanding of QFT still suffer from two important and conceptual issues (among other phenomenological aspects that fall outside the scope of this thesis):

- When it comes to strong coupling, perturbation theory is not reliable and non-perturbative techniques are often lacking to understand complicated dynamics.
- The inclusion of the gravitational interaction is challenging since we cannot make sense of it at high energy, *i.e.* it leads to non-renormalizable interactions.

Roughly speaking, in these two contexts, computations are spoiled by the appearance of infinities to which we are not able to give a sensible meaning.

This suggests that QFT has still crucial features to reveal, and possibly that another framework might play a role in our description of nature. These are our motivations to study *supersymmetry* and *string theory*. They are not, of course, the only options on the market. Nowadays, theoretical physicists enjoy a rich set of alternative or complementary approaches to these problems. We limit ourselves to name a few here: effective field theory, simulations on the lattice, asymptotic safety in quantum gravity, etc.

Supersymmetry is a particular instance of symmetry that relates particles obeying different statistics, Bose-Einstein and Fermi-Dirac, *i.e.* bosons and fermions. It was discovered in the early 1970s by several teams of physicists, see [7] and references therein. Supersymmetry imposes stringent constraints on the spectrum and interactions of physical theories. It has been extensively studied for its interesting phenomenological implications and because it significantly facilitates the acquisition of non-perturbative results. Despite its many theoretical advantages, supersymmetry was never found in particle accelerators and this is why theoretical physicists usually look for QFTs with reduced or broken (if not simply absent) supersymmetry, to balance theoretical control and pertinence of the computations.

String theory was originally developed at the end of the 1960s as a model for hadrons [8]. It was observed that the masses of the lightest hadrons were related to their spins by a unique constant with units of tension, and the latter was interpreted as the one of a rotating relativistic string. But after less than a decade, quantum chromodynamics (QCD) proved itself to be a more adequate framework to understand the physics of strong nuclear interactions. In particular, QCD consistently reproduced what we call *asymptotic freedom* [9,10], in agreement with the experimental fact that nuclear fundamental constituents become free at very high energy, and is now part of the Standard Model. It was later realized that string theory presents a very interesting feature for a quantum theory: it contains a graviton [11,12], the mediator of the gravitational interaction. Examples of different string theories emerged, but only supersymmetric variants persisted as consistent theories of strings [13]. The first superstring theories that arose were *types I*, *IIA*, and *IIB superstring theories* [14].

The first superstring revolution came with the discovery of gauge interactions in type I and two new *heterotic superstring theories* [15,16]. Then, physicists started to think about string theory as a candidate for being a quantum gravity model describing all interactions in a unified framework (a "theory of everything", whatever it means).[1]

[1]Testing string theory as a phenomenological model of all interactions in actual experiments is still beyond reach nowadays, mostly because the hypothetical size of the strings

In all these models, superstrings propagate in a ten-dimensional space. To make contact with our four-dimensional world, and at the same time gaining control on the constraints of supersymmetry, it was proposed to compactify six out of the ten dimensions on Calabi-Yau spaces [17]. This *compactification* program gave to geometry a new and important role to play in string theory.

The second superstring revolution was marked by the discovery of Witten that the five known superstring theories were actually all connected by a web of *dualities* and could be seen as limits of an eleven-dimensional theory, called *M-theory* [18]. Dualities are more general than symmetries in the sense that they exchange two complete physical theories, while the latter only map different states of a physical theory to each other. Whereas two states related by a symmetry experience the same dynamics, two dual theories should contain the same physics. In practice, and unlike symmetries, dualities can map the couplings of dual theories.

An essential ingredient in the construction of the aforementioned web of dualities is *T-duality*. It permitted the discovery of *D-branes* in superstring theories of type IIA and IIB [19, 20]. These are extended hyperplanes in spacetime that emit closed strings and to which open strings attach. T-duality thus showed that string theory is in general not only a theory of strings, but also of higher-dimensional branes, and these will be of crucial importance in what follows. Moreover, the open string sector on D-branes has been found to reproduce gauge dynamics at low energy, demonstrating once for all that gauge theories are an integral part of string theory.

Gauge/gravity dualities

By studying different aspects of D-branes at low energy, Maldacena came to the proposal in 1997 of a very special kind of duality: the celebrated *AdS/CFT correspondence* [21–23]. It is the first instance of a *gauge/gravity duality*, *i.e.* that puts on equal footing a theory of gravitation, in a negatively curved five-dimensional spacetime named Anti-de Sitter (AdS) together with a five-sphere, $AdS_5 \times S^5$, and a particular QFT symmetric under the conformal group (CFT). The original setup of branes is supersymmetric, and so are both sides of the correspondence. The QFT is actually the supersymmetric version of the Yang-Mills theory with $SU(N)$ gauge group and $\mathcal{N} = 4$ supersymmetry. This duality is important because it relates

is too tiny for the length scales probed by current accelerators. Nevertheless, we hope to convince the reader in the rest of this introduction that string theory is interesting in many other respects.

two naively very different frameworks. Most importantly, the weak coupling regime of one is tied to the strong regime of the other. So, we can for instance make computations in a gravitational background of small curvature and use the results to explore the otherwise inaccessible strong regime of the QFT, and vice versa. This duality passed many tests, especially the original version of the correspondence, and led to variants with a vast set of applications, from the study of various QFTs, black holes, to strongly coupled systems in condensed matter.

A remarkable feature of the QFT side of the duality is the absence of gravitation. This is because, in the Maldacena limit, closed and open strings decouple, the former and latter being responsible for gravitational and gauge interactions on the branes respectively. Our understanding of gauge theories was then given a dramatically new perspective when it was realized that they are not only part of string theory but define some limit of it.

In the same spirit as in the compactification program, the duality can be generalized by placing the D-branes on different singular spaces. In doing so, we can engineer a large set of different gauge theories with $\mathcal{N} = 1$ supersymmetry from D-brane setups, and use our string theory knowledge to learn about them. On the gravity side, the geometry will be of course modified too. The area of applications is, again, vast: non-trivial generalizations of the original AdS/CFT correspondence [24–33], local string phenomenology [34–38] and new perspectives, often geometric, on gauge theory dynamics and dualities [39–44].

The correspondence between gravity and gauge theory is now particularly well understood in the case where a *toric* Calabi-Yau three-folds is probed by the D-branes, for which the map is significantly streamlined by *dimer models* (equivalently known as *brane tilings*) [32, 45, 46]. All the information about the gauge theory is then encoded in a bipartite graph, *i.e.* with nodes of two different colors, embedded on a torus. See Figure 1.1 for an illustrative example of dimer model.

In addition to propagating strings on singular backgrounds, one can consider a particular gauging of an involutory isometry of the geometry together with worldsheet parity, that is, the insertion of an *orientifold plane* [19, 47–51]. They are extremely interesting for a variety of reasons. Among them, they expand the possible spectrum [52–54] (gauge groups and matter fields representations), break conformal invariance [55], play an important role in models with non-perturbative effects due to D-brane instantons [56–58] and are a key ingredient in certain models of phenomenological interest, on which we will expand below.

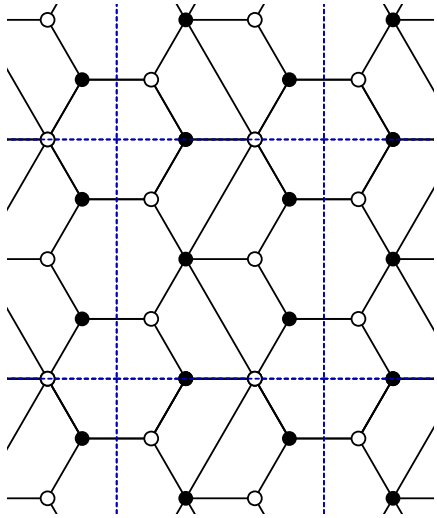

Figure 1.1: An example of dimer model on the torus, with periodic boundaries in blue.

While direct construction of orientifolds in string theory is in practice only feasible for some orbifold theories, they may be constructed directly in the dimer model [54] by identifying gauge groups and fields according to a suitable involution of the graph and possibly assigning some signs to the fixed loci in the dimer, corresponding to the different choices of orientifold plane. This makes it possible for toric singularities to be orientifolded.

It is then a question of interest to ask whether all kinds of $\mathcal{N} = 1$ supersymmetric gauge theories can be engineered in this way, or at least if it is possible to engineer theories that reproduce all kinds of low energy behavior. While confinement, generation of a mass gap and of a chiral condensate can be shown to arise in very simple models [27], as well as $\mathcal{N} = 2$ Coulomb-like branches in others [59–61], the fascinating possibility that the vacuum of the gauge theory dynamically breaks supersymmetry requires more work.

Supersymmetry can be broken in different ways. The gauge theory may have both supersymmetric vacua and meta-stable supersymmetry breaking vacua, which can be parametrically long-lived. This situation can be engineered with D-branes at singularities, see *e.g.* [62–65]. Another possibility is that there is simply no vacuum in the theory, leading to what is called a runaway. It turns out that such a situation is rather frequent in configurations of branes at singularities, see [66–69].

The last possibility that remains is that supersymmetry is dynamically

broken in a fully stable vacuum. This has proven to be a harder problem to engineer with D-branes at singularities. This is partly due to the scarcity of known gauge theories that display such a non-supersymmetric vacuum. After attempts to turn the runaway into a stable vacuum proved unsuccessful [70], it was shown in [54] that by introducing an orientifold projection it is possible to engineer configurations which at low energies reproduce the well-known dynamical supersymmetry breaking (DSB) model of [71], henceforth referred to as the $SU(5)$ *model*. The same model was argued to arise in a wider number of singularities in [72, 73].

The DSB configurations of [54, 72, 73] were more closely scrutinized in [74], where it was found that they are actually not fully stable. Indeed, when the DSB configuration is probed by N regular D3-branes, an instability appears where the regular branes split along the Coulomb branch of so-called $\mathcal{N} = 2$ fractional branes [67], eventually settling the configuration in a supersymmetric vacuum.

The difficulty in finding such models can suggest that dynamical supersymmetry breaking into stable vacua might not be a possibility in D-brane constructions and, more generally, in string theory as well. On the other hand, finding models of this kind could be of great relevance both in the context of the gauge/gravity duality and, even more interestingly, in string compactifications. In this latter setup, they could be used for model building in GKP-like constructions [75]. Eventually, they might also have an impact on the swampland program [76–78] and recent related conjectures such as [74].

Plan of the thesis

Every chapter starts with several introductory paragraphs and a plan of the chapter itself. When a chapter presents original results, the first part of these paragraphs can be thought of as an abstract.

We review in Part I all the important ingredients and tools that constitute the gauge/gravity dualities. This part does not aim at providing all the details nor proofs of the statements made but rather to collect and assemble the results that are important for our purpose. We start in Chapter 2 with basic notions of supersymmetric gauge theories and dynamical supersymmetry breaking. In Chapter 3, we present some elements of string theory with an emphasis on the type IIB superstring theory and the original AdS/CFT correspondence. We move on to Chapter 4 for reviewing notions of Calabi-Yau and toric geometries that are important for the extensions of gauge/gravity dualities. Chapter 5 covers important aspects of fractional branes. Finally, Chapter 6 reviews the construction and use of dimer models in string theory.

Part II introduces orientifold projections in dimer models and is devoted to present the original material [5] and [6]. We start in Chapter 7 with a review on the initial constructions of orientifolds in dimer models. Chapter 8 presents the results of [5], where we analyze in-depth anomaly cancellation conditions for gauge theories obtained from orientifolds of dimer models. In particular, we provide necessary geometric criteria to determine whether a singular toric CY geometry can safely be projected by an orientifold plane. Chapter 9 presents the results of [6], where we find a new kind of orientifold projection without fixed locus in dimer models, the glide projection. We expand on its important physical features: the possibility of admitting superconformal theories and fractional branes that trigger non-trivial flows of the renormalization group. We also prove the impossibility of performing an orientifold by projecting the dimer model with respect to a shift symmetry.

Part III is dedicated to my research on dynamical supersymmetry breaking in orientifolded dimer models: [2], [3] and [4]. In Chapter 10 we collect the series of results of [2] showing that dynamical supersymmetry breaking models arise in numerous examples of dimer models, together with a no-go theorem for their stability. We use dimer techniques to look for circumventing the later no-go theorem in Chapter 11, following [4], and eventually single out a candidate. The latter construction is based on a variant of the well-known $SU(5)$ model. Finally, and following [3,4], we present in Chapter 12 a first instance of stable DSB vacuum realizing this variant

of the $SU(5)$ model in a toric CY geometry, the Octagon. We comment on its stability and complete our analysis with computations in Appendix 12.B that are not yet published.

Chapters 8, 9 and 12 each have their own conclusions and perspectives for forthcoming research. They are naturally presented at the end of the aforementioned chapters.

Part I

D-Branes at Singularities

Chapter 2

Supersymmetric Gauge Theories

Supersymmetry provides a natural extension of the Poincaré group of symmetry for quantum field theories with additional charges of spin 1/2. These supercharges thus relate bosons to fermions, and vice versa. The framework of rigid supersymmetry leads then to many simplifications in the study of quantum field theories and allows to understand precisely many features of strongly coupled gauge theories. In particular, we will review in this section the nature of quantum corrections for some important models that share similar qualitative behaviors with realistic theories like quantum chromodynamics (QCD). A complete review on this subject where details can be found is [79].

In spite of its many advantages, supersymmetry is not observed in nature and we are thus looking for non-supersymmetric vacua. Models that break supersymmetry dynamically (DSB) are interesting phenomenologically because they are defined as supersymmetric theories in the ultraviolet regime and stabilize in a non-supersymmetric vacuum in the infrared. In consequence, they can be linked to UV-completed supersymmetric theories where all the constraints from supersymmetry apply but still enjoy more realistic dynamics at low energy. Moreover, the dynamical character of the breaking implies the latter does not rely on any ad-hoc or external parameter, like a vacuum expectation value (VEV) for an operator coming from another sector. They break supersymmetry all by themselves, as a consequence of their own dynamics. We will recall some features of a non-exhaustive list of DSB models that will be important in our study of string vacua. For complete reviews on DSB models, see [80–84].

2.1 Elements of supersymmetry

2.1.1 Matter, interactions and the moduli space

Gauge theories with $\mathcal{N} = 1$ rigid supersymmetry have four real supercharges, assembled in Q_α and $\bar{Q}_{\dot{\alpha}}$ with $\alpha, \dot{\alpha} = 1, 2$, and transforming as Weyl spinors of the Lorentz group. In our conventions, $\bar{Q}_{\dot{\alpha}} = Q^\dagger_\alpha$. Moreover, they satisfy the following anticommutation relation:

$$\{Q_\alpha, \bar{Q}_{\dot{\alpha}}\} = 2\sigma^\mu_{\alpha\dot{\alpha}} P_\mu \,, \tag{2.1}$$

where σ^0 is the 2×2 identity matrix and σ^i are the three Pauli matrices. We also have

$$\{Q_\alpha, Q_\beta\} = 0 \,, \quad \{\bar{Q}_{\dot{\alpha}}, \bar{Q}_{\dot{\beta}}\} = 0 \,. \tag{2.2}$$

These relations constitute together the *superalgebra* and give rise to different irreducible representations in which we will define our fields, see below. But first, it will be convenient to extend the usual four-dimensional spacetime on which the field theory is defined into a superspace. We consider the Grassmann coordinates $\theta^\alpha, \bar{\theta}^{\dot{\beta}}$ in addition to the usual Minkowski coordinates x^μ. They come together with two covariant derivates on the superspace:

$$D_\alpha = \partial_\alpha + i\sigma^\mu_{\alpha\dot{\alpha}} \bar{\theta}^{\dot{\alpha}} \partial_\mu \,, \quad \bar{D}_{\dot{\alpha}} = \bar{\partial}_{\dot{\alpha}} + i\theta^\alpha \sigma^\mu_{\alpha\dot{\alpha}} \partial_\mu \,. \tag{2.3}$$

We will mainly work with two kinds of multiplets:

- Chiral superfields Φ: They are defined by

  $$\bar{D}_{\dot{\alpha}} \Phi = 0 \,. \tag{2.4}$$

  They will give us charged matter, and we will occasionally number them in flavors. Using the superspace coordinate $y^\mu = x^\mu + i\theta\sigma^\mu\bar{\theta}$, we can write them as

  $$\Phi(y, \theta) = \phi(y) + \sqrt{2}\theta\psi(y) + \theta^2 F(y) \,, \tag{2.5}$$

  where ϕ is a complex scalar, ψ a Weyl spinor, and F an auxiliary field. In subsequent sections, we will hardly ever differentiate the notations of the chiral superfield Φ and its scalar components ϕ.

- Real superfields V: They are defined by

  $$V = \bar{V} \,. \tag{2.6}$$

They play the role of gauge vectors in the supersymmetric context. More specifically, the real multiplet takes value in the Lie algebra of a gauge symmetry group G:

$$V = V^A T^A \,, \tag{2.7}$$

where T^A is a generator of the algebra and the summation is understood on indices $A = 1, \cdots, \dim G$. The gauge transformation is now given by a chiral superfield Λ:

$$V \to V - i(\Lambda - \bar{\Lambda}) \,. \tag{2.8}$$

This freedom can be used to partially fix the gauge and express the vector superfield in a convenient form, the Wess-Zumino gauge:

$$V(x, \theta, \bar{\theta}) = \theta\sigma^\mu\bar{\theta}A_\mu(x) + i\theta^2\bar{\theta}\bar{\lambda}(x) - i\bar{\theta}^2\theta\lambda(x) + \frac{1}{2}\theta^2\bar{\theta}^2 D(x) \,, \tag{2.9}$$

where A_μ is a real vector (the gauge vector), λ a Weyl fermion (the gaugino) and D an auxiliary field. We can also build a chiral superfield in terms of V that will contain the field strength and whose lowest component is the gaugino:

$$\mathcal{W}_\alpha = \bar{D}^2(e^{-V} D_\alpha e^V) = -i\lambda_\alpha + \theta_\alpha D + i(\sigma^{\mu\nu}\theta)_\alpha F_{\mu\nu} + \theta^2(\sigma^\mu D_\mu \bar{\lambda})_\alpha \,, \tag{2.10}$$

where $\sigma^{\mu\nu} = (\sigma^\mu\bar{\sigma}^\nu - \eta^{\mu\nu})/2$.

A general gauge-invariant action for such a supersymmetric field theory with matter given by chiral multiplets Φ^i is then expressed as follows:

$$\begin{aligned} \mathcal{L} &= \mathrm{Im}\left(\tfrac{\tau}{32\pi}\int \mathrm{d}^2\theta \ \mathrm{tr}\, \mathcal{W}_\alpha \mathcal{W}^\alpha\right) + \int \mathrm{d}^2\theta \mathrm{d}^2\bar{\theta} \ \bar{\Phi}^i e^{2V} \Phi^i \\ &\quad + \int \mathrm{d}^2\theta \ W(\Phi) + \int \mathrm{d}^2\bar{\theta} \ \bar{W}(\bar{\Phi}) \,, \end{aligned} \tag{2.11}$$

where we find the complex gauge coupling,

$$\tau = i\frac{4\pi}{g^2} + \frac{\Theta}{2\pi} \,. \tag{2.12}$$

The first term contains the kinetic terms for the gauge vector and the gaugino, in addition to the topological Θ-term for the gauge vector. The second term is the kinetic term for the matter fields of the chiral multiplets, including couplings to the gauge vector through covariant derivatives, and couplings to the gaugino in trilinear terms. The last two terms involve the superpotential $W(\Phi)$ and contain extra interactions for the chiral matter fields.

This action is normalizable provided that the superpotential is at most cubic. However, we will not always take this statement as a constraint since we will often be interested in low energy supersymmetric actions, where the Lagrangian is understood as effective. In the same spirit, the low energy dynamics will often generate a kinetic term for gauge-invariant chiral multiplets that is a non-renormalizable function, based on a Kähler potential $K(\Phi, \bar{\Phi})$:

$$\int \mathrm{d}^2\theta \mathrm{d}^2\bar{\theta}\; K(\Phi, \bar{\Phi})\,. \tag{2.13}$$

The Kähler potential exposed in Equation (2.11) is the canonical one.

Equations of motion impose the following relations:

$$\bar{F}^i = \frac{\partial W}{\partial \Phi^i}(\phi) \quad D^A = -g\,\bar{\phi}\,T_R^A\,\phi\,, \tag{2.14}$$

where T_R^A is the generator defined in the representation of the chiral superfield Φ. These relations allow integrating out the auxiliary fields. They are important for computing the potential of the scalar sector in the theory:

$$V(\phi, \bar{\phi}) = \bar{F}^i(\phi)F^i(\bar{\phi}) + \frac{1}{2}D^A(\phi, \bar{\phi})D^A(\phi, \bar{\phi})\,. \tag{2.15}$$

Note that the first term in the last equation gets modified when the Kähler potential is non-trivial. In terms of $W(\Phi)$ and $K(\Phi, \bar{\Phi})$, it becomes

$$\frac{\partial W}{\partial \Phi^i}(\phi)\left(\frac{\partial^2 K}{\partial \Phi^i \partial \bar{\Phi}^{\bar{j}}}(\phi, \bar{\phi})\right)^{-1}\frac{\partial \bar{W}}{\partial \bar{\Phi}^i}(\bar{\phi})\,. \tag{2.16}$$

When we have $U(1)$ gauge factors in the gauge group, we can also add a Fayet-Iliopoulos term in the general expression of Equation (2.11):

$$\mathcal{L}_{\mathrm{FI}} = \int \mathrm{d}^2\theta \mathrm{d}^2\bar{\theta}\; \xi^B V^B\,, \tag{2.17}$$

where ξ^B is a number and B counts the $U(1)$ factors. For abelian groups, the general equation for D^B becomes

$$D^B = -g\bar{\phi}T_R^B\phi - g\xi^B\,. \tag{2.18}$$

An important property of supersymmetric vacua, which can be derived directly from the superalgebra, is that the vacuum energy is always zero. Looking at the form of the scalar potential in Equation (2.15), we understand that the only other alternative is to find positive vacuum energy,

in which case supersymmetry is broken. Supersymmetric vacua are thus parameterized by two sets of equations, the *F-term* and *D-term equations*:

$$\bar{F}^i(\phi) = 0\,, \quad D^A(\phi, \bar{\phi}) = 0\,. \tag{2.19}$$

These relations between the scalars define the (so far classical) *moduli space* of the theory. We will see in some examples below how to parametrize the latter with gauge-invariant functions of the superfields.

A last but important remark for this section is that we can have a global symmetry group acting on the supercharges. For $\mathcal{N} = 1$ supersymmetric theories, one has a $U(1)_{\mathrm{R}}$ R-symmetry, satisfying the following commutation relations:

$$[\mathrm{R}, Q_\alpha] = -Q_\alpha\,, \quad [\mathrm{R}, \bar{Q}_{\dot{\alpha}}] = +\bar{Q}_{\dot{\alpha}}\,. \tag{2.20}$$

In other words, the different components of a given multiplet will have different R-charges. For example, we can derive the following relation for the components of any chiral multiplet:

$$\mathrm{R}\,[\psi] = \mathrm{R}\,[\phi] - 1\,. \tag{2.21}$$

2.1.2 Renormalization and superconformal theories

A key feature of supersymmetry, which simplifies a lot the field theory analysis when it comes to study strongly coupled phases, are the non-renormalization theorems. They come together as a set of very restrictive results on the RG-flow for the couplings that appear in the Lagrangian of Equation (2.11).

For example, the holomorphic couplings in the superpotential $W(\Phi)$ are not renormalized at any order in perturbation theory. The reason is that loop corrections appear as integrals over the whole superspace, *i.e.* as D-terms, and thus cannot affect the superpotential.

Still, this is not the end of the story because the kinetic term for chiral superfields Φ is subject to renormalization. This is encoded in a change of the wave function normalization:

$$\bar{\Phi}\Phi \to Z_\Phi \bar{\Phi}\Phi\,. \tag{2.22}$$

This normalization will enter the physical values for the couplings (which should be thought as functions of the holomorphic ones) and the propagators for the fields. This also introduces an *anomalous dimension* γ_Φ for Φ:

$$\gamma_\Phi = -\frac{\partial \ln Z_\Phi}{\partial \ln \mu}\,. \tag{2.23}$$

It is named in this way because we can find that it changes the scaling dimension of the superfield according to the following identity:

$$\dim \Phi = 1 + \frac{1}{2}\gamma_\Phi \,. \tag{2.24}$$

On the gauge side, the coupling Θ is topological and does not run with the energy scale, as usual in quantum field theories since it does not enter equations of motion. On the contrary, the gauge coupling g runs and its evolution is prescribed by the NSVZ β function [85,86]. For a gauge theory with symmetry group G and matter fields in some representation R_i, we have

$$\beta_{\frac{8\pi^2}{g^2}} = \frac{3\,T(\mathrm{Adj}) - \sum_i T(R_i)(1-\gamma_i)}{1 - g^2\,T(\mathrm{Adj})/8\pi^2} \,, \tag{2.25}$$

where the $T(R)$ are Dynkin indices for the representation R. The latter are defined by

$$\mathrm{tr}\, T_R^A\, T_R^B = T(R)\,\delta^{AB} \,. \tag{2.26}$$

For $G = SU(N_c)$, we have

$$T(\mathrm{Adj}) = N_c \,, \quad T(\square) = \frac{1}{2} \,, \quad T(\begin{smallmatrix}\square\\\square\end{smallmatrix}) = \frac{N_c - 2}{2} \,, \quad T(\square\square) = \frac{N_c + 2}{2} \,. \tag{2.27}$$

It is common to get rid of the denominator in Equation (2.25) by making a choice of normalization for the vector superfield which differs from the canonical one [87]. In the following, we will often do so.

When the numerator of Equation (2.25) vanishes, we reach a conformal fixed point of the theory. Then, the supersymmetric version of the Poincaré algebra extends to the superconformal algebra, where we also have generators for dilatation and special conformal transformations. As a matter of fact, the R-symmetry generator enters it and this results in a constraint relating the dimension of any chiral operator $\mathcal{O}$ to its R-charge when the theory sits at the fixed point:

$$\dim \mathcal{O} = \frac{3}{2}\,\mathrm{R}\,[\mathcal{O}] \,. \tag{2.28}$$

There is a theorem for four-dimensional gauge theories stating that near a conformal fixed point any gauge-invariant operator $\mathcal{O}$ satisfies

$$\dim \mathcal{O} \geqslant 1 \,. \tag{2.29}$$

The identity saturates for free conformal fixed points.

R-charges and the related values for the anomalous dimensions constitute an important set of information about the fixed point theory and we

	$SU(N_f)_L$	$SU(N_f)_R$	$U(1)_B$	$U(1)_{\mathrm{R}}$
Q	$\overline{\square}$	$\mathbf{1}$	1	$\frac{N_f-N_c}{N_f}$
$\tilde{Q}$	$\mathbf{1}$	$\square$	-1	$\frac{N_f-N_c}{N_f}$

Table 2.1: Global charges in the classical SQCD.

will always want to compute them. We can note already that when two superfields are related by a global symmetry, their anomalous dimensions have to be the same. This combined with conformality, *i.e.* the vanishing of Equation (2.25), sometimes impose together enough relations to compute these values but it does not always happen to be the case. Fortunately, there is a more generic way to achieve this for any superconformal theory, that is maximizing its central charge $a(\mathrm{R})$ [88]:

$$a(\mathrm{R}) = \frac{3}{32}\left(3\,\mathrm{tr}\,\mathrm{R}^3 - \mathrm{tr}\,\mathrm{R}\right) . \tag{2.30}$$

2.2 SQCD and Seiberg duality

2.2.1 Setting the stage for SQCD

We study the $\mathcal{N}=1$ supersymmetric version of QCD, namely SQCD, with an arbitrary number of colors N_c and flavors N_f. The gauge group is $SU(N_c)$, with gauge fields and gauginos in the vector multiplet, and we also have N_f copies of chiral multiplets sitting in the (anti)fundamental representations of the gauge group:

$$Q^i = \square, \quad \tilde{Q}_j = \overline{\square}, \quad i,j = 1,\cdots,N_f\,. \tag{2.31}$$

The charges under the global symmetries of SQCD are shown in Table 2.1, where we refrain to exhibit the charges for the usual axial symmetry that will always be made anomalous by quantum corrections coming from instantons. The R-charges are selected in order to remain anomaly-free at the quantum level. This last statement does not apply in the absence of flavors.

In order to learn about the classical moduli space of SQCD, we will write Q and $\tilde{Q}$ as $N_f \times N_c$ matrices:

$$Q^i_a\,, \quad \tilde{Q}^a_j\,, \quad i,j = 1,\cdots,N_f\,, \quad a = 1,\cdots,N_c\,. \tag{2.32}$$

Their entries will be constraint by D-term equations:

$$D^A = \mathrm{Tr}\, Q^\dagger T^A Q - \tilde{Q}^\dagger T^A \tilde{Q} = 0\,, \quad A = 1, \cdots, N_c^2 - 1\,, \tag{2.33}$$

where we introduced $T^A \equiv T^A_{\square} = -T^A_{\overline{\square}}$.

A mass term could also be added in the superpotential but we will not consider the latter as it trivially decouples the Q and $\tilde{Q}$'s at low energy and it would be equivalent to study SQCD with a reduced N_f. As a consequence, there are no F-term equations.

For $N_f < N_c$, a generic solution to Equation (2.33) is given by matrices Q and $\tilde{Q}$ being of maximal rank N_f. Global symmetries can be used to diagonalize them, and we can find that they share the same non-zero entries. The gauge group is generically broken down to $SU(N_c - N_f)$. The moduli space has complex dimension N_f^2 and is parameterized by the VEVs for the mesonic fields:

$$M^i_{\ j} = Q^i_a \tilde{Q}^a_{\ j}\,. \tag{2.34}$$

At the origin of the moduli space, the full gauge group is recovered. It is actually singular at this point, which can be seen if you express the Kähler potential in terms of mesonic fields, and this is linked to the appearance of extra gluons in the spectrum which are left behind in the present description.

For $N_f \geqslant N_c$, the matrices Q and $\tilde{Q}$ are now of maximal rank N_c. Their entries have their norm related by the D-term equations. The gauge group is generically fully broken. We can also define baryonic fields that parametrize a new branch of the moduli space:

$$\begin{aligned} B_{k_1 \cdots k_{N_f - N_c}} &= \epsilon_{k_1 \cdots k_{N_f - N_c} i_1 \cdots i_{N_c}} \epsilon^{a_1 \cdots a_{N_c}} Q^{i_1}_{a_1} \cdots Q^{i_{N_c}}_{a_{N_c}}\,, \\ \tilde{B}^{l_1 \cdots l_{N_f - N_c}} &= \epsilon^{l_1 \cdots l_{N_f - N_c} j_1 \cdots j_{N_c}} \epsilon_{a_1 \cdots a_{N_c}} \tilde{Q}^{a_1}_{j_1} \cdots \tilde{Q}^{a_{N_c}}_{j_{N_c}}\,, \end{aligned} \tag{2.35}$$

The moduli space has complex dimension $2N_f N_c - N_c^2 + 1$, which is less than the number of mesons and baryons for the reason that there are some relations between them. In the particular example of $N_f = N_c$, one can show that

$$\mathrm{det} M - B\tilde{B} = 0\,. \tag{2.36}$$

The number of relations increases with N_f.

2.2.2 The quantum moduli space of SQCD

The phases of the quantum theory are richer than the classical one. We still have a hierarchy of results depending on N_f and N_c, and it becomes even more subtle. In this section, we recall the structure of the moduli

space by gradually increasing N_f, but we will not enter into great details for the derivation of the results. We just mention now that the main needed ingredients are holomorphy [89], R-symmetry considerations and 't Hooft anomaly matching [90]. We will also recall what important role plays Seiberg duality in this description.

$\mathbf{N_f = 0}$. We recover the vacuum of the supersymmetric version of Yang-Mills theory (SYM). This is the only case where $U(1)_{\rm R}$ is anomalous. Indeed, usual one-loop computations involving the gauginos, which have an R-charge equal to one, show that instantons are present and spoil the symmetry at the quantum level. However, the shift symmetry of Θ allows preserving a subgroup $\mathbb{Z}_{2N_c}$.

Confinement and the mass gap together imply the generation of a non-perturbative superpotential:

$$W_{\rm SYM} = N_c \Lambda^3 e^{i\frac{2\pi k}{N_c}} \,. \tag{2.37}$$

This results in a condensation of the gaugino bilinear:

$$\langle \lambda\lambda \rangle = \Lambda^3 e^{i\frac{2\pi k}{N_c}} \,, \quad k = 1, \cdots, N_c \,. \tag{2.38}$$

We thus find N_c isolated vacua, separated by domain walls, each one experiencing chiral symmetry breaking of $\mathbb{Z}_{2N_c}$ down to $\mathbb{Z}_2$.

$\mathbf{N_f < N_c}$. The classical moduli space is lifted because of the non-perturbative and runaway Affleck-Dine-Seiberg (ADS) contribution to the superpotential:

$$W_{\rm ADS} = (N_c - N_f) \left(\frac{\Lambda^{3N_c - N_f}}{\det M} \right)^{\frac{1}{N_c - N_f}} \,. \tag{2.39}$$

Note that this correction to the superpotential is permitted only due to its non-perturbative nature. The corresponding potential $V_{\rm ADS}$ is minimized at zero energy for infinite values of the VEVs of the fields, meaning that there is no stable vacuum in the theory.

$\mathbf{N_f = N_c}$. The moduli space is a deformed version of the classical one:

$$\det M - B\tilde{B} - \Lambda^{2N} = 0 \,, \tag{2.40}$$

to be compared with Equation (2.36). The whole moduli space is smooth and $SU(N_c)$ is fully broken everywhere. We also experience different kinds of chiral symmetry breaking. Along the *mesonic branch*,

$$M_i^j = \Lambda^2 \delta_i^j \quad \text{and} \quad B = \tilde{B} = 0\,, \tag{2.41}$$

one finds that the non-abelian part of the global symmetry group breaks down to its diagonal part $SU(N_f)_L \times SU(N_f)_R \to SU(N_f)_V$. While along the *baryonic branch*,

$$M_i^j = 0 \quad \text{and} \quad B = -\tilde{B} = \Lambda^{N_c}\,, \tag{2.42}$$

$U(1)_B$ is broken. For large VEVs, perturbative computations are reliable and we are in a Higgs phase, while near their smallest values we rather talk about confinement (and charge screening).

$\mathbf{N_f = N_c + 1}$. The moduli space is classically exact, in the sense that they are no quantum corrections to it. The theory confines but does not display chiral symmetry breaking at the origin of the moduli space (s-confinement). The origin is singular, but instead of gluons, the arising massless degrees of freedom are now baryons and mesons.

Seiberg duality

For $N_f > N_c + 1$, our SQCD model is known to be dual in the infrared to an alternative supersymmetric theory called mSQCD, also said to be its magnetic dual [91]. It is a slightly modified version of SQCD, with gauge group $SU(\tilde{N}_c)$ with a number of colors given by $\tilde{N}_c = N_f - N_c$ in terms of the original theory. It has also $\tilde{N}_f = N_f$ flavors q and $\tilde{q}$,

$$q_i = \overline{\square}, \quad \tilde{q}^j = \square, \quad i, j = 1, \cdots, N_f\,, \tag{2.43}$$

in addition to an extra gauge singlet chiral superfield $\Phi^i_{\ j}$,

$$\Phi^i_{\ j} = \mathbf{1}\,, \quad i, j = 1, \cdots, N_f\,. \tag{2.44}$$

It is also supplemented by a superpotential term:

$$W_{\text{mSQCD}} = h\, q_i \Phi^i_{\ j} \tilde{q}^j\,, \tag{2.45}$$

where h is a complex coupling. It is an electro-magnetic duality in the sense that

$$g^2_{\text{SQCD}} \sim g^{-2}_{\text{mSQCD}}\,. \tag{2.46}$$

See Table 2.2 for an illustration of the Seiberg duality map.

	SQCD	mSQCD
Gauge group	$SU(N_c)$	$SU(N_f - N_c)$
Matter	Q^i_a, $\tilde{Q}^a_j$	q^a_i, $\tilde{q}^j_a$, Φ^i_j
Superpotential		$q\,\Phi\,\tilde{q}$

Table 2.2: Seiberg duality map.

$\mathbf{N_c + 1 < N_f \leqslant 3N_c/2}$**.** SQCD is a strongly coupled theory enjoying confinement but is better described at low energy in terms of mSQCD, which is free in the infrared. We thus say that SQCD is in the free magnetic phase.

$\mathbf{3N_c/2 < N_f < 3N_c}$**.** This range is known as the conformal window of SQCD. The low energy theory lives on a non-trivial conformal fixed point. Near the right corner of the conformal window, the following value for the gauge coupling that can be obtained from a two-loops computation, namely we find a Banks-Zaks fixed point:

$$g^* = \frac{8\pi^2}{3}\frac{3N_c - N_f}{N_c^2 - 1}\,. \tag{2.47}$$

Note that it converges towards zero as we increase the number of flavors up to $3N_c$. Conversely, the gauge coupling of mSQCD would decrease as N_f converges towards $3N_c/2$. Both theories are not confining but are rather in an interacting Coulomb phase.

$\mathbf{3N_c \leqslant N_f}$**.** The numerator of the β function is now negative and hence the theory is free in the infrared. We call this phase the free electric phase. mSQCD turns out to be a more convenient description of the ultraviolet regime of the theory.

The different phases of SQCD are summarized in Figure 2.1.

2.3 Dynamical supersymmetry breaking

2.3.1 The $SU(5)$ model

The $SU(5)$ model is a DSB model [71, 92] that is non-calculable, in the sense that one cannot perform computations to learn about its infrared

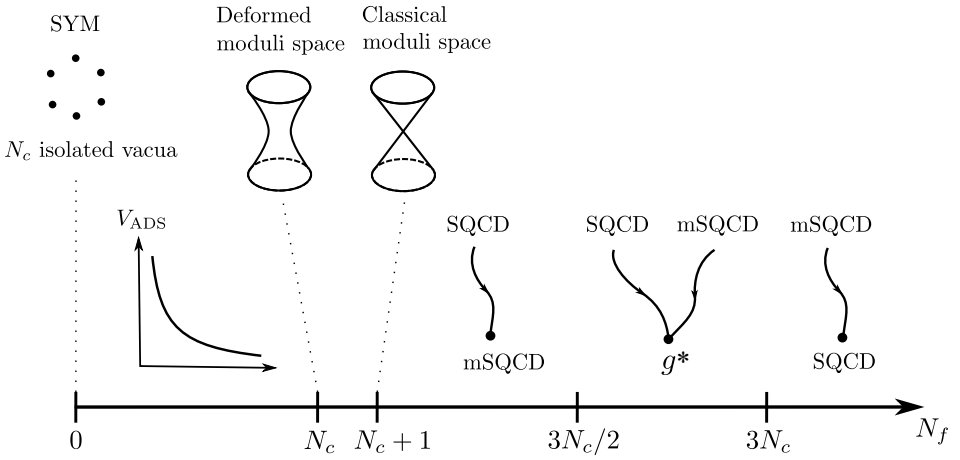

Figure 2.1: Quantum phases of SQCD. For $N_f > N_c + 1$, we draw a schematic RG-flow where the arrow links an adequate description of the ultraviolet regime of the theory to its adequate description in the infrared.

regime. Its matter content makes it look similar to a Grand Unified Theory model:

$$\tilde{Q} = \overline{\square}, \quad A = \begin{smallmatrix}\square\\\square\end{smallmatrix}. \tag{2.48}$$

The β function for the gauge coupling is positive,

$$\beta_{SU(5)} = 13\,, \tag{2.49}$$

and hence the theory is likely to confine. The theory admits no holomorphic gauge-invariant quantities and consequently no flat directions. In particular, it has a unique vacuum. The model has an exact global symmetry group $U(1)_q \times U(1)_{\rm R}$ with charges exposed in Table 2.3.

We don't know how to perform calculations in the infrared regime of the theory, but we can observe that 't Hooft anomaly matching impose weird charges assignments for hypothetical low energy fields. This leads to thinking that the global group of symmetry is (at least partially) spontaneously broken in the infrared. This should lead to the presence of one or two Goldstone bosons, and the latter cannot sit together in the same supermultiplet.[1] Still, the Goldstone boson is by essence massless and does not feel a potential at low energy, and thus because of supersymmetry, it should be found in the same chiral multiplet as an extra real scalar that is subject to identical dynamics. The presence of the latter implies a flat direction in

[1] See [71] for a full explanation of this fact.

	$U(1)_q$	$U(1)_{\mathrm{R}}$
$\tilde{Q}$	3	-9
A	-1	1

Table 2.3: Global charges in the $SU(5)$ model.

the moduli space, but they were supposed to be absent. So we conclude that the theory should break supersymmetry.

Another way to argue the breaking of supersymmetry is to couple the model to an extra pair of massive chiral multiplets [93],

$$H \oplus \tilde{H} = \square \oplus \overline{\square}, \tag{2.50}$$

with mass m. This model has four flat directions. So far, they are parameterized by VEVs for the following gauge-invariants:

$$A\tilde{Q}\tilde{H}\,, \quad AAH\,, \quad H\tilde{H} \quad \text{and} \quad H\tilde{Q}\,. \tag{2.51}$$

We can introduce a tree-level superpotential which, as for SQCD with less flavors than colors, will receive corrections from a non-perturbative ADS contribution:

$$W_{\text{eff}} = \frac{2\Lambda^6}{(A\tilde{Q}\tilde{H})^{1/2}(AAH)^{1/2}} + h(A\tilde{Q}\tilde{H}) + f(AAH) + mH\tilde{H}\,, \tag{2.52}$$

where h and f can be any coupling. For $m = 0$, F-term equations can be satisfied and the gauge group is generically broken down to $SU(2)$. However, this model cannot satisfy F-term equations for a generic non-zero mass and hence breaks supersymmetry. Sending the mass to infinity decouples the extra chiral multiplets and one recovers the initial $SU(5)$ model. The fact that the Witten index[2] is the same for finite and infinite m hints that there is no phase transition when the mass is taken to infinity. Thus, we are led to conclude that supersymmetry is broken by non-perturbative effects.

The conclusion for this model is that the potential has to be different from zero and can only be proportional to the appropriate power of the strong coupling scale:

$$V \propto \Lambda^4_{SU(5)}\,. \tag{2.53}$$

[2]The Witten index is a topological invariant that counts the difference in number between bosonic and fermionic states at any energy level. Since a supersymmetric theory has the same number of bosons and fermions at any positive energy level, this difference can only receive contributions from the vacuum, *i.e.* at zero energy.

Generalizations to higher ranks

Generalizations of the $SU(5)$ model were studied in [94]. They introduced a gauge theory with gauge group $SU(N_c)$, and matter given by N_c-4 antifundamental superfields together the usual antisymmetric:

$$\tilde{Q}^i = \overline{\square} \quad i = 1, \cdots, N_c - 4\,, \quad A = \begin{smallmatrix}\square\\\square\end{smallmatrix}. \tag{2.54}$$

It admits a R-symmetry preserving tree-level superpotential for $N_c \geqslant 6$:

$$W_{\text{tree}} = \lambda_{ij} \tilde{Q}^i \tilde{Q}^j A\,, \tag{2.55}$$

with an antisymmetric matrix of couplings, $\lambda^T = -\lambda$.

For N_c even, starting from $N_c = 4$, a runaway effective superpotential is generated. Unfortunately, the tree-level superpotential is not enough to lift every of these runaway directions, resulting in an unstable theory.

For N_c odd, starting from $N_c = 7$, there is a balance between a dynamical potential and the tree-level superpotential term of Equation (2.55) that minimizes the potential at

$$V \propto \lambda^{4\frac{N_c-5}{2N_c+3}} \Lambda^4_{SU(N_c)}\,, \tag{2.56}$$

and hence breaks supersymmetry dynamically in a stable vacuum.

2.3.2 The 3−2 model

The $3-2$ model is an instance of a calculable model [94]. The gauge group is $SU(3) \times SU(2)$ and the matter content is similar to the one of the Standard Model:

$$Q = (\square_3, \overline{\square}_2)\,, \quad \bar{U} = \overline{\square}_3\,, \quad \bar{D} = \overline{\square}_3\,, \quad L = \square_2\,, \tag{2.57}$$

with a superpotential given by

$$W = \lambda\, \bar{D} Q L\,. \tag{2.58}$$

The theory enjoys an anomaly-free global symmetry group $U(1)_Y \times U(1)_{\text{R}}$ with charges presented in Table 2.4.

We can define

$$(\bar{Q}_i) \equiv (\bar{U}, \bar{D})\,, \tag{2.59}$$

and construct three gauge-invariants that we will use to parameterize the moduli space:

$$X = \bar{U} Q L\,, \quad Y = \bar{D} Q L\,, \quad Z = \det Q \bar{Q}\,. \tag{2.60}$$

	$U(1)_Y$	$U(1)_{\mathrm{R}}$
Q	$1/3$	1
$\bar{U}$	$-4/3$	-8
$\bar{D}$	$2/3$	4
L	-1	-3

Table 2.4: Global charges in the $3-2$ model.

F-term equations force all of these operators to vanish and the moduli space is only composed of the origin. In particular, it does not have flat directions and thus we can run the same argument as for the $SU(5)$ model: if a global symmetry is broken, supersymmetry has to be broken too.

If $SU(3)$ goes to strong coupling before $SU(2)$, *i.e.* $\Lambda_3 \gg \Lambda_2$, one can easily verify that an effective superpotential term is generated because of a $SU(3)$ instanton,

$$W_{\text{eff}} = \frac{\Lambda_{SU(3)}^7}{Z} + \lambda Y \,. \tag{2.61}$$

The impossibility to satisfy the F-term equation for Y already shows that supersymmetry is broken, since $\lambda \neq 0$. It can also be seen that the first term in the effective superpotential is pushing for high values of Z. The VEV for this gauge-invariant has a non-vanishing R-charge and thus breaks $U(1)_{\mathrm{R}}$, which confirms again that supersymmetry is broken. One can find with scaling arguments that

$$V \propto \lambda^{10/7} \Lambda_{SU(3)}^4 \,. \tag{2.62}$$

For a very small λ, we can understand the VEVs in terms of UV fields and see that the non-perturbative term of the superpotential pushes for high VEVs of Q and $\bar{Q}$. This means that $SU(2)$ is fully broken and, there, the Kähler potential can be computed too. This is what makes this model calculable. This does not remain true in general, when $\Lambda_2 \gg \Lambda_3$ and up to $\Lambda_3 \approx \Lambda_2$, but it can be proved that the model still breaks supersymmetry dynamically.

Chapter 3

String Theory

There are five different ways to realize a perturbative quantum theory of propagating strings. The fundamental ingredients are exclusively closed strings in most instances. Only one starts with both open and closed strings. The amount of supersymmetry also varies. We list them below.

- *Type I* is a theory of unoriented closed and open strings with gauge symmetry $SO(32)$ and $\mathcal{N} = 1$ supersymmetry.
- *Type IIA* is a theory of closed strings. It has two supercharges with opposite chirality in spacetime, $\mathcal{N} = (1, 1)$. An open string sector arises on D-branes, which can be thought of as non-perturbative states of the theory.
- *Type IIB* differs from the previous one by having two supercharges with the same chirality in spacetime, $\mathcal{N} = (2, 0)$.
- *Heterotic* $SO(32)$ is a theory of closed strings with only one supercharge in the left or right-moving sector, $\mathcal{N} = 1$, and a $SO(32)$ gauge symmetry in the other non-supersymmetric sector.
- *Heterotic* $E_8 \times E_8$ is constructed similarly to the previous one but enjoys a $E_8 \times E_8$ gauge symmetry instead.

All these theories are linked through a web of dualities, illustrated in Figure 3.1, meaning that each of them is a valid description of another in an appropriate regime. Type I can be obtained from type IIB by introducing orientifolds. Those objects will be studied in Chapter 7. Type IIA and IIB are related by T-duality, which will be the object of Section 3.1.3. The two heterotic theories are also T-dual to each other. S-duality links the heterotic

theory with gauge group $SO(32)$ to type I. It is a non-perturbative duality, also called the strong-weak duality, because it relates the string coupling g_s of one S-dual to $1/g_s$ in the other. Type IIB is S-dual to itself, meaning that the duality is realized as symmetry in the latter. Finally, all these theories are connected to the eleven-dimensional M-theory, whose microscopic definition remains unknown but is described by eleven-dimensional supergravity at low energy. As such, the latter provides another description of string theory, even though it is not by itself a theory of strings.

- *Eleven-dimensional supergravity* is the low energy limit of M-theory.

M-theory can be compactified on a circle S^1 and gives back type IIA when the corresponding radius vanishes, or compactified on a line interval $S^1/\mathbb{Z}_2$ and then gives back the heterotic theory with $E_8 \times E_8$ again in the vanishing length limit.

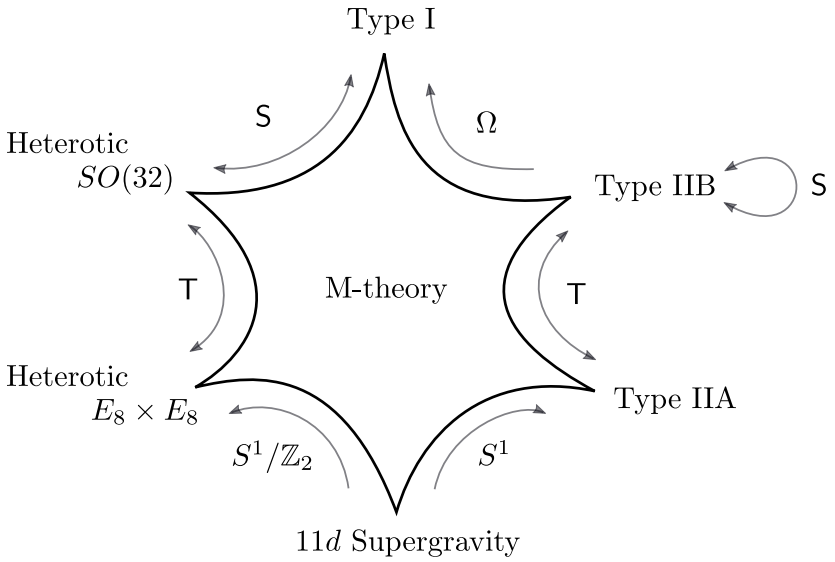

Figure 3.1: Web of dual string theories and M-theory. S stands for S-duality, T for T-duality and Ω for the addition of an orientifold plane.

For our purpose of exploring the generalizations of the gauge/gravity duality, we will mainly be interested in learning about type II superstring

theories,[1] and in particular type IIB. Our discussion follows [95–102], where more material can be found. For specific reviews on D-branes, one can look at [103–105].

3.1 Elements of string theory

3.1.1 Perturbative approach to types IIA and IIB

Since we are interested in phenomenological applications of string theory, we hope that it can reproduce a realistic spectrum, like the one of the Standard Model, at low energy. This cannot stand if string theory does not reproduce spacetime fermions from the string excitations. Indeed, quarks and leptons which constitute matter are of this type.

One way to recover spacetime fermions is to allow for worldsheet fermions, in addition to its bosons, and impose supersymmetry on the worldsheet. This is the Ramond-Neveu-Schwarz (RNS) formalism [106, 107] for which we recall some features in this section. Actually, supersymmetry appears as a necessity if one wants to work with a consistent string theory, *i.e.* free of tachyons. The absence of negative norms quantum states and Lorentz invariance will also fix the dimension of the embedding spacetime to be exactly $d = 10$. Another and equivalent way to construct these string theories with spacetime fermions is to impose supersymmetry in spacetime and is referred to as the Green-Schwarz formalism [108–110]. We will not expand on the latter in this work.

Types II superstring are theories of closed strings in the sense that those populate the perturbative vacuum. Open strings will appear in the spectrum only when attached to D-branes, which are in fact non-perturbative states. The latter will play a central role in this work, as they are the fundamental ingredients that we will use to connect string models to gauge theories, and will be reviewed in Section 3.1.2. Still, it is interesting to review some properties of the closed string spectrum, as it opens the door to gravitation and other types of interactions under which the D-branes are sensitive. Phrased differently, open strings couple to closed strings and we need the latter in order to fully appreciate the dynamics of branes.

There are two different string theories of type II, types IIA and IIB, and

[1] Although we will ultimately be interested in supersymmetry breaking, we will not comment on non-critical strings and other non-supersymmetric realizations of string theory. We will restrict ourselves to a textbook approach of superstring theory before considering implementing a supersymmetry breaking scenario.

we now review what is the content of their massless spectra of closed strings. We start with a common action for a two-dimensional worldsheet W_2 that admits as many bosonic as fermionic excitations, respectively denoted X^M and ψ^M where M is an index counting dimensions of the embedding space-time, and we anticipate $M = 0, \cdots, 9$. Each ψ^M is a Majorana fermion on the worldsheet. The action on the worldsheet is given by

$$S = -\frac{1}{4\pi\alpha'} \int_{\mathsf{W}_2} \mathrm{d}^2\sigma \, \left(\partial X_M \partial X^M + \bar{\psi}_M \not{\partial} \psi^M \right) . \tag{3.1}$$

The worldsheet theory is supersymmetric. X^M and ψ^M are respectively regarded as scalars and spinors from the worldsheet point of view but are both vectors in the embedding space. The prefactor in the action is the tension of the string, where α' is related to the string scale l_s by

$$\alpha' = l_s^2 \, . \tag{3.2}$$

Closed strings excitations can be decomposed in left and right-moving sectors. It is useful to do so since they turn out to be decoupled sectors, up to a level matching condition for the masses. Let be

$$\begin{array}{rcl} X(\sigma_0, \sigma_1) & = & X_L(\sigma_0 + \sigma_1) + X_R(\sigma_0 - \sigma_1) \\ \psi(\sigma_0, \sigma_1) & = & \psi_L(\sigma_0 + \sigma_1) + \psi_R(\sigma_0 - \sigma_1) \end{array} \tag{3.3}$$

for each component M, where ψ_L and ψ_R are now Majorana-Weyl spinors.

We have to impose a boundary condition for closed strings that translates into a periodicity on σ_1, with a period chosen to be 2π. For the bosonic excitations, this is uniquely fixed by

$$X_{L,R}\big|_{\sigma_1 + 2\pi} = X_{L,R}\big|_{\sigma_1} \, . \tag{3.4}$$

For the fermionic partners, we have two choices:

$$\begin{array}{lcrcl} \text{Neveu-Schwarz (NS)} & : & \psi_{L,R}\big|_{\sigma_1 + 2\pi} & = & -\psi_{L,R}\big|_{\sigma_1} \\ \text{Ramond (R)} & : & \psi_{L,R}\big|_{\sigma_1 + 2\pi} & = & +\psi_{L,R}\big|_{\sigma_1} \end{array} , \tag{3.5}$$

that can be made independently for both left and right-movers. Hence, it leads to four different sectors for closed strings: NSNS, NSR, RNS, and RR.

There are different ways to quantize the strings: in the light-cone gauge or covariantly. The first one is generally exposed in a first course on string theory. It prescribes to write worldsheet fields in light-cone coordinates: X^+, X^-, ψ^+, ψ^- in addition to transverse components $X^2, \cdots, X^9$, $\psi^2, \cdots, \psi^9$, and then use the reparametrizations of the worldsheet to reach

the so-called light-cone gauge. The latter satisfies automatically the Virasoro constraints inherited from the superconformal invariance of the RNS strings and, together with the equations of motion, fix the values of X^+, X^-, ψ^+, ψ^-. On-shell degrees of freedom are obtained from the eight transverse components of the worldsheet fields and will transform in representations of the little group $SO(8)$.

After quantization, Gliozzi-Scherk-Olive (GSO) projections [13] are performed in order to avoid tachyons in the spectrum. This results in two alternative massless spectra, corresponding to types IIA and IIB. In short, the NS sector brings a vector in the representation $\mathbf{8}_v$ of $SO(8)$ for each type II theory. From the R sector, type IIA gets two spinors with opposite chirality in the $\mathbf{8}$ and $\mathbf{8}'$, while those of type IIB have identical chirality in the $\mathbf{8}$, all of them from the $SO(8)$ group too. The tensor product of left and right-movers gives rise to fields in the ten-dimensional spacetime. In contrast with the worldsheet content of spinors, Type IIA ends up being non-chiral and IIB chiral in spacetime:

$$\begin{aligned}
\text{IIA} \quad : \quad & [\mathbf{8}_v \oplus \mathbf{8}] \otimes [\mathbf{8}_v \oplus \mathbf{8}'] \;=\; [\mathbf{1} \oplus \mathbf{28} \oplus \mathbf{35}]_{\text{NSNS}} \oplus [\mathbf{8} \oplus \mathbf{56}']_{\text{NSR}} \\
& \qquad \oplus [\mathbf{8}' \oplus \mathbf{56}]_{\text{RNS}} \oplus [\mathbf{8}_v \oplus \mathbf{56}_t]_{\text{RR}} \,, \\
\text{IIB} \quad : \quad & [\mathbf{8}_v \oplus \mathbf{8}] \otimes [\mathbf{8}_v \oplus \mathbf{8}] \;=\; [\mathbf{1} \oplus \mathbf{28} \oplus \mathbf{35}]_{\text{NSNS}} \oplus [\mathbf{8} \oplus \mathbf{56}]_{\text{NSR}} \\
& \qquad \oplus [\mathbf{8} \oplus \mathbf{56}]_{\text{RNS}} \oplus [\mathbf{1} \oplus \mathbf{28} \oplus \mathbf{35}_*]_{\text{RR}} \,.
\end{aligned} \tag{3.6}$$

The fields in components are presented in Table 3.1.

Sectors		Type IIA	Type IIB
NSNS	dilaton	ϕ	ϕ
	2-form	B_{MN}	B_{MN}
	graviton	G_{MN}	G_{MN}
NSR RNS	dilatinos	$\lambda^1_\alpha \quad \lambda^2_{\dot\alpha}$	$\lambda^1_\alpha \quad \lambda^2_\alpha$
	gravitinos	$\psi^1_{M\dot\alpha} \quad \psi^2_{M\alpha}$	$\psi^1_{M\alpha} \quad \psi^2_{M\alpha}$
RR	p-forms	C_M C_{MNP}	C C_{MN} C_{MNPQ}

Table 3.1: Massless closed string spectra of type IIA and IIB superstring theories.

The NS-NS sector is common to both type II theories. It contains a

graviton G that mediates the usual gravitational interactions. There is a 2-form field B_2 that couples electrically to the fundamental strings through a topological term that one can add to their action,

$$\frac{1}{2\pi\alpha'}\int_{\mathsf{W}_2} B_2\,. \tag{3.7}$$

The theories are consequently invariant under the gauge transformation

$$B_2 \to B_2 + \mathrm{d}\Lambda_1\,. \tag{3.8}$$

Finally, we find a dilaton whose VEV defines the string coupling constant:

$$g_s = e^{\phi}\,. \tag{3.9}$$

The latter is the parameter for the loop expansion of strings interactions and thus controls quantum corrections

Other sectors differ from one theory to the other. The RNS and NSR contain fermions, among which we find two gravitinos, of spin 3/2, which sit in supersymmetric gravity multiplets together with the graviton. This is an important consequence of the GSO projections since it implies that both theories have spacetime supersymmetry. They have 32 real components of supercharges, which in the ten-dimensional spacetime correspond to two Majorana-Weyl spinors Q^1 and Q^2 generating the supersymmetries. More precisely, gravitinos have opposite/identical chirality in type IIA/IIB, and so the same can be said for the chirality of Q^1 and Q^2:

$$\text{IIA} \quad : \quad Q^1 = \mathbf{16},\, Q^2 = \mathbf{16'}\,, \qquad\qquad \text{IIB} \quad : \quad Q^1,\, Q^2 = \mathbf{16}\,. \tag{3.10}$$

The situation is usually summarized by noting the number of supersymmetries for both type II theories as follows:

$$\text{IIA} \quad : \quad \mathcal{N} = (1,1)\,, \qquad\qquad \text{IIB} \quad : \quad \mathcal{N} = (2,0)\,. \tag{3.11}$$

As such, type IIB can be suspected to generate chiral anomalies. However, as it was shown in [111], all contributions to these anomalies cancel and type IIB is eventually well-defined. We also note that the presence of gravitinos comes together with the fact that types II theories at low energy theory are actually different theories of supergravity.

The RR p-forms C_p (or equivalently, $C_{M_1\cdots M_p}$ in components) imply that the theories are invariant under the following gauge transformations:

$$C_p \to C_p + \mathrm{d}\Lambda_{p-1}\,, \tag{3.12}$$

with p odd/even in type IIA/IIB. They do not appear to be sourced by any object in the perturbative spectrum, but this silence speaks volumes. Such objects exist and are the D-branes that we will introduce soon. Note also that the 4-form field C_4 of type IIB can be consistently defined in the **35** only if its flux is self-dual under Hodge duality:

$$F_5 = *F_5 \,. \tag{3.13}$$

The low energy action of IIB, which we do not present here, enjoys a $SL(2,\mathbb{R})$ symmetry and it is conjectured that a $SL(2,\mathbb{Z})$ subgroup is maintained at the quantum level. It corresponds to the S-duality mentioned in the introduction of the present chapter. It acts on the NSNS B_2 and RR C_2 fields as a doublet:

$$\begin{pmatrix} C_2 \\ B_2 \end{pmatrix} \to \begin{pmatrix} a & b \\ c & d \end{pmatrix} \begin{pmatrix} C_2 \\ B_2 \end{pmatrix} \,, \tag{3.14}$$

and on the axio-dilaton field, defined by

$$\tau_{\text{IIB}} = ie^{-\phi} + \frac{C_0}{2\pi} \,, \tag{3.15}$$

in a non-linear fashion:

$$\tau_{\text{IIB}} \to \frac{a\,\tau_{\text{IIB}} + b}{c\,\tau_{\text{IIB}} + d} \,, \tag{3.16}$$

for $a, b, c, d \in \mathbb{Z}$ satisfying $ad - bc = 1$. In particular, a bridge from weak to strong coupling g_s is built for $a = d = 0$ and $b = -c = 1$:

$$\tau_{\text{IIB}} \to -\frac{1}{\tau_{\text{IIB}}} \,. \tag{3.17}$$

3.1.2 Branes

D-branes and open strings

Although type II superstring theories are perturbatively defined as theories of closed strings, the discovery of D-branes in the spectrum [112] opened a path to an open string sector in both of them. These are non-perturbative objects in nature and this is essentially the reason why open strings can arise consistently with our initial will to consider closed strings at the perturbative level.

Starting with the same supersymmetric action as in Equation (3.1), the open string requires proper boundary conditions at its ends, $\sigma_1 = 0$ and

$\sigma_1 = \pi$. The left and right-moving fermions can be identified with the same relative sign on both ends, or with an opposite sign. This introduces two different sectors:

$$\begin{array}{lcll} \text{Neveu-Schwarz (NS)} & : & \psi_L\big|_{\sigma_1=0} = +\psi_R\big|_{\sigma_1=0}\,, & \psi_L\big|_{\sigma_1=\pi} = -\psi_R\big|_{\sigma_1=\pi}\,, \\ \text{Ramond (R)} & : & \psi_L\big|_{\sigma_1=0} = +\psi_R\big|_{\sigma_1=0}\,, & \psi_L\big|_{\sigma_1=\pi} = +\psi_R\big|_{\sigma_1=\pi}\,. \end{array} \tag{3.18}$$

From what we said for the closed strings, we can anticipate that a quantization combined with a suitable GSO projection would lead to a vector in the $\mathbf{8}_v$ and a spinor in the $\mathbf{8}$ from the NS and R sectors respectively. But now come the branes.

A Dp-brane is a surface extending in p spatial directions on which open strings can end. This means that our open strings are free to move in the worldvolume of a D-brane but are fixed at its position in its transverse directions. Thus, they satisfy Neumann boundary conditions on p spatial directions and Dirichlet on the remaining $9-p$:

$$\begin{array}{lcccccll} \text{Neumann} & : & \partial_{\sigma_1} X^\mu\big|_{\sigma_1=0} & = & \partial_{\sigma_1} X^\mu\big|_{\sigma_1=\pi} & = & 0\,, & \mu = 0, \cdots, p\,, \\ \text{Dirichlet} & : & \delta X^i\big|_{\sigma_1=0} & = & \delta X^i\big|_{\sigma_1=\pi} & = & 0\,, & i = p+1, \cdots, 9\,. \end{array} \tag{3.19}$$

Quantizing the open string with such boundary conditions results in the massless spectrum presented in Table 3.2. The vector of the NS sector will split into a gauge vector in the worldvolume of the Dp-branes and real scalars in the transverse directions, one for each $9-p$ coordinates. They originate from a specific Fourier mode of ψ^M at the quantum level, and it is common to note them as such:

$$\text{NS} \quad : \quad \left(\psi^M_{-1/2}\,|k\rangle\right) = \left(A^\mu\,|k\rangle\,, \phi^i\,|k\rangle\right)\,, \tag{3.20}$$

for a NS quantum state of momentum k. The excitations of the scalars describe the displacement of the Dp-brane along its transverse coordinates.

Sectors		Type IIA and IIB
NS	gauge vector	A_μ
	scalars	ϕ^i
R	fermions	λ_α

Table 3.2: Massless spectra of open strings in type IIA and IIB superstring theories.

In addition to removing a tachyon and an excess of fermions from the spectrum, the GSO projection constrains the dimension of D-branes p to be even/odd for type IIA/B superstring theories.

D-brane interactions

The only points that can be meaningfully distinguished on an open string are its endpoints, and so we can introduce degrees of freedom on them. It turns out that these are non-dynamical and called the Chan-Paton factors [113]. We can formally introduce N different sorts of endpoints and decompose a quantum state a with momentum k as follows:

$$|k;a\rangle = \sum_{m,n}^{N} \lambda^a_{mn} \, |k;mn\rangle \ , \tag{3.21}$$

where i and j label the endpoints of the open string. Since the open string gives rise to real vector states, the matrix λ should be diagonalizable to real values. Hence, the Chan-Paton factors have to satisfy the reality condition of being hermitian:

$$\lambda^a = \lambda^{a\dagger} \, . \tag{3.22}$$

Any interaction of open strings will a product of such matrices. Moreover, the trivial dynamics of the endpoints implies that such a factor should appear in the form of a trace in the computation of amplitudes, as in the example with four open strings:

$$\delta^{mm'}\delta^{nn'}\delta^{pp'}\delta^{qq'}\lambda^a_{q'm}\lambda^b_{m'n}\lambda^c_{n'p}\lambda^d_{p'q} = \mathrm{tr}\,\lambda^a\lambda^b\lambda^c\lambda^d \, . \tag{3.23}$$

Interactions are thus invariant under any global transformation on the worldsheet given by

$$\lambda \to U\,\lambda\,U^{-1} \, , \tag{3.24}$$

where $U \in U(N)$ in order to preserve the reality condition. Thus, one endpoint transforms in the fundamental representation of $U(N)$ while the other transforms in the antifundamental, illustrating the oriented nature of the open string. It results that both the vector A^μ and the scalars ϕ^i transform in the adjoint of $U(N)$. The symmetry can be promoted to a *gauge symmetry* in spacetime since it can be performed at any point in the latter. In the context of open strings attached to D-branes, these Chan-Paton factors naturally encode on which D-brane an endpoint is attached. Thus, we will remember that a stack of N coincident D-branes support a $U(N)$ gauge theory on their worldvolume.

The effective action for a Dp-brane is composed by the Dirac-Born-Infeld action:

$$S_{\mathrm{DBI}} = -T_{\mathrm{d}p} \int_{\mathsf{W}_{p+1}} \mathrm{d}^{p+1}\sigma \, \sqrt{-\det\left(G + B_2 + 2\pi\alpha' F_2\right)} \,, \tag{3.25}$$

computed at fixed value for the dilaton, $g_s = e^{\phi}$. B_2 is present because it arises from the same sector as G. F_2 is the field strength for the gauge vector A^{μ} and its presence guarantees gauge invariance of the action when considering contributions from boundaries of the worldsheet. The tension can be computed from an exchange of closed string between two D-branes:

$$T_{\mathrm{d}p} = \frac{1}{(2\pi)^p \alpha'^{(p+1)/2} g_s} \,, \tag{3.26}$$

where the dependence in g_s shows the non-perturbative nature of the D-branes.

Expanding in α', the action becomes

$$S_{\mathrm{DBI}} = -\frac{\alpha'^{-(p-3)/2}}{4 g_s (2\pi)^{p-2}} \int \mathrm{d}^{p+1}\sigma \, \sqrt{-G} \, \mathrm{tr}\, F^{\mu\nu} F_{\mu\nu} + \cdots \tag{3.27}$$

Thus, the gauge coupling g of the Yang-Mills theory on the D-branes is related to g_s by

$$g^2 = 2(2\pi)^{p-2} \alpha'^{(p-3)/2} g_s \,. \tag{3.28}$$

The effective action is also made of a Chern-Simons term that includes the coupling to RR fields C_{p+1} at the lowest order in α':

$$S_{\mathrm{CS}} = T_{\mathrm{D}p} \int_{\mathsf{W}_{p+1}} C_{p+1} \, + \cdots \tag{3.29}$$

It implies that Dp-branes couple "electrically" to the RR $(p+1)$-forms exposed in Table 3.1. By considering the Hodge dual of RR fluxes,

$$F_{8-p} = * F_{p+2} \,, \tag{3.30}$$

we get that Dp-branes also couple "magnetically" to RR $(7-p)$-forms. We thus find which are the D-branes that carry RR charges in each type II superstring theories:[2]

$$\begin{array}{ll} \text{type IIA}: & \mathrm{D0}, \mathrm{D2}, \mathrm{D4}, \mathrm{D6}, \mathrm{D8} \\ \text{type IIB}: & \mathrm{D}(-1), \mathrm{D1}, \mathrm{D3}, \mathrm{D5}, \mathrm{D7} \end{array} \tag{3.31}$$

[2]Some entries in the list may seem rather exotic. D8-branes are related to 9-form gauge field and so 10-form field strength. The latter is non-dynamical and thus the 9-form gauge field didn't enter our perturbative description. The D(-1)-brane couples electrically to the 0-form gauge field C and is interpreted as a D-instanton since it is localized both in time and space.

An important result for brane dynamics included in Equation (3.29) is the equality between their tension and their RR charges,

$$Q_{\mathrm{RR,D}p} = T_{\mathrm{D}p}\,. \tag{3.32}$$

This means that the attraction resulting from the exchange of NSNS fields is balanced with the repulsive exchange of RR fields. Hence, the D-branes mentioned in Equation (3.31) are stable. They are actually BPS states[3] and as such, they preserve half of the supersymmetries. Indeed, the two supercharges identified for closed strings excitations can be related to the left and right-moving sectors of fermions on the worldsheet respectively, and those end up being identified by the open string boundary condition. If Q^1 and Q^2 are the two Marojana-Weyl supercharges, a Dp-brane extending along $x^0, x^1, \cdots, x^p$ preserves the linear combination

$$Q^1 + \Gamma^{01\cdots p}\, Q^2\,. \tag{3.33}$$

The number of supersymmetries is thus reduced by half, leaving only 16 real components of supercharges on the worldvolume of the Dp-brane.

In the weak coupling limit, $g_s \to 0$, D-branes become more rigid but their tension increases slower than a typical soliton, for which the tension grows like $1/g_s^2$. As a matter of fact, the gravitational backreaction of the D-branes is controlled by the product of the Newton constant G_N, which scales like g_s^2, with their tension. The latter is thus found to be small in the weak coupling limit:

$$G_N T_{\mathrm{D}p} \propto g_s\,, \tag{3.34}$$

so we can treat the D-branes as probes on a given background geometry.

The gauge theory on a stack of D3-branes

We can go into greater details in order to describe the $U(N)$ gauge theory living on the worldvolume of a stack of N coincident D3-branes. First of all, it has 16 real components of supercharges, and we have in consequence a $\mathcal{N} = 4$ supersymmetric theory on the four-dimensional worldvolume. The massless bosonic matter is composed of a gauge vector A^μ and six real scalars ϕ^i. Moreover, one finds that the massless elements of the R sector can be arranged as four complex Weyl fermions, λ_α^I with $I = 0, \cdots, 3$. All

[3] BPS states have a mass that is equal to the norm of a central charge entering the supersymmetry algebra when $\mathcal{N} > 1$. Here, the tension generalizes the notion of mass. In general, BPS multiplets have a lower number of states than other multiplets. They are thus robust against a change of parameters in theory or quantum corrections since the number of states cannot jump when corrections are taken into account.

these fields are defined in the adjoint representation of the gauge group and combine together into a $\mathcal{N} = 4$ real multiplet. In order to see this, it is convenient to assemble the real scalars into complex ones,

$$\Phi^1 = \phi^4 + i\phi^5\,, \quad \Phi^2 = \phi^6 + i\phi^7\,, \quad \Phi^3 = \phi^8 + i\phi^9\,, \tag{3.35}$$

so that they would correspond to the complex scalars of three $\mathcal{N} = 1$ chiral multiplets. Then, the real multiplet of $\mathcal{N} = 4$ can be decomposed into a $\mathcal{N} = 1$ real multiplet and three chiral multiplets:

$$V_{\mathcal{N}=4} = (\lambda^0_\alpha, A^\mu) \oplus (\Phi^1, \lambda^1_\alpha) \oplus (\Phi^2, \lambda^2_\alpha) \oplus (\Phi^3, \lambda^3_\alpha)\,. \tag{3.36}$$

Written in these terms, the kinetic term in the action for $V_{\mathcal{N}=4}$ decomposes into kinetic terms for the four $\mathcal{N} = 1$ multiplets and a superpotential given by

$$W = \mathrm{tr}\,\Phi^1[\Phi^2, \Phi^3]\,. \tag{3.37}$$

More can be said regarding the symmetries of this theory. First of all, it enjoys a $SU(4)_\mathrm{R}$ R-symmetry, under which the set of scalars ϕ^i transforms in the **6** and the Weyl fermions λ^A_α in the **4**.

One can also remark that the $U(N)$ gauge group can be decomposed as a product of $SU(N)$ and $U(1)$ (up to some $\mathbb{Z}_N$ that are only relevant for global considerations). The $U(1)$ vector multiplet contains six scalars whose excitations displace of the center of mass of the stack of D-branes. It decouples at low energy, and we will consider that the gauge theory has a $SU(N)$ symmetry group. We will thus refer to it as $\mathcal{N} = 4$ SYM.

Finally, it can be checked that $\mathcal{N} = 4$ SYM is also superconformal since its β function vanishes:

$$\beta_{\mathcal{N}=4} = 0\,, \tag{3.38}$$

where the Φ^i do not have an anomalous dimension, $\gamma_\Phi = 0$.

NS5-branes

NS5-branes are other BPS objects present in both type IIA and IIB superstring theories that carry magnetic charges under the B_2 field. They are present both in type IIA and B theories. Their tension is different from the one of the D-branes:

$$T_{\mathrm{NS5}} = \frac{1}{(2\pi)^5 \alpha'^3 g_s^2}\,, \tag{3.39}$$

and are then of pure solitonic nature. Since B_2 and C_2 sit in a doublet of the S-duality group, the NS5-brane is the $SL(2,\mathbb{Z})$ partner of the D5-brane.

3.1.3 T-duality

T-duality is a perturbative duality in the sense that it is manifest at any order in perturbation theory, *i.e.* in an expansion in g_s. It acts on a theory compactified on a circle S^1, or more generally on any theory whose embedding space has a S^1 fiber, by exchanging the Kaluza-Klein and windings modes of the closed strings. It also exchanges the boundary conditions of the open string on the cycle. Consequently, T-duality acting on a coordinate $x_\perp$ transverse to a Dp-brane exchanges the Dirichlet condition for a Neumann:

$$\text{D}p\text{-brane} \quad \xrightarrow{\mathsf{T}_\perp} \quad \text{D}(p+1)\text{-brane}\,. \tag{3.40}$$

and vice versa for a T-duality acting on a worldvolume coordinate $x_\parallel$:

$$\text{D}p\text{-brane} \quad \xrightarrow{\mathsf{T}_\parallel} \quad \text{D}(p-1)\text{-brane}\,. \tag{3.41}$$

The radius R of the S^1 is also modified:

$$R \xrightarrow{\mathsf{T}} \frac{\alpha'}{R}\,, \tag{3.42}$$

and the string coupling constant g_s changes as follows:

$$g_s \xrightarrow{\mathsf{T}} \frac{\sqrt{\alpha'}}{R} g_s\,. \tag{3.43}$$

We call it a duality because the overall spectrum is left unchanged.

We can guess from the change of D-branes that T-duality switches type IIA and IIB. Indeed, it is possible to check that it interchanges the two GSO projections, as it is possible to work out the precise action on the massless bosonic sector. We expose a rough picture of the T-duality map in Table 3.3. While the NSNS fields mix non-trivially according to the Buscher rules [114] that we refrain to exhibit, the map presented for the RR fields can be trusted in a trivial NSNS background.

The exchange of B_2 with the graviton suggests that NS5-branes can be exchanged with a background geometry. Indeed, this geometry is known to be an asymptotically locally flat geometry with a singularity of type A_{N-1} if N parallel NS5-branes were present [115, 116], and we find it after a T-duality on a transverse direction of the NS5-brane. A T-duality on the geometry sends the configuration back to the NS5-brane:

$$\text{NS5-brane} \quad \xleftrightarrow{\mathsf{T}_\perp} \quad \text{ALF geometry}\,. \tag{3.44}$$

Type IIA		$\overset{\mathsf{T}_9}{\longleftrightarrow}$	Type IIB	
G_{9m}	B_{9m}		B_{9m}	G_{9m}
C_9	C_m		C	C_{9m}
C_{9mn}	C_{mnr}		C_{mn}	C_{9mnr}

Table 3.3: A rough picture of the T-duality map on the bosonic sector of closed strings. The duality is operated on the coordinate x^9. m, n, r span the values $0, \cdots, 8$.

Consider again having a NS5-brane in flat space. A T-duality along its worldvolume simply turns a NS5-brane of type IIA into a NS5-brane of type IIB, and the other way around:

$$\text{NS5-brane} \quad \overset{\mathsf{T}_\parallel}{\longleftrightarrow} \quad \text{NS5-brane}\,. \tag{3.45}$$

3.2 AdS-CFT correspondence

In his seminal work [21], Maldacena introduced the first realization of a *gauge/gravity duality*, also called *gauge-string duality* or *holographic correspondence*. It puts on equal footing the four-dimensional conformal gauge theory $\mathcal{N} = 4$ SYM and a theory of closed strings propagating on the curved space $AdS_5 \times S^5$, hence the specific name of AdS/CFT correspondence. An important feature of this correspondence is that it relates the weak coupling regime of one to the strong of the other, and vice versa. We review some of its important features in this section but see [117] for more details.

We place a stack of coincident N D3-branes in a flat Minkowski spacetime in 10 dimensions. Consider it first from a string theory point of view. In the low energy limit, lower than l_s^{-1}, the surviving string modes include only the massless ones. On the closed strings side, the gravitons propagate on flat space without interacting with the D-branes. The reason is essentially that gravity becomes free at low energy. Indeed, in superstring theory the Newton constant is proportional to $g_s^2 l_s^8$ and tends to vanish for small l_s. On the D-branes however, the massless open strings attached to them also survive the low energy limit and describe a $\mathcal{N} = 4$ $SU(N)$ gauge theory. This is basically the SYM theory living on the four-dimensional worldvolume of the D3-branes that we introduced in the previous section since a small l_s implies a small α'. Remember that the gauge coupling g is

expressed in terms of the string coupling g_s,

$$g^2 = 4\pi g_s \,. \tag{3.46}$$

This gauge dynamics is of course trapped on the worldvolume of the D-branes, so that the two sectors of closed and open strings do not talk to each other. The low energy limit of the setup divides itself into two parts:

$$\text{Free gravitons in flat space} \quad \oplus \quad \mathcal{N}{=}4 \text{ SYM gauge theory} \,. \tag{3.47}$$

This system has an alternative description. From the supergravity point of view, the tension of the D-branes induces a backreaction on the geometry, which turns out to become the following supergravity solution for the metric:

$$\mathrm{d}s^2 = f(r)^{-1/2}(-\mathrm{d}t^2 + \mathrm{d}x_1^2 + \mathrm{d}x_2^2 + \mathrm{d}x_3^2) + f(r)^{1/2}(\mathrm{d}r^2 + r^2\mathrm{d}\Omega_5) \,, \tag{3.48}$$

with

$$f(r) = 1 + \frac{R^4}{r^4} \,, \quad R^4 = 4\pi g_s \alpha'^2 N \,, \tag{3.49}$$

in the presence of a RR self-dual 5-form flux on the S^5,

$$F_5 = (1 + *)\mathrm{d}t \wedge \mathrm{d}x_1 \wedge \mathrm{d}x_2 \wedge \mathrm{d}x_3 \wedge \mathrm{d}f^{-1} \,, \tag{3.50}$$

that satisfies

$$\int_{S^5} F_5 = N \,. \tag{3.51}$$

This solution depicts a throat centered around $r = 0$ for $r \lesssim R$, and a flat space for $r \gg R$. In the low energy limit, some gravitons with a wavelength larger than R survive and do not feel the throat anymore. Moreover, physical phenomena happening arbitrarily close enough to the horizon $r = 0$ are not visible for an external observer, since their energy measured from infinity will be redshifted to an arbitrarily small value:

$$E_{\text{measured}} = f(r)^{-1/4} E_r \,. \tag{3.52}$$

Excitations in this region are thus completely decoupled from the outside of the throat, no matter how high are their energies as far as they are close enough to the horizon. We can obtain the metric Equation (3.48) in this region by considering the *near-horizon limit*:

$$\mathrm{d}s^2 = \frac{r^2}{R^2}(-\mathrm{d}t^2 + \mathrm{d}x_1^2 + \mathrm{d}x_2^2 + \mathrm{d}x_3^2) + \frac{R^2}{r^2}\mathrm{d}r^2 + R^2\mathrm{d}\Omega_5 \,. \tag{3.53}$$

This metric is simply the one of $AdS_5 \times S^5$ where both elements are of radius R. AdS is known to be a maximally symmetric solution to the Einstein equations with negative cosmological constant. We come to the conclusion that the theory at low energy divides again in two parts:

$$\text{Free gravitons in flat space} \quad \oplus \quad \text{Type IIB on } AdS_5 \times S^5 \,. \tag{3.54}$$

Now, anybody (and in particular Maldacena) would be tempted to associate the two RHS of Equations (3.47) and (3.54). The resulting equivalence is the celebrated and first example of a gauge/gravity duality:

$$\boxed{\mathcal{N}\text{=4 SYM gauge theory} \quad \leftrightarrow \quad \text{Type IIB on } AdS_5 \times S^5} \tag{3.55}$$

This duality relates the strong coupling of one theory to the weak coupling of the other. First of all, recall that when an arbitrary number of colors N is introduced for the gauge theory, the actual gauge coupling that dictates the perturbative theory is the 't Hooft coupling:

$$\lambda = g^2 N \,. \tag{3.56}$$

One can use the definition of R in Equation (3.49) to check that

$$\lambda = \frac{R^4}{l_s^4} \,. \tag{3.57}$$

Hence, when we have a weak curvature and the supergravity approximation holds, the 't Hooft coupling is large and the gauge theory is strongly coupled. Reciprocally, when string corrections are important, we experience a high curvature and it corresponds to a small 't Hooft coupling.

The perturbative expansion of $\mathcal{N} = 4$ SYM reveals interesting features when N is large, and λ is kept fixed. The dominant Feynman diagrams are planar and this simplifies a lot the computations. This limit is referred to as the *large N limit*. In string theory, we find

$$\frac{\lambda}{N} = g_s \,, \tag{3.58}$$

and so we learn that the expansion in $1/N$ controls the loop expansion like g_s does. In other words, the large N limit provides better control of quantum corrections in the string theory.[4]

[4]This can also be expressed in terms of the radius R by introducing the Planck length, $l_{\rm P} = g_s^{1/4} l_s$, and casting Equation (3.58) as

$$N = \frac{1}{4\pi} \frac{R^4}{l_{\rm P}^4} \,. \tag{3.59}$$

We can also check that the symmetries on both sides of the duality match. The isometries of AdS_5 and S^5 are $SO(2,4)$ and $SO(6)$ respectively. On the field theory side, these groups are part of the superconformal algebra. The first group corresponds to the four-dimensional conformal group of symmetry and the second is isomorphic to the $SU(4)_{\mathrm{R}}$ R-symmetry. As we explained before, the presence of D-branes breaks half of the supersymmetries of type IIB. In other words, 16 supercharges are preserved and the broken 16 others still realize a supersymmetry but act non-linearly on the fields. They correspond to the 32 supercharges that we find in the bulk of $AdS_5 \times S^5$. The $SL(2,\mathbb{Z})$ S-duality of type IIB corresponds to the electric-magnetic duality of $\mathcal{N} = 4$ SYM. In this context, it makes sense to generalize Equation (3.46) into the following identification:

$$\tau = \tau_{\mathrm{IIB}}\,, \tag{3.60}$$

where τ is the complex coupling of $\mathcal{N} = 4$ SYM.

Chapter 4

String Geometry

So far, we discussed superstring theories whose excitations propagate in a ten-dimensional spacetime. In this respect, strings seem rather inappropriate to reproduce the behavior of usual field theories, where the number of dimensions typically reduces from ten to four. Compactification has been the key to make contact between these two realms by declaring that six out of the nine spatial dimensions were actually compact. Then, one should send their characteristic scales to very small values, so that we cannot see these extra dimensions naively. Calabi-Yau manifolds were introduced in physics [17] to provide a rich variety of compact spaces that lead to different four-dimensional low energy theories. They have the important advantage of preserving a certain amount, but reduced, of supersymmetry. Otherwise, we would lose control of the UV completion of our theory.

In the context of the gauge/gravity duality, the compactness of the extra dimensions is not an issue anymore. Indeed, we saw in the example of AdS/CFT that the radial coordinate transverse to the D3-branes extends towards infinity. Still, changing the background on which we place D-branes is an open door to a vast set of generalizations of the known correspondence. In particular, things get interesting when the transverse space bears singularities. Of course, we would like to introduce such singular spaces while keeping the advantages of supersymmetry, so we are interested in finding non-compact Calabi-Yau cones. For this topic, we follow the references [100, 101, 118–122].

Knowing that we will deal with Calabi-Yau cones is not enough to concretely propose extensions of the gauge/gravity duality. We need details about the geometry itself. In this respect, toric geometry comes to the rescue as a robust framework for producing a large amount of different non-compact

and singular Calabi-Yau geometries. The power of toric geometry resides in the combinatorial control that one has over the geometrical properties of each toric variety. It was introduced in brane physics in [123]. We will review some of the important ingredients to construct Calabi-Yau toric geometries and illustrate them with examples, following [118, 121, 124–127].

4.1 Calabi-Yau cones

4.1.1 Preserving supersymmetry

Assume that we compactify a type II superstring theory from the 10-dimensional flat space $\mathbb{R}^{1,9}$ to a more general $\mathbb{R}^{1,3} \times \mathcal{M}_6$, where $\mathcal{M}_6$ is any six-dimensional manifold. Supersymmetry would typically be broken. The reason is that the supercharges previously defined in the **16** now transform in the $(\mathbf{2}_L, \mathbf{4})$ and $(\mathbf{2}_R, \bar{\mathbf{4}})$ of the $SO(1,3) \times SO(6)$ group:

$$\mathbf{16} \to (\mathbf{2}_L, \mathbf{4}) \oplus (\mathbf{2}_R, \bar{\mathbf{4}})\,, \tag{4.1}$$

As such, they might experience a non-trivial rotation after making a tour around a closed loop in $\mathcal{M}_6$. They would then be ill-defined.

Instead of this catastrophic scenario, we would like to find $\mathcal{M}_6$ such that we can define a covariantly constant spinor ξ on the manifold, *i.e.* a Killing spinor:

$$\nabla_{\mathcal{M}_6} \xi = 0\,, \tag{4.2}$$

guaranteeing that some supercharges survive. The way out is to consider particular manifolds for which the holonomy group $\mathcal{H}(\mathcal{M}_6)$ is the subgroup $SU(3) \subset SO(6)$ because it admits a trivial representation as we decompose the **4** into representations of $SU(3)$:

$$\mathbf{4} \to \mathbf{1} \oplus \mathbf{3}\,. \tag{4.3}$$

From the initial 16 components of the supercharges, only four coming from $(\mathbf{2}_L, \mathbf{1})$ and $(\mathbf{2}_R, \mathbf{1})$ will survive. We would thus have a total of eight supercharges giving us an $\mathcal{N} = 2$ four-dimensional theory. If D3-branes also extend along $\mathbb{R}^{1,3}$, then it would reduce the amount of supersymmetry to $\mathcal{N} = 1$. For spaces with a smaller holonomy group, an enhancement of supersymmetry is also possible. A manifold $\mathcal{M}_6$ has $SU(3)$ holonomy if and only if it is Calabi-Yau (CY, or CY_3 in the present context). See Table 4.1 for other kinds of special holonomies.

Originally, a CY is defined to be a compact Kähler manifold with vanishing first Chern class c_1. It was conjectured by Calabi and proved by Yau

$\mathcal{M}_{2n}$	$\mathcal{H}(\mathcal{M}_{2n})$
Kähler	$U(n)$
Calabi-Yau	$SU(n)$
Hyper-Kähler	$Sp(n/2)$
Quaternionic Kähler	$Sp(n/2) \cdot Sp(1)$

Table 4.1: Varieties $\mathcal{M}_{2n}$ with special holonomies $\mathcal{H}(\mathcal{M}_{2n})$.

that such a manifold admits a Ricci-flat metric. We now explain briefly the content of these statements and how they ensure that the holonomy group will be $SU(3)$.

Being Kähler means several things. The manifold $\mathcal{M}_{2n}$ has to be complex, *i.e.* a $2n$-dimensional space, with a globally defined complex structure[1] I that acts linearly on the tangent space $T_p\mathcal{M}_{2n}$, and satisfies the following condition:

$$I^j_{\ j} I^j_{\ k} = -\delta^i_{\ k} \,. \tag{4.4}$$

There is a theorem that stipulates that a complex manifold always admits a Hermitian metric g, *i.e.* satisfying

$$g(I\bullet, I\bullet) = g(\bullet, \bullet) \,. \tag{4.5}$$

Now, the complex manifold with Hermitian metric g is Kähler if it is endowed with a Kähler form J_2 such that

$$g(\bullet, \bullet) = J_2(\bullet, I\bullet) \,, \quad \mathrm{d}J_2 = 0 \,. \tag{4.6}$$

A direct implication of being Hermitian for g is that, once written in complex coordinates, only its components with mixed entries are non-vanishing:

$$g_{ij} = g_{\bar{i}\bar{j}} = 0 \,. \tag{4.7}$$

Consequently, the Kähler form J_2 is actually a 2-form of bidegree $(1,1)$:

$$J_2 = J_{i\bar{j}} \, \mathrm{d}z^i \wedge \mathrm{d}\bar{z}^{\bar{j}} \,. \tag{4.8}$$

Since the Kähler form is closed, we also find extra relations for the metric,

$$\partial_i g_{j\bar{k}} = \partial_j g_{i\bar{k}} \,, \quad \partial_{\bar{i}} g_{\bar{j}k} = \partial_{\bar{j}} g_{\bar{i}i} \,, \tag{4.9}$$

[1] As presented in the main text, I is an almost complex structure. It is really a complex structure if the Nijenhuis tensor, $N^i_{jk} = I^l_{\ j}(\partial_l I^i_{\ k} - \partial_k I^i_{\ l}) - I^l_{\ k}(\partial_l I^i_{\ j} - \partial_j I^i_{\ l})$, vanishes identically.

which imply in turn that the Levi-Civita connection does not mix holomorphic and antiholomorphic indices:

$$\Gamma^{i}_{\bar{j}k} = \Gamma^{\bar{i}}_{\bar{j}k} = \Gamma^{i}_{\bar{j}\bar{k}} = \Gamma^{\bar{i}}_{jk} = 0\,. \tag{4.10}$$

In other words, parallel transport does not mix holomorphic and antiholomorphic indices on a Kähler manifold. Since the length of a vector is also preserved, the holonomy group is at most $U(n)$ if the manifold has dimension $2n$. In order to reduce it to $SU(n)$, one has to verify the absence of $U(1)$ holonomy. For a simply connected manifold, it can be shown easily that the $U(1)$ holonomy contributes with a term proportional to the Ricci curvature 2-form $\mathcal{R}_{i\bar{j}}$ in Equation (4.2). Therefore, a Ricci-flat metric comes together with a $SU(n)$ holonomy group.

For a Kähler manifold, the first Chern class is given by

$$c_1 = \frac{1}{2\pi}[\mathcal{R}]\,. \tag{4.11}$$

The vanishing of c_1 was proved to ensure the existence of a number $h^{1,1}(\mathcal{M}_6)$ of Ricci-flat metrics for the CY manifolds. It counts the Kähler parameters of the CY. Moreover, c_1 vanishes if and only if the manifold has a trivial canonical bundle. We will exemplify this notion in the context of toric geometry in Section 4.2. This guarantees the existence of a globally-defined and nowhere vanishing holomorphic n-form Ω_n. For our case of interest where the CY is connected and of complex dimension three, it is uniquely defined with a choice of Kähler 2-form J_2 and holomorphic 3-form Ω_3. Moreover, these can be constructed out of the Killing spinor ξ as follows:

$$J_{i\bar{j}} = -i\xi^{\dagger}\Gamma_i\Gamma_{\bar{j}}\xi\,, \quad \Omega_{ijk} = \xi^{T}\Gamma_i\Gamma_j\Gamma_k\xi\,, \tag{4.12}$$

where the Γ_i are matrices of $\mathrm{Cliff}(6,0)$.

The non-compact and singular CY that we will deal with in the rest of this work can be thought as regions, or open neighborhoods, cut from a compact CY. The definitions for compact CY introduced above thus hold in non-compact cases up to specific boundary conditions at infinity.

4.1.2 Conical singularities

We now focus on non-compact CY threefolds with cone-type singularities. The CY is constructed as a cone over a base that is a five-dimensional Sasaki-Einstein manifold SE_5,

$$\mathrm{CY} = C(\mathrm{SE}_5)\,, \tag{4.13}$$

in the sense of the following construction of the CY metric:

$$\mathrm{d}s^2_{\mathrm{CY}} = \mathrm{d}r^2 + r^2 \mathrm{d}s^2_{\mathrm{SE}_5} \,, \tag{4.14}$$

where r is a radial coordinate. In general, a $(2n-1)$-dimensional Sasaki-Einstein manifold satisfies the following relation for the Ricci curvature,

$$R_{ij} = 2(n-1) g_{ij} \,, \tag{4.15}$$

and is thus of positive curvature. This moreover guarantees that the full cone is Ricci-flat and is thus a non-compact CY. Its metric is said to be of conical-type because there exists a diffeomorphism that rescales the metric,

$$r \to \lambda r \quad \forall \lambda \in \mathbb{R}_{>0} \,. \tag{4.16}$$

In the present scenario, we could write

$$\mathrm{SE}_5 = \frac{\mathrm{CY} \setminus \{0\}}{\mathbb{R}^+} \,. \tag{4.17}$$

Note in passing that we can always find a $U(1)_{\mathrm{R}}$ isometry on such a CY cone generated by the following Killing *Reeb vector*:

$$\xi = I \left(r \frac{\partial}{\partial r} \right) \,. \tag{4.18}$$

In the original version of the gauge/gravity correspondence presented in Section 3.2, before considering their backreaction, D3-branes are placed on flat space. More precisely, the stack is localized at a point in $\mathbb{R}^6 \cong \mathbb{C}^3$, which is the simplest instance of non-compact CY threefold. The metric for their transverse coordinates can thus be written as

$$\mathrm{d}s^2_{\mathbb{R}^6} = \mathrm{d}r^2 + r^2 \mathrm{d}\Omega^2_5 \,, \tag{4.19}$$

where $\mathrm{d}\Omega^2_5$ is the metric for the 5-sphere S^5, which is, in turn, the simplest instance of five-dimensional Sasaki-Einstein manifold. This metric is of the same form as Equation (4.14), even though the latter is typically singular at the origin. In the case of the AdS/CFT correspondence, the backreaction of the branes onto the geometry led to a 10-dimensional space $AdS_5 \times S^5$ with a F_5-flux on the S^5. For a conical singularity, we thus expect to find a correspondence between a gauge theory and a supergravity solution $AdS_5 \times \mathrm{SE}_5$ with a F_5-flux on the Sasaki-Einstein manifold. Naturally, the non-compact CY has infinite volume and will thus admit any amount of D3-branes, and in particular, a large N limit, since their RR fluxes can escape all the way to infinity.

The number of preserved supercharges on SE_5 is given by the dimension of the space of Killing spinors on the manifold. A theorem [119, 128] establishes an isomorphism between the spaces of covariantly constant spinors on the cone $C(\mathrm{SE}_5)$ and SE_5 itself. Since the cone is CY, we know that we will have well-defined supercharges in $AdS_5 \times \mathrm{SE}_5$.

Given a CY cone, it is not easy to find the corresponding and explicit form of the metric in Equation (4.14). Nevertheless, they were found for infinite families of singularities denoted by $Y^{p,q}$ and then enlarged to $L^{a,b,c}$ [28, 31]. In the present work, we will be essentially focused on the gauge theory side of the correspondence and will comment on particular metrics only in some instances.

4.2 Toric varieties

4.2.1 Fans and cones

To introduce the subject of toric geometry, we start with a familiar construction of a compact space that is a particular instance of toric variety, the complex projective plane $\mathbb{CP}^2$. It is built from an ambient space $\mathbb{C}^3\backslash\{0\}$ with an equivalence relation on the three *homogeneous coordinates* (z_1, z_2, z_3) given by

$$(z_1, z_2, z_3) \sim (\lambda z_1, \lambda z_2, \lambda z_3) \quad \forall \lambda \in \mathbb{C}^* \,. \tag{4.20}$$

This definition can be summarized by

$$\mathbb{CP}^2 = \frac{\mathbb{C}^3\backslash\{0\}}{\mathbb{C}^*} \,. \tag{4.21}$$

We can introduce different sets of two local coordinates to describe $\mathbb{CP}^2$ on some patches. Take for instance the patch defined by $z_3 \neq 0$, we can use the following coordinates:

$$\zeta_1 = \frac{z_1}{z_3} \,, \quad \zeta_2 = \frac{z_2}{z_3} \,. \tag{4.22}$$

Similarly, we can define coordinates for the patches $z_1 \neq 0$ and $z_2 \neq 0$. Altogether, these three patches cover the whole complex manifold and this leads us to the observation that $\mathbb{CP}^2$ has a dense open subset isomorphic to the algebraic torus $(\mathbb{C}^*)^2$.[2] Note also that $(\mathbb{C}^*)^2$ acts freely on the manifold

[2] We call any algebraic group that is a product of $\mathbb{C}^*$ an algebraic torus by analogy with the abelian "torus" action $U(1)$ in Lie group theory. Indeed, acting with $\mathbb{C}^*$ can be seen as a complex generalization of acting with a $U(1)$ phase.

by multiplication on the coordinates, minus some points. This is at the origin of a $U(1)^2$ isometry in the complex manifold. This fact is important because it applies to all toric varieties.

In general, a toric variety $\mathcal{X}_\Delta$ is an algebraic variety of complex dimension n containing an algebraic torus $(\mathbb{C}^*)^n$ as a dense open subset, and such that the torus action on itself extends to an algebraic action on $\mathcal{X}_\Delta$. This n-dimensional variety is obtained as the quotient of a complex plane of higher dimension $m \geqslant n$:

$$\mathcal{X}_\Delta = \frac{\mathbb{C}^m \backslash Z_\Delta}{(\mathbb{C}^*)^{m-n} \times \Gamma}\,, \tag{4.23}$$

where $Z_\Delta \subset \mathbb{C}^m$ is a suitably chosen set of points and Γ is a finite discrete group. The name *toric variety* comes from the presence of the algebraic torus action. In our case of interest where the toric variety has $n = 3$ complex dimensions, it will always enjoy a $U(1)^3$ isometry.

One can construct toric varieties by implementing their data combinatorially into fans and cones. Consider a set of m given integer vectors $\mathbf{n}_i$, $i = 1, \cdots, m$, in a n-dimensional lattice $N \cong \mathbb{Z}^n$. We introduce a (strictly convex rational polyhedral) cone $\sigma \subset N_\mathbb{R}$, where $N_\mathbb{R} \cong \mathbb{R} \otimes N$, generated by the vectors $\mathbf{n}_i$:

$$\sigma = \Big\{ \sum_{i=1}^{m} a_i \mathbf{n}_i \in N_\mathbb{R} \,|\, a_i \in \mathbb{R}_{\geqslant 0},\, \mathbf{n}_i \in N \Big\}\,, \tag{4.24}$$

and such that it satisfies the strong convexity condition:

$$\sigma \cap (-\sigma) = \{0\}\,. \tag{4.25}$$

We define a face of a cone as the intersection of the cone with a supporting hyperplane. Then, a fan is a collection of cones in $N_\mathbb{R}$ such that each face of a cone is a cone, and each intersection of two cones is a face of a cone. See the fan of $\mathbb{CP}^2$ in Figure 4.1 for an illustration.

Given a fan, the toric variety is then constructed as follows:

- For each $\mathbf{n}_i$ we introduce a new coordinate z_i, so that we collect the set of coordinates of $\mathbb{C}^m$.
- Each of the $m - n$ actions $\mathbb{C}^*$ labelled by A is defined by a set of m numbers $(Q_1^A, \cdots, Q_m^A)$:

$$\mathbb{C}_A^* : \mathbb{C}^m \to \mathbb{C}^m : (z_1, \cdots, z_m) \mapsto (\lambda^{Q_1^A} z_1, \cdots, \lambda^{Q_m^A} z_m) \quad \forall \lambda \in \mathbb{C}^*\,, \tag{4.26}$$

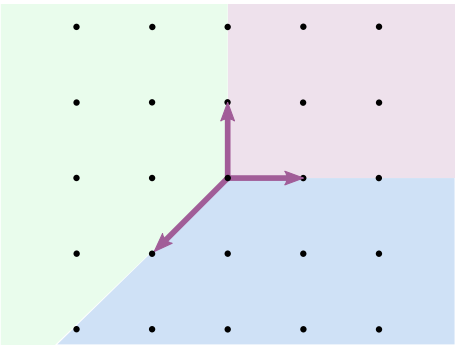

Figure 4.1: Fan of $\mathbb{CP}^2$ with its three two-dimensional cones (bounded by the vectors), three one-dimensional cones (along the vectors) and a zero-dimensional cone (the point at the origin).

and are found to satisfy

$$\sum_{i=1}^{m} Q_i^A \mathbf{n}_i^k = 0\,, \quad \forall A = 1, \cdots, m-n \quad \forall k = 1, \cdots, n. \tag{4.27}$$

- If the vectors $\mathbf{n}_i$ generate only a sublattice lattice $N' \subset N$, then the discrete group is
$$\Gamma = N/N'\,. \tag{4.28}$$
- For each subset $\{\mathbf{n}_{i_1}, \cdots, \mathbf{n}_{i_l}\}$ that does not generate a cone, we define
$$V_l = \{z_{i_1} = \cdots = z_{i_l} = 0\}\,, \tag{4.29}$$
such that
$$Z_\Delta = \bigcup_l V_l\,. \tag{4.30}$$

We will now familiarize ourselves with this procedure by considering two examples, $\mathbb{CP}_2$ and the orbifold $\mathbb{C}^2/\mathbb{Z}_2$.

Example of $\mathbb{CP}_2$

In the case of $\mathbb{CP}_2$, we have obtained from Figure 4.1 that

$$\mathbf{n}_1 = (1,0)\,, \quad \mathbf{n}_2 = (0,1)\,, \quad \mathbf{n}_3 = (-1,-1)\,. \tag{4.31}$$

This sets a relation,

$$\mathbf{n}_1 + \mathbf{n}_2 + \mathbf{n}_3 = 0\,, \tag{4.32}$$

such that we find one action $\mathbb{C}^*$ with

$$(Q_1, Q_2, Q_3) = (1, 1, 1)\,, \tag{4.33}$$

and hence reproduces Equation (4.20). It is easy to see that $\langle \mathbf{n}_1, \mathbf{n}_2, \mathbf{n}_3 \rangle$ is not a cone since it does not satisfy the strong convexity condition, see Equation (4.25). Therefore, one finds

$$Z_{\mathbb{CP}^2} = \{z_1 = z_2 = z_3 = 0\} = \{0\}\,. \tag{4.34}$$

Example of the orbifold $\mathbb{C}^2/\mathbb{Z}_2$, part I

The fan is generated by

$$\mathbf{n}_1 = (1, -1)\,, \quad \mathbf{n}_2 = (1, 1)\,, \tag{4.35}$$

see Figure 4.2 for an illustration. There is no relation between $\mathbf{n}_1$ and $\mathbf{n}_2$. Thus, there is no $\mathbb{C}^*$ action that will quotient $\mathbb{C}^2$. However, the lattice N' covers only half of N and thus $\Gamma = \mathbb{Z}_2$. One can extract the precise finite action on homogeneous coordinates in the following way.

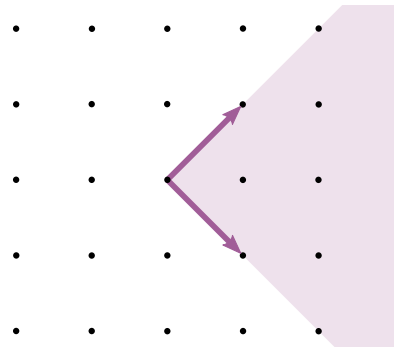

Figure 4.2: Fan of $\mathbb{C}^2/\mathbb{Z}_2$.

Start with N' the fan of $\mathbb{C}^2$, illustrated in Figure 4.3a, which is made of a single two-dimensional cone together with its faces. Its one-dimensional cones coincide with the generators of its two-dimensional cones:

$$\mathbf{n}'_1 = \mathbf{e}'_1 = (1, 0)\,, \quad \mathbf{n}'_2 = \mathbf{e}'_2 = (0, 1)\,. \tag{4.36}$$

Now, we introduce the following relation to define the lattice N in terms of N':

$$N = N' + (1/2, 1/2)\mathbb{Z}\,. \tag{4.37}$$

In terms of the generators of N', N is generated by

$$\mathbf{e}_1 = \frac{1}{2}(\mathbf{e}'_1 - \mathbf{e}'_2)\,, \quad \mathbf{e}_2 = \frac{1}{2}(\mathbf{e}'_1 + \mathbf{e}'_2)\,. \tag{4.38}$$

In this new base, we find that the vectors $\mathbf{n}'_1$ and $\mathbf{n}'_2$ have the same coefficients as the vectors presented in Equation (4.35):

$$\mathbf{n}'_1 = \mathbf{e}_1 - \mathbf{e}_2\,, \quad \mathbf{n}'_2 = \mathbf{e}_1 + \mathbf{e}_2\,, \tag{4.39}$$

so that they are actually the same vectors. We thus understand how to construct the fan of $\mathbb{C}^2/\mathbb{Z}_2$ out of $\mathbb{C}^2$. Notice that Figure 4.2 and Figure 4.3b are the same fan. Since N' and $N' + (1,1)\mathbb{Z}$ are the same lattices, we find that Equation (4.37) indeed implies

$$N/N' = \mathbb{Z}_2\,. \tag{4.40}$$

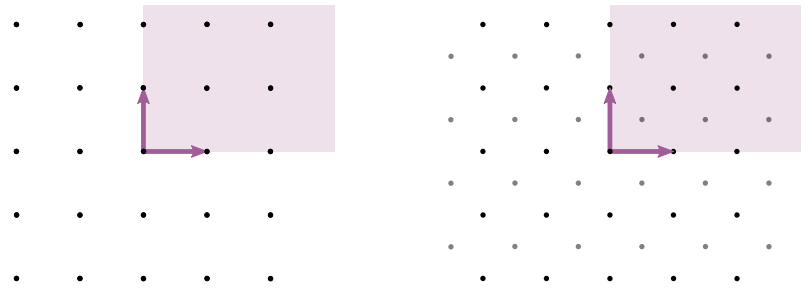

(a) (b)

Figure 4.3: (a) Fan of $\mathbb{C}^2$, named N'. (b) Fan N obtained by adding $(1/2, 1/2)\mathbb{Z}$, in grey in the picture, to N'.

One can also read how $\mathbb{Z}_2$ acts on the homogeneous coordinates. Start with N' the fan of $\mathbb{C}^2$ and introduce as usual the coordinates z_1 and z_2 for $\mathbf{n}'_1$ and for $\mathbf{n}'_2$ respectively. The prefactors of $\mathbb{Z}$ in Equation (4.37) appear as powers of $e^{i2\pi}$ when multiplying the coordinates:

$$\mathbb{Z}_2 \quad : \quad (z_1, z_2) \to (e^{\frac{1}{2}i2\pi} z_1, e^{\frac{1}{2}i2\pi} z_2) = (-z_1, -z_2)\,. \tag{4.41}$$

Finally, since the union of the two one-dimensional cones is itself a cone, one finds an empty Z_Δ. The singular space is thus $\mathbb{C}^2/\mathbb{Z}_2$, as expected.

4.2.2 The Calabi-Yau and non-compactness conditions

To each $\mathbf{n}_i$ we associated a homogeneous coordinate z_i. It can be understood that each $\mathbf{n}_i$ corresponds to a toric divisor

$$D_i = \{z_i = 0\} \cap \mathcal{X}_\Delta \,. \tag{4.42}$$

A divisor is in general a codimension one (in complex dimension) subvariety. Then, to any formal sum of toric divisors $\sum_i a_i D_i$, we can associate a line bundle $\mathcal{O}(\sum_i a_i D_i)$ whose sections are generated by the monomials of the form

$$z_1^{a_1} \cdots z_n^{a_n} \,, \tag{4.43}$$

such that they vanish on D_i with a zero to the power of a_i, or they have a pole of order $-a_i$. For this monomial, we have a transformation under the algebraic torus given by

$$\mathbb{C}_A^* : z_1^{a_1} \cdots z_n^{a_m} \mapsto \lambda^{Q_1^A a_1} z_1^{a_1} \cdots \lambda^{Q_m^A a_m} z_m^{a_m} = \lambda^{\sum_i^m Q_i^A a_i} z_1^{a_1} \cdots z_m^{a_m} \,. \tag{4.44}$$

The power of λ vanishes if we consider $a_i = \mathbf{m} \cdot \mathbf{n}_i$, for some element of the dual lattice $\mathbf{m} \in M = \mathrm{Hom}(N, \mathbb{Z})$. In this case, the monomial is a globally defined meromorphic function on the toric variety and $\mathcal{O}(\sum_i \mathbf{m} \cdot \mathbf{n}_i \, D_i)$ is a trivial line bundle, which can be noted as

$$\sum_i \mathbf{m} \cdot \mathbf{n}_i \, D_i \sim 0 \,. \tag{4.45}$$

The converse relation holds. If

$$\sum_i a_i \, D_i \sim 0 \,, \tag{4.46}$$

then we can find $\mathbf{m} \in M$ such that $a_i = \mathbf{m} \cdot \mathbf{n}_i$ for any i.

It can be shown for toric varieties that the canonical bundle K_Δ is equal to $\mathcal{O}(-\sum_i D_i)$, so that K_Δ is trivial if and only if

$$\sum_i D_i \sim 0 \,, \tag{4.47}$$

which means in particular that the toric variety is CY if and only if there exists an $\mathbf{m} \in M$ such that

$$\mathbf{m} \cdot \mathbf{n}_i = 1 \quad \forall i = 1, \cdots, m \,. \tag{4.48}$$

In other words, all $\mathbf{n}_i$ lie in the same hyperplane of the lattice N. In particular, since the fan Δ for a toric variety with three complex dimensions is

defined in a three-dimensional lattice N, a toric CY threefold can always be drawn as a convex polygon in a two-dimensional lattice. The latter is the common hyperplane where the $\mathbf{n}_i$ end, and the convex polygon is the convex hull of their endpoints. It is usually convenient to perform a $SL(3,\mathbb{Z})$ transformation to bring all vectors $\mathbf{n}_i$ to the following form:

$$\mathbf{n}_i = (a_i, b_i, 1)\,, \tag{4.49}$$

where the pairs (a_i, b_i) specify the position of the extremal points of the convex polygon. We will call this convex polygon the *toric diagram* and will occasionally refer to it as Δ. Note that there is a leftover $SL(2,\mathbb{Z})$ that one can use to redefine the couples (a_i, b_i).

The CY condition in Equation (4.48) can be rephrased in terms of the charges for the torus actions:

$$\sum_{i=1}^{m} Q_i^A = 0 \quad \forall A\,. \tag{4.50}$$

Similarly, the charges of the discrete group Γ sum to zero modulo one since they appear as arguments in the complex exponential.

Another proposition that we will not develop is that the fan of a compact toric variety spans the whole lattice N. It can be checked in the simple examples of Figure 4.1 and Figure 4.2.

The example of flat space $\mathbb{C}^3$

The fan of $\mathbb{C}^3$ is defined by the three vectors

$$\mathbf{n}_1 = (1,0,0)\,, \quad \mathbf{n}_2 = (0,1,0)\,, \quad \mathbf{n}_3 = (0,0,1)\,, \tag{4.51}$$

so that we indeed find three coordinates z_1, z_2 and z_3 without any action on it. We can find $\mathbf{m} = (1,1,1)$ such that Equation (4.48) is satisfied, as expected. The latter vector identifies the sublattice of the hyperplane.

A $SL(3,\mathbb{Z})$ transformation sends the vectors of Equation (4.51) into the new set,

$$\mathbf{n}_1 = (1,0,1)\,, \quad \mathbf{n}_2 = (0,1,1)\,, \quad \mathbf{n}_3 = (0,0,1)\,, \tag{4.52}$$

see Figure 4.4a, and so we can draw the toric diagram for $\mathbb{C}^3$, illustrated in Figure 4.4b.

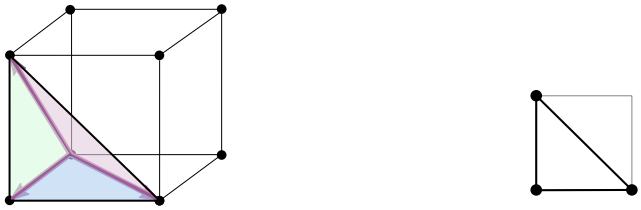

(a) (b)

Figure 4.4: Flat space $\mathbb{C}^3$: (a) Fan. (b) Toric diagram.

The example of the orbifold $\mathbb{C}^2/\mathbb{Z}_2$, part II

If instead of the fan of Figure 4.2, one starts instead with the fan in Figure 4.5a, with vectors given by

$$\mathbf{n}_1 = (1,1,0)\,, \quad \mathbf{n}_2 = (1,-1,0)\,, \quad \mathbf{n}_3 = (1,0,1)\,, \tag{4.53}$$

the resulting singularity is $\mathbb{C}^2/\mathbb{Z}_2 \times \mathbb{C}$. This is the actual singular space that we will use for compactification when mentioning $\mathbb{C}^2/\mathbb{Z}_2$. The complete action of the discrete group on $\mathbb{C}^3$ is

$$\mathbb{Z}_2 \quad : \quad (z_1, z_2, z_3) \to (-z_1, -z_2, +z_3)\,. \tag{4.54}$$

A $SL(3,\mathbb{Z})$ permutation of the coordinates in Equation (4.53) sends the vectors into the new set:

$$\mathbf{n}_1 = (1,0,1)\,, \quad \mathbf{n}_2 = (-1,0,1)\,, \quad \mathbf{n}_3 = (0,1,1)\,, \tag{4.55}$$

and so we can draw the toric diagram for $\mathbb{C}^3$, illustrated in Figure 4.5b.

4.2.3 Dual cones and ring of coordinates

We can define local coordinates as monomials x invariant under the overall action $\mathbb{C}^{*m-n} \times \Gamma$. It is not difficult to show that for

$$x = z_1^{p_1} \cdots z_m^{p_m} \tag{4.56}$$

to be invariant, we need the p_i to satisfy

$$\sum_{i=1}^{m} Q_i^A p_i = 0\,, \tag{4.57}$$

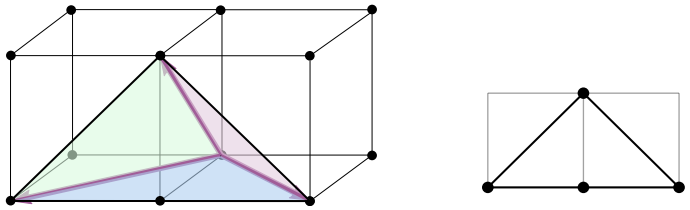

(a) (b)

Figure 4.5: Orbifold of flat space $\mathbb{C}^2/\mathbb{Z}_2 \times \mathbb{C}$: (a) Fan. (b) Toric diagram.

and a similar relation for the charges of the discrete action Γ. It implies in turn that

$$p_i = \mathbf{m} \cdot \mathbf{n}_i \,, \quad \forall \mathbf{m} \in M = \mathrm{Hom}(N, \mathbb{Z}) \,. \tag{4.58}$$

The introduction of the lattice $M \cong \mathbb{Z}^n$ suggests to define the dual cone:

$$\sigma^\vee = \left\{ a\mathbf{m} \in M_{\mathbb{R}} \,|\, a \in \mathbb{R}_{>0},\, \mathbf{m} \cdot \mathbf{n}_i \geqslant 0 \quad \forall \mathbf{n}_i \in \sigma \right\} . \tag{4.59}$$

To find all the possible coordinates as in Equation (4.56), we need to find the generators of the integer cone $\sigma^\vee \cap M$ which typically has more generators than $\sigma^\vee$ alone. The ring of coordinate is then defined by

$$\mathbb{C}[\sigma^\vee \cap M] \,, \tag{4.60}$$

in the sense that each generator $\mathbf{m}_i$ of $\sigma^\vee \cap M$ is in one-to-one correspondence with a complex coordinate x_i. Finally, the equations defining our singularity are given by associating the linear relations between the $\mathbf{m}_i$ to algebraic equations P for the x_i. For example,

$$\mathbf{m}_1 + \mathbf{m}_2 = \mathbf{m}_3 + \mathbf{m}_4 \quad \rightarrow \quad P(x_1, x_2, x_3, x_4) \equiv x_1 x_2 - x_3 x_4 = 0 \,. \tag{4.61}$$

Assume that we end up with r coordinates x_i and a collection of $l < r$ algebraic equations P_k, this sets a new identity for the ring of coordinates:

$$\mathbb{C}[\sigma^\vee \cap M] = \frac{\mathbb{C}[x_1, \cdots, x_r]}{\langle P_1, \cdots, P_l \rangle} \,. \tag{4.62}$$

For toric CY threefolds, we can use these to compute the holomorphic 3-form Ω_3 using the Poincaré residue formula:

$$\Omega_3 = \mathrm{Res} \frac{\mathrm{d}x_1 \wedge \cdots \wedge \mathrm{d}x_r}{P_1 \cdots P_{r-3}} \,. \tag{4.63}$$

We show below how to compute the ring of coordinates and the holomorphic 3-form for specific examples.

Example of the orbifold $\mathbb{C}^2/\mathbb{Z}_2$, part III

The dual cone of the fan in Figure 4.5a is generated by

$$\mathbf{m}_1 = (-1, 0, 1)\,, \quad \mathbf{m}_2 = (1, 0, 1)\,, \quad \mathbf{m}_3 = (0, -1, 1)\,. \tag{4.64}$$

They will correspond to local coordinates x, y and z. In order to generate the full integer dual cone $\sigma^\vee \cap M$, one needs to introduce an extra generator:

$$\mathbf{m}_4 = (0, 0, 1)\,, \tag{4.65}$$

which will correspond to the coordinate w. This gives the relation

$$\mathbf{m}_1 + \mathbf{m}_2 = 2\,\mathbf{m}_4\,, \tag{4.66}$$

and so, in terms on local coordinates:

$$xy = w^2\,. \tag{4.67}$$

This is in agreement with the definition of this orbifold space. If one takes (z_1, z_2, z_3) as coordinates of $\mathbb{C}^3$, with the action $\mathbb{Z}_2$ action determined before in Equation (4.41), then one can build invariant coordinates:

$$x = z_1^2\,, \quad y = z_2^2\,, \quad w = z_1 z_2\,, \quad z = z_3\,, \tag{4.68}$$

and recover Equation (4.67). We can also use its defining equation to check that the variety is singular at $x = y = w = 0$ for any z:

$$f(x, y, w, z) \equiv xy - w^2 = 0\,, \quad \mathrm{d}f_{|x=y=w=0} = 0\,. \tag{4.69}$$

Finally, we can compute the holomorphic 3-form for this space. Let be

$$\begin{aligned} \Omega_3 &= \mathrm{Res}\frac{\mathrm{d}x \wedge \mathrm{d}y \wedge \mathrm{d}z \wedge \mathrm{d}w}{xy - w^2} \\ &= \frac{1}{2\pi i}\oint_{xy-w^2=0} \frac{\mathrm{d}x \wedge \mathrm{d}y \wedge \mathrm{d}z \wedge \mathrm{d}w}{xy - w^2} \\ &= \frac{\mathrm{d}x \wedge \mathrm{d}y \wedge \mathrm{d}z}{2w}\,, \end{aligned} \tag{4.70}$$

where w is now a function of x and y.

Example of the conifold $\mathcal{C}$

The fan for the conifold $\mathcal{C}$ is generated by

$$\mathbf{n}_1 = (0, 0, 1)\,, \quad \mathbf{n}_2 = (1, 0, 1)\,, \quad \mathbf{n}_3 = (1, 1, 1)\,, \quad \mathbf{n}_4 = (0, 1, 1)\,, \tag{4.71}$$

see Figure 4.6a. We find the relation

$$\mathbf{n}_1 - \mathbf{n}_2 + \mathbf{n}_3 - \mathbf{n}_4 = 0\,, \tag{4.72}$$

such that we have one $\mathbb{C}^*$ action with

$$Q = (+1, -1, +1, -1)\,. \tag{4.73}$$

The full lattice is generated by the $\mathbf{n}_i$ such that Γ is trivial. Z_Δ is not empty since $\langle \mathbf{n}_1, \mathbf{n}_3 \rangle$ and $\langle \mathbf{n}_2, \mathbf{n}_4 \rangle$ are not cones of the fan. We thus find

$$\mathcal{C} = \frac{\mathbb{C}^4 \backslash \{z_1 = z_3 = 0\} \cup \{z_2 = z_4 = 0\}}{\mathbb{C}^*}\,. \tag{4.74}$$

Starting with the toric diagram in Figure 4.6b, we find the defining equations for the conifold. The dual cone is generated by

$$\mathbf{m}_1 = (1, 0, 0)\,, \quad \mathbf{m}_2 = (0, 1, 0)\,, \quad \mathbf{m}_3 = (-1, 0, 1)\,, \quad \mathbf{m}_4 = (0, -1, 1)\,. \tag{4.75}$$

Together, they generate the full integer dual cone $\sigma^\vee \cap M$ and we do not need to introduce extra generators. Moreover, they are linked by the relation:

$$\mathbf{m}_1 + \mathbf{m}_3 = \mathbf{m}_2 + \mathbf{m}_4\,, \tag{4.76}$$

and so, in terms on four local coordinates:

$$xy = uv\,. \tag{4.77}$$

It can be checked to be singular at the origin. We can also compute the holomorphic 3-form for this space. Let be

$$\begin{aligned} \Omega_3 &= \mathrm{Res} \frac{\mathrm{d}x \wedge \mathrm{d}y \wedge \mathrm{d}u \wedge \mathrm{d}v}{xy - uv} \\ &= \frac{\mathrm{d}x \wedge \mathrm{d}y \wedge \mathrm{d}u}{u}\,. \end{aligned} \tag{4.78}$$

4.2.4 Cycles and (p, q)-web

It will be of particular importance for us to identify the different cycles in the base of the CY cone that shrink at the singularity. We briefly introduce some tools of toric geometry that are relevant in this context.

The integer dual cone of a toric CY threefold can be projected onto a two-dimensional plane in order to recover the (p, q)-web. This diagram

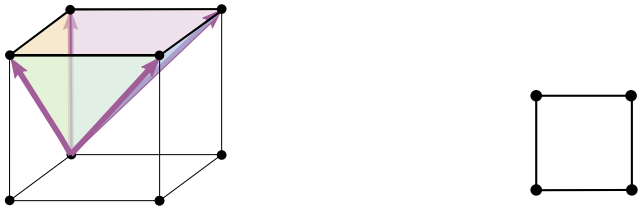

(a) (b)

Figure 4.6: The conifold $\mathcal{C}$: (a) Fan. (b) Toric diagram.

(a) (b)

Figure 4.7: The Hirzebruch surface F_0: (a) Triangulated toric diagram. (b) (p, q)-web.

is found to be dual to the toric diagram once triangulated, see Figure 4.7 for an example. (p, q) labels refer to the directions of external legs in the web. We will see in Chapter 6 how to connect this new diagram to webs of fivebranes.

The (p, q)-web delimitates the distinct regions of the dual cone for which the element $\mathbf{m}$ satisfies the strict equality

$$\mathbf{m} \cdot \mathbf{n}_i = 0\,, \tag{4.79}$$

for exactly one value of i. Now, we use the $U(1)^3$ isometry to think about the toric variety as a $\mathbb{T}^3$-fibration over the dual cone, and hence the (p, q)-web. Regions bounded by two external legs represent the four-dimensional toric divisors D_i mentioned earlier, where a one-cycle shrinks and $\mathbb{T}^3$ degenerates into a $\mathbb{T}^2$. External legs are the intersections of two toric divisors, and there $\mathbb{T}^3$ shrinks into a S^1. At the singularity, all external edges would meet, and the full $\mathbb{T}^3$ would degenerate, but this is not shown in the (p, q)-web of Figure 4.7b precisely because the singularity is resolved in this picture.

The triangulation of the toric diagram has a precise geometrical mean-

ing. It actually corresponds to a *small resolution* of the singular locus, where the latter is excised from the variety to be replaced by a certain number of smooth two-spheres $S^2 \cong \mathbb{CP}^1$. In general, there can be different ways to triangulate a toric diagram and hence different resolutions. See for instance that the conifold admits two distinct resolutions in Figure 4.8. The transition from one to the other is called a *flop*. The S^2 can be seen in the (p, q)-web as an intermediate segment linking two external legs. It corresponds to a two-cycle that is normally shrinking at the non-resolved singularity.

(a) (b)

Figure 4.8: Two small resolutions of the conifold.

Another way to do resolutions consists of *blowing up* the singularity in the variety of complex dimension n by inserting one or several $\mathbb{CP}^{n-1}$ at the singular locus.[3] This is done by adding extra divisors to the variety and hence new points in the toric diagram. In particular, when a toric diagram has internal points, compact four-cycles $\mathbb{CP}^2$ will be present where we expect to find the singularity. Those are shown in the (p, q)-web as finite areas surrounded by the intermediate segments, like in the center of Figure 4.7b.

Example of the orbifold $\mathbb{C}^2/\mathbb{Z}_2$, part IV

We study the blow-up resolution of the singular locus of the orbifold $\mathbb{C}^2/\mathbb{Z}_2$ in two complex dimensions. As prescribed above, we add an extra generator in the fan, see Figure 4.9. The fan is now composed of two two-dimensional cones, together with their respective faces.

Keeping the same conventions as before and introducing an extra coordinate z_4 corresponding to the new one-dimensional cone, it can be

[3]The terminology *blow-up* is sometimes used to refer to *small resolutions* too.

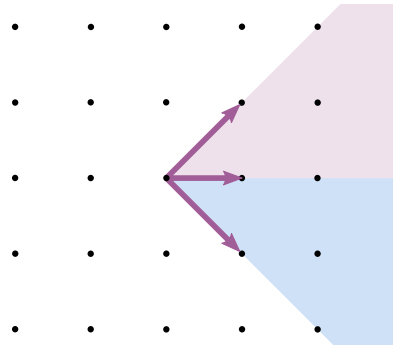

Figure 4.9: Blow-up of the $\mathbb{C}^2/\mathbb{Z}_2$ orbifold.

checked that this fan defines a variety parameterized by (z_1, z_2, z_4) in $\mathbb{C}^3\backslash\{z_1 = z_2 = 0\}$ and subject to the equivalence relation:

$$(z_1, z_2, z_4) \sim (\lambda z_1, \lambda z_2, \lambda^{-2} z_4)\,, \quad \forall \lambda \in \mathbb{C}^*\,. \tag{4.80}$$

At $z_4 \neq 0$, this freedom can be used to set $z_4 = 1$ and we find a residual equivalence relation:

$$(z_1, z_2, 1) \sim (\lambda z_1, \lambda z_2, 1)\,, \quad \text{for } \lambda^2 = 1\,, \tag{4.81}$$

which reproduces the geometry of the orbifold space away from the singular locus, since $(0, 0, z_4)$ is not part of the toric manifold. At $z_4 = 0$, we find

$$(z_1, z_2, 0) \sim (\lambda z_1, \lambda z_2, 0)\,, \quad \forall \lambda \in \mathbb{C}^*\,. \tag{4.82}$$

λ is not constrained anymore and the equivalence relation defines a $\mathbb{CP}^1 \cong S^2$ compact manifold.

From the point of view of the $\mathbb{C}^2/\mathbb{Z}_2 \times \mathbb{C}$ threefold, the extra generator corresponds to a point of the toric diagram placed on its perimeter and we find indeed that the $\mathbb{CP}^1$ is an intermediate segment in the (p, q)-web, see Figure 4.10.

del Pezzo surfaces

Blow-ups can also be used to reach new instances of CY cones. For example, we can add one-dimensional cones in the fan of $\mathbb{CP}^2$ and generate toric *del Pezzo* surfaces, noted dP_n when n one-dimensional cones are added in the fan (up to three). See the fan of dP_1 in Figure 4.11a. For our purpose of considering non-compact varieties with three complex dimensions, we will be interested in complex cones over del Pezzo surfaces which are obtained

(a) (b)

Figure 4.10: The orbifold of flat space $\mathbb{C}^2/\mathbb{Z}_2$: (a) Triangulated toric diagram. (b) (p, q)-web.

by extending the fan of the surface to a three-dimensional lattice. See the toric diagram for the complex cone over dP_1 in Figure 4.11b. We will also refer to complex cones over *pseudo del Pezzo* surfaces for toric varieties with non-isolated singularities that are obtained from additional blow-ups of $\mathbb{CP}^2$ and resemble non-toric del Pezzo surfaces [129].

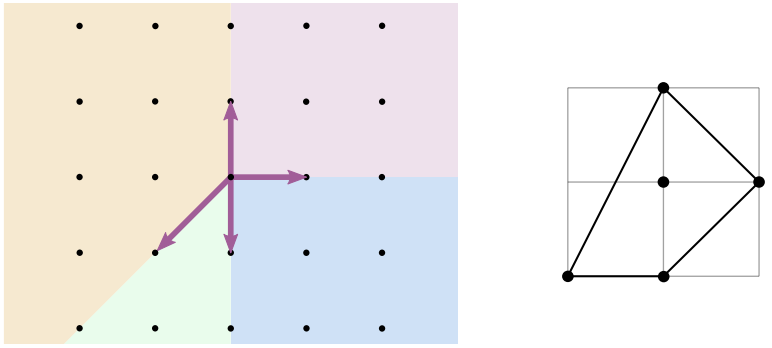

(a) (b)

Figure 4.11: dP_1 surface obtained as a blow-up of $\mathbb{CP}^1$ at one point. (a) Fan of the dP_1 surface. (b) Toric diagram of the complex cone over dP_1.

Chapter 5

Quivers and Fractional Branes

Branes at singularities have a rich history of developments in string theory. See [24–27, 30, 53, 119, 130–136] for some of the first investigations on the subject. In this section, we shall however focus on the simplest examples on the market: orbifolds of flat space and the conifold.

The orbifold $\mathbb{C}^2/\mathbb{Z}_2$ will guide us on a path to $\mathcal{N} = 2$ gauge dynamics. This geometry has the advantage to be easy to construct and we know a simple prescription to access the D-branes low energy gauge theory via world-sheet techniques. We present it in the hope of clarifying some ideas about quivers and fractional branes in general. We will not however present the dual supergravity solution $AdS_5 \times S^5/\mathbb{Z}_2$. See [137] and references therein for a more detailed description.

We will then move on to the conifold. Although being one of the simplest examples of toric CY geometry, it leads to a very rich $\mathcal{N} = 1$ dynamics. We will explore the SCFT that one obtains as the dual gauge theory, the Klebanov-Witten model, and then describe a kind of fractional branes that trigger a cascading RG-flow: the deformation branes. We will review both the gauge theory and the supergravity dual in this case. See [138] for more details on this subject.

Finally, we will discuss some geometrical features of fractional branes [139] and their intimate relation to anomalies [134, 140, 141] when arising on toric CY singularities. This will hopefully enlighten some of the general features of $\mathcal{N} = 1$ gauge theories that one can obtain by applying the gauge/gravity duality into the context of toric geometry.

5.1 Orbifolds of flat space

5.1.1 A first encounter with quivers

Consider placing a stack of N D3-branes at a generic point of the orbifold space $\mathbb{C}^2/\mathbb{Z}_2 \times \mathbb{C}$. If one thinks about this configuration in the universal cover of the space, it is like looking at two identical stacks of branes placed in $\mathbb{C}^3$ symmetrically with respect to the origin in $\mathbb{C}^2$, where is the singular locus of the orbifold space. Open strings can link a stack to itself or its mirror. However, only the first kind of strings will produce massless modes due to the distance separating the two stacks. The low energy spectrum for a given stack is thus simply the usual four-dimensional $U(N)$ gauge theory with three adjoints, as in flat space. Mathematically speaking, the sets of D3-branes are mapped into each other by the regular representation $\mathcal{R}$ of the discrete group.

Now, we change this situation by moving the stacks towards the origin. We expect to find new massless modes since the distance between the two mirror stacks is vanishing. In fact, the whole low energy gauge theory can a priori be changed and will be constrained by one principle: its spectrum has to be invariant under the orbifold action since the stack is placed on its fixed point. We now show how to simply derive it using worldsheet techniques. Recall first that the massless bosonic states coming from the open strings sector are given by the following quantum states in the NS sector:

$$\lambda \otimes \psi^M_{-1/2} \left|k\right\rangle \ . \tag{5.1}$$

We start with a $2N \times 2N$ Chan-Paton matrix λ, for the two stacks of N D-branes, and ask for the states that are invariant under the orbifold action. First, we need to define the action on Chan-Paton matrix with a matrix γ_g that satisfies the group law of $\mathbb{Z}_2$:

$$\mathbb{Z}_2 \quad : \quad \lambda \to \gamma_g \lambda \gamma_g^{-1} \,, \tag{5.2}$$

such that

$$\gamma_g^2 = \gamma_{g^2} = \gamma_{\rm id} = \mathbb{1}_{2N\times 2N} \,. \tag{5.3}$$

It will be convenient for a latter purpose to diagonalize the regular action of $\mathbb{Z}_2$:

$$\gamma_g = \begin{pmatrix} \mathbb{1}_{N\times N} & 0 \\ 0 & -\mathbb{1}_{N\times N} \end{pmatrix} . \tag{5.4}$$

This action has to accompanied by the orbifold spatial action on $\psi^M_{-1/2}$. This is because the orbifold acts on spatial coordinates x^M, and so acts

equivalently on the worldsheet fields X^M. Supersymmetry then imposes the same action on ψ^M components. In the present case, the action on the complex coordinates of $\mathbb{C}^3 \cong \mathbb{R}^6$ is

$$\mathbb{Z}_2 \quad : \quad (z_1, z_2, z_3) \to (-z_1, -z_2, +z_3)\,. \tag{5.5}$$

For a general orbifold, always acting on the coordinates transverse to the D3-branes, we can introduce a general matrix S related to the spatial action:

$$\text{Orbifold} \quad : \quad \psi^i_{-1/2} \to S^i_j\, \psi^j_{-1/2}\,, \tag{5.6}$$

where $i, j = 1, 2, 3$. For the specific orbifold $\mathbb{C}^2/\mathbb{Z}_2 \times \mathbb{C}$, we thus have

$$S = \begin{pmatrix} -1 & 0 & 0 \\ 0 & -1 & 0 \\ 0 & 0 & 1 \end{pmatrix}. \tag{5.7}$$

Massless states from the open strings sector living at the tip of the orbifold will thus be constrained by

$$A^\mu = \gamma_g A^\mu \gamma_g^{-1}\,, \quad \Phi^1 = -\gamma_g \Phi^1 \gamma_g^{-1}\,, \quad \Phi^2 = -\gamma_g \Phi^2 \gamma_g^{-1}\,, \quad \Phi^3 = \gamma_g \Phi^3 \gamma_g^{-1}\,. \tag{5.8}$$

The resulting spectrum is then given by

$$\begin{aligned} A^\mu &= \begin{pmatrix} A_1^\mu & 0 \\ 0 & A_2^\mu \end{pmatrix}, \quad \Phi^1 = \begin{pmatrix} 0 & X_{12} \\ X_{21} & 0 \end{pmatrix}, \\ \Phi^2 &= \begin{pmatrix} 0 & Y_{12} \\ Y_{21} & 0 \end{pmatrix}, \quad \Phi^3 = \begin{pmatrix} Z_{11} & 0 \\ 0 & Z_{22} \end{pmatrix}, \end{aligned} \tag{5.9}$$

where A_1^μ and A_2^μ are two gauge fields for two different gauge groups $SU(N)_1$ and $SU(N)_2$. The two $U(1)$ parts of the gauge groups are discarded because one is related to the center of mass of the D-branes and decouples in the infrared, the other is also infrared-free and becomes a global baryonic symmetry $U(1)_B$ at low energy. The other fields are defined in a bifundamental or adjoint representation and imply that the theory is non-chiral:

$$X_{12}, Y_{12} \in (\overline{\square}_1, \square_2)\,, \quad X_{21}, Y_{21} \in (\overline{\square}_2, \square_1)\,, \quad Z_{11} \in \text{Adj}_1 \quad \text{and} \quad Z_{22} \in \text{Adj}_2\,. \tag{5.10}$$

We can recover the superpotential easily starting with the one for D3-branes in flat space,

$$W = \Phi^1[\Phi^2, \Phi^3]\,, \tag{5.11}$$

and simply plugging in the expressions found in Equation (5.9). We thus find

$$W = X_{12}Y_{21}Z_{11} + X_{21}Y_{12}Z_{22} - X_{12}Z_{22}Y_{21} - X_{21}Z_{11}Y_{12}\,. \tag{5.12}$$

Each of the gauge group is a $SU(N)$ $\mathcal{N}=2$ theory with $2N$ flavors. See for instance that for $SU(N)_1$ we can group the $\mathcal{N}=1$ multiplets into one $\mathcal{N}=2$ real multiplet and two hypermultiplets (where we refrain to show the fermions):

$$V_{\mathcal{N}=2} = A_1^\mu \oplus Z_{11}\,, \quad H^1_{\mathcal{N}=2} = X_{12} \oplus Y_{21}\,, \quad H^2_{\mathcal{N}=2} = Y_{12} \oplus X_{21}\,. \tag{5.13}$$

The same can be done for $SU(N)_2$. Finally, the β functions vanish and the model is thus superconformal with $\mathcal{N}=2$ supersymmetries.

This computation is easy to carry on for any kind of orbifold of flat space $\mathbb{C}^3/\mathbb{Z}_n$ or $\mathbb{C}^3/\mathbb{Z}_p \times \mathbb{Z}_q$.[1] See for instance that for an orbifold with a $\mathbb{Z}_n$ action defined by

$$(z_1, z_2, z_3) \to (e^{i2\pi\frac{a}{n}} z_1, e^{i2\pi\frac{b}{n}} z_2, e^{i2\pi\frac{c}{n}} z_3)\,, \tag{5.14}$$

with the CY condition:

$$a + b + c = 0 \bmod n\,, \tag{5.15}$$

one just has to consider

$$\gamma_g = \begin{pmatrix} \mathbb{1}_{N\times N} & 0 & \cdots & 0 \\ 0 & e^{i2\pi\frac{1}{n}}\mathbb{1}_{N\times N} & \cdots & 0 \\ & & & \\ 0 & 0 & \cdots & e^{i2\pi\frac{n-1}{n}}\mathbb{1}_{N\times N} \end{pmatrix}, \qquad S = \begin{pmatrix} e^{i2\pi\frac{a}{n}} & 0 & 0 \\ 0 & e^{i2\pi\frac{b}{n}} & 0 \\ 0 & 0 & e^{i2\pi\frac{c}{n}} \end{pmatrix}, \tag{5.16}$$

and run the same machinery as before.

Of course, the same construction does not hold so easily for any generic toric singularity. However, the outcome for the massless spectrum is quite illustrative of what can happen in general. For instance, the presence of singularity will always enlarge the number of gauge factors in the whole

[1] The discrete groups in the orbifold quotients are chosen to be subgroups of $SU(3)$, as a necessary condition for the orbifold to be CY.

gauge symmetry group. And since open strings will always link a stack of branes to itself or to another one, we can always expect to find fields defined in an adjoint or bifundamental representation respectively. These limited possibilities are a good motivation to describe the low energy theories of these stacks of branes at singularities in terms of *quivers*.

Quivers are oriented graphs where the nodes are the different SU gauge groups and arrows represent matter fields: an arrow linking a gauge group i to the gauge group j is a bifundamental field $(\overline{\square}_i, \square_j)$ and an arrow joining a gauge group k to itself is defined in the adjoint Adj_k. We present the quiver for the orbifold $\mathbb{C}^2/\mathbb{Z}_2$ in Figure 5.1. Similarly, we can obtain the quiver for any $\mathbb{C}^2/\mathbb{Z}_n$, see Figure 5.2. Since $\mathbb{Z}_n$ is a subgroup of $SU(2)$, it can be noted that they are all $\mathcal{N} = 2$ quivers. Take also a moment to contemplate the correspondence between these quiver gauge theories and the extended A_{n-1} Dynkin diagrams, which is a manifestation of the McKay correspondence between discrete groups of $SU(2)$ and simple Lie groups falling into the ADE classification [142].

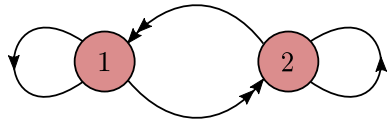

Figure 5.1: The quiver of the orbifold of flat space $\mathbb{C}^2/\mathbb{Z}_2$.

Unfortunately, the quiver as it is presented here misses a crucial piece of information: the superpotential of the theory. We will introduce in Chapter 6 a more appropriate tool that encodes the superpotential in addition to the usual quiver information.

5.1.2 $\mathcal{N} = 2$ fractional branes

If one looks for gauge groups with different rank assignments,[2] most quivers will still admit a certain number of non-anomalous solutions. This statement is trivial for non-chiral theories but applies for some chiral too. We will refer to these new solutions in general as *fractional D3-branes*,

[2] All over this work, we mention the *rank* of a gauge group where we should, strictly speaking, talk about the dimension of its fundamental representation.

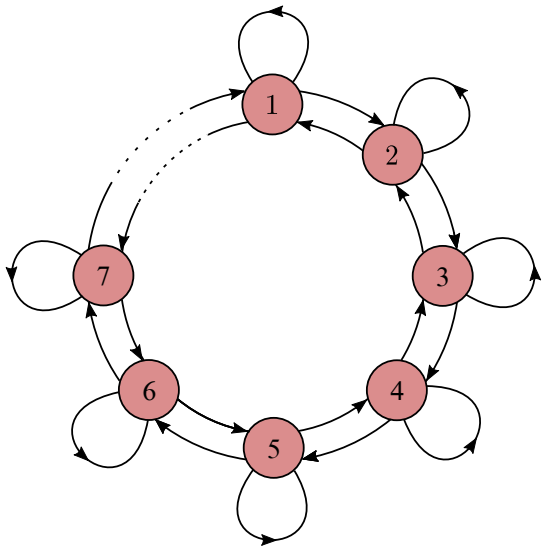

Figure 5.2: The quiver of the orbifold of flat space $\mathbb{C}^2/\mathbb{Z}_n$.

or *fractional branes* for short. The reason is that, contrarily to *regular branes*, which are configurations obtained as above (D3-branes that can be displaced to any point of the space), fractional branes are obtained by wrapping higher-dimensional D-branes on cycles that shrink at the singularity. In our orbifold example, $\mathbb{C}^2/\mathbb{Z}_2 \times \mathbb{C}$ has one non-trivial two-cycle that shrinks at the singularity and on which we can wrap D5-branes with two possible orientations, and hence opposite fluxes. Their tension forbids them to leave the singularity. The result is that they effectively look like D3-branes with fractional RR charges.

In the case of $\mathbb{C}^2/\mathbb{Z}_2$, the gauge theory point of view on fractional branes is that non-abelian anomalies are trivially satisfied for any N_1 and N_2 since the theory is non-chiral. We can consider turning off N_2 while keeping $N_1 = N$. The gauge theory of these N fractional branes is thus $SU(N)$ with an adjoint field Z_{11}. The theory is still $\mathcal{N} = 2$ but with only one $\mathcal{N} = 2$ vector multiplet:

$$V_{\mathcal{N}=2} = A_1^\mu \oplus Z_{11}\,. \tag{5.17}$$

For this reason, we call these fractional branes $\mathcal{N} = 2$ *fractional brane*. In the present situation, the number of supersymmetries does not change but we will see later that $\mathcal{N} = 2$ fractional branes can be present in $\mathcal{N} = 1$

quivers too. Note also that the theory is not conformal anymore. Fractional branes are indeed an important tool to generalize the gauge/gravity duality to non-conformal setups.

A peculiarity of these kinds of fractional branes, that will play an important role in Part III, is the presence of a flat direction in the moduli space of the gauge theory. For $\mathbb{C}^2/\mathbb{Z}_2$, we can go on the Coulomb branch by giving a VEV to the adjoint field Z_{11} since it does not appear in the superpotential anymore once $N_2 = 0$. This freedom is reflected in the geometry by the fact that we have a non-isolated singularity (coming from the extra $\mathbb{C}$ in $\mathbb{C}^2/\mathbb{Z}^2 \times \mathbb{C}$) onto which the stack of fractional branes can freely move.

We said before that regular branes transform in the regular representation $\mathcal{R}$ of the finite group. It appears that fractional branes transform in irreducible representations. Decompose the reducible $\mathcal{R}$ in irreducible representations of $\mathbb{Z}_2$:

$$\mathcal{R} = \mathcal{D}_0 \oplus \mathcal{D}_1 \,. \tag{5.18}$$

Now, see that $\mathcal{D}_0$ an $\mathcal{D}_1$ correspond to the diagonal actions in Equation (5.4). Comparing it with Equation (5.9), we find that $\mathcal{D}_0$ an $\mathcal{D}_1$ act on A_1^μ and A_2^μ respectively. Each irreducible representation is thus identified to a fractional brane, and the combination of two of these fractional branes gives rise to a regular brane. This one-to-one correspondence can be generalized to other orbifolds.

5.2 The conifold and cascading gauge theories

5.2.1 The Klebanov-Witten model

The Klebanov-Witten model is a superconformal field theory that one obtains by placing a stack of D3-branes at the tip of another singular geometry, the conifold. The latter has its defining equation given by

$$z_1^2 + z_2^2 + z_3^2 + z_4^2 = 0 \,. \tag{5.19}$$

Its isometries are $SO(4) \cong SU(2) \times SU(2)$, where z_i transform in the **4**, and a $U(1)$ for a common change of phase for the coordinates. There is a singularity at the origin, $z_i = 0$ for every $i = 1, \cdots, 4$. Alternatively, we can run the machinery of toric geometry to extract the equation of the conifold from its toric diagram in Figure 4.6b and find

$$xy = uv \,. \tag{5.20}$$

The link between the two equations is a simple change of coordinates:

$$\begin{aligned} x &= z_1 + iz_2\,, \quad y = z_1 - iz_2\,, \\ u &= z_3 + iz_4\,, \quad v = -z_3 + iz_4\,. \end{aligned} \tag{5.21}$$

It is possible to define a radial coordinate r to write the metric of this space[3] as a cone over a base $T^{1,1}$:

$$\mathrm{d}s^2_{\mathcal{C}} = \mathrm{d}r^2 + r^2 \mathrm{d}s^2_{T^{1,1}}\,, \tag{5.22}$$

where the base itself is defined as a coset,

$$T^{1,1} = \frac{SU(2) \times SU(2)}{U(1)}\,, \tag{5.23}$$

and has the topology of $S^2 \times S^3$.

We place a stack of N D3-branes at the tip of the conifold and consider the limit where supergravity is a good approximation of string theory, *i.e.* taking $N \gg 1$ and $g_s \ll 1$ while keeping $g_s N \gg 1$ fixed. In the near-horizon limit, we find that the backreaction of the D3-branes onto the metric changes it into

$$\begin{aligned} \mathrm{d}s^2 &= \frac{r^2}{R^2}\eta_{\mu\nu}\mathrm{d}x^\mu \mathrm{d}x^\nu + \frac{R^2}{r^2}(\mathrm{d}r^2 + r^2 \mathrm{d}s^2_{T^{1,1}}) \\ &= R^2(\mathrm{d}s^2_{AdS_5} + \mathrm{d}s^2_{T^{1,1}})\,, \end{aligned} \tag{5.24}$$

with

$$R^4 = \frac{27}{16} 4\pi g_s \alpha'^2 N\,. \tag{5.25}$$

As expected, the resulting metric is similar to the one of the original AdS/CFT correspondence where the metric of S^5 has been replaced by the metric for the base $T^{1,1}$. The AdS_5 part of the metric highlights the fact that the dual four-dimensional gauge theory will be conformal. The radius of space R differs by a ratio of the volumes of S^5 and $T^{1,1}$. The dilaton is constant and there is still a self-dual F_5-flux, but that is now integrated over $T^{1,1}$:

$$\int_{T^{1,1}} F_5 = N\,. \tag{5.26}$$

Klebanov and Witten found the dual gauge theory [24] to be $SU(N)_1 \times SU(N)_2$. Again, one $U(1)$ decouples and the other is IR-free, becoming a

[3]The metric $\mathrm{d}s^2_{T^{1,1}}$ is actually known. You can find it explicitly in [24].

baryonic global symmetry $U(1)_B$. It is accompanied by four chiral superfields, $A_1, A_2 \in (\overline{\square}_1, \square_2)$ and $B_1, B_2 \in (\overline{\square}_2, \square_1)$, see the quiver in Figure 5.3. There is a superpotential given by

$$W = h \det_{i,j} A_i B_j = h \left(A_1 B_1 A_2 B_2 - A_1 B_2 A_2 B_1 \right) . \tag{5.27}$$

The latter preserves a global $SU(2)_L \times SU(2)_R \times U(1)_B \times U(1)_{\mathrm{R}}$ symmetry group with charges depicted in Table 5.1. It is possible to check that the moduli space that is exactly N copies of the conifold, symmetrized under the permutation of the N D-branes.

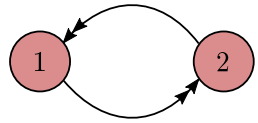

Figure 5.3: The quiver of the conifold $\mathcal{C}$.

	$SU(2)_L$	$SU(2)_R$	$U(1)_B$	$U(1)_{\mathrm{R}}$
A_i	$\square$	$\mathbf{1}$	-1	$1/2$
B_j	$\mathbf{1}$	$\square$	1	$1/2$

Table 5.1: Global charges in the Klebanov-Witten model.

The group of global symmetries is large enough to ensure that all the chiral superfields have the same anomalous dimension γ_0. Conformality then requires

$$\gamma_0 = -\frac{1}{2} , \tag{5.28}$$

which emphasizes the strong interacting nature of the fixed point. The superpotential is thus exactly marginal and the theory is self-dual under Seiberg duality.

τ_{IIB} in the string theory should correspond to a parameter on the space of conformal space for theories and should be symmetric under the exchange of τ_1 and τ_2 in the gauge theory. Consequently,

$$e^{-\phi} \propto \frac{1}{g_1^2} + \frac{1}{g_2^2} . \tag{5.29}$$

Another parameter, related to the difference $\tau_1 - \tau_2$, is linked in string theory to the presence of a non-trivial two-cycle and thus to the values of 2-form fields,

$$e^{-\phi}\left(\int_{S^2} B_2 - \frac{1}{2}\right) \propto \frac{1}{g_1^2} - \frac{1}{g_2^2}\,. \tag{5.30}$$

The baryonic symmetry $U(1)_B$ has also a readable interpretation from the string theory point of view. As always in the gauge/gravity duality, a global symmetry in the field theory corresponds to a gauge symmetry in the bulk. The gauge field comes from the reduction of the RR bulk field C_4 on the three-cycle of $T^{1,1}$, since it topologically contains a S^3. We correspondingly have charged dibaryons in the field theory:

$$\begin{array}{rcl} \mathcal{A}_{(i_1\cdots i_N)} & = & (A_{i_1})^{\alpha_1}_{\beta_1}\cdots(A_{i_N})^{\alpha_N}_{\beta_N}\,\epsilon_{\alpha_1\cdots\alpha_N}\epsilon^{\beta_1\cdots\beta_N}\,, \\ \mathcal{B}_{(i_1\cdots i_N)} & = & (B_{i_1})^{\beta_1}_{\alpha_1}\cdots(B_{i_N})^{\beta_N}_{\alpha_N}\,\epsilon^{\alpha_1\cdots\alpha_N}\epsilon_{\beta_1\cdots\beta_N}\,. \end{array} \tag{5.31}$$

Since $\pi_3(T^{1,1}) = \mathbb{Z}$, the baryons are interpreted as D3-branes wrapped an integer number of times on the three-cycles on the string theory side. They have a mass $R^4/g_s \propto N$ and dimension $3N/4$.

5.2.2 Deformation branes

The fact that $T^{1,1}$ contains topologically a S^2 leads us to another kind of fractional branes, the *deformation branes*. Indeed, it translates the fact that $\pi_2(T^{1,1}) = \mathbb{Z}$ and thus branes of that extend in a high enough number of spatial directions can be wrapped on a non-trivial two-cycle of $T^{1,1}$. In particular, we can modify the dual gauge theory previously found by wrapping D5-branes on the two-cycle [135]. Those are fractional branes, like D3-branes with fractional charges.

Consider adding M D5-branes to the system. They are a magnetic source of RR F_3-flux, since it is the Hodge-dual of a 7-form, and so introduce a non-trivial background for C_2. This breaks the S-duality of type IIB and generates a F_3-flux over the S^3, such that

$$\int_{S^3} F_3 = M\,. \tag{5.32}$$

This flux will have a dramatic impact on our setup, notably on the geometry and the flux F_5, to which F_3 couples. B_2 will have non-trivial value too, and so will $H_3 = \mathrm{d}B_2$. The metric will not be $AdS_5 \times T^{1,1}$, which is consistent with the fact that the gauge theory is not conformal anymore. For instance,

having placed M deformation branes at the tip of the conifold and probing it with a single D3-brane leads to the geometry for the *deformed* conifold:

$$z_1^2 + z_2^2 + z_3^2 + z_4^2 = \epsilon^2 \,. \tag{5.33}$$

This manifold is smooth. More precisely, as S^2 shrinks towards small values of the radial coordinate, S^3 keeps a finite radius, see Figure 5.4. It is still CY but not toric anymore since ϵ explicitly breaks one of the $\mathbb{C}^*$ actions.

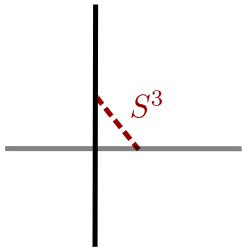

Figure 5.4: In presence of deformation branes, the conifold geometry is smoothed out, and we represent the corresponding inflated S^3 with a dashed line in the (p, q)-web.

The cascade

The gauge theory is the one of the conifold with modified ranks in the gauge group: $SU(N+M)_1 \times SU(N)_2$, where N and M are the numbers of regular and deformation branes respectively. For $N \gg M$, one tends to recover the superconformal Klebanov-Witten as a good approximation of the model. In particular, it is possible to find

$$\gamma_0 = -\frac{1}{2} + \mathcal{O}\left(\frac{M}{N}\right)^2 \,. \tag{5.34}$$

The beta-functions are given by

$$\begin{aligned} \beta_1 &= N + 2N\gamma_0 + 3M &&= +3M + N\,\mathcal{O}\left(\tfrac{M}{N}\right)^2 \,, \\ \beta_2 &= N + 2N\gamma_0 - 2(1-\gamma_0)M &&= -3M + N\,\mathcal{O}\left(\tfrac{M}{N}\right)^2 \,. \end{aligned} \tag{5.35}$$

A consequence is that the two gauge groups never reach a simultaneous fixed point. This will give to the RG-flow the trajectory of a cascade, that we now describe qualitatively.

Suppose that we start near the fixed point g_2^*, where g_1 and the superpotential coupling h are very small. There, $\gamma_0 > -1/2$ and only g_1 is a relevant operator so that the RG-flow inevitably deviates towards the fixed point g_1^* for the first gauge factor. Near this point, $\gamma_0 < -1/2$ and h becomes relevant and deviates the flow towards larger values of g_1^*, keeping g_2 comparatively small. A Seiberg duality on the first factor is necessary to understand the theory in the infrared, and thus the gauge theory becomes better described by $SU(N-M)_1 \times SU(N)_2$ with a small new coupling $\tilde{g}_1$ and h irrelevant. We are in a region similar to the one where we started, but the rank is decreased by $2M$. The RG-flow thus follows a cascade of Seiberg dualities until we reach small values for k. See Figure 5.5 for an illustration of the cascading RG-flow. This goes on until we reach $SU(M+l) \times SU(l)$ for $0 < l \leqslant M$.[4]

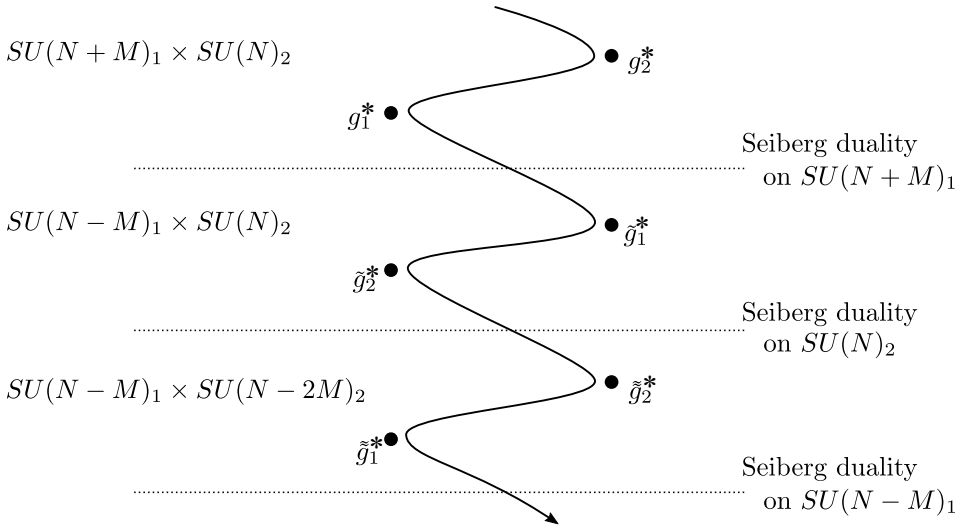

Figure 5.5: A cascade of Seiberg duality triggered by M fractional branes on top of $N \gg M$ regular branes.

[4]Actually, the steps where $M < l \leqslant 3M$ do not have fixed points for the gauge group of higher rank but rather enjoy free magnetic phases which do not change the qualitative behavior of the RG-flow described in the paragraph.

The *mesonic branch* of $SU(M+l) \times SU(l)$ for $0 < l \leqslant M$ can be easily worked out, although we restrict ourselves to describe it qualitatively here. The $U(1)_{\mathrm{R}}$ symmetry being anomalous leaves only a $\mathbb{Z}_{2M}$ R-symmetry in the quantum theory, regardless of the number of regular branes. In the infrared, the latter breaks down to $\mathbb{Z}_2$, which is explicit from the presence of ϵ in Equation (5.33), so that the moduli space has to be composed of M branches. One eventually finds that the mesonic branch corresponds to the moduli space for l regular branes moving on the deformed geometry. In other words, each branch is l copies of the deformed conifold, symmetrized under the permutation of l regular branes, see Figure 5.6.

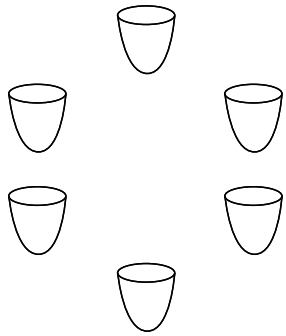

Figure 5.6: The mesonic branch for $M = 6$ deformation branes with $l = 1$ regular brane consists of $M = 6$ deformed conifolds.

We can see that something particular happens when $N = kM$ for a given $k \geqslant 1$. We eventually reach $SU(2M) \times SU(M)$, *i.e.* $l = M$, at the bottom of the cascade. $SU(2M)$ still runs faster towards the infrared and the second still can be seen as a global symmetry. Now we have baryons $\bar{\mathcal{B}} = [A]^{2M}$ and $\mathcal{B} = [B]^{2M}$, and mesons $M_{ij} = (A_i)_\alpha (B_j)^\alpha$ where $SU(2M)$ indices are contracted. This is nothing but SQCD with the same number of colors than flavors, so that we are in the scenario where SQCD has deformed moduli space. A new thing to do, with respect to the cases $l < M$, is then to go on the *baryonic branch*:

$$\mathcal{B} = \bar{\mathcal{B}} = i\Lambda_{2M}^{2M}\,, \quad M = 0\,. \tag{5.36}$$

This breaks fully the $SU(2M)$ and leaves $SU(M)$ unbroken since baryons are singlets under the latter. The mesons get a mass and are integrated out. We thus recover the M isolated vacua of pure $\mathcal{N} = 1$ SYM in addition to an extra massless chiral superfield containing the Goldstone boson for the

breaking of $U(1)_B$. The theory thus enjoys a discrete spectrum of glueballs, confinement and chiral symmetry breaking due to a gaugino condensate. The M vacua are separated by domain walls. Even if in principle there is no mass gap anymore, the massless superfield does not couple relevantly in the IR to the $SU(M)$ sector and thus we can neglect it (at least at weak 't Hooft coupling).

The supergravity flow

Klebanov and Tseytlin [26] proposed a dual supergravity solution where the breaking of conformal invariance, *i.e.* the impossibility to simultaneously cancel the two expressions in Equation (5.35), is translated into a radial dependence of the field B_2:

$$\int_{S^2} B_2 = \frac{3Me^{\phi}}{2\pi} \ln\left(r/r_0\right) \equiv k(r)\,, \tag{5.37}$$

where the dilaton ϕ is kept constant. In addition to the effect on the geometry, the deformation branes have also an effect on the H_3 and F_5-fluxes. In particular, one can expect to find new dependences in the radial coordinate r in the Gauss law:

$$\int_{T^{1,1}} F_5 = N(r)\,. \tag{5.38}$$

One thus finds

$$N(r) = Mk(r) \propto \ln\left(r/r_0\right)\,, \tag{5.39}$$

which reproduces the effective lowering of regular branes in the geometry as we move towards the infrared. We also know from geometrical considerations that N should be proportional to R^4, which is then also expected to be a function of r.

Klebanov and Tseytlin thus proposed a warped version of the Klebanov-Witten metric:

$$\begin{aligned} \mathrm{d}s^2 &= \frac{r^2}{R(r)^2}\eta_{\mu\nu}\mathrm{d}x^{\mu}\mathrm{d}x^{\nu} + \frac{R(r)^2}{r^2}(\mathrm{d}r^2 + r^2\mathrm{d}s^2_{T^{1,1}}) \\ &= R(r)^2(\mathrm{d}s^2_{AdS_5} + \mathrm{d}s^2_{T^{1,1}})\,, \end{aligned} \tag{5.40}$$

where $R(r)$ can be computed:

$$R(r)^4 = (81/8)(g_sM)^2\alpha'^2\ln(r/r_0)\,. \tag{5.41}$$

However, this solution is still singular and needs to be corrected if we want to learn about confinement and chiral symmetry breaking. To solve this

issue, Klebanov and Strassler [27] proposed instead that the metric should be

$$\mathrm{d}s^2 = h(r)^{-1/2}\eta_{\mu\nu}\mathrm{d}x^\mu \mathrm{d}x^\nu + h(r)^{1/2}\mathrm{d}s^2_{\mathrm{def.}\mathcal{C}}\,, \tag{5.42}$$

where $\mathrm{d}s^2_{\mathrm{def.}\mathcal{C}}$ is the metric of the deformed conifold and $h(r)$ should asymptote to $R(r)^4/r^4$ at large r. They also assume a constant dilaton and $h(r)$ nonsingular, without horizons, and vanishing at a finite value $r = r_{\mathrm{min}}$.

The solution that they found successfully displayed a discrete spectrum for glueballs, as it can be effectively made compact with the limiting value $r = r_{\mathrm{min}}$; confinement by attaching Wilson loops to the boundary; chiral symmetry breaking with the $\mathbb{Z}_2$ R-symmetry that follows automatically from the equation of the deformed conifold, together with a division of the moduli space in M distinct branches; domain walls constructed with D5-branes wrapped on S^3.

In order to connect these solutions to the cascading gauge theories, we recall that any supergravity solution is reliable only at large 't Hooft coupling. Assuming $N = kM$ in the gauge theory, the solution has to be placed in a region of the space of couplings where the varying 't Hooft coupling $\lambda_k = g_s kM$ is large. This region is somehow distant from the fixed points that we described above, where the field theory is more adequate to learn about physics. It is however interesting to note that as you go backward in the RG-flow, towards the UV regime of the theory, k effectively increases and you will reach $\lambda_k \gg 1$. This is true except for flows that travel extremely close to the fixed points. Conversely, for RG-flows with $g_s M \ll 1$, the field theory description starts to be necessary at a step $k \sim 1/g_s M$ and below. A corollary is that starting with a small $\lambda_k = g_k^2 kM$ keeps you near the fixed points themselves, see Figure 5.7

A fascinating conclusion is the following: whatever is the flow that you follow in your journey towards the infrared, you always end up in a vacuum that shares the same features as $\mathcal{N} = 1$ SYM. This does not mean that the corresponding low energy theories are the same, for instance they can have different massive spectra, but rather that they sit in the same infrared universality class.

5.3 Symmetries and anomalies

The ranks N_i of the gauge groups associated with nodes in the quiver reflect the configuration of branes at the singularity. These branes include both regular and fractional D3-branes.

The configuration with a democratic assignment for every node $N_i = N$

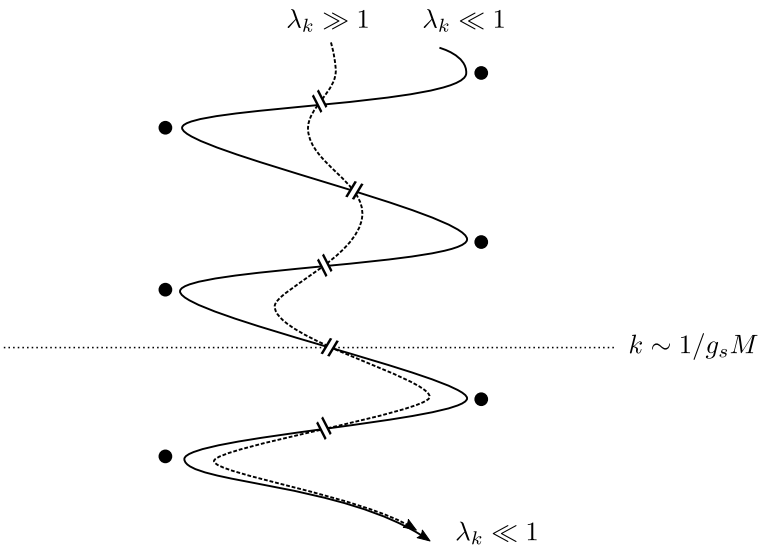

Figure 5.7: Different RG-flows in the case where $g_s M \ll 1$. A flow with $\lambda_k \ll 1$ is better described as a gauge theory, and $\lambda_k \gg 1$ as the supergravity dual.

corresponds to having N regular D3-branes and no fractional branes. This configuration is always tadpole free since the CY is non-compact and the RR flux sourced by regular D3-branes can escape all the way to infinity.

Configurations with unequal ranks are obtained by adding fractional branes. It is a general fact that the latter correspond to D5-branes wrapped on vanishing compact two-cycles [139]. We already met these cycles when talking about small resolutions in Chapter 4. When compact four-cycles are also present at the singularity, *i.e.* when the toric diagram of the singularity has internal points, these D-branes source RR tadpoles that must be canceled. This is the geometric counterpart of being a chiral dual gauge theory and having non-abelian anomalies to cancel [143], see the familiar one-loop Feynman diagram in Figure 5.8.

In other words, tadpole cancellation amounts to canceling the flux sourced by the branes in compact homology. This equivalence of tadpole and anomaly cancellation holds even formally for gauge groups with zero rank. In this work, we will use anomaly cancellation conditions (ACC) and tadpole cancellation interchangeably.

The number of independent, anomaly-free fractional brane configura-

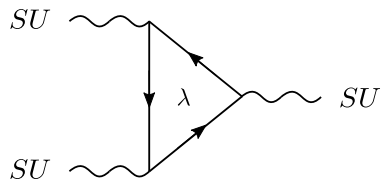

Figure 5.8: One-loop Feynman diagram with fermions running in the loop and non-abelian gauge vectors in the external legs.

tions is thus in one-to-one correspondence with the number of compact two-cycles whose Hodge duals in the CY are non-compact four-cycles. Indeed, D5 branes wrapped on these (and only these) two-cycles are tadpole free since the RR flux can again escape to infinity. For toric geometries, we know how to compute the number of anomaly-free fractional branes based on the perimeter of the toric diagram n, *i.e.* the number of external points of the convex polygon [134, 140]:

$$\#\text{Fractional Branes} = n - 3 \ . \tag{5.43}$$

Pictorially, the quiver is really a convenient object for checking the absence of local gauge anomalies in the low energy theory. In practice, the cancellation of anomalies at a given node corresponds to having the same number of incoming and outgoing arrows (weighted by the ranks of the nodes at their other endpoints). This is encoded in the (antisymmetric) matrix A defined as

$$A = \text{adj}(\mathcal{Q}) - \text{adj}(\mathcal{Q})^T \, , \tag{5.44}$$

where $\text{adj}(\mathcal{Q})$ is the adjacency matrix of the quiver. The latter is a matrix whose elements $\text{adj}(\mathcal{Q})_{ij}$ count the number of bifundamental chiral superfields $(\overline{\square}_i, \square_j)$ charged under the gauge group i and the gauge group j. With abuse of language in the following, we will call A the adjacency matrix, for simplicity. The matrix A is only sensitive to the chiral content of the theories (*e.g.* it is zero for $\mathbb{C}^2/\mathbb{Z}_2$ and the conifold). Cancellation of anomalies amounts to solving the homogeneous system of equations defined by this matrix,

$$\text{For each } SU(N_i) \quad : \quad \sum_j A_{ij} N_j = 0 \, , \tag{5.45}$$

that is, finding $\text{Ker}(A)$. Vectors in $\text{Ker}(A)$ are the ranks associated with regular and fractional branes.

The quiver of the complex cone over dP_1, see Figure 5.9, was found to yield a chiral gauge theory and to host an additional kind of fractional

brane. The latter is known to break supersymmetry in an unstable runaway vacuum [66]. From the quiver, we get

$$A = \begin{pmatrix} 0 & 2 & -1 & -1 \\ -2 & 0 & -1 & 3 \\ 1 & 1 & 0 & -2 \\ 1 & -3 & 2 & 0 \end{pmatrix} . \tag{5.46}$$

Ker(A) is generated by

$$\mathbf{N} = (N_1, N_2, N_3, N_4) = (1,1,1,1)\, N + (3,1,0,2)\, M\,. \tag{5.47}$$

N and M parametrize the regular and fractional branes respectively, in accordance with the fact that the toric diagram of the singularity has a perimeter equal to four. $N = 0$ and $M = 1$ indeed reproduce the incriminated fractional brane.

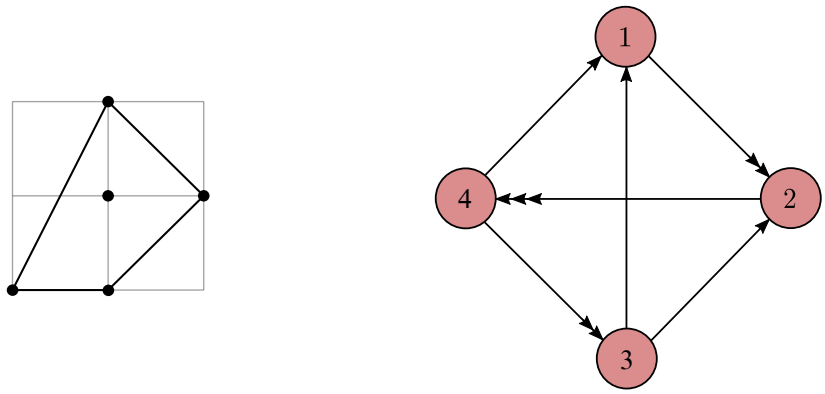

(a) (b)

Figure 5.9: The complex cone over dP_1 (a) Toric diagram. (b) Quiver.

Initially, the gauge theory on the worldvolume of the D-branes is a product $U(N)$ gauge groups and one can ask why we did neglect the $U(1)$ factors in the above discussion. First of all, one can identify a $U(1)$ under which all matter fields are charged, and that decouples in the infrared, similarly to what happens for D-branes on flat space. Secondly, in chiral gauge theories some $U(1)$ factors can be anomalous and become massive through a generalization of the Green-Schwarz mechanism [144]. Finally, the leftover and non-anomalous $U(1)$ factors become global symmetries at low energy

and we will call them *baryonic symmetries* for the following reason. They correspond to gauge vectors in the bulk of the dual supergravity solution obtained by integrating the RR field C_4 over non-trivial three-cycles in the base SE_5 of the CY cone. The number of baryonic symmetries was thus computed to be exactly the number of such independent three-cycles in the case of a smooth base [32]. In fact, it was also shown earlier that the number of baryonic symmetries corresponds exactly the number of fractional branes [134], such that we find in general a global group of baryonic symmetries $U(1)_B^{n-3}$ for any gauge theory extracted from a toric singularity with perimeter n.

Since we are talking about global symmetries, note also that, as usual in the framework of the gauge/gravity duality, isometries in the bulk are dual to global symmetries in the gauge theory. Hence, when dealing with toric singularities, the $U(1)^3$ isometry of the geometry will be associated with a $U(1)_F^2 \times U(1)_{\mathrm{R}}$ global symmetry group. One of these $U(1)$ isometry is generated by the Reeb vector in the CY cone and, as such, is recognized to generate the R-symmetry in the gauge theory. The $U(1)_F^2$ will play the role of *flavor symmetries*.

Chapter 6

Branes and Dimers

By the early 2000s, the efforts devoted to the description of supersymmetric gauge theories obtained from D-branes on singular geometries resulted in two algorithms: the *Forward algorithm* that links a quiver to a toric diagram, and the *Inverse algorithm* that links a toric diagram to possibly many quivers [39, 40]. However, these algorithms are somewhat heavy to run for large quivers and toric diagrams. Moreover, we know that quivers miss the superpotential of the gauge theory. These facts called for new tools and methods and led to the discovery that *dimer models* have an important role to play in brane physics [45, 46].

We introduce dimer models in this chapter first by recalling their physical origin as a brane system [46,145,146], and then their more conventional construction as a statistical model of perfect matchings. In particular, we will explain how to use them to read the supersymmetric gauge theories. We will also review how to connect it to the toric variety with the Kasteleyn matrix in one way, and using zig-zag paths in the other, see Figure 6.1. Reviews on the subject can be found in [147, 148]. For a more exhaustive list of applications of dimer models in physics and mathematics, see [32, 149].

6.1 Brane tiling

In this section, we recall how dimer models arise as a physical picture of branes after a sequence of two T-dualities on our familiar setup, a stack of D3-branes placed at the tip of a toric CY threefold singularity.

Start with N coincident D3-branes extending along $\mathbb{R}^{1,3}$, as pictured in Table 6.1, and perform two T-dualities on the transverse coordinates to

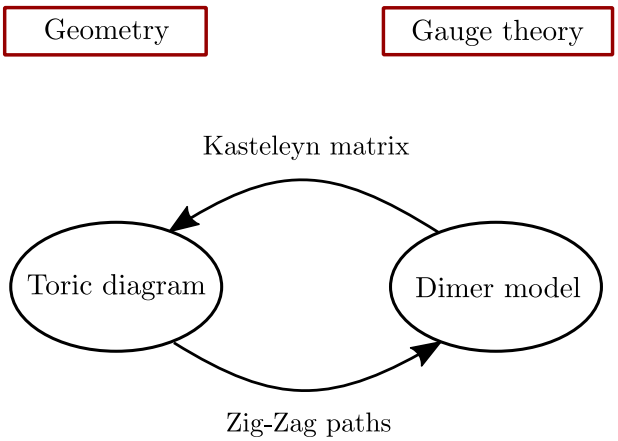

Figure 6.1: Quiver of algorithms: to go from the geometry to the gauge theory, and vice versa.

the branes. These T-dualities are performed on cycles that are found in toric CY threefolds since we know that they have at least a $U(1)^3$ as part of their isometry group. This sequence of T-dualities will bring us to a fivebrane system made of D5 and NS5-branes in flat spacetime, illustrated in Table 6.2.

	0	1	2	3	4	$5_\circ$	6	$7_\circ$	8	$9_\circ$
CY					×	×	×	×	×	×
N D3	×	×	×	×						

Table 6.1: D3-branes sitting at the tip of a CY singular geometry. Coordinates parametrizing the cycles have a circle subscript.

	0	1	2	3	4	$5_\circ$	6	$7'_\circ$	8	$9'_\circ$
NS5	×	×	×	×			–	–	Σ	– –
N D5	×	×	×	×				×		×

Table 6.2: The brane tiling. Σ is the holomorphic curve in the $67'89'$-space wrapped by the NS5-brane.

In more details, say that the cycles that we T-dualize are parameterized

by the coordinates 7 and 9. After T-duality, we call them $7'$ and $9'$ respectively. Since they were transverse to the D3-branes, they are now wrapped by a stack of D5-branes. The CY geometry, signaled by a non-trivial G_{ij}, gave way for a NS5-brane, paired with a non-trivial background for the 2-form B_{ij}. The NS5-brane now wraps a holomorphic curve Σ, in addition to extend in the $\mathbb{R}^{1,3}$ part of spacetime. Σ determined by the geometry of the CY, it can be seen as a "thickened" version of the (p,q)-web,[1] see Figure 6.2. This holomorphic curve Σ is two-dimensional and intersects the D5-branes in a non-trivial manner on some one or two-dimensional regions. In real coordinates, it is indeed defined by a set of two equations on four coordinates, chosen to 6, $7'$, 8, and $9'$ in Table 6.2. The intersections give rise to a graph on $\mathbb{T}^2$. This is the origin of the *brane tiling*.

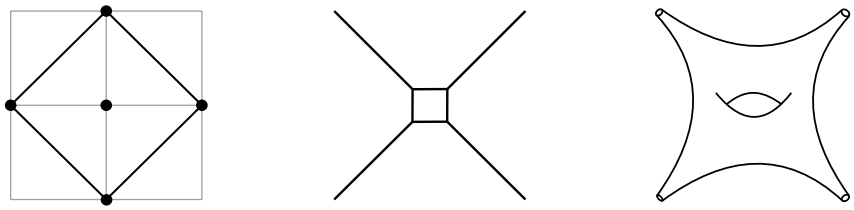

(a) Toric diagram. (b) (c)

Figure 6.2: The Hirzebruch surface F_0: (a) Toric diagram. (b) (p,q)-web. (c) Curve Σ.

The tensions of the fivebranes have different dependence in the string coupling constant:

$$T_{\text{D5}} \propto \frac{1}{g_s}\,, \quad T_{\text{NS5}} \propto \frac{1}{g_s^2}\,. \tag{6.1}$$

If we look at this system in a strong coupling limit defined by sending $g_s \to \infty$, the D5-branes become flat and are found to form disks attached to the NS5-brane, which ban be either perpendicular or parallel to them and makes sharp angles to connect these regions. In the torus $\mathbb{T}^2$ of the $7'9'$-plane that support the D5-branes, this limit draws a simpler picture where we find three different kind of regions, all of them being bound states of (D5,NS5)-branes: $(N,0)$ and $(N,\pm 1)$-branes, see the example for the F_0 singularity in Figure 6.3a.

In this limit, the NS5-brane can also be seen as a sum of different rigid NS5-branes that together reproduce the same pattern as the unique and

[1]The holomorphic curve Σ is defined by $P(x,y)=0$ where P is the characteristic polynomial of the toric diagram, and equivalently the determinant of the Kasteleyn matrix, defined below.

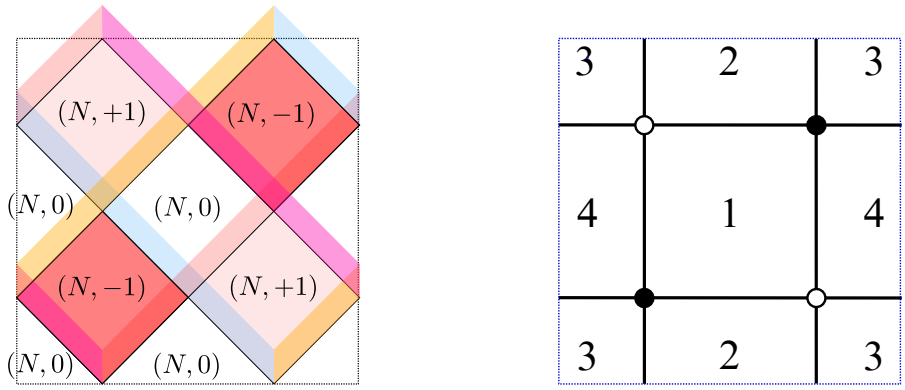

(a) (b)

Figure 6.3: The Hirzebruch surface F_0: (a) Fivebrane system on the torus $\mathbb{T}^2$. (b) Dimer model.

curved NS5-brane in the strong coupling limit. In other words, Σ is thinned by the strong coupling limit such that it can be seen as an intersection of many semi-cylinders of NS5-branes ending on $\mathbb{T}^2$ and whose directions coincide with the direction of the asymptotic "tubes" of Σ. This is consistent with Figure 6.3a where in practice the directions of NS5-branes are given by the external legs of the graph dual to the toric diagram, the (p, q)-web.

We now wish to extract the gauge theory living on this fivebranes system. The radii of the torus $\mathbb{T}^2$ can be taken to small values in order to get rid of Kaluza-Klein modes, $R \to 0$. We also set the string length to small values $l_s \to 0$ in order to make sense of the gauge coupling of the low energy theory at finite and fixed value:

$$\lambda = \frac{R^4}{l_s^4} \quad \text{fixed.} \tag{6.2}$$

The gauge theory on the worldvolume of the D5-branes is determined in the following way. On the $(N, 0)$-branes, the story is just the same as for D3-branes, we find a $U(N)$ gauge theory where the $U(1)$ factor decouples to leave a $SU(N)$ gauge theory. Regions with $(N, \pm 1)$-branes enjoy a $U(1)$ gauge symmetry but the latter is found to be non-dynamical and related to anomalous global symmetry of the quiver gauge theory [141, 150]. At every point where two different $(N, 0)$-branes meet, we find a massless open string connecting the two regions. It corresponds to a bifundamental field in the gauge theory, and is oriented because the NS5-brane itself is. The regions $(N, \pm 1)$ can be spanned by a tree-level disk amplitude connecting several matter fields and thus correspond to terms in the tree-level superpotential,

with a sign obtained according to the orientation of the NS5-brane:

$$W = +X_{ij}Y_{jk}Z_{ki} - X_{ij}U_{jk}V_{kl}W_{li} + \cdots . \tag{6.3}$$

The couplings are taken to be equal to one in order to get a superconformal theory.

Note in passing that an extra T-duality on the remaining cycle, the coordinate 5 in Tables 6.1 and 6.2, leads to the mirror picture [145]. NS5-branes give way back for a geometry known to be the mirror CY of our original singular space. The mirror is again fully specified by Σ. It is defined as a double fibration over a complex plane W: there is a punctured Riemann surface $P(x, y) = W$, and a circle $W = uv$ degenerating at the origin. D5-branes are replaced by D6-branes. Gauge fields are associated with different three-cycles in the mirror CY wrapped by D6-branes, matter fields to intersections among these cycles and superpotential terms arise from open string worldsheet instantons supported at disks in this Riemann surface. We will not need to enter further details now, but more comments will be made in Chapter 9.

Bipartite graph on the torus

This decomposition of the torus into regions suggests drawing the brane tiling as a bipartite graph on the torus $\mathbb{T}^2$, a *dimer model*. It consists of edges linking vertices of different colors, black to white. The faces encircled by edges will be the gauge groups. The edges together with their natural orientation will be matter fields. Finally, white and black vertices will be superpotential terms with a positive or negative sign respectively. The correspondence is illustrated in Figure 6.3 and the rules are summarized in Table 6.3, where we also set some conventions.

The bipartite nature of this graph constrains it on some aspects. First, we note that every face is surrounded by an even number of edges. Secondly, since every edge connects a black node to a white node, it follows that every field appears twice in the superpotential, once in a positive term and once in a negative term, like X_{ij} in the example of Equation (6.3). The latter fact is called the *toric condition* on the superpotential since it follows directly from toric geometry.

In general, the vertices in dimer models will always be of valence strictly greater than two. The reason is that a one-valent node does not make sense (both from the point of view of the gauge theory and in the above brane construction), while a two-valent is a mass term and can be consistently

Dimer model	Quiver gauge theory
Face	$SU(N_i)$ gauge factor
Edge between faces i and j	Chiral superfield in the bifundamental representation of groups i and j (adjoint representation if $i = j$). The chirality, *i.e.* orientation, of the bifundamental is such that it goes clockwise around black nodes and counterclockwise around white nodes.
k-valent node	Superpotential term made of k chiral superfields. Its sign is $+/-$ for a white/black node, respectively.

Table 6.3: Dictionary relating the dimer model to quiver gauge theories.

integrated out. See the following contribution to the superpotential:

$$W = Y(X_3, \cdots, X_n)\, X_1 - X_1 X_2 + X_2\, Z(X_3, \cdots, X_n) + \cdots, \tag{6.4}$$

where Y and Z are arbitrary products of fields. Using the toric condition, we know that F-term equations for X_1 and X_2 read

$$X_2 = Y(X_3, \cdots, X_n)\,, \quad X_1 = Z(X_3, \cdots, X_n)\,. \tag{6.5}$$

The fields X_1 and X_2 can be integrated out and the superpotential thus simplifies into

$$W = Y(X_3, \cdots, X_n)\, Z(X_3, \cdots, X_n) + \cdots\,. \tag{6.6}$$

See Figure 6.4 for an illustration on the dimer.

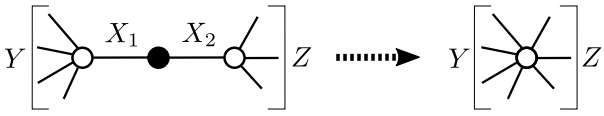

Figure 6.4: A two-valent node in a dimer model corresponds to a mass term and is integrated out at low energy.

If one limits its interest in finding the gauge groups, matter content, and superpotential of a field theory, the angles between edges in a dimer

model do not matter and can be deformed. However, the authors of [146] showed that when *isoradial embeddings* are admissible in a dimer model, angles between edges were directly related to R-charges for the fields. This fact strengthens the idea that the dimer model is a physical construction more than an ad-hoc mathematical tool.

The advantage of the dimer model over quivers is to provide the tree-level superpotential of the gauge theory. We can however link one to the other by embedding the quiver on $\mathbb{T}^2$ and making it periodic, see Figure 6.5. We see that the *periodic quiver* is actually the dual graph of the dimer, in the sense that faces and nodes are exchanged. Closed loops of arrows in the periodic quiver are thus the superpotential terms. In the rest of the thesis, we will stick to dimer models.

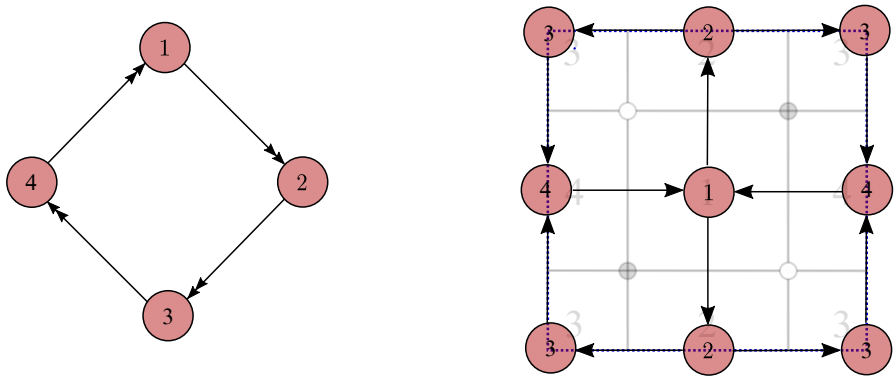

Figure 6.5: The Hirzebruch surface F_0 (a) Quiver. (b) Periodic quiver on $\mathbb{T}^2$.

Finally, let us comment that the above correspondence between dimer models and the gauge theory has been proved to hold for any toric singularity in a more precise way [151]. We will not review the proof here, but we will introduce some of its relevant tools in the subsequent sections for our purpose of studying orientifolds and dynamical supersymmetry breaking.

6.2 Dimer models

6.2.1 Conformality on the graph

We now develop some reasons that help to understand why bipartite graphs on the torus are suited for describing our superconformal gauge theories.

Let be F faces the number of faces, N_W the number of vertices of both colors and E the number of edges in the bipartite graphs. The Euler formula links these quantities to the genus g of the embedding surface. In the case of the torus, $g = 1$ and we find

$$F + N_W - E = 2g - 2 = 0\,. \tag{6.7}$$

Recall now that F is also the number of SU factors in the gauge symmetry group, N_W is the number of superpotential terms and E is the number fields. This is an interesting identity from the point of view of gauge theories since it can be derived exactly from superconformal theories.

Use the identity at the conformal fixed point between the anomalous dimensions and R-charges for the fields, labeled by i, of each gauge factor to write its β function.[2]

$$\text{For each gauge factor} \quad : \quad 2 + \sum_i (R_i - 1) = 0\,. \tag{6.8}$$

We can sum the LHS of the above equation over each different gauge group f, remembering that every edge belongs to two faces:

$$2F + \sum_{i,f} R_i - 2E = 0\,. \tag{6.9}$$

All superpotential terms have a R-charge equal to 2, and so we find

$$2F + 2N_W - 2E = 0\,. \tag{6.10}$$

Thus, superconformality of SU gauge theories implies $g = 1$. This is satisfied for the torus and the Klein bottle.

We already saw that the torus appeared naturally from toric geometries after the sequence of T-dualities. The authors of [151] then anticipated that bipartite graphs embedded on Klein bottles could also lead to superconformal gauge theories. We will explicitly realize such construction with orientifolds in Chapter 9.

[2]The reasoning is presented assuming only the presence of bifundamental fields for simplicity, although it works with adjoints too.

6.2.2 From dimers to the geometry

Dimer models were initially introduced as statistical tools in condensed matter in order to describe bonds in substances made of two monomers, hence the bipartite nature of the graph. In general, dimer models are the statistical mechanical models for *perfect matchings*, a generalization of these bonds. A perfect matching is a subset of edges in the graph such that every vertex is an endpoint of only one edge in the set. They play the role of fields in a gauged linear sigma model (GLSM), the field theory one obtains after imposing F and D-terms equations on the fields obtained from the quiver of a given singularity. See how we can extract the different perfect matchings from the dimer model of the zeroth Hirzebruch surface F_0 in Figure 6.6.

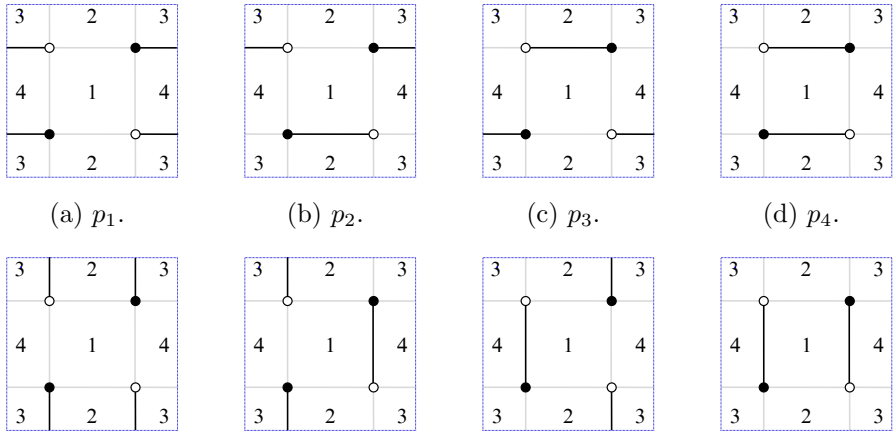

(a) p_1. (b) p_2. (c) p_3. (d) p_4.

(e) p_5. (f) p_6. (g) p_7. (h) p_8.

Figure 6.6: The perfect matchings of F_0.

As discussed in [45, 46, 152, 153], to any dimer model one can associate a weighted (with two variables x and y), signed adjacency matrix K, named the *Kasteleyn matrix*, whose determinant takes the form of a Laurent polynomial:

$$P(x, y) = \det K(x, y) = \sum_{i,j} c_{i,j} x^i y^j \,. \tag{6.11}$$

It is the characteristic polynomial of the dimer model, and can be understood as its partition function. In fact, the data contained in this Laurent polynomial allows recovering the geometry on which D3-branes are placed and that corresponds to this dimer model.[3] This procedure is known as the

[3]The equation $P(x, y) = 0$ defines the holomorphic curve Σ wrapped by the NS5-brane in the fivebranes system associated with the dimer model.

Fast Forward Algorithm [46]. We review it here with the example of the zeroth Hirzebruch surface F_0.

To obtain the Kasteleyn matrix of a dimer model, we assign a plus or minus sign to every edge in the dimer such that for every face the product of signs is $+1$ if its number of edges is $2 \bmod 4$ and -1 if its number of edges is $0 \bmod 4$. We then draw two closed oriented (gauge-invariant) paths γ_x, γ_y with holonomy $(1,0)$ and $(0,1)$ on $\mathbb{T}^2$. Every edge crossed by γ_x is multiplied by x or $1/x$, depending on the relative orientation, and respectively by y or $1/y$ if the edge is crossed by γ_y. See the example of these assignments in Figure 6.7.

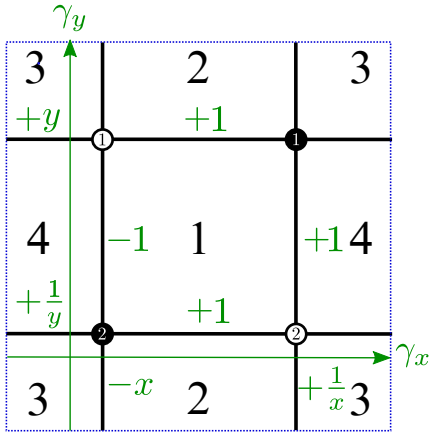

Figure 6.7: Dimer model of the Hirzebruch surface F_0 with an assignment for the Fast Forward Algorithm.

The adjacency matrix of the graph for the nodes, black (b) and white (w), with such weights, is the Kasteleyn Matrix. For F_0, it reads

$$K = \left(\begin{array}{c|cc} & b_1 & b_2 \\ \hline w_1 & 1+y & -1-x \\ w_2 & x^{-1}+1 & y^{-1}+1 \end{array} \right) , \tag{6.12}$$

where rows and columns correspond to white and black nodes in the dimer respectively, with the same numbers as in the dimer of Figure 6.7. Its determinant is

$$\det K = x^{-1} + y^{-1} + 4 + x + y \, . \tag{6.13}$$

We may compute the Newton Polygon of the above expression and the latter corresponds to the toric diagram of the singular toric geometry related to the dimer model [45]. For every monomial $x^{p_x} y^{p_y}$ one draws a point in a

two-dimensional lattice with coordinates (p_x, p_y). In doing so, we finally recover the toric diagram of the zeroth Hirzebruch surface F_0 depicted in Figure 6.2a.

Each point (p_x, p_y) in the toric diagram corresponds actually to a perfect matching with a multiplicity given by the coefficient of $x^{p_x} y^{p_y}$ in the Laurent polynomial. The perfect matchings are distinguished in different classes. There are the *internal* and the *external points* in the toric diagram. The external lie on the perimeter and can be further divided in two sets, the *extremal points* that are placed on corners of the toric diagram and the *non-extremal*. In the GLSM, extremal perfect matchings are the only ones with a non-zero R-charge.

An intuitive way to see how perfect matchings are related to points in the toric diagram is to consider formal differences of perfect matchings $p - p_0$ with respect to a reference perfect matching p_0. The corresponding configurations are closed loops on $\mathbb{T}^2$ and have a definite winding number, corresponding to its position in the toric diagram. See in Figure 6.8 the different closed loops when p_4 is the reference perfect matching for F_0 and in Figure 6.9 the result of this construction.

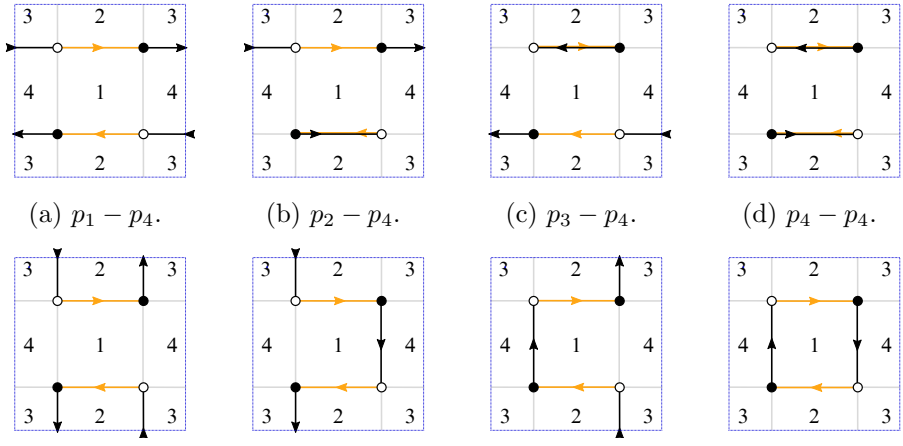

(a) $p_1 - p_4$. (b) $p_2 - p_4$. (c) $p_3 - p_4$. (d) $p_4 - p_4$.

(e) $p_5 - p_4$. (f) $p_6 - p_4$. (g) $p_7 - p_4$. (h) $p_8 - p_4$.

Figure 6.8: Closed loops obtained from the difference of perfect matchings of F_0, $p - p_4$, where $-p_4$ is shown in orange.

There is a set of consistency conditions that the dimer model has to satisfy to correspond appropriately to the toric diagram extracted from the Fast Inverse Algorithm.

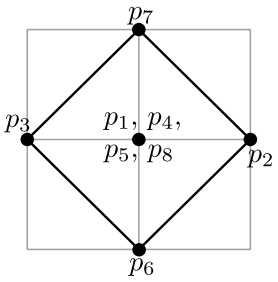

Figure 6.9: Toric diagram of F_0 with perfect matchings, in the case where p_4 is the reference perfect matching.

- The number of faces in the dimer model is equal to twice the area of the toric diagram, where the smallest square has an area equal to one.
- No face in the dimer model is two-sided. The minimal number of edges surrounding a face is thus four.
- No extremal perfect matching has multiplicity different than one in absolute value.

Indeed, it can be checked that the toric diagram of F_0 has an area equal to two from Figure 6.2a, and that its internal point is the only one with a multiplicity different than one from Equation (6.13).

Toric duality

It has been observed that several gauge theories, and hence dimer models, correspond to the same toric geometry. See for instance the dimer model of Figure 6.10b. With similar conventions as before, we reach the following Kasteleyn matrix:

$$K = \left(\begin{array}{c|cccc} & b_1 & b_2 & b_3 & b_4 \\ \hline w_1 & y & -x & 1 & 0 \\ w_2 & x^{-1} & y^{-1} & 0 & 1 \\ w_3 & 1 & 0 & 1 & 1 \\ w_4 & 0 & 1 & -1 & 1 \end{array}\right) \tag{6.14}$$

Its determinant reads

$$\det K = -x^{-1} - y^{-1} + 5 - x - y\,, \tag{6.15}$$

and we recover the toric diagram of F_0. No consistency condition has been violated even though the gauge theories look naively different. This is an

expression of the *toric duality*, where a single toric diagram knows about different dimer models.

This toric duality is understood to take its origin in Seiberg duality [41]. We present in Figure 6.10 the dimer models for the two phases of F_0 that are linked by Seiberg duality on face 1. The Kasteleyn matrices are not the same, but this results in similar characteristic polynomials. Actually, only the coefficients for the internal points of the toric diagram are different. If in the two phases, all gauge groups can have an identical rank, we call these different *toric phases*.

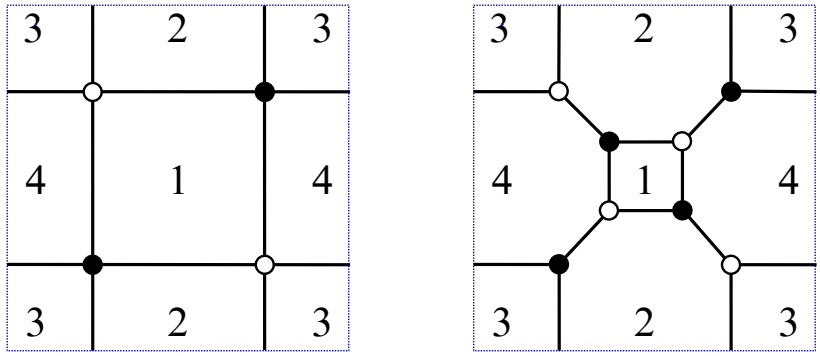

(a) Phase I. (b) Phase II.

Figure 6.10: Two toric phases of F_0. Seiberg duality on face 1 links one to the other.

6.2.3 Zig-Zag paths

Zig-Zag paths (ZZPs) are oriented paths on the dimer that capture global properties of the geometry. They can be computed as the oriented differences of external perfect matchings. They are constructed by following edges in the graph and turning maximally left (right) at white (black) nodes. The ZZPs of the conifold dimer are shown in Figure 6.11. These form non-selfintersecting closed loops on the torus with non-trivial homology around the two fundamental cycles. These homology numbers can be associated with charges for two of the three $U(1)$ isometries of the toric CY threefold, the remaining one being associated with the $U(1)_{\mathrm{R}}$ R-symmetry. ZZPs are also in one-to-one correspondence with legs in the (p, q)-web diagram, obtained as the dual graph to the toric diagram. The (p, q) labels of the external legs are exactly the homology charges of the ZZPs.

(a) (b)

Figure 6.11: Zig-Zag paths in the conifold: (a) Toric diagram. (b) Dimer model.

In the way they are defined, ZZPs constitute a route to go from the toric diagram to dimers. Given a toric diagram, one has a definite set of ZZPs at disposal and can try to place them on a blank torus $\mathbb{T}^2$ in order to generate a dimer model. Of course, the ZZPs cannot intersect in a complete arbitrary way. In addition to the consistency conditions of Section 6.2.2, a ZZP cannot intersect with any other ZZP that has the same winding number, including itself [154]. Thurston [155, 156] provided a convenient algorithm to assemble the ZZPs in a consistent way using *triple crossings*, but we will not review it here. For large toric diagrams, one will typically find different ways to arrange the ZZPs and these can lead to different toric phases. See Figure 6.12 in the two toric phases of F_0.

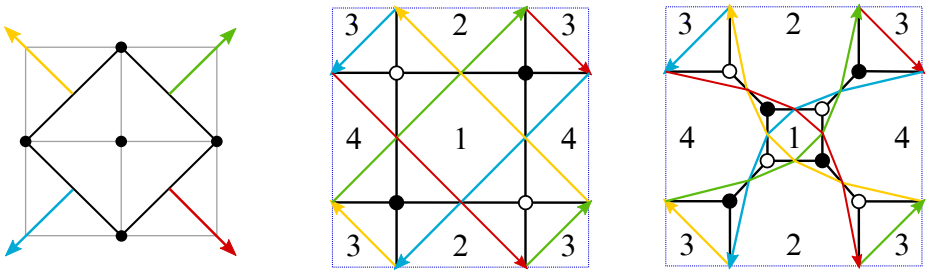

(a) (b) (c)

Figure 6.12: Zig-Zag paths in F_0: (a) Toric diagram. (b) Dimer model of phase I. (c) Dimer model of phase II.

6.2.4 Partial resolutions

A *partial resolution*, or *blow-down*, consists of removing one or several external points in a toric diagram. In the dimer model, this corresponds to performing a higgsing, as we now explain and illustrate.

Removing points from the perimeter of a toric diagram changes its ZZPs content. See for instance the partial resolution of F_0, presented in Figure 6.13a, and leading to the orbifold $\mathbb{C}^2/\mathbb{Z}_2$. In that case, some ZZPs that were crossing each other in the dimer model before the resolution will not be allowed to do so anymore. In general, the number of ZZPs also changes.

In the dimer model, we have an algorithm [157] that performs the partial resolution based on the ZZPs. It prescribes the "merging" of the ZZPs that are identified in the toric diagram by the partial resolution. This ensures that they will not cross each other anymore. Consistently, the edges that result from their crossings are deleted from the dimer model, see Figure 6.13b. From the gauge theory viewpoint, VEVs are assigned to these edges and they are integrated out. Different faces and hence gauge groups are identified according to this higgsing pattern. We finally recover the dimer model of $\mathbb{C}^2/\mathbb{Z}_2$, with its two hexagonal faces.

We note that the partial resolution of Figure 6.13 can be performed similarly in the dimer model of the second phase of F_0, shown in Figure 6.12c. This results in the same dimer model than in Figure 6.13b, consistently with the fact that the orbifold of flat space admits only one toric phase.

6.3 Fractional branes revisited

6.3.1 Anomalies and zig-zag paths

We now review a method for finding anomaly-free rank assignments of dimers based on ZZPs [140]. We can regard every ZZP as defining an "anomaly-free wall" on the dimer. This is because due to its definition, every time a ZZP overlaps with a face in the dimer, it does so over exactly a pair of consecutive edges.[4] These two consecutive edges correspond to an incoming and an outgoing arrow in the quiver for the gauge group associated with the face under consideration.[5] This implies that if we add some constant to

[4]By overlapping with a face, we mean sharing an edge with it, not just touching it at a node.

[5]More generally, a ZZP might overlap with a given face more than once. Every overlap involves a pair of consecutive edges, so the previous discussion still applies. For an

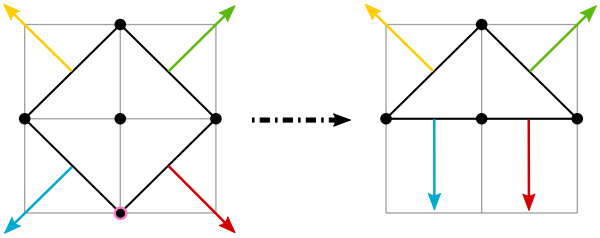

(a)

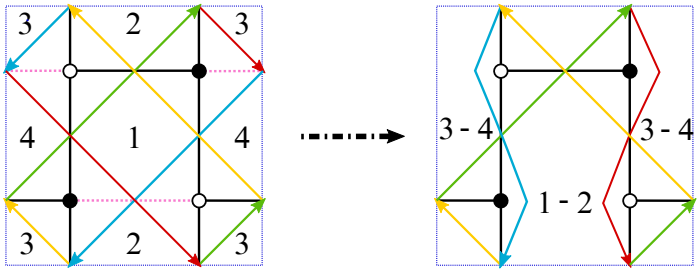

(b)

Figure 6.13: Partial resolution of F_0 yielding the orbifold $\mathbb{C}^2/\mathbb{Z}_2$, illustrated in (a) the toric diagram, (b) the dimer model of phase I.

the ranks of all the faces on one side of the ZZP, the ACC of the faces on the other side of the ZZP do not change, as illustrated in Figure 6.14.

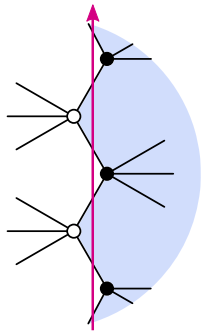

Figure 6.14: A ZZP as an anomaly wall.

explicit example of this situation, see the yellow ZZP in the dP_1 dimer model shown in Figure 6.15b.

With this insight, one recovers the algorithm to construct anomaly-free rank assignments for dimer models outlined in [140]:

1. The set of ZZPs is given by $\{(p_\Gamma, q_\Gamma) \,|\, \Gamma = 1, \ldots, n\}$, where p_Γ and q_Γ are the winding numbers of the ZZP Γ, with respect to a fixed unit cell. To every (p_Γ, q_Γ) assign an integer coefficient v_Γ.

2. Choose one face and assign rank zero to it.

3. In going from face a to an adjacent face b, the rank of the latter will be
$$N_b = N_a + v_\Gamma - v_\Delta \,, \tag{6.16}$$
where v_Γ is the coefficient of the ZZP moving to the left with respect to the path from a to b, and v_Δ is the one in the opposite direction. This operation is well defined since we are working on an oriented surface, which implies that we can consistently speak of "right" and "left" of a ZPP.

4. Finally, one must impose two constraints that ensure that the rank assignment is single-valued. Consider, for instance, moving along a loop along with one of the two cycles of the fundamental cell. When returning to the initial face, the rank should be unchanged. This is granted by imposing
$$\Lambda = \sum_\Gamma v_\Gamma p_\Gamma = 0, \quad M = \sum_\Gamma v_\Gamma q_\Gamma = 0 \,. \tag{6.17}$$
We will refer to these two conditions as the Λ and M *topological constraints*.

Every choice of values for the v_Γ's consistent with the topological constraints Equation (6.17) gives rise to an anomaly-free rank assignment. Moreover, notice that, by construction, every rank assignment is invariant under a global shift $v_\Gamma \to v_\Gamma + k$. One may use this freedom to fix one of the v_Γ's (equivalently, one of the ZZPs is not independent). There are thus two constraints and one redundancy to be fixed, such that we find

$$\#\text{ZZPs} - 3 = \#\text{Fractional Branes} \,, \tag{6.18}$$

which is also the number of non-compact four-cycles. In other words, this construction can account for the most general anomaly-free rank assignment, up to an overall shift of the ranks (*i.e.* regular branes). Generically, this algorithm can produce negative ranks for some faces, which cannot be

directly interpreted as ranks of gauge groups. Of course, one may always add regular branes until all ranks are positive.[6]

Let us illustrate Butti's algorithm with two examples, to which we will return when discussing orientifolds.

Example of dP_1

Consider the toric phase of the complex cone over dP_1, or dP_1 for short, which is shown in Figure 6.15. Let us apply the method described above for the computation of the fractional branes.

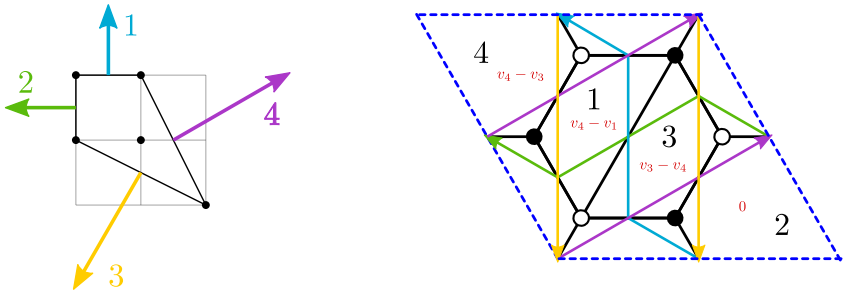

(a) (b)

Figure 6.15: ZZPs of dP_1 and the rank assignments coming from them: (a) Toric diagram. (b) Dimer model.

Let us choose $N_2 = 0$. Applying the algorithm, the other faces are assigned the following ranks:

$$\begin{array}{lcl} N_1 & \leftrightarrow & v_4 - v_1 \\ N_2 & \leftrightarrow & 0 \\ N_3 & \leftrightarrow & v_3 - v_4 \\ N_4 & \leftrightarrow & v_4 - v_3 \end{array} \tag{6.19}$$

[6]It is worth noting that this procedure is closely related to the algorithm for constructing fractional brane rank assignments introduced in [134], in which the difference in the ranks between two nodes in the quiver is proportional to the baryonic $U(1)_B$ charge of the bifundamental field connecting them, with one independent vector for each baryonic $U(1)_B$. The relation between the two methods is through the correspondence between baryonic $U(1)_B$ symmetries and extremal perfect matchings [158] or, equivalently, ZZPs (which correspond to differences between consecutive external perfect matchings). Our procedure is also equivalent to the one for labeling cluster variables associated with plabic (*i.e.* planar bicolored) graphs using ZZPs [159], and to the even more similar one in the context of cluster integrable systems [160] that associates a divisor at infinity on the spectral curve, to each face of the bipartite fat graph under consideration [161].

From the toric diagram we read the two topological constraints:

$$\left\{\begin{array}{rcrcl} \Lambda &=& -v_2 - v_3 + 2v_4 &=& 0 \\ M &=& v_1 + v_4 - 2v_3 &=& 0 \end{array}\right. \Leftrightarrow \left\{\begin{array}{rcl} v_1 &=& 2v_3 - v_4 \\ v_2 &=& -v_3 + 2v_4 \end{array}\right. \tag{6.20}$$

We can further use a global shift of the v_i to set $v_4 = 0$ and find the following rank assignment:

$$\begin{array}{rcrcl} \mathbf{v} &=& (v_1, v_2, v_3, v_4) &=& (2, -1, 1, 0)v_3\,, \\ \mathbf{N} &=& (N_1, N_2, N_3, N_4) &=& (-2, 0, 1, -1)v_3\,. \end{array} \tag{6.21}$$

Example of $\mathbf{PdP_4}$

As a slightly more complicated example, let us study the case of the PdP_4 singularity [129] in the toric phase considered in [2] and given in Figure 6.16.

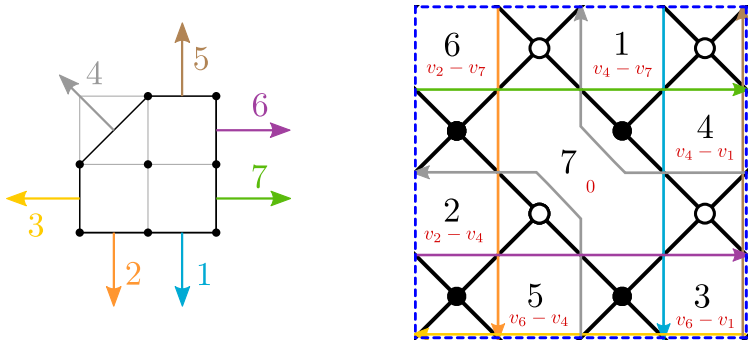

(a) (b)

Figure 6.16: ZZPs of PdP_4 and the rank assignments coming from them: (a) Toric diagram. (b) Dimer model.

From the toric diagram we read:

$$\left\{\begin{array}{rcl} \Lambda &=& v_6 + v_7 - v_3 - v_4 = 0 \\ M &=& v_5 + v_4 - v_1 - v_2 = 0 \end{array}\right. \Leftrightarrow \left\{\begin{array}{rcl} v_3 &=& v_6 + v_7 - v_4 \\ v_5 &=& v_1 + v_2 - v_4 \end{array}\right. \tag{6.22}$$

Since a global shift in the v_i does not change the rank assignments, we can impose $v_4 = 0$. We then find the following rank assignment,

$$\begin{array}{l} \mathbf{v} = (v_1, v_2, v_6 + v_7, 0, v_1 + v_2, v_6, v_7) \\ \quad \rightarrow \quad \mathbf{N} = (-v_7, v_2, v_6 - v_1, -v_1, v_6, v_2 - v_7, 0)\,. \end{array} \tag{6.23}$$

6.3.2 Classification of fractional branes

A classification of fractional branes based on the IR dynamics of the gauge theories living on them was introduced in [67]. According to it, fractional branes fall into three classes: deformation, $\mathcal{N} = 2$ and DSB fractional branes. We also know how to detect them from the toric diagram. Moreover, we can use Butti's algorithm in order to the set of definite values v_Γ that allow to turn on the fractional branes.

Deformation branes

These branes correspond to isolated faces in the dimer touching each other at nodes (so, only gauge groups and no bifundamental fields are involved) or to isolated clusters of faces surrounding a given node (where the corresponding superpotential term and fields are turned on). The gauge theory is then either a set of decoupled SYM theories, or SYM theories coupled via a superpotential term, respectively. In both cases, the low energy effective theory leads to confinement and the geometry undergoes a complex structure deformation.

Two examples of deformation branes are reported in figure 6.17. Note

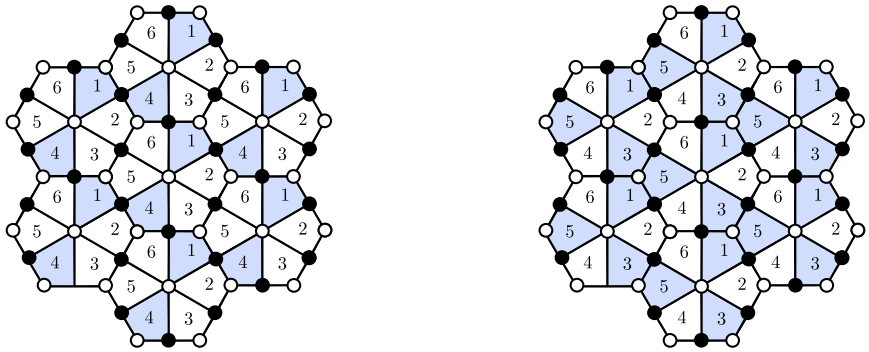

(a) (b)

Figure 6.17: The dimer of the $dP3$ singularity, which admits both classes of deformation branes. (a) Deformation fractional branes corresponding to isolated nodes. (b) Deformation fractional branes corresponding to loops in the quiver.

that single faces are allowed deformation branes only for non-chiral theories. Chiral theories may admit deformation branes but these correspond to

clusters, or two or more isolated faces. The $dP3$ dimer in the figure is one such chiral example.

The presence of deformation branes can be inferred from the toric diagram, or the (p, q)-web [140, 162] and equivalently from the set of ZZPs. They are present whenever the toric diagram can be decomposed in several Minkowski summands. In terms of ZZPs, the theory will have a deformation fractional brane if there is a subset of m ZZPs in equilibrium $\{v_\sigma\} \subset \{v_\Gamma\}$, such that

$$\sum_{i=1}^{m} (p_{\sigma_i}, q_{\sigma_i}) = 0\,. \tag{6.24}$$

The deformation brane is turned on whenever all v_σ have the same value, distinguished from the one of all others $v_\tau \notin \{v_\sigma\}$, see Figure 6.18 for an example.

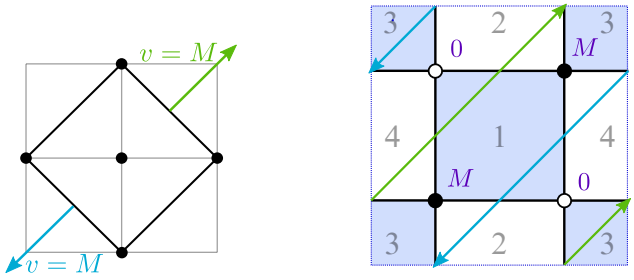

(a) Toric diagram. (b) Dimer model.

Figure 6.18: M deformation branes in a phase of F_0 turned on with two ZZPs having $v = M$.

$\mathcal{N} = 2$ fractional branes

These fractional branes support a gauge-invariant operator that does not appear in the superpotential. In dimer language, they correspond to a collection of faces forming a stripe, which gives rise to the closed path in the quiver associated with this gauge-invariant operator. The VEV of such an operator parametrizes a flat direction along which the dynamics reduces to an $\mathcal{N} = 2$ theory. Geometrically, $\mathcal{N} = 2$ fractional branes arise in the case of non-isolated singularities, which have complex curves of singularities passing through the origin. Such fractional branes wrap a two-cycle collapsed at the singularity, which exists at every point along the curve.

In the case of toric geometries, the singularity on the curve is always

$\mathbb{C}^2/\mathbb{Z}_k$, $k \geqslant 2$. Such a singularity translates into edges on the boundary of the toric diagram with $k-1$ consecutive external but non-extremal points. Equivalently, they correspond to k parallel legs in the dual (p,q)-web diagram [123, 163, 164]. Indeed, the stripe of faces in the dimer describing an $\mathcal{N}=2$ stretches between a pair of ZZP with the same holonomy, say (p_μ, q_μ). From Butti's algorithm, we learn that they are turned on whenever only some of these v_μ, among the whole set of ZZPs $\{v_\Gamma\}$, are non-vanishing. The stripe bounded by consecutive ZZPs μ_1 and μ_2 is turned on when

$$v_{\mu_1} = -v_{\mu_2} \neq 0\,, \qquad \text{and} \qquad v_\nu = 0 \quad \text{for } \nu \neq \mu_1,\, \mu_2\,. \tag{6.25}$$

Finally, let us emphasize that the previous discussion implies that the gauge theories/dimers associated with toric diagrams without external but non-extremal points, *i.e.* without non-isolated singularities, do not support $\mathcal{N}=2$ fractional branes.

Figure 6.19 shows an example, based on the PdP_3 geometry [2, 129], illustrating the ideas presented above. The collection of phases shaded in blue defines an $\mathcal{N}=2$ fractional brane (its complement is obviously also an $\mathcal{N}=2$ fractional brane). These faces stretch between the parallel red and green ZZPs.

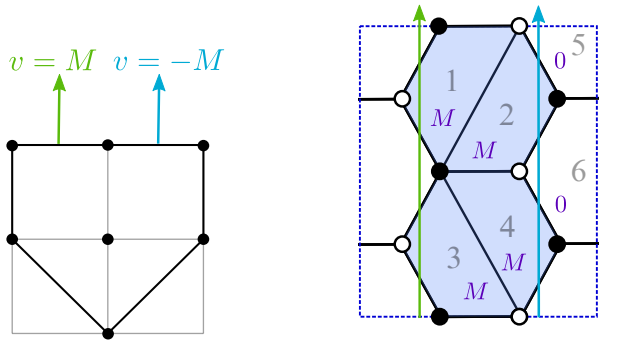

(a) Toric diagram of PdP_3.

(b) Dimer model of PdP_{3b}.

Figure 6.19: M copies of a $\mathcal{N}=2$ fractional brane phase b of PdP_3 turned on with two ZZPs having $v = \pm M$.

Dynamical SUSY breaking branes

Any other kind of anomaly-free rank assignment usually leads to a dynamically generated superpotential and hence breaks supersymmetry dynamically [165] (usually into runaway directions [66–68]). These branes are

called DSB fractional branes. The ranks found for dP_1 in Equation (6.21) correspond to a well-known DSB fractional brane.

Generically, combinations of several fractional branes may provide other types of fractional branes. For example, the combination of an $\mathcal{N} = 2$ fractional brane with a deformation fractional brane may correspond to a DSB one. Similarly, the combination of two deformation fractional branes can be a DSB brane, when the corresponding complex structure deformations are incompatible with each other.

Part II

Orientifolds in Dimer Models

Chapter 7

Orientifolds

Orientifolds are non-dynamical extended objects in string theory. They may be thought of as a generalization of orbifolds with an action on the worldsheet. Hence, they open the door to extra non-oriented sectors of propagating strings. They share some common features with D-branes, as they have tension and are charged under RR fields. The two kinds of extended objects can be placed on top of each other, and this has the effect to change the low energy gauge theory accordingly. We will mostly think about orientifolds in these terms, as a way to find new kinds of quivers, with SO/USp nodes and (anti)symmetric matter. They play an important role in the construction of dynamical supersymmetry breaking models in string theory.

We start by reviewing the construction of orientifolds in string theory, see [52, 166–170] for further details. We then move on to their implementation in dimer models [54].

7.1 Orientifolds from the worldsheet

7.1.1 Orientifolds and supersymmetry

An orientifold projection of a string theory is obtained by gauging an involution symmetry acting on the worldsheet. It is typically combined with an action on the embedding spacetime $\mathbb{R}^{1,3} \times \mathcal{M}_6$, where we will impose $\mathcal{M}_6$ to be a CY threefold.

In the present case, we want the elements g_Ω of the orientifold group

G_Ω to be composed of a parity action on the worldsheet:

$$\Omega \quad : \quad \begin{cases} (\sigma_0, \sigma_1) \to (\sigma_0, 2\pi - \sigma_1) & \text{for closed strings,} \\ (\sigma_0, \sigma_1) \to (\sigma_0, \pi - \sigma_1) & \text{for open strings.} \end{cases} \tag{7.1}$$

We thus have to find an element R such that $g_\Omega = \Omega R$ is an actual symmetry of the theory. In type IIB superstring theory, R will generically be a product of $(-1)^{F_L}$ and σ, where F_L counts the number of left-moving fermions in spacetime, and σ is a holomorphic involution and an isometry of the CY. The orientifold plane will be defined as the fixed loci of σ. We will refer to it as the Op-plane, where p counts the number of spatial dimensions fixed by σ. This plane is non-dynamical because it is fixed by the latter geometrical action.

In type IIB theories, in order for σ to be an involution, it has to satisfy

$$\sigma(J_2) = +J_2 \,, \quad \sigma(\Omega_3) = \pm\Omega_3 \,. \tag{7.2}$$

This follows from the fact that σ is holomorphic. The orientifold action will act on spinors, and in particular the supercharges. In consequence, σ will be subject to further supersymmetry preserving constraints. As for D-branes, the dimension of the plane p is fixed to be odd by supersymmetry so that they preserve a common set of supercharges. We then find

$$\begin{array}{lll} \text{O3/O7} & : & R = (-1)^{F_L}\sigma \,, \quad \sigma(\Omega_3) = -\Omega_3 \,, \\ \text{O5/O9} & : & R = \sigma \,, \qquad\quad\; \sigma(\Omega_3) = +\Omega_3 \,. \end{array} \tag{7.3}$$

As explained in [171], this is valid for any CY space.

Since we will focus on D3-branes at singularities. We will admit only O3 and O7 planes, thus considering a type IIB superstring theory on

$$\mathbb{R}^{1,3} \times \frac{\text{CY}}{\Omega(-1)^{F_L}\sigma} \,, \tag{7.4}$$

where σ will distinguish between the two possible dimensions of the Op-planes, $p = 3$ and 7. Note in passing that $\Omega(-1)^{F_L}$ is an element of the $SL(2,\mathbb{Z})$ of type IIB. In the conventions of Section 3.1.1, we find

$$\Omega(-1)^{F_L} = \begin{pmatrix} -1 & 0 \\ 0 & -1 \end{pmatrix} \in SL(2,\mathbb{Z}) \,. \tag{7.5}$$

7.1.2 Orientifold charge and tension

Just like D-branes, orientifolds have charge and tension, the main difference being that they are non-dynamical. A complete review of the classification of orientifolds according to their charge is provided in [172] and we summarize it here.

To compute the charge of an Op-plane, we need to integrate fluxes over a "sphere" surrounding the plane. The action σ will typically act as an involution on space transverse to the Op-plane, such that we have to integrate the flux over $S^{8-p}/\mathbb{Z}_2 \simeq \mathbb{RP}^{8-p}$. This allows for twisted forms to have non-trivial backgrounds[1]. Since $\tilde{H}^3(\mathbb{RP}^5) = \tilde{H}^3(\mathbb{RP}^1) = \mathbb{Z}_2$ we find that both O3-planes and O7-planes can have two kind of charges with respect to the flux $H_3 = \mathrm{d}B_2$. In general, we will say that Op^- and Op^+-planes have trivial and non-trivial charges under this flux respectively. In general, an Op-plane can also have a charge with respect to the flux of $F_{6-p} = \mathrm{d}C_{5-p}$. In our case of interest, we note that O3-planes can have a discrete torsion charge $\mathbb{Z}_2$ with respect to the $F_3 = \mathrm{d}C_2$ flux. We label O3-planes with non-trivial RR discrete torsion charges $\widetilde{\mathrm{O3}}$. In units of D-branes charges, those of the orientifolds and, more importantly for us, the gauge groups for D-branes placed on Op-planes are recalled in Table 7.1.

Op-planes	RR charges	Gauge groups
Op^-	-2^{p-5}	$SO(N)$ with N even
Op^+	$+2^{p-5}$	$USp(N)$ with N even
$\widetilde{\mathrm{O}p}^-$	$1/2 - 2^{p-5}$	$SO(N)$ with N odd
$\widetilde{\mathrm{O}p}^+$	$+2^{p-5}$	$USp(N)$ with N even

Table 7.1: RR charges (in units of D-branes charge) and gauge groups for the different kinds of orientifolds.

Orientifolds can sometimes have negative tension. For instance, it can be computed for O9-planes exchanging unoriented strings that

$$T_{\mathrm{O9}^-} = -16 T_{\mathrm{D9}}\,. \tag{7.8}$$

[1]It can be checked that the orientifold action sends B_2 and C_2 to minus themselves, *i.e.* they are twisted, while other forms are preserved. We thus need to distinguish usual cohomologies H^q with twisted cohomologies $\tilde{H}^q$. One has

$$H^q(\mathbb{RP}^{8-p}) = \begin{cases} \mathbb{Z}_2 & \text{for } q > 0 \text{ even} \\ \mathbb{Z} & \text{for } q = 0 \text{ or } q = 8-p \text{ odd} \\ 0 & \text{otherwise} \end{cases}, \tag{7.6}$$

and

$$\tilde{H}^q(\mathbb{RP}^{8-p}) = \begin{cases} \mathbb{Z}_2 & \text{for } q \text{ odd} \\ \mathbb{Z} & \text{for } q = 8-p \text{ even} \\ 0 & \text{otherwise} \end{cases}. \tag{7.7}$$

Note that there exists an alternative notation for cohomologies: $H^q(\bullet) \equiv H^q(\bullet, \mathbb{Z})$ and $\tilde{H}^q(\bullet) \equiv H^q(\bullet, \tilde{\mathbb{Z}})$.

D-branes can be added on top of this O-plane at the price to balance this NSNS repulsion. We can thus add 16 D9-branes on top of an O9$^-$-plane, knowing that there is an attraction between them due to RR fields:

$$Q_{\mathrm{RR,O9^-}} = -16 Q_{\mathrm{RR,D9}} \,. \tag{7.9}$$

A gauge theory is obtained from the low energy of unoriented open strings on the worldvolume of the D-branes, and it has gauge group $SO(32)$ (the strings can attach to the 16 D-branes or to their orientifold mirrors). From the 32 supersymmetries of type IIB, half are broken by the presence of extended planes. What we just described is how to get type I superstring theory from type IIB.

Finally, let us comment that orientifolds placed at the tip of CY singularities will behave similarly as fractional branes and in particular can also have fractional charges. Hence, we expect to generically lose conformality in presence of orientifolds.

7.1.3 Orientifolded open string sector

Since we will be interested in the gauge theory living on the worldvolume of D3-branes, we look at the projection on open string states. Let be

$$\lambda^a_b \otimes \psi^M_{-1/2} \, |k\rangle \tag{7.10}$$

an open string state of impulsion k. We saw in Section 3.1.2 that for $M = \mu = 0, \cdots, 3$, the state is a (generically non-abelian) gauge boson. For $M = i = 4, \cdots, 9$, it is a real scalar. We introduce a non-trivial action on Chan-Paton factors that has to be consistent with the orientifold projection:

$$\lambda \to \gamma_\Omega \lambda^T \gamma_\Omega^{-1} \quad \text{with} \quad \gamma_\Omega^T \gamma_\Omega^{-1} = \mathbb{1}_{N\times N} \,. \tag{7.11}$$

The transposition is necessary because the worldsheet parity reverses the endpoints of the open string. The condition on γ_Ω comes from the fact that the orientifold should be an involution. It can be seen from vertex algebra that the worldsheet parity does not treat gauge vectors and scalars in the same way. For instance, the gauge vector is sent to minus itself. Knowing that the scalars are mixed by σ, we can define the following orientifold action on $\psi^M_{-1/2}$:

$$\psi^M_{-1/2} \to R^M_N \psi^N_{-1/2} \quad \text{with} \quad R = \begin{pmatrix} -\mathbb{1}_{4\times 4} & 0 \\ 0 & \sigma \end{pmatrix} . \tag{7.12}$$

The states surviving the orientifold projection are those invariant under the combination of Equation (7.11) and Equation (7.12).

Examples of O3-planes on flat space

As usual, start with a stack of N D3-branes on flat space. We can choose to place the stack on different kind of orientifold planes. These different choices are hidden in the solutions of the constraint on γ_Ω shown in Equation (7.11).

Orthogonal gauge group. A first choice is to take γ_Ω to be the identity matrix. Initially, we have gauge bosons defined as

$$(A^\mu)^a_b = \lambda^a_b \otimes \psi^\mu_{-1/2}\,. \tag{7.13}$$

The surviving gauge bosons will thus be projected in the adjoint of the group $SO(N)$:

$$\gamma_\Omega = \mathbb{1}_{N\times N} \;:\quad A^\mu = -(A^\mu)^T\,. \tag{7.14}$$

One needs to know σ in order to get the action on the three complex matter fields

$$(\Phi^I)^a_b = \lambda^a_b \otimes \psi^I_{-1/2}\,. \tag{7.15}$$

Consider the O3-plane action defined by σ inverting all the (holomorphic) coordinates of flat space:

$$\gamma_\Omega = \mathbb{1}_{N\times N}\,,\quad \sigma = -\mathbb{1}_{3\times 3} \quad:\quad \Phi^I = -(\Phi^I)^T = \begin{array}{|c|}\hline\;\;\\\hline\end{array}\,. \tag{7.16}$$

Symplectic gauge group. For N even, one can consider γ_Ω to be the antisymmetric matrix defined by

$$\mathbb{J}_N \equiv \begin{pmatrix} 0 & \mathbb{1}_{N\times N} \\ -\mathbb{1}_{N\times N} & 0 \end{pmatrix}\,. \tag{7.17}$$

Then, the resulting gauge bosons are elements of the Lie algebra of $USp(N)$,

$$\gamma_\Omega = \mathbb{J}_N \;:\quad A^\mu = -\mathbb{J}_N (A^\mu)^T \mathbb{J}_N^{-1}\,. \tag{7.18}$$

Consider the same action σ as before,

$$\gamma_\Omega = \mathbb{J}_N\,,\quad \sigma = -\mathbb{1}_{3\times 3} \quad:\quad \Phi^I = -\mathbb{J}_N (\Phi^I)^T \mathbb{J}_N^{-1} = \square\!\square\,. \tag{7.19}$$

In each of these cases, the superpotential is not modified because the chiral superfields are mapped onto themselves. However, when two different fields will be mapped onto each other, we can expect to see the number of superpotential terms reduced.

7.1.4 Fractional branes and orientifolds

Orientifold projections generically change the number of independent fractional branes that one can obtain at the tip of a given CY singularity. This can be understood from the projection of the $\mathcal{N} = 1$ multiplets as follows.

- When a gauge vector A_i^μ is mapped onto itself, as in the examples of the previous section,
$$A_i^\mu \sim A_i^{\mu T}\,, \tag{7.20}$$
it replaces the gauge group $SU(N_i)$ by $SO(N_i)$ or $USp(N_i)$. None of these new gauge groups have complex fundamental representations.[2] Hence, they are not subject to ACC and this reduces the number of equations to consider.

  When a gauge vector A_i^μ is not mapped onto itself, it is identified to another vector A_j^μ:
$$A_i^\mu \sim A_j^{\mu T} \quad \text{for } i \neq j\,. \tag{7.21}$$
This results in the identification of $SU(N_i)$ and $SU(N_j)$, and in particular of N_i and N_j. The number of ACC for these kinds of gauge groups is thus halved, but also is the number of independent parameters N_i.

- When a chiral superfield is self-identified, we saw that it becomes a symmetric or antisymmetric tensor. If it is defined as a representation of a gauge group $SU(N)$, it contributes to ACC with coefficients given by
$$d_{\square\!\square} = (N+4)d_{\square}\,, \quad d_{\substack{\square\\\square}} = (N-4)d_{\square}\,, \tag{7.22}$$
where $d_{\square}$ is the weight of the fundamental representation. Remember also that
$$d_{\overline{\mathbf{R}}} = -d_{\mathbf{R}}\,. \tag{7.23}$$
The effect of the extra ± 4 will be very important because it turns the ACC into a non-homogeneous problem. In particular, the existence of solutions is not guaranteed anymore.

This discussion boils down to say that ACC, as we knew them, will be heavily affected by the orientifold projection. It is difficult to anticipate naively what kind of singularity may lead to a non-anomalous orientifolded

[2] The fundamental representations of $SO(N)$ and $USp(N)$ are real and pseudo-real respectively.

theory. Of course, dimer models will come to the rescue, and clarifying this situation will actually be the subject of Chapter 8. Note in passing that one way to cure anomalous orientifolds is to modify the initial brane setup by adding D7-branes that participate to the gauge dynamics as *flavor branes*. Those can effectively balance the ± 4 and lead to trivially satisfied ACC after orientifold projection. However, we will limit ourselves to regular and fractional D3-branes in this work and try to fulfil the non-trivial task of finding orientifold solutions in the absence of flavor branes.

Orientifolds may change the nature of fractional branes too. Again, no clear rules are established but examples of different phenomena have been collected in the past. We will focus on deformation branes to exemplify our purpose in this section.

An orientifold version of the deformation brane in the conifold was studied in [173]. The gauge group is projected to $SO(N_1) \times USp(N_2)$ with two fields in the bifundamental representation $(\Box_1, \Box_2)$. Using Seiberg duality for orthogonal and symplectic gauge groups and their NSVZ β functions, the authors found the following cascading RG-flow:

$$\begin{aligned} SO(N+M+2)_1 \times USp(N)_2 &\to SO(N-M+2)_1 \times USp(N)_2 \\ &\to SO(N-M+2)_1 \times USp(N-2M)_2 \,, \end{aligned} \tag{7.24}$$

that can be continued until confinement is reached. Note that the two steps together reduce all the effective number of regular branes N by $2M$. This example is a straightforward generalization of the usual cascade, and the authors argue that it leads to a deformed moduli space in the infrared too.

This is quite different from what has been observed in [55]. There, an orientifold of F_0 is presented and leads to a gauge groups product $USp(N_1) \times SU(N_2) \times USp(N_3)$. The latter combination admits a deformation such that $N_1 = N_3 = N + M$ and $N_2 = N$. We can compute the following sequence of Seiberg dualities:

$$\begin{aligned} & USp(N+M)_1 \times SU(N)_2 \times USp(N+M)_3 \\ \to \quad & USp(N-M-4)_1 \times SU(N)_2 \times USp(N-M-4)_3 \\ \to \quad & USp(N-M-4)_1 \times SU(N-2M-8)_2 \times USp(N-M-4)_3 \,, \end{aligned} \tag{7.25}$$

A special feature of this cascading RG-flow is thus to change the effective number of fractional branes, in addition to the regular ones. Indeed, a full sequence in the cascade decreases N by $2M+8$, and increases M by 4.[3] This implies that the cascade is triggered even in the absence of fractional branes

[3] An instance of quiver with flavors, without orientifold projection, proposed in [174] led to cascade with a *decreasing* effective number of fractional branes.

and generates them on its way towards the infrared. Moreover, climbing the RG-flow towards the UV, one finds that the cascade stops at a definite value for the ranks. For suitably chosen M, the gauge theory at the top of the cascade can be made UV-free.

The difference between these two cascades can be understood technically from the number of SO and USp factors. The balance of these in the example of the conifold led Seiberg dualities to generate a cascade similar to the one experienced on a non-orientifolded conifold, whereas the excess of USp in the case of F_0 drastically changed its behavior. Indeed, the ranks of the gauge groups were modified by Seiberg dualities such that M had to be affected. Once again, this conclusion is sensible to the addition of flavor branes [175].

7.2 Fixed points and lines in dimer models

Orientifold projections on D-branes at singularities and their description on dimers were studied in [54]. Related works include [176–178]. In this framework, the orientifold projection corresponds to a $\mathbb{Z}_2$ involution acting on the torus that identifies faces, edges and vertices in an appropriate way. The authors of [54] studied involutions with fixed loci, see Figure 7.1 to contemplate the three explored possibilities, and resulting in a set of rules needed to construct the projected theory that we summarize below.

1. Self-identified faces project to SO/USp groups, depending on the fixed locus charge, + or − respectively.[4] All other faces are identified with their image, merging to one SU group.

2. Every edge on top of a fixed locus becomes a symmetric or antisymmetric tensor (or their conjugate), depending on the fixed locus charge, + or − respectively. The remaining edges are identified with their images, merging to bifundamental fields. More concretely, bifundamentals are identified as follows:

$$(\overline{\square}_i, \square_j) \sim (\overline{\square}_{j'}, \square_{i'}) \to (\overline{\square}_i, \square_j)\,, \tag{7.26}$$

   where i', j' are the images of gauge groups i, j.

3. The superpotential is found upon the projection of the fields.

[4] Charges of fixed loci are related to the charges of the O-planes [54, 176], even though they are not always of the same sign in our conventions.

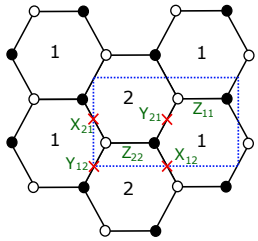

(a)

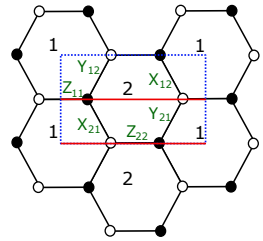

(b)

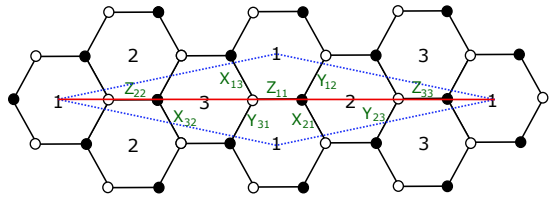

(c)

Figure 7.1: (a) Orientifold of $\mathbb{C}^2/\mathbb{Z}_2$ with fixed points. (b) Orientifold of $\mathbb{C}^2/\mathbb{Z}_2$ with two fixed lines. (c) Orientifold of $\mathbb{C}^2/\mathbb{Z}_3$ with a single fixed line.

Before moving on to the next section, we present in detail the three kind of orientifold involutions studied in [54] with examples.

Fixed points

In an orientifold of this type, there are four fixed points in a unit cell. In order to preserve SUSY, their signs must satisfy the so-called *sign rule* [54]: their product must be $(-1)^{N_W/2}$ where N_W is the number of superpotential terms.

In the example of Figure 7.1a, we choose the signs $(-+-+)$, starting with the fixed point at the origin of the unit cell and going clockwise. We have that face 1 is identified with face 2, meaning that the resulting theory will have only one gauge group $SU(N)$. The bifundamental fields are

identified as follows

$$\begin{array}{lllll} Y_{12} \sim Y_{12} & \to & \begin{array}{|c|}\hline \\ \hline \\ \hline \end{array}, & X_{21} \sim X_{21} & \to \quad \square\square, \\ Y_{21} \sim Y_{21} & \to & \begin{array}{|c|}\hline \\ \hline \\ \hline \end{array}, & X_{12} \sim X_{12} & \to \quad \overline{\square\square}, \end{array} \qquad (7.27)$$
$$Z_{11} \sim Z_{22} \to \text{Adj}\,.$$

and the superpotential is given by

$$W = X_{12}Y_{21}Z_{11} - X_{21}Y_{12}Z_{11}\,, \qquad (7.28)$$

where we implicitly take a trace over gauge indices.

To be sure that this projection preserves some supersymmetry, we need to check the action of the involution on Ω_3. To do so, we need to link the action on the fields to a spatial action on the coordinate of the CY variety. We compute the mesonic moduli space of our theory, which correspond to the singularity D3-branes are probing. Mesonic operators are given by

$$\begin{array}{lllllll} x & = & X_{12}X_{21}\,, & y & = & Y_{12}Y_{21}\,, \\ w_1 & = & Y_{12}X_{21}\,, & w_2 & = & Y_{21}X_{12}\,, \\ z_1 & = & Z_{11}\,, & z_2 & = & Z_{22}\,. \end{array} \qquad (7.29)$$

F-term equations impose

$$w_1 = w_2 \equiv w\,, \qquad (7.30)$$

and

$$z_1 = z_2 \equiv z\,, \qquad (7.31)$$

and the classical relation between the fields gives

$$xy = w^2\,. \qquad (7.32)$$

Thus, the mesonic moduli space is the symmetric product of N copies of the A_1 singularity, consistently with what was found in Chapter 4 and where N is the number of probe D3-branes. The holomorphic 3-form Ω_3 can be easily computed using the Poincaré residue formula:

$$\Omega_3 = \text{Res}\frac{\mathrm{d}x \wedge \mathrm{d}y \wedge \mathrm{d}w \wedge \mathrm{d}z}{w^2 - xy} = \frac{\mathrm{d}x \wedge \mathrm{d}y \wedge \mathrm{d}z}{2w}\,. \qquad (7.33)$$

Under the involution, the fields are mapped in the following way

$$\begin{array}{ll} x \to x\,, & y \to y\,, \\ w \to -w\,, & z \to z\,, \end{array} \qquad (7.34)$$

where the sign taken by a meson is given by the product of the fixed point charges it crosses. The orientifold action on the holomorphic 3-form is thus odd, $\Omega_3 \to -\Omega_3$, meaning that the O-plane is compatible with the supersymmetry charges preserved by the D3-branes. It is easy to see that sign configuration not respecting the sign rule is not supersymmetric.

Horizontal/Vertical fixed lines

In the example of Figure 7.1b, we have two fixed lines, each one coming with a sign, + or −, which is unconstrained. We chose to assign − to the bottom line and + to the other. The faces are self-identified, leading to a gauge group $USp(N_1) \times SO(N_2)$. The identification of fields gives

$$\begin{array}{ll} Y_{12} \sim X_{21} \to Q^1_{12}\,, & X_{12} \sim Y_{21} \to Q^2_{12}\,, \\ Z_{11} \sim Z_{11} \to \begin{array}{|c|}\hline \\ \hline \end{array}\,, & Z_{22} \sim Z_{22} \to \square\square\,. \end{array} \tag{7.35}$$

and the superpotential is given by

$$W = (Q^2_{12}Q^{2T}_{12} - Q^1_{12}Q^{1T}_{12})Z_{11} + (Q^{2T}_{12}Q^2_{12} - Q^{1T}_{12}Q^1_{12})Z_{22}\,. \tag{7.36}$$

The mesons are the same as in the previous example since the geometry is the same, but the action of the orientifold is different and given by

$$x \leftrightarrow y\,, \quad w \to -w\,, \quad z \to -z\,, \tag{7.37}$$

where the fixed line exchanges two mesons and introduces a sign to the self-mapped mesons given by the product of the signs of the two fixed lines crossed. We can again see that the SUSY condition is respected

$$\Omega_3 = \frac{\mathrm{d}x \wedge \mathrm{d}y \wedge \mathrm{d}z}{2w} \to \frac{\mathrm{d}y \wedge \mathrm{d}x \wedge \mathrm{d}z}{2w} = -\Omega_3\,. \tag{7.38}$$

In particular, we see that the signs of the fixed lines play no role in the last relation.

Diagonal fixed line

Finally, we have a single fixed line in the example of Figure 7.1c. Again, the choice of sign for the line is unconstrained. We choose a + sign. All faces are self-identified, and the gauge factors are thus $SO(N_1) \times SO(N_2) \times SO(N_3)$. The identification of fields is as follows:

$$\begin{array}{lll} Y_{12} \sim X_{21} \to Q_{12}\,, & X_{13} \sim Y_{31} \to Q_{31}\,, & Y_{23} \sim X_{32} \to Q_{23} \\ Z_{11} \sim Z_{11} \to \square\square\,, & Z_{22} \sim Z_{22} \to \square\square\,, & Z_{33} \sim Z_{33} \to \square\square\,. \end{array} \tag{7.39}$$

The superpotential is originally given by

$$W = X_{21}Y_{12}Z_{22} - Y_{23}X_{32}Z_{22} + X_{13}Y_{31}Z_{11} - X_{21}Y_{12}Z_{11} + X_{32}Y_{23}Z_{33} - Y_{31}X_{13}Z_{11}\,, \tag{7.40}$$

and becomes

$$W = Q_{12}^2 Z_{22} - Q_{23}^2 Z_{22} + Q_{31}^2 Z_{11} - Q_{12}^2 Z_{11} + Q_{23}^2 Z_{33} - Q_{31}^2 Z_{11} \,. \quad (7.41)$$

As before, we can find the mesonic invariants:

$$\begin{array}{rclcrcl} x & = & X_{13}X_{32}X_{21}\,, & & y & = & Y_{12}Y_{23}Y_{31}\,, \\ w_1 & = & Y_{12}X_{21}\,, & & w_2 & = & Y_{23}X_{32}\,, \\ w_3 & = & Y_{31}X_{13}\,, & & z_1 & = & Z_{11}\,, \\ z_2 & = & Z_{22}\,, & & z_2 & = & Z_{33}\,. \end{array} \quad (7.42)$$

From F-terms equations, we find

$$\begin{array}{c} w_1 = w_2 = w_3 \equiv w\,, \\ z_1 = z_2 = z_3 \equiv z\,, \end{array} \quad (7.43)$$

and then

$$xy = w^3\,. \quad (7.44)$$

The action of the orientifold on mesons in the dimer model is found to be

$$x \leftrightarrow y\,, \quad w \to +w\,, \quad z \to +z\,. \quad (7.45)$$

Consistently, the orientifold action on Ω_3 is odd:

$$\Omega_3 = \frac{\mathrm{d}x \wedge \mathrm{d}y \wedge \mathrm{d}z}{3w^2} \to \frac{\mathrm{d}y \wedge \mathrm{d}x \wedge \mathrm{d}z}{3w^2} = -\Omega_3\,. \quad (7.46)$$

Chapter 8

Anomalies

This chapter is devoted to the study of non-abelian anomalies in gauge theories coming from D-branes at orientifolds of toric singularities, in the *absence* of flavor branes. We will introduce a new geometric algorithm for constructing anomaly-free theories and identify geometric necessary criteria for the existence of such solutions for orientifolds realized as "fixed points" and "fixed line(s)" involutions in dimer models. Remarkably, our results allow us to determine whether an orientifold singularity can admit anomaly-free D-brane gauge theories just by analyzing its geometric structure and avoiding any case-by-case analysis, which has been so far the only known approach for this class of theories. This geometric criterion is therefore a new addition to the list of connections between the geometry of singularities and general properties of the resulting gauge theories, some of which were mentioned in the previous chapters. Our results were originally presented in [5].

The presentation is organized as follows. In Section 8.1, we consider anomalies in orientifolds, for which cancellation conditions generically correspond to non-homogeneous linear systems of equations due to the presence of tensor matter. In Section 8.2, we generalize the algorithm for solving anomaly cancellation conditions based on zig-zag paths to the case of orientifolds. This analysis will lead to the main result of the chapter, which we present in Section 8.3: a purely geometric criterion for anomaly cancellation conditions in orientifold field theories just based on the toric data of the singularity. Section 8.4 contains a summary of our results and an outlook.

8.1 Anomaly cancellation conditions in orientifolds

Determining whether an orientifolded theory admits anomaly-free solutions and, if so, finding them is a relatively straightforward task on a case-by-case basis. Indeed, writing down the set of anomaly equations for every gauge group and looking for solutions is not more complicated than for non-orientifolded models. In this section we systematize this calculation, introducing an algorithm for finding anomaly-free solutions in the presence of orientifolds. This, in turn, will allow us to relate the calculation to the one in the unorientifolded theory and, at a later stage, to extend the geometric determination of solutions in terms of zig-zag paths to orientifolds.

In what follows, we will refer to the original, unorientifolded theory as the *mother theory*. Similarly, we will dub the orientifolded theory the *daughter theory*. As described in Section 5.3 finding an anomaly-free rank assignment for the mother theory amounts to finding the kernel of its adjacency matrix. More precisely, we are looking for the kernel of

$$A = \mathrm{adj}(\mathcal{Q}) - \mathrm{adj}(\mathcal{Q})^T \,, \tag{8.1}$$

with $\mathrm{adj}(\mathcal{Q})$ is the proper adjacency matrix of the quiver, see the discussion in Section 5.3. Tensor matter in the daughter theory modifies the ACC, dovetailing the contribution of the O-planes to the RR-charges that must cancel in compact homology. In general, the anomaly/tadpole problem of orientifolded theories corresponds to a non-homogeneous linear system of the form:

$$\bar{A} \cdot N = f \,, \tag{8.2}$$

where $\bar{A}$ is the adjacency matrix of the daughter theory, and f stands for the additional contribution of tensor matter. The difference between two solutions of the system Equation (8.2) is a solution of the corresponding homogeneous one, *i.e.* it is in the kernel of $\bar{A}$. If one knows a particular solution N_{part} of Equation (8.2), every solution N can be expressed as:

$$N = N_{\mathrm{hom}} + N_{\mathrm{part}} \,, \tag{8.3}$$

where N_{hom} is a solution of the homogeneous system,

$$\bar{A} \cdot N_{\mathrm{hom}} = 0 \,. \tag{8.4}$$

Remarkably, we will show that whether Equation (8.2) has solutions or not can be directly determined from the toric diagram of the singularity under consideration. In other words, we will establish a geometric criterion for the satisfiability of the ACC in orientifolded theories.

8.1.1 The adjacency matrix of orientifolded theories

Consider a toric singularity and a corresponding dimer admitting a $\mathbb{Z}_2$ involution. We can divide the n_g gauge groups of the mother theory into two sets: pairs of faces identified under the involution, and self-identified ones. Therefore, the adjacency matrix of the mother theory, A_{IJ} with $I, J = 1, \ldots, n_g$, can be suitably rearranged as follows:

$$A = \left(\begin{array}{c|c|c} B_{11} & B_{12} & B_{13} \\ \hline B_{21} & B_{22} & B_{23} \\ \hline B_{31} & B_{32} & B_{33} \end{array}\right) \begin{array}{l} \Big\} i \\ \Big\} i+k \\ \Big\} a \end{array} \quad . \tag{8.5}$$

$$\underbrace{\phantom{B_{11}}}_{j} \quad \underbrace{\phantom{B_{12}}}_{j+k} \quad \underbrace{\phantom{B_{13}}}_{b}$$

Here faces $i, j = 1, \ldots, k$ are the surviving ones out of those in the pairs of faces that are mapped into each other (for every pair, we are free to keep any of the two faces). Faces $i+k, j+k$, with $i, j = 1, \ldots, k$, are their images. Finally, the remaining faces $a, b = 1, \ldots, n_g - 2k$ are those that are self-identified. The B matrices are the adjacency matrices between these different subsets. For example, B_{13} is the adjacency matrix between surviving faces and self-identified faces, while B_{23} is the adjacency matrix between the image faces and the self-identified ones. The matrix A is by definition antisymmetric, which in terms of the submatrices B implies that

$$\begin{aligned} &B_{11} = -B_{11}^T\,, \quad B_{22} = -B_{22}^T\,, \quad B_{33} = -B_{33}^T\,, \\ &B_{12} = -B_{21}^T\,, \quad B_{13} = -B_{31}^T\,, \quad B_{23} = -B_{32}^T\,. \end{aligned} \tag{8.6}$$

The $\mathbb{Z}_2$ symmetry of the phase under consideration endows it with further symmetry properties. The $\mathbb{Z}_2$ projection acts on the bifundamental fields as follows:

Mother theory		Daughter theory
$(\overline{\square}_i, \square_j)$, $(\overline{\square}_{j+k}, \square_{i+k})$	$\to$	$(\overline{\square}_i, \square_j)$
$(\overline{\square}_i, \square_{j+k})$, $(\overline{\square}_j, \square_{i+k})$	$\to$	$(\overline{\square}_i, \overline{\square}_j)$
$(\overline{\square}_{i+k}, \square_j)$, $(\overline{\square}_{j+k}, \square_i)$	$\to$	$(\square_i, \square_j)$
$(\overline{\square}_a, \square_i)$, $(\overline{\square}_{i+k}, \square_a)$	$\to$	$(\square_a, \square_i)$
$(\overline{\square}_i, \square_a)$, $(\overline{\square}_a, \square_{i+k})$	$\to$	$(\square_a, \overline{\square}_i)$
$(\overline{\square}_a, \square_b)$, $(\overline{\square}_b, \square_a)$	$\to$	$(\square_a, \square_b)$

. (8.7)

These projections imply that:

$$\begin{aligned} B_{11} &= B_{22}^T\,, \quad B_{12} = B_{12}^T\,, \quad B_{21} = B_{21}^T\,, \\ B_{31} &= B_{23}^T\,, \quad B_{13} = B_{32}^T, \quad B_{33} = B_{33}^T\,. \end{aligned} \tag{8.8}$$

We can apply Equations (8.6) and (8.8) together to find further relations between the B's,

$$\begin{aligned} B_{11} &= -B_{22}\,, \quad B_{12} = -B_{21}\,, \\ B_{13} &= -B_{23}\,, \quad B_{31} = -B_{32}\,, \quad B_{33} = 0\,, \end{aligned} \tag{8.9}$$

so that eventually the adjacency matrix is entirely determined by B_{11}, B_{12}, and B_{13}:

$$A = \begin{pmatrix} B_{11} & B_{12} & B_{13} \\ -B_{12} & -B_{11} & -B_{13} \\ -B_{13}^T & B_{13}^T & 0 \end{pmatrix}\,. \tag{8.10}$$

In order to illustrate these relations, let us consider the complex cone over PdP_{3b}, as studied in [2]. The dimer, which is shown in Figure 8.1, admits a $\mathbb{Z}_2$ symmetry with two fixed lines. The numbering of the faces has

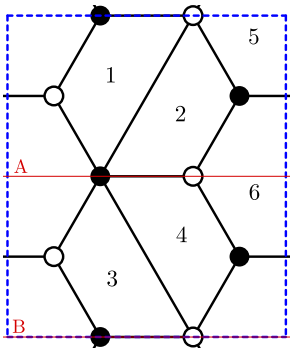

Figure 8.1: Dimer diagram for PdP_{3b} with two horizontal fixed lines (in red).

already been chosen such that the adjacency matrix reads

$$A = \left(\begin{array}{cc|cc|cc} 0 & 1 & -1 & 0 & 1 & -1 \\ -1 & 0 & 0 & 1 & 1 & -1 \\ \hline 1 & 0 & 0 & -1 & -1 & 1 \\ 0 & -1 & 1 & 0 & -1 & 1 \\ \hline -1 & -1 & 1 & 1 & 0 & 0 \\ 1 & 1 & -1 & -1 & 0 & 0 \end{array}\right)\,, \tag{8.11}$$

which showcases the general structure in Equations (8.6), (8.8) and (8.9).

Let us now turn our attention to the daughter theory. To compute the ACC for the orientifolded theory we first note that SO/USp groups are automatically anomaly-free and play no role.[1] Further, for the ACC of the non-self-identified faces we have to take into account both the contributions from fields such as $(\overline{\square}_i, \square_j)$, that are counted by B_{11}, and fields such as $(\square_i, \square_j)$ and $(\overline{\square}_i, \overline{\square}_j)$ that are counted by B_{12}, see Equation (8.7). This leads to the homogeneous ACC for the projected theory given by

$$\overline{A} = \left(\begin{array}{c|c} B_{11} + B_{12} & B_{13} \end{array} \right) . \tag{8.12}$$

Applying this to the PdP_{3b} example we get

$$\overline{A} = \left(\begin{array}{cc|cc} -1 & 1 & 1 & -1 \\ -1 & 1 & 1 & -1 \end{array} \right) . \tag{8.13}$$

8.1.2 The homogeneous problem

In the previous section, we have constructed the homogeneous part of the ACC for an orientifolded theory. We now show how solutions to the homogeneous problem, namely elements of $\mathrm{Ker}(\overline{A})$, are obtained from symmetric rank assignments of the mother theory, which form a subspace of $\mathrm{Ker}(A)$. This will allow us to extend the method explained in Section 6.3.1 to the homogeneous problem of orientifolded theories.

We say that a rank assignment of the mother theory N_I^S is symmetric with respect to the $\mathbb{Z}_2$ involution if it satisfies

$$N_i^S = N_{i+k}^S , \quad N_a^S \text{ free} . \tag{8.14}$$

If this rank assignment is anomaly-free in the mother theory (*i.e.* if it is in the kernel of A), we have

$$A_{IJ} N_J^S = 0 , \tag{8.15}$$

where here and henceforth, summation over repeated indices is understood.

[1] There could have been, however, Witten anomalies à la $SU(2)$ in SO/USp groups. Yet, as discussed in [176], cancellation of local anomalies ensures that the number of fermions is even and the Witten anomaly vanishes.

Expanding this equation in terms of the B matrices and exploiting the symmetry properties given in Equation (8.14), it becomes

$$\begin{aligned}(B_{11}+B_{12})_{ij}N_j^S+(B_{13})_{ia}N_a^S&=0\,,\\(B_{21}+B_{22})_{ij}N_j^S+(B_{23})_{ia}N_a^S&=0\,,\\(B_{31}+B_{32})_{aj}N_j^S+(B_{33})_{ab}N_b^S&=0\,.\end{aligned}\tag{8.16}$$

From Equation (8.9), we conclude that the first two equations are actually one and the same, while the third equation is trivially satisfied for any symmetric rank assignment. From the first two equations we learn that any symmetric rank assignment N_I^S in the mother theory which satisfies the ACC, defines a solution of the homogenous ACC system of the daughter theory given in Equation (8.2):

$$N_{\rm hom}=(N_i^S|N_a^S)\,.\tag{8.17}$$

Equation (8.16) indeed implies that such a vector satisfies:

$$\overline{A}\cdot N_{\rm hom}=0\,.\tag{8.18}$$

Conversely, if one starts with a vector $(N_i^S|N_a^S)$ satisfying Equation (8.18), the vector $(N_i^S|N_{i+k}^S|N_a^S)$ is a symmetric rank assignment of the mother theory. The definition of $\overline{A}$ in Equation (8.12) implies that the equations in Equation (8.16) hold for $(N_i^S|N_{i+k}^S|N_a^S)$, *i.e.* that the latter satisfies the ACC of the mother theory. Hence, we have proved the following:

> Rank assignments in the daughter theory which satisfy the homogeneous ACC are in one-to-one correspondence with symmetric rank assignments in the mother theory which satisfy the ACC.

In the special case where tensors are absent from the daughter theory, the ACC are actually a homogeneous problem and the symmetric rank assignments in the mother theory provide directly the orientifold solutions. The regular brane is such a solution that always exists and thus guarantees that an orientifold without tensors always admits a non-anomalous solution.

8.1.3 The non-homogeneous problem

Finding solutions to the ACC in orientifolded theories with tensors is not trivial because their very existence is not guaranteed, since the full system of ACC given in Equation (8.2) has a non-homogeneous part coming

from the tensor matter. The Rouché-Capelli theorem gives us a criterion for its solvability: a non-homogeneous system,

$$\bar{A} \cdot N = f \,, \tag{8.19}$$

admits a solution if and only if

$$\text{rank}(\bar{A}) = \text{rank}(\bar{A}|f) \,, \tag{8.20}$$

where $(\bar{A}|f)$ is the matrix obtained appending the column f to the matrix $\bar{A}$. For us f encodes the contribution to the ACC of the tensor matter, *i.e.* of the self-identified chiral fields.

In other words, every set of numbers r_i such that

$$r_i \bar{A}_{i\bar{J}} = 0 \tag{8.21}$$

holds for all $\bar{J} = j, a$, must satisfy

$$r_i f_i = 0 \tag{8.22}$$

for the system to be solvable. In this section, we show that the coefficients r_i which satisfy Equation (8.21) correspond precisely to the antisymmetric rank assignments of the mother theory.

Suppose that some coefficients r_i satisfying Equation (8.21) exist. Using Equation (8.9) for $\bar{J} = j$, one can show that it implies

$$r_i (B_{11})_{ij} - r_i (B_{21})_{ij} = 0 \,. \tag{8.23}$$

Using Equation (8.9), this is equivalent to

$$r_i (B_{12})_{ij} - r_i (B_{22})_{ij} = 0 \,. \tag{8.24}$$

For $\bar{J} = a$, using Equation (8.9), we find that

$$r_i (B_{13})_{ia} - r_i (B_{23})_{ia} = 0 \,. \tag{8.25}$$

We write

$$N_I^A = (r_i| - r_i|0) \,, \tag{8.26}$$

and equations Equation (8.23) to Equation (8.25) can be expressed as

$$N_I^A A_{IJ} = 0 = A_{JI} N_I^A \,, \tag{8.27}$$

where the second equality merely uses the antisymmetry property of A. Hence, we have proved that any set of r_i satisfying Equation (8.21) defines

an antisymmetric rank assignment N_I^A of the mother theory, which satisfies the mother ACC.

Conversely, starting with an antisymmetric rank assignment N_I^A in the mother theory

$$N_i^A = -N_{i+k}^A, \quad N_a^A = 0\,, \tag{8.28}$$

which satisfies the ACC, one can use equations Equation (8.23) to Equation (8.25) backward, and thus obtain a set of r_i such that Equation (8.21) holds for all $\bar{J} = j, a$.

Let us emphasize that while symmetric rank assignments in the mother theory are in one-to-one correspondence with solutions of the homogeneous system of ACC in the daughter theory (which by definition form the kernel of $\overline{A}$), the antisymmetric rank assignments in the mother theory correspond rather to the elements of the cokernel of $\overline{A}$, that we will see merely as technical tools. They are useful for determining whether a given daughter theory admits an anomaly-free rank assignment, since the elements in the cokernel of $\overline{A}$ encode the relations between the lines of $\overline{A}$, from which one can row-reduce $\overline{A}$.

Coefficients of the trivial linear combination of lines of $\overline{A}$ are in one-to-one correspondence with the anomaly-free antisymmetric rank assignments in the mother theory.

To rephrase what we wrote at the beginning of the section, there are anomaly-free rank assignments in the daughter theory if and only if

$$N_i^A f_i = 0 \tag{8.29}$$

for every antisymmetric solution N_I^A of the mother theory, where f is easily computed from the dimer and its orientifold. We call this the "Rouché-Capelli condition".

In general, note that any rank assignment N_I can be split into a symmetric and an antisymmetric component,

$$(N_i|N_{i+k}|N_a) = \frac{1}{2}(N_i + N_{i+k}|N_{i+k} + N_i|2N_a) + \frac{1}{2}(N_i - N_{i+k}|N_{i+k} - N_i|0)\,. \tag{8.30}$$

Both parts are then half-integer valued. Multiplying such a possibly unphysical (in the case it is half integer-valued) rank vector by an even number yields a physical rank vector with the required (anti)symmetry. All of the reasoning of the last two subsections is pure linear algebra, and does not know about the need for integrality for rank assignments, which entirely comes from physics.

8.2 A zig-zag algorithm for orientifolds

We will now generalize the procedure discussed in Section 6.3.1 to find (anti)symmetric rank assignments in orientifolded theories. The precise details of the algorithm depend on whether the $\mathbb{Z}_2$ involution leaves fixed lines or points. This difference comes from the fact that involutions with fixed lines map nodes to nodes of the same color, while involutions with fixed points map nodes to nodes of opposite color.

We illustrate this difference in Figure 8.2. There we can see that ZZPs around a node make a clockwise or counterclockwise loop. If a node is mapped to a node of the same color it means that the orientation of the loop is preserved, while, in the opposite case, it is reversed.[2] This observation will become crucial when we define (anti)symmetric rank assignment in both the case of fixed lines and points.

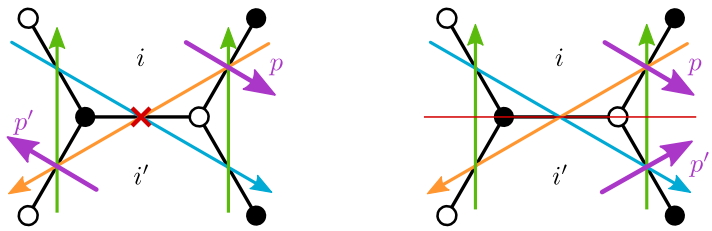

Figure 8.2: The orientifold actions with (a) fixed points and (b) fixed lines. p is a path from one face to an adjacent one, and p' its image. In (a) the orange and blue ZZPs are self-identified, while the green ones are mapped into each other. In (b), the orange and blue ZZPs are mapped into each other, and the green ones are self-identified.

For the forthcoming analysis, we find it useful to introduce the notation $\{\Gamma\} = \{\alpha, \overline{\alpha}, \gamma\}$ to describe the set of ZZPs: every pair $(\alpha, \overline{\alpha})$ corresponds to ZZPs mapped into each other under the orientifold projection, while γ labels self-identified ZZPs.

[2] We recall that under both involutions, a dimer is sent to a dimer with all ZZPs going in the opposite direction. The map between ZZPs is understood after additionally reversing the direction of every ZZP, as in [73].

8.2.1 Fixed line(s) orientifolds

Due to how they act on ZZPs, orientifolds with fixed lines in the dimer correspond to toric diagrams with axes of $\mathbb{Z}_2$ reflection symmetry.[3] Figure 8.3 illustrates the general structure of such axes and the map between a ZZP and its image in the cases of orientifolds with diagonal and horizontal O-lines (which is analogous to the case with vertical O-lines). Let us elaborate on this kind of figure. Naively, the orientation of the reflection axis in these toric diagrams can be modified by an $SL(2,\mathbb{Z})$ transformation, potentially eliminating the distinction between the diagonal and vertical/horizontal O-line cases. However, the toric diagram after such $SL(2,\mathbb{Z})$ transformation would no longer be symmetric with respect to the axis. Alternatively, we can think about the toric diagrams with reflection axes as coming from specific dimers with fixed lines. In this context, an $SL(2,\mathbb{Z})$ transformation translates into a change of the unit cell of the dimer. But the unit cell is fixed by the specific orientifold under consideration: not any $SL(2,\mathbb{Z})$ transformation is permitted once we have chosen an orientifold identification. In other words, the orientifold obstructs $SL(2,\mathbb{Z})$ transformations.

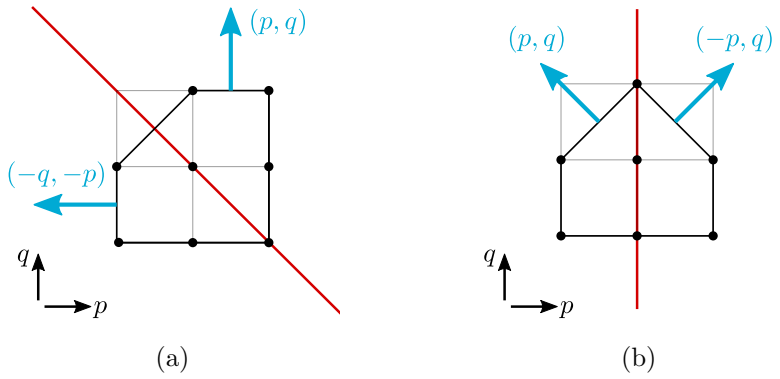

Figure 8.3: The toric diagrams for fixed line orientifolds have an axis of reflection symmetry. The corresponding axes for: (a) diagonal and (b) horizontal O-lines. In both cases we show in blue a generic ZZP and its image.

[3] We will refer to such lines of reflection symmetry in the toric diagram as *axes* in order to avoid confusion with the fixed lines in the dimer (which we also call O-lines).

Symmetric rank assignments. For $\mathbb{Z}_2$ involutions with fixed lines, symmetric rank assignments correspond to symmetric ZZP value assignments:

$$v_\alpha = v_{\overline{\alpha}}, \quad v_\gamma \text{ free} \tag{8.31}$$

First, recall from Section 6.3.1 that the difference between the ranks of any two faces in the dimer is equal to a sum (with signs) of the values of the ZZPs one crosses as one goes between the two faces. ACC at each face of the dimer ensure that the value of this sum is invariant under smooth (homological) deformations of the path one follows. Furthermore, the topological constraints guarantee that the value of the sum is independent of the homology class of the path on the torus.

Consider two faces i and j and a path p connecting them, and i', j' and p' their respective images under the $\mathbb{Z}_2$ symmetry. Every time p crosses a ZZP α, its image p' crosses α', and these two crossings have the same sign since the orientation is preserved. From this, it is clear that, if the ZZP value assignment is symmetric, the rank assignment generated by the method in Section 6.3.1 is also symmetric.

In the case of dimer models with involutions fixing lines, symmetric rank assignments correspond bijectively to symmetric ZZP value assignments (up to the global shift in the values, and such that the topological constraints are satisfied).

For symmetric value assignments, the topological constraints read:

- Diagonal line ($p_{\bar{\alpha}} = -q_\alpha, q_{\bar{\alpha}} = -p_\alpha$):

$$0 = \Lambda = \sum_\alpha v_\alpha (p_\alpha - q_\alpha) + \frac{1}{2} \sum_\gamma v_\gamma (p_\gamma - q_\gamma) = -M = 0\,. \tag{8.32}$$

- Vertical lines ($p_{\bar{\alpha}} = -p_\alpha, q_{\bar{\alpha}} = q_\alpha$):

$$\begin{array}{rcl} M & = & 2\sum_\alpha v_\alpha q_\alpha + \sum_\gamma v_\gamma q_\gamma \;\; = \;\; 0\,, \\ \Lambda & = & 0\,, \end{array}$$

  The case of horizontal lines follows exchanging p_Γ with q_Γ and Λ with M.

We can now compute the total number of symmetric rank assignments. If the dimer under consideration has n ZZPs, symmetric rank assignments

correspond to a choice of v_Γ, such that $v_\alpha = v_{\overline{\alpha}}$, and such that topological constraints hold. We also have the freedom to shift the rank of all gauge groups, since regular branes respect the required symmetry. Putting all this together, the number of independent symmetric rank assignments modulo some (possibly half-integer) number of regular branes is

$$\dim(\mathrm{Ker}(\overline{A})) - 1 = \frac{1}{2}(n + n_s) - 2\,, \tag{8.33}$$

where n_s is the number of self-identified ZZPs.

Antisymmetric rank assignments. Antisymmetric rank assignments are found in a similar fashion, by imposing the antisymmetry explicitly on the ZZP values, *i.e.* $v_\Gamma = -v_\Gamma$, or equivalently

$$v_\alpha = -v_{\overline{\alpha}}, \quad v_\gamma = 0\,. \tag{8.34}$$

This follows from the same reasoning as in the symmetric case: due to the geometric action of the symmetry, it is clear that antisymmetric ZZP value assignments lead to antisymmetric rank assignments in the dimer. Furthermore, if the ZZP value assignment is not antisymmetric *up to a shift*, it is straightforward to see that the rank assignment cannot be antisymmetric either.

In this case, there is a subtlety that was not present in the symmetric case. First, the ZZP value method only knows about differences of ranks in the dimer. Equivalently, it only describes anomaly-free rank assignments up to some (half-integer) number of regular branes. The relevant point here is that regular branes are not antisymmetric. Hence, starting from an antisymmetric value assignment, it can well be that the rank assignment one constructs is not antisymmetric per se, but merely antisymmetric after having added some number of regular branes (we will see examples of this later). Then, in the method of Section 6.3.1, a global shift of the ZZP values does not change the resulting rank assignment. The global shift does not preserve antisymmetry, so among the family of value assignments corresponding to a given rank assignment (modulo regular branes), there is a special representative which is an antisymmetric value assignment. Thus instead of focusing on the bijection between the set of antisymmetric rank assignments up to a (half-integer) number of regular branes, and the set of ZZP value assignments which satisfies the topological constraints, and which can be transformed into antisymmetric value assignments thanks to the global shift, one can consider the only representative of such a class of ZZP value assignments, which is antisymmetric. We have proven the following:

In the case of dimer models with involutions fixing lines, antisymmetric rank assignments correspond bijectively to antisymmetric ZZP value assignments which satisfy the topological constraints.

When combined with Equation (8.34), the topological constraints $\Lambda = M = 0$ again merge into a single constraint, regardless of the type of fixed line orientifold. The surviving combination however depends on the nature of the fixed lines:

- Diagonal line:

$$\Lambda = \sum_{\alpha} v_{\alpha}(p_{\alpha} + q_{\alpha}) = -M = 0\,. \tag{8.35}$$

- Vertical lines:

$$\begin{aligned} &\Lambda = 2\sum_{\alpha} v_{\alpha} p_{\alpha} = 0\,, \\ &M = 0\,. \end{aligned} \tag{8.36}$$

  For horizontal lines we merely need to exchange p_{α} with q_{α}, and Λ with M.

The number of antisymmetric rank assignments is easily computed to be

$$\dim(\mathrm{coker}(\overline{A})) = \frac{1}{2}(n - n_s) - 1 \tag{8.37}$$

Adding Equation (8.33) and Equation (8.37), we find that the total number of independent either symmetric or antisymmetric anomaly-free rank assignments is $n - 3$, as should be the case since it is the number of anomaly-free rank assignments in the mother theory, up to (half) regular branes.

Below we illustrate these ideas with a few explicit examples, containing both diagonal and vertical/horizontal fixed lines.

No anomaly-free solution: dP_1 with diagonal fixed line

Consider the complex cone over dP_1, which we discussed in Section 6.3.1 as an example of the ZZP method for the mother theory. It admits a $\mathbb{Z}_2$ involution with a fixed line, as shown in Figure 8.4.

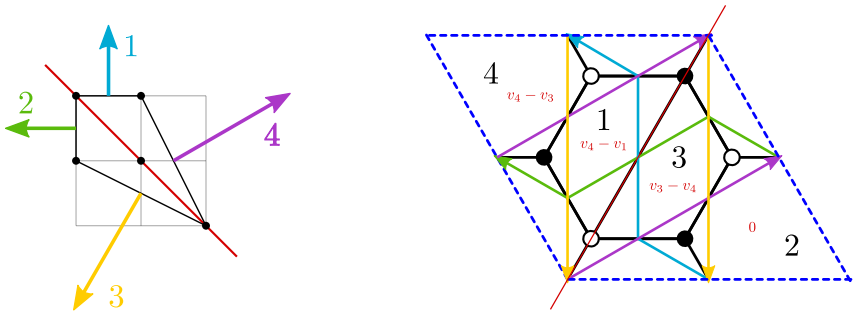

(a) (b)

Figure 8.4: (a) The toric diagram with the orientifold symmetry axis. (b) Dimer diagram for dP_1 with a diagonal fixed line (in red). We show the ZZPs and the rank assignments coming from them.

Adjacency matrices. The adjacency matrix of the mother theory is easily read from the dimer, and it is given by

$$A = \left(\begin{array}{cc|cc} 0 & 2 & -1 & -1 \\ -2 & 0 & -1 & 3 \\ \hline 1 & 1 & 0 & -2 \\ 1 & -3 & 2 & 0 \end{array}\right) \tag{8.38}$$

For concreteness, let us consider the case of a positive O-line. The adjacency matrix for the orientifolded theory is found using Equation (8.12). It is supplemented with the inhomogeneous part and becomes

$$(\bar{A}|f) = \left(\begin{array}{cc|c} -1 & 1 & +4 \\ -3 & 3 & -4 \end{array}\right) . \tag{8.39}$$

We will later discuss how to determine systematically the f_is. Here it is sufficient to see that since the O-line has a + sign, both tensors are symmetric. The sign of $f_i = \pm 4$ has to be correlated with the sign of the diagonal elements of $\bar{A}$, so that in the ACC we eventually find $\pm(N_i + 4)$ for symmetric tensors and $\pm(N_i - 4)$ for antisymmetric ones (recall that f is on the right-hand side of the ACC equations Equation (8.2)).

One may directly solve the simple system Equation (8.39), but we will rather use the algorithm we developed. In the dimer in Figure 8.4b we indicate the linear combination of ZZPs that corresponds to every face (we have chosen face 2 to have rank 0). In Section 6.3.1 we studied the anomaly-free rank assignments in the mother theory and found a one-parameter family (besides the regular brane):

$$\mathbf{N} = (-2, 0, 1, -1)v_3 , \tag{8.40}$$

which can be decomposed into symmetric and antisymmetric parts,

$$(-2,0,1,-1)v_3 = -\frac{1}{2}(1,1,1,1)v_3 + \frac{1}{2}(-3,1,3,-1)v_3 \tag{8.41}$$

We see that there is one antisymmetric rank vector $(-3,1,3,-1)$ and no symmetric one (except the regular brane). We now show how to find them directly from the ZZPs.

The antisymmetric rank vector is found by imposing $v_1 = -v_2$ and $v_3 = -v_4$. We cannot use the global shift, since it is not antisymmetric. The periodicity constraints are $\Lambda = M = v_1 - 3v_3 = 0$. We thus find the antisymmetric rank assignment $\mathbf{N} = (-3,1,3,-1)v_3$. In the daughter theory this vector is $\overline{\mathbf{N}} = (-3,1)v_3$. However, it is not in $\mathrm{Ker}(\overline{A})$, but in the cokernel. We can use it to row reduce $\overline{A}$ and study whether the linear system $(\overline{A}|f)$ has solutions. Denote $\mathbf{f} = (+4,-4)^T$ the inhomogeneous part of $(\overline{A}|f)$. If $\overline{\mathbf{N}} \cdot \mathbf{f} \neq 0$, the theory is anomalous. This is indeed the case in this example, so we conclude that the daughter theory does not admit an anomaly-free solution.

No anomaly-free solution: PdP_4 with diagonal fixed line

Consider now PdP_4, which we previously discussed in Section 6.3.1. Figure 8.5 shows the dimer and toric diagram for the orientifold under consideration. In Section 6.3.1 we saw that anomaly-free rank assignments of the mother theory are given by:

$$\mathbf{N} = (-v_7, v_2, v_6 - v_1, -v_1, v_6, v_2 - v_7, 0)\,. \tag{8.42}$$

The topological constraints are:

$$\Lambda : v_4 + v_3 = v_6 + v_7\ , \tag{8.43}$$

$$M : v_4 + v_5 = v_1 + v_2\,. \tag{8.44}$$

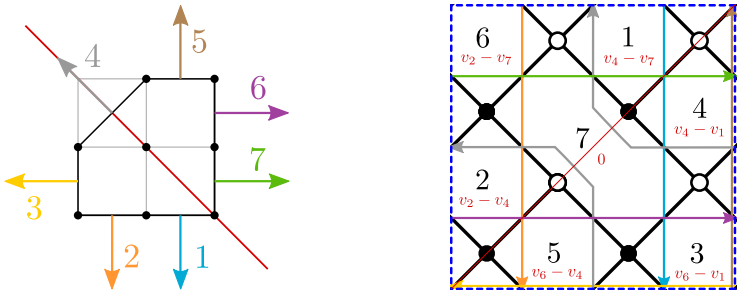

(a) (b)

Figure 8.5: (a) The toric diagram with the orientifold symmetry axis. (b) Dimer diagram for PdP_4 with a diagonal fixed line (in red). We show the ZZPs and the rank assignments coming from them.

Adjacency matrices. The adjacency matrices of the mother and daughter theories are:

$$A = \left(\begin{array}{ccc|ccc|c} 0 & 0 & 1 & -1 & -1 & 0 & 1 \\ 0 & 0 & 1 & -1 & -1 & 0 & 1 \\ -1 & -1 & 0 & 0 & 0 & 1 & 1 \\ \hline 1 & 1 & 0 & 0 & 0 & -1 & -1 \\ 1 & 1 & 0 & 0 & 0 & -1 & -1 \\ 0 & 0 & -1 & 1 & 1 & 0 & -1 \\ \hline -1 & -1 & -1 & 1 & 1 & 1 & 0 \end{array}\right) , \qquad (8.45)$$

$$(\bar{A}|f) = \left(\begin{array}{ccc|c|c} -1 & -1 & 1 & 1 & -4 \\ -1 & -1 & 1 & 1 & -4 \\ -1 & -1 & 1 & 1 & +4 \end{array}\right) ,$$

where, for concreteness, we have assumed that the sign of the orientifold line is negative.

Symmetric rank assignments. Impose $v_3 = v_5$, $v_2 = v_6$, $v_1 = v_7$. The constraints $M = 0$, $\Lambda = 0$ combine into $v_4 = v_1 + v_2 - v_3$. We can use the global shift freedom to set $v_4 = 0$, which leads to $\mathbf{v^S} = (v_1, v_2, v_1 + v_2, 0, v_1 + v_2, v_2, v_1)$. The resulting symmetric rank assignments in the mother and daughter theories are

$$\begin{aligned} \mathbf{N^S} &= (-v_1, v_2, v_2 - v_1, -v_1, v_2, v_2 - v_1, 0) \\ \overline{\mathbf{N}}^{\mathbf{S}} &= (-v_1, v_2, v_2 - v_1, 0) \ . \end{aligned} \qquad (8.46)$$

Note that $\overline{\mathbf{N}}^{\mathbf{S}}$ should be understood as the column vector whose first three elements refer to the faces 1–3 that have an image, while the last refers to the self-identified face 7. When considered as a row vector, one should drop the last element.

Antisymmetric rank assignments. Impose $v_1 = -v_7$, $v_2 = -v_6$, $v_3 = -v_5 = 0$, $v_4 = 0$. We also need to impose the constraint $v_1 + v_2 = -v_3$ with no global shift freedom. We then find a two-parameter family of antisymmetric assignments for the v_Γ, $\mathbf{v}^{\mathbf{A}} = (v_1, v_2, -v_1 - v_2, 0, v_1 + v_2, -v_2, -v_1)$. The corresponding antisymmetric rank assignment is

$$\mathbf{N}^{\mathbf{A}} = (v_1, v_2, -v_1 - v_2, -v_1, -v_2, v_1 + v_2, 0) \ . \tag{8.47}$$

In the daughter theory, this rank assignment gives rise to the two row vectors

$$\overline{\mathbf{N}}_{\mathbf{1}}^{\mathbf{A}} = (1, 0, -1)v_1, \quad \overline{\mathbf{N}}_{\mathbf{2}}^{\mathbf{A}} = (0, 1, -1)v_2 \tag{8.48}$$

Let us denote by $\mathbf{f} = (-4, -4, 4)^T$ the inhomogeneous part of $(\overline{A}|f)$. We find $\overline{\mathbf{N}}_{\mathbf{1}}^{\mathbf{A}} \cdot \mathbf{f} = -8$ and $\overline{\mathbf{N}}_{\mathbf{2}}^{\mathbf{A}} \cdot \mathbf{f} = -8$. We conclude that anomalies cannot be canceled in this theory.

This example and the previous one consist of orientifolds with a diagonal fixed line. Both cases turned out to lead to theories in which anomalies cannot be cancelled. In Section 8.3.1 we will present a more detailed general analysis and discuss under which conditions such orientifolds can admit anomaly-free solutions.

An anomaly-free example: PdP_{3b} with two fixed lines

Figure 8.6 shows the dimer and toric diagram for an orientifold of PdP_{3b} with two fixed lines. This theory was studied in [2], where it was shown that the daughter theory admits an anomaly-free rank assignment if the two O-lines have opposite signs. Note that the horizontal fixed lines in the dimer correspond to a vertical axis of symmetry in the toric diagram.

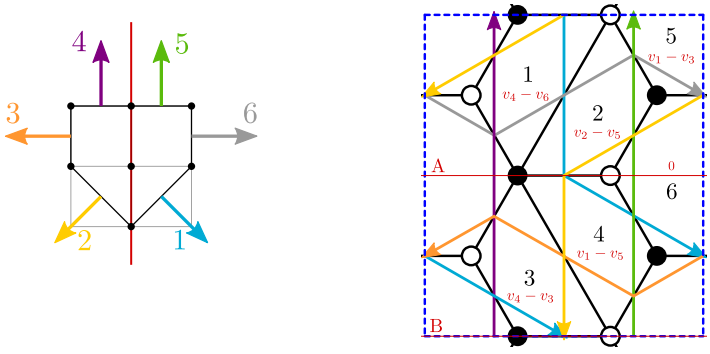

(a) (b)

Figure 8.6: (a) The toric diagram with the orientifold symmetry axis. (b) Dimer diagram for PdP_{3b} with two horizontal fixed lines (in red). We show the ZZPs and the rank assignments coming from them.

Adjacency matrices. The adjacency matrices of the mother and daughter theories are:

$$A = \left(\begin{array}{cc|cc|cc} 0 & -1 & 1 & 0 & -1 & 1 \\ 1 & 0 & 0 & -1 & -1 & 1 \\ \hline -1 & 0 & 0 & 1 & 1 & -1 \\ 0 & 1 & -1 & 0 & 1 & -1 \\ \hline 1 & 1 & -1 & -1 & 0 & 0 \\ -1 & -1 & 1 & 1 & 0 & 0 \end{array}\right), \tag{8.49}$$

$$(\bar{A}|f) = \left(\begin{array}{cc|cc|c} 1 & -1 & -1 & 1 & -4\cdot\mathrm{sign}(B) \\ 1 & -1 & -1 & 1 & +4\cdot\mathrm{sign}(A) \end{array}\right),$$

where $\mathrm{sign}(A)$, $\mathrm{sign}(B)$ are the signs of the two O-lines. Let us now turn to the study of symmetric and antisymmetric rank assignments.

Symmetric rank assignments. Let us impose $v_2 = v_1$, $v_6 = v_3$. The constraint $\Lambda = 0$ is trivially satisfied, while $M = 0$ becomes (keeping v_1 and v_3):

$$2v_1 - v_4 = v_5\,. \tag{8.50}$$

Setting $v_4 = 0$, we get

$$\mathbf{v^S} = (v_1, v_1, v_3, 0, 2v_1, v_3)\,, \tag{8.51}$$

giving in turn

$$\mathbf{N^S} = (-v_3, -v_1, -v_3, -v_1, v_1 - v_3, 0)\,. \tag{8.52}$$

Projecting down this vector, we obtain the solutions to the homogeneous problem in the daughter theory.

Antisymmetric rank assignments. We now impose $v_2 = -v_1$, $v_3 = -v_6$, $v_4 = v_5 = 0$. As expected, M is trivially satisfied and one just needs to impose $\Lambda = 0$, which reads $v_3 = v_1$. Remember that the global shift has already been fixed. We then find a one-dimensional family of antisymmetric assignments for the v_Γ:

$$\mathbf{v^A} = (v_1, -v_1, v_1, 0, 0, -v_1)\,. \tag{8.53}$$

The corresponding antisymmetric rank assignment is given by $\mathbf{N^A} = (v_1, -v_1, -v_1, v_1, 0, 0)$. In the daughter theory this rank assignment gives $\overline{\mathbf{N}}^{\mathbf{A}} = (1, -1)v_1$. One may now use it to row reduce $\overline{A}$. Denote by $\mathbf{f} = (-4 \cdot \mathrm{sign}(B), +4 \cdot \mathrm{sign}(A))^T$ the inhomogeneous part of $(\overline{A}|f)$. We find $\overline{\mathbf{N}}^{\mathbf{A}} \cdot \mathbf{f} = -4 \cdot \mathrm{sign}(B) - 4 \cdot \mathrm{sign}(A)$. If $\overline{\mathbf{N}}^{\mathbf{A}} \cdot \mathbf{f} \neq 0$, the theory is anomalous, so we need $\mathrm{sign}(A) = -\mathrm{sign}(B)$, as anticipated.

Anomaly-free rank assignments. As explained in the introduction of the current section, since we have a parametrization of the symmetric rank assignments, we merely need a single solution of the tadpole-cancellation system to write all of them.

Looking at the adjacency matrix of the daughter theory in Equation (8.49) with $\mathrm{sign}(A) = +$ and $\mathrm{sign}(B) = -$, a straightforward solution to the rank assignment is $N_1 = 4$ and $N_2 = N_5 = N_6 = 0$ (in the daughter theory we keep faces $1, 2, 5$ and 6). This gives the following three-parameter family of solutions to the ACC, where we have added $N + v_1 + v_3$ regular branes:

$$\begin{cases} N_1 &= N + v_1 + 4 \\ N_2 &= N + v_3 \\ N_5 &= N + 2v_1 \\ N_6 &= N + v_1 + v_3\ . \end{cases} \tag{8.54}$$

8.2.2 Fixed points orientifolds

In orientifolds with fixed points, every ZZP is mapped to a ZZP with the same winding numbers [73]. The image of a ZZP can therefore be either

itself or another ZZP, if more than one ZZP with the same winding numbers exist.

Contrarily to the cases with fixed lines, in fixed point orientifolds nodes in the dimer are mapped to nodes of the opposite color. In analogy with the case of line orientifolds, let us consider a path p going from a face i to a face j, and its image p' going from the image of i to the image of j. If p crosses a ZZP α, then p' crosses its image α', but since the color of the nodes is inverted in the image, the signs of the crossings are opposite. This implies that a symmetric, respectively antisymmetric, rank assignment is associated with an antisymmetric, respectively symmetric, value assignment for the ZZP. We therefore have:

> In dimer models with fixed point involutions, symmetric rank assignments up to (half)-regular branes correspond bijectively to antisymmetric ZZP value assignments which satisfy the topological constraints. Similarly, antisymmetric rank assignments correspond bijectively to symmetric ZZP value assignments which satisfy the topological constraints and up to a global shift.

We have seen that in the cases of fixed point orientifolds, symmetric rank assignments correspond to ZZP value assignments such that:

$$v_\alpha = -v_{\overline{\alpha}}, \quad v_\gamma = 0\,. \tag{8.55}$$

One can easily verify that the topological constraints are always satisfied by this choice of v_Γ, hence the number of symmetric rank assignment is:

$$\dim(\mathrm{Ker}(\overline{A})) = \frac{1}{2}(n - n_s)\,. \tag{8.56}$$

Antisymmetric rank assignments, conversely, correspond to:

$$v_\alpha = v_{\overline{\alpha}}, \quad v_\gamma = \text{free}\,. \tag{8.57}$$

In this case both topological constraints Λ and M are not trivial:

$$\begin{cases} \Lambda = \sum_\alpha p_\alpha v_\alpha + \sum_{\overline{\alpha}} p_{\overline{\alpha}} v_{\overline{\alpha}} + \sum_\gamma p_\gamma v_\gamma = 2\sum_\alpha p_\alpha v_\alpha + \sum_\gamma p_\gamma v_\gamma = 0 \\ M = \sum_\alpha q_\alpha v_\alpha + \sum_{\overline{\alpha}} q_{\overline{\alpha}} v_{\overline{\alpha}} + \sum_\gamma q_\gamma v_\gamma = 2\sum_\alpha q_\alpha v_\alpha + \sum_\gamma q_\gamma v_\gamma = 0 \end{cases} \tag{8.58}$$

This leads to:

$$\dim(\mathrm{coker}(\overline{A})) = \frac{1}{2}(n + n_s) - 3\,. \tag{8.59}$$

Upon summing the contributions of symmetric and antisymmetric rank assignments, we retrieve the total number of fractional branes, $n-3$, modulo regular branes.

An example: PdP_{3b}

Let us return to PdP_{3b}, already studied in Section 8.2.1 but now with fixed points instead of lines. The dimer is shown in Figure 8.7. Note that we have changed the unit cell and face numbering with respect to Figure 8.6 to make it consistent with fixed point reflections.

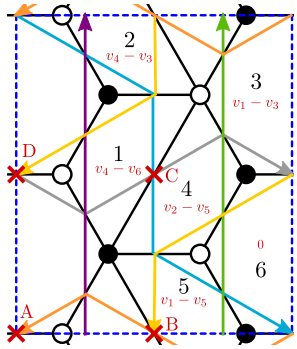

Figure 8.7: Dimer diagram for PdP_{3b} with fixed points. We show the ZZPs and the rank assignments coming from them.

Adjacency matrices. The adjacency matrices of the mother and daughter theories are:

$$A = \left(\begin{array}{ccc|ccc} 0 & 1 & -1 & -1 & 0 & 1 \\ -1 & 0 & 1 & 0 & 1 & -1 \\ 1 & -1 & 0 & 1 & -1 & 0 \\ \hline 1 & 0 & -1 & 0 & -1 & 1 \\ 0 & -1 & 1 & 1 & 0 & -1 \\ -1 & 1 & 0 & -1 & 1 & 0 \end{array}\right), \tag{8.60}$$

$$(\bar{A}|f) = \left(\begin{array}{ccc|c} -1 & 1 & 0 & +4\cdot\mathrm{sign}(C) \\ -1 & 1 & 0 & -4\cdot\mathrm{sign}(B) \\ 2 & -2 & 0 & -4\cdot\mathrm{sign}(A)+4\cdot\mathrm{sign}(D) \end{array}\right),$$

where $\mathrm{sign}(A)$ to $\mathrm{sign}(D)$ are the signs of the O-points. Note that the ZZPs 4 and 5 are interchanged by the projection, while all other ZZPs are

mapped to themselves. Let us now turn to the study of antisymmetric and symmetric rank assignments.

Symmetric rank assignments. This time we start with antisymmetric ZZP assignments, since for point orientifolds they provide symmetric rank assignments. Let us impose $v_4 = -v_5$, $v_1 = v_2 = v_3 = v_6 = 0$. As already said, the topological constraints are both trivially satisfied. Note that there is no global shift to fix. We obtain a one-parameter family of v_Γ assignments:

$$(0, 0, 0, 1, -1, 0)v_4 \,. \tag{8.61}$$

The corresponding rank assignment is:

$$\mathbf{N^S} = (1, 1, 0, 1, 1, 0)v_4 \,, \tag{8.62}$$

which is symmetric, as expected. Projecting down this vector, one obtains the solutions to the homogeneous problem in the daughter theory.

Antisymmetric rank assignments. We now turn to symmetric ZZP assignments, responsible for the antisymmetric rank assignments. We only need to impose $v_4 = v_5$. We further fix the global shift by choosing $v_4 = 0$. The topological constraints become:

$$\begin{aligned} \Lambda : v_3 &= v_1 - v_2 + v_6 \ , \\ M : v_2 &= -v_1 \ . \end{aligned} \tag{8.63}$$

We find a two-dimensional family of symmetric assignments for the v_Γ:

$$(1, -1, 2, 0, 0, 0)v_1 + (0, 0, 1, 0, 0, 1)v_6 \,. \tag{8.64}$$

The corresponding antisymmetric rank assignments are:

$$\mathbf{N}^A = (0, -2, -1, -1, 1, 0)v_1 + (-1, -1, -1, 0, 0, 0)v_6 \ . \tag{8.65}$$

Which, up to half regular branes is equal to:

$$\mathbf{N}^A = (1, -3, -1, -1, 3, 1)\frac{v_1}{2} + (-1, -1, -1, 1, 1, 1)\frac{v_6}{2} \,, \tag{8.66}$$

which is antisymmetric, as expected. Let us split it into two vectors and project them down to the daughter theory to obtain,

$$\overline{\mathbf{N}}_1^A = (1, -3, -1)\frac{v_1}{2}, \quad \overline{\mathbf{N}}_2^A = (-1, -1, -1)\frac{v_6}{2} \ . \tag{8.67}$$

Again, let us use these rank assignments to row reduce $\overline{A}$ by denoting $\mathbf{f} = (+4 \cdot \text{sign}(C), -4 \cdot \text{sign}(B), -4 \cdot \text{sign}(A) + 4 \cdot \text{sign}(D))^T$. One finds that, for the theory to admit non-anomalous solutions, one must satisfy,

$$\begin{aligned} \overline{\mathbf{N}}_1^A \cdot \mathbf{f} =& \frac{v_1}{2} \left(\text{sign}(C) + 3\text{sign}(B) + \text{sign}(A) - \text{sign}(D) \right) = 0 \ , \\ \overline{\mathbf{N}}_2^A \cdot \mathbf{f} =& \frac{v_6}{2} \left(-\text{sign}(C) + \text{sign}(B) + \text{sign}(A) - \text{sign}(D) \right) = 0 \ . \end{aligned} \tag{8.68}$$

Anomaly-free rank assignments. The solution to Equation (8.68) depends on the sign choices for the four fixed points. Consider for example

$$\text{sign}(A) = \text{sign}(C) = +, \quad \text{sign}(B) = \text{sign}(D) = - \ , \tag{8.69}$$

which is consistent with the sign rule for fixed point orientifolds. In this case, we go back to Equation (8.60) to find a two-parameter family of solutions:

$$\begin{cases} N_1 &= N + v_4 \\ N_2 &= N + v_4 + 4 \\ N_3 &= N \ . \end{cases} \tag{8.70}$$

8.3 General criteria for anomaly-free orientifolds

In this section, we present a general study of the solutions to the non-homogeneous system of ACC of the daughter theory. Remarkably, we can exploit the algorithm of the previous section to determine the existence of such solutions directly from toric data, regardless of the particular phase of the theory. This gives purely geometric necessary criteria determining whether an orientifolded theory may admit a toric phase with non-anomalous rank assignments.

8.3.1 Diagonal line orientifolds

Let us consider orientifolds with a diagonal fixed line. Without loss of generality, we assume that the fixed line has winding numbers $(1, 1)$ in the fundamental cell of the dimer. The mapping of ZZPs in this kind of orientifolds has been studied in [73] and we presented a preliminary discussion in Section 8.2.1. The diagonal fixed line in the dimer translates into a reflection symmetry axis in the toric diagram with slope -1, as we already illustrated in Figure 8.3a. This 90° rotation of the symmetry axis of the toric diagram with respect to the fixed line in the dimer was explained in [148].

Reflection with respect to the axis of the toric diagram maps a ZZP with winding (p, q), to a ZZP with winding $(-q, -p)$. Figure 8.8 shows an example of a generic toric diagram with a diagonal line orientifold.

- Let l be the number of pairs $\{v_\alpha, v_{\overline{\alpha}}\}$,with $\alpha = 1, .., l$, of ZZPs mapped one to another, which are not parallel to the symmetry axis of the toric diagram.
- Let $l_\parallel$ be the number of self-identified ZZPs $\{v_\gamma\}$ for $\gamma = 1, ..., l_\parallel$, which are parallel to the symmetry axis of the toric diagram.

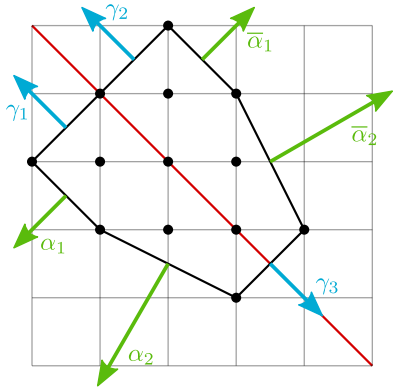

Figure 8.8: A generic toric diagram with a diagonal axis symmetry.

From the previous section, we know how to produce the coefficients of the trivial linear combinations of rows. They are the ranks of the projected SU groups that result from imposing the following conditions on the v_Γ:

$$\begin{aligned} v_\alpha &= -v_{\overline{\alpha}}\,, \\ v_\gamma &= 0 \end{aligned} \tag{8.71}$$

for all α and γ's. The topological constraints Λ and M are given by:

$$\Lambda = \sum_{\alpha,\overline{\alpha}} (v_\alpha p_\alpha + v_{\overline{\alpha}} p_{\overline{\alpha}}) = \sum_\alpha v_\alpha (p_\alpha + q_\alpha) = -M \tag{8.72}$$

where we used $p_{\overline{\alpha}} = -q_\alpha$.

We now recall the Rouché-Capelli theorem: A non-homogeneous linear system has solution *iff* the rank of the associated homogeneous matrix is equal to the rank of the matrix associated with the full system. A trivial linear combination of rows of the homogenous matrix is still trivial when

considering the matrix associated with the full system. This can be stated as:

$$\sum_i N_i f_i = 0 \tag{8.73}$$

where f_i is the non-homogeneous contribution to the ACC matrix of the orientifolded theory, coming from the tensor matter.

We now need to derive an expression for N_i in terms of the v_Γ. The Rouché-Capelli theorem tells us that the ACC system admits a solution *iff* Equation (8.73) holds for every value of v_Γ consistent with the topological constraints.

Faces with at most one tensor

Let us first focus on the simpler case where every gauge group has at most one tensor field. This result will be easily extended later to cases with more tensors. Consider a face of the mother theory with an edge on top of a fixed line. The rank assignment providing the coefficients for row reduction is given by the condition $N_i = -N_{i+k}$, $v_\alpha = -v_{\overline{\alpha}}$, and the difference between the ranks of two adjacent faces is given by $N_i - N_{i+k} = v_\alpha - v_{\overline{\alpha}}$. Combining these two results, we obtain

$$2N_i = N_i - N_{i+k} \;=\; v_\alpha - v_{\overline{\alpha}} = 2v_\alpha \,. \tag{8.74}$$

Let us now determine the f_i from the toric data. The method we are going to discuss below can be regarded as a generalization to orientifolds of the algorithm for finding the (minimal) matter content of a quiver in terms of basic knowledge of the (p, q) winding numbers of its ZZPs (equivalently of the external legs of the (p, q) web dual to the toric diagram). The intersection number between a given ZZP and the fixed line is

$$\det \begin{pmatrix} p & 1 \\ q & 1 \end{pmatrix} = p - q \,. \tag{8.75}$$

At every such crossing this ZZP, if not self-identified, will intersect its image on the line. The edge on which they cross will produce a tensor or conjugate tensor field, depending on the orientation of the crossing. This is depicted in Figure 8.9.

From the discussion above, it is clear that the non-vanishing components of f_i are exactly those corresponding to the faces with a tensor, for which we have just determined the rank in terms of the ZZP values. Taking

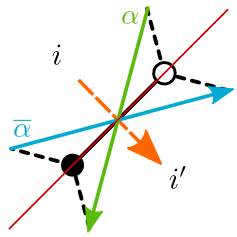

Figure 8.9: Crossing between a ZZP (and its image) over an edge on top of a diagonal fixed line. We show the corresponding bifundamental field in the mother theory.

into account that the same ZZP can be related to $p_\alpha - q_\alpha$ tensors, this allows us to write Equation (8.73) as

$$\sum_i N_i f_i = (\pm 4) \sum_\alpha v_\alpha (p_\alpha - q_\alpha) = 0\,, \tag{8.76}$$

where we have factorized the choice of sign for the diagonal O-line.

It is worth noting that the intersection with sign is a topological quantity that counts the minimal number of intersections of the ZZP with the fixed line in the dimer. This is, in fact, a homological invariant. In principle, more intersections are allowed, but they will come in pairs, one with positive and one with negative intersection, as shown in Figure 8.10. When computing the total contribution they cancel, leaving us with Equation (8.76), which does not depend on the particular phase we are considering.

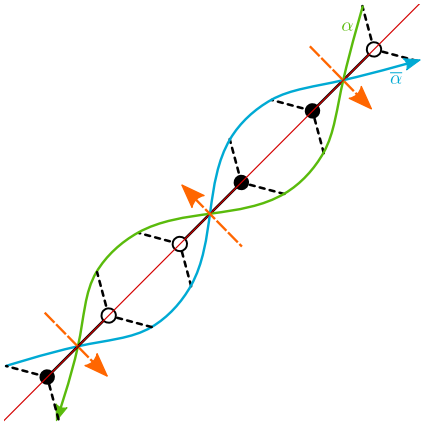

Figure 8.10: When ZPPs are deformed, additional intersections are added in pairs. We show the corresponding bifundamental fields in the mother theory.

We use the topological constraint Equation (8.72) to express the value assigned to v_1, as

$$v_1 = -\frac{1}{p_1 + q_1} \sum_{\alpha \neq 1} v_\alpha (p_\alpha + q_\alpha) \,. \tag{8.77}$$

Plugging this expression into (8.76) and rearranging the terms, we reach the following equality:

$$\sum_{\alpha \neq 1} v_\alpha \left(p_\alpha q_1 - p_1 q_\alpha \right) = 0 \,. \tag{8.78}$$

Then, the Rouché-Capelli theorem can be satisfied for generic v_α *iff*

$$p_\alpha q_1 - p_1 q_\alpha \equiv \det \begin{pmatrix} p_\alpha & p_1 \\ q_\alpha & q_1 \end{pmatrix} = 0 \ , \tag{8.79}$$

which implies that $p_\alpha = p_1, q_\alpha = q_1$ for every α. This implies that the toric diagram has a maximum of 4 edges, 2 of which are orthogonal to the symmetry axis. We dub the corresponding class of toric diagrams the *trapezoids*. An example of such a trapezoid is shown in Figure 8.11. Among trapezoids, we of course include also *triangles*.

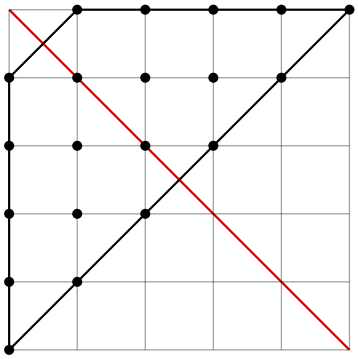

Figure 8.11: An example of a trapezoid for which you can find a non-anomalous diagonal line orientifold.

Note also that there is a subset of trapezoids for which (8.76) is trivially satisfied. They have $p_\alpha = q_\alpha$ for every α so we refer to them as the *rectangles*, and describe orbifolds of F_0. See Figure 8.12 as an example. We remark that rectangles are the toric diagrams that give rise to line orientifolds without tensors in the spectrum. Thus, we recover the result that the latter always admit a non-anomalous solution.

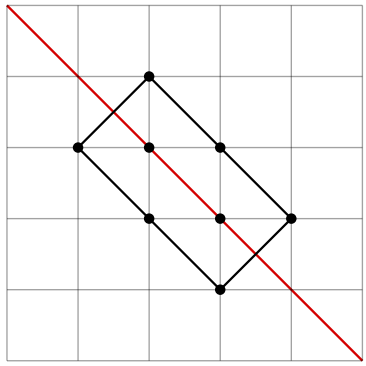

Figure 8.12: An example of a rectangle toric diagram with its diagonal axis of symmetry.

Preliminary result for diagonal line orientifolds: Unless the toric diagram of the singularity under consideration is a trapezoid, any orientifold theory obtained from a dimer symmetric with respect to its diagonal, *and in which every face has at most one edge along this diagonal*, does not admit anomaly-free solutions.

Faces with multiple tensors

Faces with multiple tensors arise in examples as simple as the conifold or $\mathbb{C}^2/\mathbb{Z}_{2n+1}$ orbifolds, upon orientifolding with respect to a diagonal line. We now discuss how the previous discussion is extended to these cases. We start by considering how multi-tensor faces may be embedded in the dimer. We will see that there are restrictions on the number of tensors a face can have. Moreover, their existence is non-trivial and imposes constraints on the toric diagrams. The analysis of this case is slightly different from the one in the previous section but will lead to the same result.

Interestingly, it is possible to find an upper bound on the number of tensors a face in the dimer can have. Figure 8.13 shows a face with two self-identified edges on the same side of the O-line. If they were adjacent, they would be connected at a 2-valent node, which corresponds to a mass term, and then they could be integrated out. Naively, we might imagine that this can be avoided by introducing additional structure between the two edges, which is represented as a blob in Figure 8.13. But the ZZPs generating the edges on the line are the only ones that participate in the blob. In other words, the orange and purple ZZPs in Figure 8.13 must be identified with the blue and green ZZPs, with the precise identification depending on the

number of intermediate edges. Therefore, the blob can only correspond to a sequence of edges connected by mass terms. After integrating them out, we are left with either zero or one tensor for an even or odd number of edges, respectively. This implies that a given face can only support more than one tensor in two cases: if they belong to different O-lines or if they belong to the same O-line but are coming from different copies of the unit cell as illustrated in Figure 8.14. In both cases, the previous analysis applies to each instance that the face touches a fixed line, so we conclude that the maximum possible number of tensors at a given face is two. The total number of tensors in the full theory is, however, unrestricted.

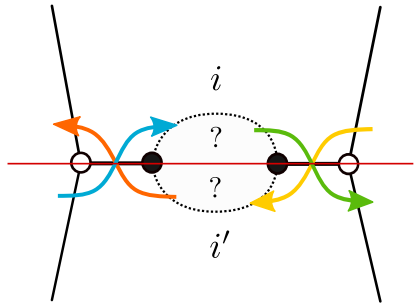

Figure 8.13: Two edges of a given face on a fixed line, separated by a general structure.

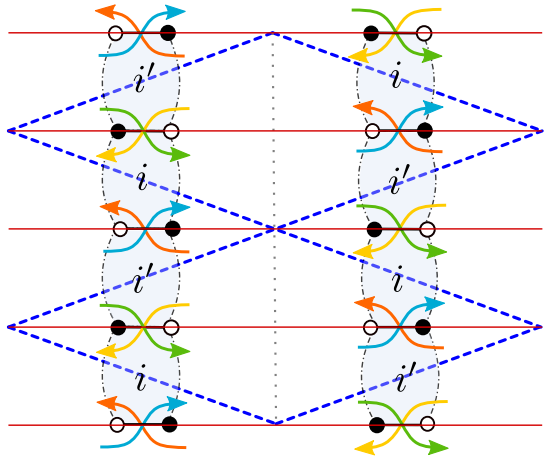

Figure 8.14: Faces with edges on top of the fixed line at different copies of the unit cell.

From Figure 8.14, we see that there can be three types of ZZPs: ZZPs parallel to the fixed line, which are forbidden since they would have to go through the face with two tensors, spoiling it; ZZPs orthogonal to the fixed

line, *i.e.* self-identified ZZPs, which do not give rise to tensors; finally, ZZPs which intersect in pairs on self-identified edges giving rise to tensors. Thus, the singularity can only have self-identified ZZPs, those of the γ kind, and at most two couples of ZZPs of the α kind. Moreover, the (p, q) numbers of the latter are also subject to constraints. They cannot cross faces i and i' otherwise than passing by the O-lines, so they can intersect the grey dotted axis in Figure 8.14 at most twice if only one couple of ZZPs α is involved:

$$|p_\alpha + q_\alpha| \leq 2 \quad \text{for } \alpha = 1\,, \tag{8.80}$$

and once in the case of two couples:

$$|p_\alpha + q_\alpha| = 1 \quad \text{for } \alpha = 1, 2\,. \tag{8.81}$$

Those relations apply both for ZZPs α and $\bar{\alpha}$, for which the sums are respectively negative and positive.

If there is only one couple, the singularity corresponds to a trapezoid as the ones discussed in the previous section. Indeed, we have only one couple of ZZPs of the α kind and the topological constraint imposes $v_1 = 0$ for them, turning the RC condition into a trivial equation.

For two couples, the topological constraints and (8.81) impose

$$v_1 = -v_2\,. \tag{8.82}$$

This is the counterpart of the fact that faces i and i' in Figure 8.14 have to be of opposite ranks, following (8.74). Now, we can write the RC condition allowing faces to support one or two tensors in terms of v_1 only:

$$\sum_i N_i f_i = (\pm 4)(v_1(p_1 - q_1) - v_1(p_2 - q_2)) = 0\,. \tag{8.83}$$

Knowing (8.81), the only solution is $(p_1, q_1) = (p_2, q_2)$ so that we recover trapezoids. Let us note that the last equation considered with (8.82) can be brought to the form of (8.78) for two couples of ZZPs α, hence it is not surprising that a subset of trapezoids appears again as solutions in this context. For instance, the conifold does not provide a non-anomalous diagonal line orientifold while $\mathbb{C}^2/\mathbb{Z}_{2n+1}$ orbifolds do.

We conclude with a general result for diagonal line orientifolds:

Diagonal line orientifolds: Unless the toric diagram of the singularity is a *trapezoid*, any orientifold theory obtained from a dimer with a diagonal O-line is anomalous.

See Figure 8.15 for more examples.

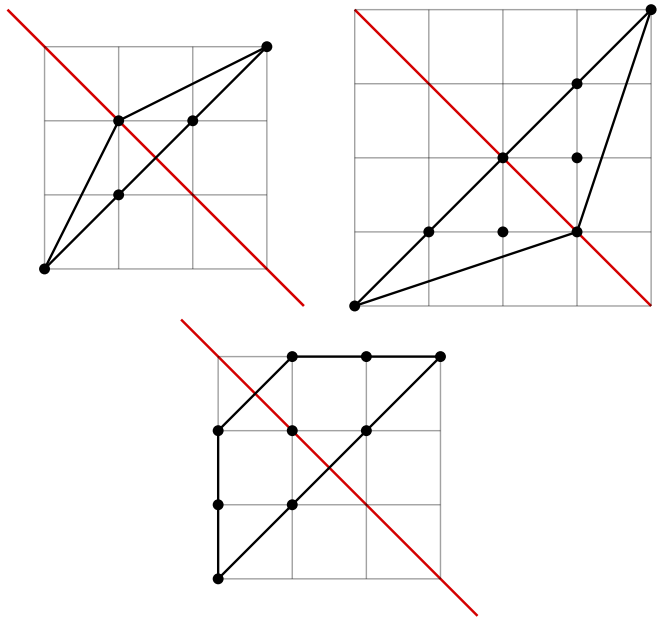

Figure 8.15: Examples of trapezoids, which admit anomaly-free fixed line orientifolds.

8.3.2 Horizontal/Vertical lines orientifolds

In this section, we consider horizontal fixed lines. The case of vertical lines is trivially related by rotation. The reasoning is essentially the same as the one described previously for the case of diagonal lines. This allows us to go fast to the main result for this class of orientifolds. In particular, we will not comment here about rectangles and faces with many tensors since the previous results are easily generalized.

Horizontal symmetry lines in the dimer correspond to a vertical symmetry in the toric diagram. The $\mathbb{Z}_2$ action maps a ZZP with winding (p, q) to a ZZP with winding $(-p, q)$. Again, we distinguish two different types of ZZPs:

- Pairs of ZZPs $\{v_\alpha, v_{\overline{\alpha}}\}$ for $\alpha = 1, ..., l$, where v_α and $v_{\overline{\alpha}}$ are exchanged under the symmetry, thus not parallel to the axis of symmetry.
- Self-identified ZZPs $\{v_\gamma\}$ for $\gamma = 1, ..., l_{\|}$, with winding numbers $(0, 1)$ or $(0, -1)$.

A general illustration of this is depicted in Figure 8.16.

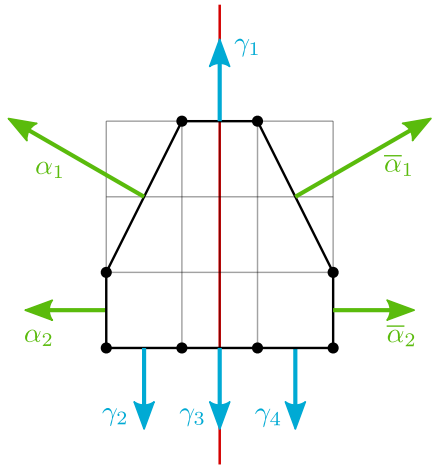

Figure 8.16: A generic singularity with a vertical axis symmetry.

In order to find the antisymmetric solutions to the ACC, we need to look at the antisymmetric value assignments of the ZZPs and impose the topological constraint

$$\Lambda = 2\sum_{\alpha} v_\alpha p_\alpha = 0 \ . \tag{8.84}$$

Let us now consider the Rouché-Capelli condition. A ZZP of type α with winding numbers (p, q) crosses both fixed lines $-q$ times, counted with sign. The Rouché-Capelli condition can be expressed as

$$\sum_i N_i f_i = -\sum_{\alpha} v_\alpha q_\alpha (4 \text{ sign}(A) + 4 \text{ sign}(B)) = 0 \,, \tag{8.85}$$

where sign(A) and sign(B) indicate the signs of the two fixed lines. Unlike the case of diagonal lines, the Rouché-Capelli condition in (8.85) becomes trivial as soon as sign(A) and sign(B) are different. In that case, the orientifold theory is always anomaly-free.

If the two fixed lines have the same sign, (8.84) allows us to express v_1 in terms of the remaining v_α, as in the case of diagonal lines. Plugging this expression into Equation (8.85) leads to

$$\sum_{\alpha \neq 1} v_\alpha \left(p_\alpha q_1 - p_1 q_\alpha\right) = 0 \,. \tag{8.86}$$

With the same analysis of the previous section, we find that singularities with two horizontal lines of the same sign admit a solution to the ACC only if they are trapezoids, just as in the case of diagonal lines. See Figure 8.17 for examples.

Horizontal/vertical lines orientifolds: Toric diagrams symmetric with respect to a horizontal/vertical axis always lead to anomaly-free orientifold theories when the two O-lines have *opposite signs*. When the signs are the same, instead, in order to yield a non-anomalous orientifold theory the toric diagram of the singularity must be a *trapezoid*.

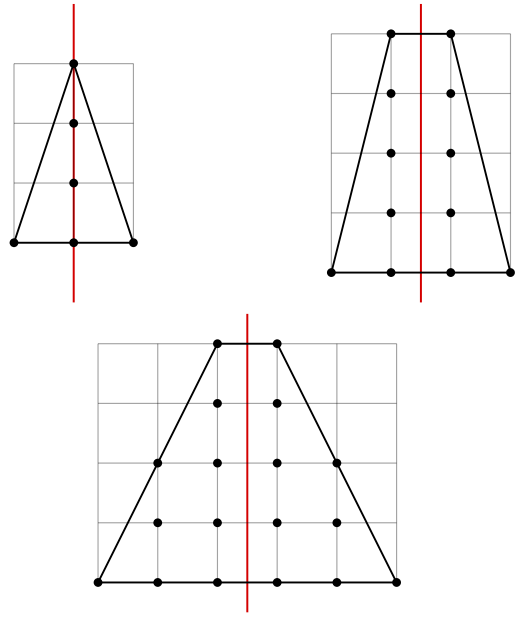

Figure 8.17: Examples of trapezoids, which admit anomaly-free horizontal fixed line orientifolds.

8.3.3 Fixed points orientifolds

Finally, we address the case of fixed point orientifolds. We should state right away that the results in this case are less conclusive than for fixed lines. Indeed, one can easily anticipate that having a larger number of signs to fix (at the four fixed points), it will be straightforward to satisfy the ACC just by a wise choice, similarly to the case with horizontal/vertical line. On the other hand, if one sticks with a 'wrong' choice, the restriction on the allowed geometries is not as nicely characterizable as in the previous case.

As already explained in Section 8.2, the action of the orientifold on every ZZP is to map it either to itself or to another ZZP with the same winding numbers. We thus divide the ZZPs into two sets:

- Pairs of distinct ZZPs $\{v_\alpha, v_{\overline{\alpha}}\}$ for $\alpha = 1, \cdots, k$ that are exchanged.
- Self-identified ZZPs $\{v_\gamma\}$, for $\gamma = 1, \cdots, l$.

The total number of ZZPs is $n = 2k + l$.

In this kind of orientifolds, tensors arise whenever a pair of self-identified ZZPs intersect over a fixed point. Moreover, a ZZP going through a fixed point necessarily goes through a second fixed point [73]. As a result, it is easy to convince oneself that the number of tensors, if present at all, must be between 2 and 4, and it coincides with the total number of self-identified ZZPs that cross a fixed point.

In order to find the antisymmetric solutions to the ACC, we need to consider symmetric value assignments for the ZZPs, as explained in Section 8.2, subject to the topological constraints

$$\begin{array}{rcl} \Lambda & = & 2\sum_\alpha v_\alpha p_\alpha + \sum_\gamma v_\gamma p_\gamma \;=\; 0\,, \\ M & = & 2\sum_\alpha v_\alpha q_\alpha + \sum_\gamma v_\gamma q_\gamma \;=\; 0\,. \end{array} \tag{8.87}$$

The RC equation becomes

$$\sum_i N_i f_i = \sum_{\gamma \neq \gamma'} (v_\gamma - v_{\gamma'})(\pm 4) = 0\,. \tag{8.88}$$

where the sum in the middle runs over the tensors. The signs depend on the sign of the fixed points and on the orientations of the self-identified edges. Depending on which of the two faces adjacent to the edge we preserve in the projection, we get tensors or their conjugates, contributing with opposite signs to the ACC.

We recall that the signs of the fixed points, in contrast with fixed lines, are constrained by the *sign rule* [54]. The rule prescribes that the product of the four signs is $(-1)^{n_W/2}$, with n_W the number of superpotential terms.[4]

We now consider the different possibilities, *i.e.* $l = 2$, 3 and 4 tensors. Our analysis is general and does not distinguish between faces with single or multiple tensors.

- $l = 2$: In this case we have two tensors, meaning that two ZZPs cross each other on two fixed points. Equation (8.88) reads

$$(v_1 - v_2)(\pm_1 4) \pm (v_1 - v_2)(\pm_2 4) = 0\,, \tag{8.89}$$

[4]Generically, it is not known whether the parity of $n_W/2$ can be deduced from the toric diagram.

where the $\pm_i$ indicate the signs of the fixed points, while the additional $\pm$ signs depends on whether the tensors are conjugated or not.

Since only two fixed points are involved in this case, their signs can always be chosen such that this equation is trivially satisfied, while satisfying the sign rule. However, it is interesting to consider whether there are other ways to satisfy this constraint. We can impose $v_1 = v_2$ using the two equations of the topological constraint. Expressing v_1 and v_2 as function of the other v_α's we get

$$\begin{aligned} v_1 &= \frac{2}{p_1 q_2 - p_2 q_1}(p_2 \sum_\alpha v_\alpha q_\alpha - q_2 \sum_\alpha v_\alpha p_\alpha)\,, \\ v_2 &= \frac{2}{p_1 q_2 - p_2 q_1}(q_1 \sum_\alpha v_\alpha p_\alpha - p_1 \sum_\alpha v_\alpha q_\alpha)\,, \end{aligned} \tag{8.90}$$

where we have assumed $p_1 q_2 - p_2 q_1 \neq 0$. Equating v_1 and v_2, we obtain

$$\sum_\alpha v_\alpha (p_\alpha (q_1 + q_2) - q_\alpha (p_1 + p_2)) = 0\,. \tag{8.91}$$

Since this equation must hold for all v_α, the only possibility is that all terms in the summation vanish, thus $p_\alpha(q_1 + q_2) = q_\alpha(p_1 + p_2)$ for all α. Solutions are of the form $p_1 = -p_2$ and $p_\alpha = 0$, up to $SL(2, \mathbb{Z})$ transformations. Those correspond to trapezoids (not necessarily symmetric with respect to any axis) with an even number of ZZPs on each base and only one ZZP on each side.

If $p_1 q_2 - p_2 q_1 = 0$, it means that $(p_1, q_1) = -(p_2, q_2)$, since the two ZZPs are parallel and, in order to intersect in a consistent way, they must have opposite winding numbers. In this case, the topological constraint imposes $v_1 = v_2$ if $p_\alpha q_{\alpha'} - q_\alpha p_{\alpha'} = 0$ where $\alpha \neq \alpha'$. It means that all non-self-identified ZZPs have to be either parallel or anti-parallel to each other. This condition is satisfied by all toric diagrams with the shape of a rectangle or a parallelogram where there is an even number of non self-identified ZZPs. Together with the solutions of the previous paragraph, they constitute a class of trapezoids for which any sign assignment for the fixed points leads to an anomaly-free theory when two tensors are involved.

As an illustration, consider fixed point orientifolds of $\mathbb{C}^3/\mathbb{Z}_6$ with actions (1,1,4) and (1,2,3), whose toric diagrams are shown in Figure 8.18. Both of them admit an orientifold with two tensors. Our analysis implies that only the first one admits tensors with any sign, as it can easily be checked by explicitly solving the ACC.

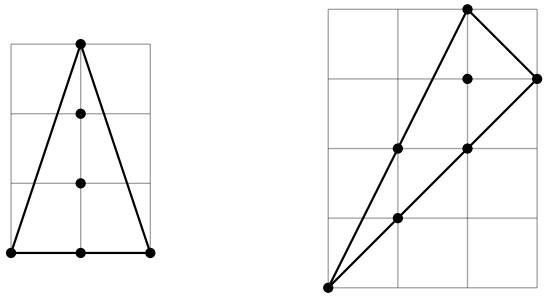

(a) (b)

Figure 8.18: The toric diagrams for the $\mathbb{C}^3/\mathbb{Z}_6$ orbifolds with actions: (a) (1,1,4) and (b) (1,2,3).

An interesting scenario is when tensors arise from the orientifold projection of adjoints in the mother theory, namely from edges separating self-identified faces. In this case, the ACC of the self-identified gauge group is trivially zero, since it is either SO or USp. In this situation, the two self-identified ZZPs intersect all other ZZPs only once. This can be understood as follows. Let us consider a line passing through the fixed points under consideration. All the non self-identified ZZPs must be parallel to this line, since otherwise their intersections with the line would imply that they go through the self-identified face, which in turn would spoil the fact that it is self-identified. The $\mathbb{C}^2/\mathbb{Z}_{2m}$ orbifolds are examples in this class, see Figure 8.19.

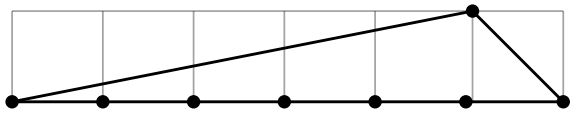

Figure 8.19: The toric diagram of $\mathbb{C}^2/\mathbb{Z}_6$, as an example of the $\mathbb{C}^2/\mathbb{Z}_{2m}$ family.

- $l = 3$: In this case we have three tensors, *i.e.* three ZZPs intersecting on three fixed points. Equation (8.88) reads

$$(v_1 - v_2)(\pm_1 4) \pm (v_2 - v_3)(\pm_2 4) \pm (v_3 - v_1)(\pm_3 4) = 0 \ . \qquad (8.92)$$

Since only three of the fixed points are involved, it is possible to pick their signs such that this equation is trivially satisfied. These choices in turn determine the sign of the fourth fixed point due to the sign rule.

If instead we have a different combination of signs, we end up with an

equation of the form

$$v_\gamma - v_{\gamma'} = 0\,, \tag{8.93}$$

with γ and γ' two of the three ZZPs above. The missing $v_{\gamma''}$ in the previous equation depends on the choice of fixed point signs in Equation (8.92). Therefore, in order to have a solution for all possible fixed point sign assignments we need to impose $v_1 = v_2 = v_3$ with the topological constraint. This means that the ZZPs have winding numbers of the form $(p_1, 0)$, $(-p_1, q_2)$ and $(0, -q_2)$, up to $SL(2, \mathbb{Z})$ transformations. The only solution is $p_1 = q_2 = 1$, corresponding to $\mathbb{C}^3$, *i.e.* flat space.

A face with multiple tensors imposes constraint(s) of the form $v_1 - v_2 = \pm(v_2 - v_3)$, leading to an RC constraint of the form

$$(v_1 - v_2)(\pm_1 4) \pm (v_1 - v_2)(\pm_2 4) \pm (v_3 - v_1)(\pm_3 4) = 0\ . \tag{8.94}$$

Again, the existence of solutions depends on the signs of the fixed points. Solutions for generic signs can be obtained only when $v_1 = v_2 = v_3$, *i.e.* for flat space.

- $l = 4$: This case, in contrast with the previous ones, does not always admit a solution to the ACC. The reason for this is that the four fixed points are used, their signs are constrained by the sign rule and we no longer have the freedom of unused fixed points.

  The RC equation can take two different forms, depending on the ZZP intersections:

$$\begin{aligned}(v_1 - v_2)(\pm_1 4) \pm (v_2 - v_3)(\pm_2 4)& \\ \pm (v_3 - v_4)(\pm_3 4) \pm (v_4 - v_1)(\pm_4 4) &= 0\ , \end{aligned} \tag{8.95}$$

$$\begin{aligned}(v_1 - v_2)(\pm_1 4) \pm (v_1 - v_2)(\pm_2 4)& \\ \pm (v_3 - v_4)(\pm_3 4) \pm (v_3 - v_4)(\pm_4 4) &= 0\ . \end{aligned} \tag{8.96}$$

  Since the signs of the fixed points are constrained, it is not always possible to trivially solve the RC equation.

  Moreover, it is also impossible to find general non-trivial solutions by using the topological constraint to force some of the v_i to be equal. For the first equation, we need all the v_i to be equal. To do so, we need at least three equations, but the topological constraint provides only two. In the second case, we can impose $v_1 = v_2$ and $v_3 = v_4$ with the following ZZPs: $(1, 0)$, $(-1, 0)$, $(0, 1)$ and $(0, -1)$, which define the conifold singularity. Unfortunately, the conifold gives rise to an RC of the first kind, not of the second one.

To conclude, this partial analysis retained only one toric diagram that can accommodate any signs for its fixed points: flat space. We eventually found some particular trapezoids for which we can freely choose the signs of the tensors when only two are present, but those singularities also allow *in principle* for fixed point orientifolds with four tensors, where our analysis showed its limits. Thus, we cannot say in general that they provide every kind of anomaly-free orientifolds. As an illustrative example, one can check that the orientifold of Figure 8.18a with four tensors does not allow for every combination of signs satisfying the sign rule, although it does with only two tensors.

It would be interesting to investigate further whether it is possible to determine the solvability of the ACC from the toric diagram. We leave this question for future work. In the meantime, orientifolds with four self-identified ZZPs need to be studied on a case-by-case basis.

8.4 Conclusions

In this chapter we studied anomalies in gauge theories living on D-branes probing orientifolds of toric singularities, focusing on pure D3-brane theories, namely without the addition of extra flavors.

We introduced a new, geometric algorithm for finding anomaly-free solutions based on zig-zag paths. The main virtue of this procedure is not so much its practicality over the direct solution of the ACC in explicit examples, but the fact that it allows us to make general statements regarding anomalies directly from geometry. Indeed, we managed to derive stringent no-go theorems that establish the conditions for anomaly-free solutions in these orientifolds. Such results are extremely useful since until now the cancellation of anomalies in this class of theories was analyzed on a case-by-case basis.

We can summarize our findings as follows, from the most stringent case to the less conclusive one:

- For orientifolds with a fixed diagonal line, for which one has to choose only one sign, we find that only singularities whose toric diagram is a trapezoid with respect to the diagonal axis of symmetry allow for a non-anomalous D-brane gauge theory.
- For orientifolds with fixed horizontal lines, we have two signs to choose. All singularities can lead to anomaly-free theories if the two signs are chosen to be opposite to each other. If the singularity has a toric

diagram which is a trapezoid with respect to the vertical axis of symmetry, then the theory can be non-anomalous also for equal signs.

- For orientifolds with fixed points, there are four signs to choose, up to a constraint on their product. Moreover, the relation between the fixed points in the dimer and the toric diagram of the singularity is less direct. Because of these two facts, it is more difficult to summarize the few instances where a restriction is indeed obtained on the singularities that lead to non-anomalous theories. The particular cases have been detailed in Section 8.3.3.

As an illustration of the power of the ideas introduced in this work, we will exploit them in Part III to guide the search of models of D-branes at singularities that display dynamical supersymmetry breaking. Such models necessarily involve orientifolds, but have a potential instability as soon as the singularity allows for a partial resolution which is non-isolated (in D-brane jargon, this translates to the presence of $\mathcal{N} = 2$ fractional branes [74]). In terms of the toric diagram, this property manifests itself through points within the external edges of diagram, or in other words, parallel ZZPs.[5] It is straightforward to see that toric diagrams that fall in the class of trapezoids always include such points on the boundary, except for few very simple cases (namely F_0 and orbifolds with a toric diagram which is an isosceles triangle with a unit base). As a consequence, if one is to look for fixed line orientifolds which allow for anomaly-free D-brane configuration, and with no non-isolated partial resolution, the only option one is left with is horizontal/vertical fixed lines with opposite signs.

[5] In [179, 180] the existence of such flat directions in moduli space was exploited to add relevant mass deformations in dimers with and without orientifolds.

Chapter 9

Dimers in a Bottle

In the pioneer work [54], orientifolds were classified in three groups, depending on the involution, those that leave four fixed points, a single fixed line, or two fixed lines in the dimer. Interestingly, these correspond to three out of the five possible smooth involutions on the torus [181]. The remaining ones correspond to a shift of the fundamental cell and a glide reflection, *i.e.* combining a shift and a reflection.

The main purpose of this chapter is to study the two last cases, that leave no fixed loci and assess whether they correspond to sensible orientifolds in string theory. We will argue that only the glide reflection leads to SUSY preserving orientifolds, while the shift is always breaking it. Moreover, we will show how the orientifold projection corresponding to a glide reflection has remarkable properties. Not only, the projected theory always has a conformal fixed point, but also admits, in some cases, a non-trivial RG-flow described by a cascade of Seiberg dualities, analogous to the one of the conifold [27, 91]. Our results were originally presented in [6].

The organization of the chapter is as follows. In Section 9.1 we review the list of torus involutions and connect them to orientifolds in dimer models to find the missing cases. In Section 9.2 we describe glide orientifolds starting from orbifolds and describing their general properties. The absence of fixed loci is tackled in Section 9.3, where we understand it to be dual to a pair of opposite sign orientifold planes and use T- and mirror duality to give a global picture. In Section 9.4 we study the action on the toric geometry through the zig-zag paths, allowing the study of fractional branes in the orientifolded theory. A proof of the non-existence of SUSY preserving shift orientifolds is finally provided in Section 9.5. Some string computations and a cascade analysis are presented in Appendices 9.A and 9.B.

9.1 Torus involutions

There are five inequivalent non-trivial smooth involutions [181], *i.e.* involutory diffeomorphisms, on a torus.[1] Three of them have a fixed locus and the two others do not. To list all of them we consider a square torus, with a complex structure[2] $\tau = i$. We take z as the complex coordinate on the torus and the periodicity condition is $z \sim z + m + ni$, with $m, n \in \mathbb{Z}$. The involutions are given by:

1. Two fixed lines: $z \to \bar{z}$. The fixed loci are two parallel lines located at $\mathrm{Im}(z) = 0, 1/2$ along the real axis. Under this involution, the torus is projected to an annulus.

2. Single fixed line: $z \to i\bar{z}$. The fixed line is $\mathrm{Re}(z) = \mathrm{Im}(z)$, corresponding to a diagonal line of the unit cell. The resulting surface is a Moebius strip.

3. Fixed points: $z \to -z$. In this case we have four fixed points, $z = 0, 1/2, i/2$ and $(1+i)/2$. The resulting topology is that of a sphere.

4. Glide reflection: $z \to \bar{z} + 1/2$. There are no fixed loci. The resulting topology is that of a Klein bottle.

5. Shift: $z \to z + 1/2$. Again, the involution has no fixed loci. The torus is projected to another torus.

As already mentioned, 1, 2 and 3 are involutions with fixed loci correspond to orientifold operations already studied in the literature. In this chapter, we will focus on 4, the glide reflection, studying the consistency of such projection and its properties. Regarding involution 5, we will show that the shift is not compatible with the required properties to preserve supersymmetry.

Let us conclude this section with few comments. First, involutions with fixed loci teach us that if the involution is holomorphic, $z \to f(z)$, nodes in the dimer are mapped to nodes of the opposite color, while if it is antiholomorphic, $z \to f(\bar{z})$, nodes are mapped to nodes of the same color. This is a requirement from the orientifold mapping of chiral superfields.

[1] They are classified by the topology of their orbit set which is always one of the parabolic two-orbifolds listed in [182].

[2] We are interested only in smooth involutions, the complex structure doesn't play any role in the analysis, thus we fixed it to a handy value. The use of complex coordinates will be useful for later observations.

It gives us a hint for the unexplored involutions. Indeed, we expect 5 to be consistent with an orientifold identification only if nodes are mapped to nodes of the opposite color, while 4 would be consistent only if the mapping is between vertices of the same color. Second, we stress that the involution should be not only a symmetry for the torus, but also for the embedded dimer model. In particular, a generic fundamental cell for a dimer model has the shape of a parallelogram. The symmetry may be present in the abstract graph, but in order to be shown explicitly, consider the case of say 2, one has to deform the embedding in such a way that the resulting fundamental cell is now a rhombus, displaying a symmetry with respect to one of the diagonals. From this observation, we conclude that in order to display a glide symmetry, the fundamental cell must be a rectangle. Third, a $\mathbb{Z}_2$ glide reflection with diagonal axis is described by the map $z \to i\bar{z} + (1+i)/2$ which has $\mathrm{Re}(z) = \mathrm{Im}(z) + 1/2$ as fixed line, hence they are nothing else than reflections about a diagonal axis. In particular, they do not correspond to a class of smooth involutions not listed above.

Even if we can deform the embedding to make the involution explicit, it is possible that the model can be endowed with extra structures, capturing some physical properties. For example, isoradial embeddings described in [146] encode the R-charges of the fields. In this work, though, we are not interested in these particular cases.

9.2 Glide orientifolds

In this section, we investigate glide reflection orientifolds. We start with orbifold examples, motivating our results in the dimer from the open string projection on the Chan-Paton indices. We also explicitly check that it preserves supersymmetry, in particular, it acts on the CY 3-form as $\Omega_3 \to -\Omega_3$. We extend our results to orbifolds of the conifold, considering the cascade in the presence of deformation fractional branes. Finally, we discuss anomalies, or rather their absence, and conformality in the presence of these orientifolds.

9.2.1 Orbifold $\mathbb{C}^2/\mathbb{Z}_2$

We consider the recipe directly applied in the dimer and then check that it is indeed predicted by open-string computation.

Projection on the dimer model

(a) (b)

Figure 9.1: (a) Dimer diagram for the orbifold $\mathbb{C}^2/\mathbb{Z}_2 \times \mathbb{C}$. The unit cell and the reflection axis are depicted in blue and red respectively. (b) The Klein bottle we obtain with the orientifold projection.

We present in Figure 9.1 the dimer for the orbifold $\mathbb{C}^2/\mathbb{Z}_2$ where the glide reflection is a combined operation of a horizontal shift by one half of the length of the unit cell followed by a reflection with respect to the dashed red horizontal axis. Nodes are mapped to nodes of the same color, as we want from the analysis in Section 9.1. Note that this operation leaves no fixed loci in the unit cell. The projected theory is embedded in a Klein Bottle drawn on one half of the original unit cell, as illustrated in Figure 9.1b.

The edge X_{12} is identified with Y_{12}, X_{21} with Y_{21} and Z_{11} with Z_{22}. Following the rules summarized in Section 7.2, the resulting theory has gauge group $SU(N)_1$ with matter content given by two tensors[3] and one adjoint field. Note that the tensor fields are not in an irreducible representation, so we split them in their symmetric and antisymmetric parts;

$$\begin{aligned} \mathcal{X}_{S,A} &= \overline{\square\square}_1, \overline{\begin{smallmatrix}\square\\\square\end{smallmatrix}}_1 \,, \\ \mathcal{Y}_{S,A} &= \square\square_1, \begin{smallmatrix}\square\\\square\end{smallmatrix}_1 \,, \\ \mathcal{Z} &= \mathrm{Adj}_1 \,. \end{aligned} \tag{9.1}$$

The superpotential is obtained by explicitly projecting the original one and keeping half of the terms,

$$W = \mathcal{X}\mathcal{Y}\mathcal{Z}^T - \mathcal{Y}\mathcal{X}\mathcal{Z} = \mathcal{X}_A\mathcal{Y}_S\mathcal{Z} - \mathcal{X}_S\mathcal{Y}_A\mathcal{Z} \,. \tag{9.2}$$

In a SUSY-preserving orientifold in type IIB, the holomorphic 3-form must map to minus itself. This is easy to check by noting that the orientifold

[3]The two tensors are of the form $(\overline{\square}_1, \overline{\square}_1)$ and $(\square_1, \square_1)$.

action on the mesons is

$$x \leftrightarrow y \qquad w \to w \qquad z \to z\,. \tag{9.3}$$

The action on the 3-form is then

$$\Omega_3 = \frac{\mathrm{d}x \wedge \mathrm{d}y \wedge \mathrm{d}z}{2w} \to \frac{\mathrm{d}y \wedge \mathrm{d}x \wedge \mathrm{d}z}{2w} = -\Omega_3\,. \tag{9.4}$$

It is also clear from the matter content and the first equality of Equation (9.2) that the gauge theory preserves $\mathcal{N} = 2$ supersymmetry.[4]

It is worth noting that the theory, unlike many examples of projections with fixed loci, is free from any local gauge anomaly, regardless of the gauge group rank. Although this example is rather trivial, we will see that this feature is general and related to tensor fields being absent or coming in pairs, symmetric and antisymmetric, canceling each other's contribution to the anomaly cancellation conditions (ACC). We also note that the projected theory is actually conformal. Indeed, the β-function of the gauge group can be shown to be zero. The fact that these orientifolds naturally lead to SCFT's will be discussed in Section 9.2.4.

Open string projection

We now consider the orientifold projection on the Chan-Paton indices of the open string spectrum. For D-branes localized on the $\mathbb{C}^2/\mathbb{Z}_2 \times \mathbb{C}$ singularity the open string spectrum is obtained by promoting the flat space one to $2N \times 2N$ matrices with a restricted set of non-zero entries:

$$\begin{aligned} A_\mu &= \begin{pmatrix} A_{1\mu} & 0 \\ 0 & A_{2\mu} \end{pmatrix}, \quad \Phi_1 = \begin{pmatrix} 0 & X_{12} \\ X_{21} & 0 \end{pmatrix}, \\ \Phi_2 &= \begin{pmatrix} 0 & Y_{12} \\ Y_{21} & 0 \end{pmatrix}, \quad \Phi_3 = \begin{pmatrix} Z_{11} & 0 \\ 0 & Z_{22} \end{pmatrix}, \end{aligned} \tag{9.5}$$

where the gauge group is $SU(N)_1 \times SU(N)_2$ and matther fields transform in the following representations,

$$X_{ij}, Y_{ij} = (\square_i, \overline{\square}_j), \quad Z_{ii} = \mathrm{Adj}_i\,. \tag{9.6}$$

[4]The attentive reader might have noticed that this orientifolded theory is identical to the one obtained with fixed points in Section 7.2, although the involution acts differently on the coordinates. This is however an artifact of the orbifold $\mathbb{C}^2/\mathbb{Z}_2$ since glide reflections will not provide tensors in general.

Decomposing the $\mathbb{C}^3$ fields the orbifold superpotential becomes,

$$\begin{aligned} W &= [\Phi_1, \Phi_2]\, \Phi_3 \\ &= X_{12}Y_{21}Z_{11} - Y_{21}X_{12}Z_{22} + X_{21}Y_{12}Z_{22} - Y_{12}X_{21}Z_{11}\,, \end{aligned} \tag{9.7}$$

where an overall trace over gauge indices is understood.

A general orientifold projection on the $\mathbb{C}^3$ fields acts as,

$$A_\mu = -\gamma_\Omega A_\mu^T \gamma_\Omega^{-1}\,, \tag{9.8}$$

$$\Phi_i = R_{ij}\gamma_\Omega \Phi_j^T \gamma_\Omega^{-1}\,, \tag{9.9}$$

where γ_Ω is a $2N \times 2N$ matrix acting on gauge group (Chan-Paton) indices and R_{ij} acts on space indices i, j running from 1 to 3. Different choices for these matrices lead to different orientifold projections. In order to reproduce the glide reflection orientifold, we specifically choose

$$\gamma_\Omega = \begin{pmatrix} 0 & \mathbb{1}_N \\ \mathbb{1}_N & 0 \end{pmatrix}\,, \quad \text{and} \quad R = \begin{pmatrix} 0 & 1 & 0 \\ 1 & 0 & 0 \\ 0 & 0 & 1 \end{pmatrix}\,, \tag{9.10}$$

so that Φ_1 and Φ_2 coordinates are exchanged by the orientifold. Equation Section 9.2.1 translates into

$$A_{1\mu} = -A_{2\mu}^T\,, \tag{9.11}$$

which tells us that the two gauge groups are now identified as one $SU(N)_1$ in the orientifolded theory. Equation Section 9.2.1 maps the superfields in the following way:

$$\begin{aligned} X_{12} &= Y_{12}^T \equiv \mathcal{X}_{A,S}\,, \\ Y_{21} &= X_{21}^T \equiv \mathcal{Y}_{A,S}\,, \\ Z_{11} &= Z_{22}^T \equiv \mathcal{Z}\,. \end{aligned} \tag{9.12}$$

We recognize the same field content of the theory obtained with the dimer technique. It is easy then to show that we recover the superpotential advertised in Equation (9.2) (up to an irrelevant numerical factor). We thus conclude that the glide reflection on the dimer reproduces the orientifold projection we just computed in string theory.

In the following, we discuss the dimer construction in more involved examples. It is clear that not all dimer models have the required symmetry, and in Section 4.2 we provide a necessary condition for a given toric CY_3 to admit a glide reflection directly from its toric diagram.

9.2.2 More orbifold examples

The previous example has so much symmetry that it could be misleading. Let us start our journey to less symmetric theories by considering $\mathbb{C}^2/\mathbb{Z}_4$, whose dimer model and relevant involution we present in Figure 9.2. From the four initial gauge groups, only two of them are kept after the

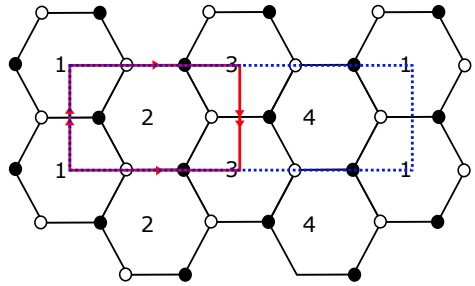

Figure 9.2: Dimer diagram for the orbifold $\mathbb{C}^2/\mathbb{Z}_4$. The unit cell is depicted in blue and we show in red the Klein bottle obtained from the orientifold projection.

projection, $SU(N_1)_1 \times SU(N_2)_2$. The surviving fields are

$$\begin{array}{lll} \mathcal{X}_{12} = (\overline{\square}_1, \square_2)\,, & \mathcal{X}_{21} = (\overline{\square}_2, \overline{\square}_1)\,, & \mathcal{Y}_{21} = (\overline{\square}_2, \square_1)\,, \\ \mathcal{Y}_{12} = (\square_1, \square_2)\,, & \mathcal{Z}_{11} = \mathrm{Adj}_1\,, & \mathcal{Z}_{22} = \mathrm{Adj}_2\,. \end{array} \tag{9.13}$$

and the resulting superpotential is found to be

$$W = \mathcal{X}_{12}\mathcal{Y}_{21}\mathcal{Z}_{11} - \mathcal{Y}_{21}\mathcal{X}_{12}\mathcal{Z}_{22} + \mathcal{X}_{21}\mathcal{Y}_{12}\mathcal{Z}_{22} - \mathcal{Y}_{12}\mathcal{X}_{21}\mathcal{Z}_{11}^T\,. \tag{9.14}$$

The open string projection computation for this example can be found in Appendix 9.A. Note that despite its similarities with the orbifold $\mathbb{C}^2/\mathbb{Z}_2$ (without orientifold), this model has a different matter content, which cannot be obtained from dimer models.

The mapping of the mesons is the same as for $\mathbb{C}^2/\mathbb{Z}_2$ so that the holomorphic 3-form transforms as follows:

$$\Omega_3 = \frac{\mathrm{d}x \wedge \mathrm{d}y \wedge \mathrm{d}z}{4w^3} \to \frac{\mathrm{d}y \wedge \mathrm{d}x \wedge \mathrm{d}z}{4w^3} = -\Omega_3\,, \tag{9.15}$$

and hence suggests that our projection is indeed supersymmetric and the resulting gauge theory preserves $\mathcal{N} = 2$ supersymmetry. Note that the usual orientifold techniques in the dimer, fixed points and line(s), are not able to reproduce it.

Our observations make it clear that any orbifold $\mathbb{C}^2/\mathbb{Z}_{2n} \times \mathbb{C}$ will admit a glide reflection, for any integer n. More general orbifolds, such as $\mathbb{C}^3/\mathbb{Z}_n$ or $\mathbb{C}^3/\mathbb{Z}_p \times \mathbb{Z}_q$, can also enjoy the glide reflections, see an example in Figure 9.5a. In Section 9.4 we will discuss the general geometric condition a singularity should meet to admit such orientifold.

$\mathcal{N} = 2$ fractional branes

Let us briefly comment on the fractional branes of the orientifolded theory [67]. The glide orientifold of $\mathbb{C}^2/\mathbb{Z}_4$ is free of local gauge anomalies for any rank N_1 and N_2. Hence, it has a fractional brane. We find that it is an $\mathcal{N} = 2$ fractional brane corresponding to a subset of the $\mathcal{N} = 2$ fractional branes of the parent theory. In Section 9.4.2 we will discuss this fact in detail.

9.2.3 Conifold-like singularities

As we will explain in Section 9.4, the conifold $\mathcal{C}$ itself does not admit a glide reflection, but conifold-like singularities like its orbifold $\mathcal{C}/\mathbb{Z}_2$ or the zeroth Hirzebruch surface F_0 do. We now study those examples in turn.

Non-chiral orbifold of the conifold $\mathcal{C}/\mathbb{Z}_2$

The dimer model and the glide orientifold of $\mathcal{C}/\mathbb{Z}_2$ are shown in Figure 9.3. The resulting gauge theory has gauge group $SU(N_1) \times SU(N_2)$

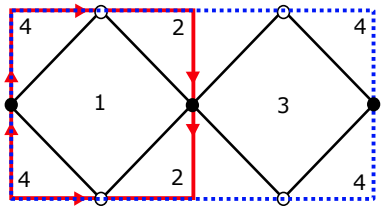

Figure 9.3: Dimer diagram for the orbifold of the conifold $\mathcal{C}/\mathbb{Z}_2$. The unit cell is depicted in blue and we show in red the Klein bottle obtained from the orientifold projection.

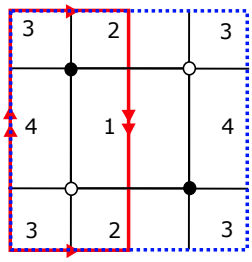

Figure 9.4: Dimer diagram for the Hirzebruch surface F_0. The unit cell is depicted in blue and we show in red the Klein bottle obtained from the orientifold projection.

with matter content given by

$$\begin{array}{rclcrcl} A & = & (\overline{\square}_1, \overline{\square}_2)\,, & & B & = & (\square_1, \square_2)\,, \\ C & = & (\overline{\square}_1, \square_2)\,, & & D & = & (\square_1, \overline{\square}_2)\,, \end{array} \tag{9.16}$$

Note in passing that the ACC do not impose any constraint on the ranks, so that N_1 and N_2 may be chosen independently. The superpotential reads

$$W = ABCD - BAC^T D^T\,. \tag{9.17}$$

For details of computations using worldsheet techniques and a proof that the 3-form is odd under the orientifold action, see Appendix 9.B.1.

Zeroth Hirzebruch surface F_0

We show the dimer model and the glide orientifold of F_0 in Figure 9.4. After projection the gauge group becomes $SU(N_1) \times SU(N_2)$, while the matter content is given by

$$\begin{array}{rclcrcl} X & = & (\square_1, \overline{\square}_2)\,, & & Y & = & (\square_1, \overline{\square}_2)\,, \\ U_{S,A} & = & \overline{\square\square}_1, \overline{\begin{array}{c}\square\\\square\end{array}}_1\,, & & Z_{S,A} & = & \square\square_2, \begin{array}{c}\square\\\square\end{array}_2\,, \end{array} \tag{9.18}$$

In this case the ACC impose non-trivial constraints on the gauge group ranks, in particular they must be the same, $N_1 = N_2$. The superpotential reads

$$W = XU_S Y^T Z_A - X^T Z_S Y U_A\,. \tag{9.19}$$

The Chan-Paton computation and a proof that the 3-form is odd under the orientifold action are exposed in Section 9.B.2.

Deformation fractional branes

We have seen that the $\mathcal{C}/\mathbb{Z}_2$ glide reflection admits fractional brane since the ranks of the two gauge groups may be chosen freely. It is in fact a deformation brane [67, 140] of the parent theory that survives the orientifold projection, in the precise sense described in [5]. A natural question is whether such fractional branes may trigger a non-trivial RG-flow giving rise to a cascade of Seiberg dualities [27, 91]. We study this process in Section 9.B.3 and verify that the cascade steps are: $SU(N+M)_1 \times SU(N)_2 \to SU(N-M)_1 \times SU(N)_2$, with the same matter content and superpotential, as we flow towards the IR. For N being a multiple of M, the deep IR of this gauge theory is expected to reproduce the same features as for a deformed conifold. Notably, on the baryonic branch, one finds the vacuum of SYM, displaying confinement and chiral symmetry breaking.

We will see later that it is a fact that the orbifolds of the conifold $\mathcal{C}/\mathbb{Z}_m \times \mathbb{Z}_n$ compatible with the glide projection preserve some of their deformation branes. The compatibility of fractional branes of the parent theory with the glide reflection is discussed in Section 9.4.

9.2.4 General properties

As we have seen, and since the glide reflection leaves no fixed loci, we don't expect any self-identified face (*i.e.* SO or USp gauge group) to show up in the dimer projection. This restricts the number of gauge groups of the parent theory to be even. A further consequence of not having fixed loci is that there are no self-identified bifundamentals, therefore, tensor matter, if present, always comes in antisymmetric-symmetric pairs, canceling the contributions to the chiral anomaly. This is precisely what happens in the $\mathbb{C}^2/\mathbb{Z}_2$ orbifold, where two edges, charged under two identified groups, are identified, leading to a reducible two index tensor, which splits into the sum of a symmetric and an antisymmetric one. We now see how these facts translates in the absence of non-homogenous terms in the anomaly cancellation conditions, allowing always a solution to the latter, and how such projected theories are actually SCFTs.

Borrowing the notation of Chapter 8, we know that the ACC matrix of the projected theory is deduced from that of the parent theory. Denote

the latter as,

$$A = \left(\begin{array}{c|c|c} B_{11} & B_{12} & B_{13} \\ \hline B_{21} & B_{22} & B_{23} \\ \hline B_{31} & B_{32} & B_{33} \end{array} \right) \begin{array}{l} \left.\vphantom{\begin{array}{c} a \\ a \\ a \end{array}}\right\} i \\ \left.\vphantom{\begin{array}{c} a \\ a \\ a \end{array}}\right\} i+k \\ \left.\vphantom{\begin{array}{c} a \\ a \\ a \end{array}}\right\} a \end{array} \quad , \tag{9.20}$$

$$\underbrace{\phantom{B_{11}}}_{j} \quad \underbrace{\phantom{B_{12}}}_{j+k} \quad \underbrace{\phantom{B_{13}}}_{b}$$

where indices $i, j = 1, \ldots, k$ label the gauge groups surviving the orientifold projection and the corresponding entries represent the anomaly contribution of the field between faces i and j. Indices $i+k$ and $j+k$ represent gauge groups that are identified with i and j under the orientifold action, respectively. The a, b indices label the self identified gauge groups. Finally, the ACC system takes the form

$$A \cdot N = 0 \,, \tag{9.21}$$

where N is a vector whose entries, $N_{(j|j+k|a)}$ are the ranks of the corresponding gauge group.

From what we said earlier, we know that $B_{\star 3} = B_{3\star} = B_{33} = 0$, since there are no self-identified gauge groups. Furthermore, we have no net contributions from tensors to the ACC, meaning that there are no non-homogeneous terms in the projected theory ACC. From [5], we know that the projected ACC can be written as

$$\overline{A} \cdot N = \Big(\; B_{11} + B_{12} \; \Big) \cdot N = 0 \,. \tag{9.22}$$

It is then easy to see that the all-equal-rank solution in the parent theory is still a solution. Indeed, a general solution for the orientifolded theory has a trivial part, corresponding to a stack of regular branes in the parent theory, and a non-trivial part, corresponding to "symmetric" fractional branes of the parent theory.

Fixed loci orientifolds have the remarkable property of producing, in general, non-conformal theories. However, this is not true for glide orientifolds. The theory they describe is an SCFT when the ranks of the gauge

groups are all the same. This fact can be seen as follows, consider the β-function of the parent theory with N probes D-branes,

$$\beta_{SU(N)_i} = 3N - \sum_{i=1}^{n} \frac{N}{2}(1-\gamma_i) = 0\,, \tag{9.23}$$

where γ_i are the anomalous dimensions of the matter fields.[5] From this, we can read the β-function of the projected theory whose general form is

$$\beta_{SU(N)_i} = 3N - \sum_{i=1}^{n} \frac{N+b_i}{2}(1-\gamma_i)\,, \tag{9.24}$$

where the coefficients b_i vanish for fundamental fields and are ± 2 for, respectively, symmetric or antisymmetric fields. If we assume that the anomalous dimensions of the fields are the same up to $1/N$ corrections and, since all tensors come in pairs of opposite parity, we see that the β-function of the gauge groups of the projected theory vanishes as long as all ranks are equal. This dovetails the fact that a Klein Bottle has zero Euler characteristic and, as explained in [151], such surfaces may embed a dimer model describing an SCFT.[6] Franco and Vegh pointed out that the Franklin graph would be a good candidate to be embedded in a Klein Bottle and host an SCFT not embedded in a torus. Indeed, it can be readily found via a glide reflection of $\mathbb{C}^3/\mathbb{Z}_{12}$, see Figure 9.5. This not only confirms their intuition, but it is, to the best or our knowledge, the first instance of such construction within string theory.

9.3 T-duals of the glide orientifold

9.3.1 Type IIA picture and the brane tiling

Fixed loci in the dimer have been related to actual orientifold planes in the physical realization of the dimer [46,176]. In fact, one may consider the D3-branes probing a singularity with an orientifold and track the position of the orientifold in the ambient space to the fixed loci in the dimer through T-dualities. An immediate puzzle arises in the case of glide orientifolds, since there are no fixed loci on the torus, *i.e.* in the brane tiling. In this section, we look at $\mathbb{C}^2/\mathbb{Z}_2$ and argue that these orientifolds, which have 8-dimensional fixed loci in the D3 picture (they are O7-planes), don't have

[5] We consider Adj fields as a couple of antifundamentals fields charged under the same gauge group.

[6] Other kinds of surfaces obtained from orientifolds with fixed loci were found to accommodate SCFTs in [173, 183].

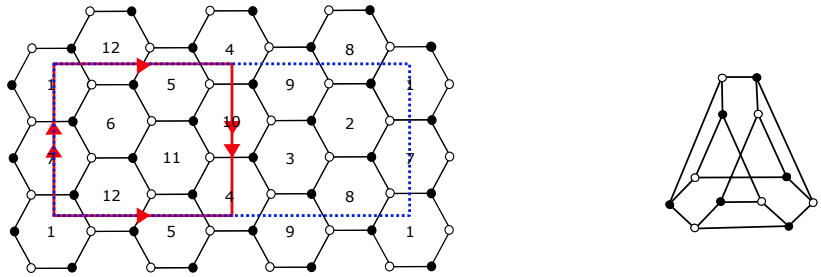

(a) (b)

Figure 9.5: (a) Dimer diagram for the orbifold $\mathbb{C}^3/\mathbb{Z}_{12}$ with action $(1, 5, 6)$. The unit cell and the Klein bottle are depicted in blue and red respectively. (b) The Franklin graph.

a fixed locus in the tiling in the precise sense of [166, 184]. In the latter reference, the shift action is deduced to be T-dual to a pair of opposite charge O-planes on a circle.

Let us again consider N D3-branes at the tip of a singular toric CY_3. As reviewed in the introduction, the dimer presented in Figure 9.1 is physically realized as a web of D5 and NS5-branes. It is obtained by T-duality along with two of the three toric cycles of the toric variety. In particular along those corresponding to mesonic symmetries in the field theory, rather than R-symmetry. Focusing on the case at hand, $\mathbb{C}^2/\mathbb{Z}_2 \times \mathbb{C}$, one may take local coordinates such that x_7, x_9 correspond to the two toric cycles that are to be T-dualized. The D-brane configuration is then as in Table 9.1 which, after two T-duality should become that of Table 9.2. Note that we have avoided including an orientifold plane in the T-dual, as the dimer shift seems to suggest.

After T-duality one finds D5-branes wrapping the dual cycles with local coordinates x'_7, x'_9. These are in turn identified as the coordinates of the torus $\mathbb{T}^2$ where the 5-brane web lives.

	0	1	2	3	4	5	6	7	8	9
$\mathbb{C}^2/\mathbb{Z}_2$					×	×	×	×		
D3	×	×	×	×						
O7	×	×	×	×	×	×			×	×

Table 9.1: D3-branes sitting at the tip of $\mathbb{C}^2/\mathbb{Z}_2$ in the presence of O7-planes.

	0	1	2	3	4	5	6	$7'$	8	$9'$
NS5	×	×	×	×			–	–	Σ	– –
D5	×	×	×	×				×		×

Table 9.2: The brane tiling. Σ is the holomorphic curve in the $67'89'$-space wrapped by the NS5-brane.

To study the location of the O-plane in the singular geometry, let us introduce the coordinates z_1, z_2 and z_3 of flat space $\mathbb{C}^3$. We define the coordinates of the variety transverse to the D3-branes, $\mathbb{C}^2/\mathbb{Z}_2 \times \mathbb{C}$, by constructing invariants under the orbifold action:

$$x = z_1^2\,, \quad y = z_2^2, \quad w = z_1 z_2, \quad \text{and} \quad z = z_3\,, \tag{9.25}$$

with the following relation holding,

$$xy = w^2\,. \tag{9.26}$$

As explained in Section 9.2.1, the orientifold action on the dimer implies that it acts on z_1, z_2, z_3 as $z_1 \leftrightarrow z_2$,. In terms of the orbifold invariant coordinates the orientifold action is then,

$$x \leftrightarrow y\,, \quad w \text{ and } z \text{ fixed.} \tag{9.27}$$

Thus, the orientifold plane extends on the surface defined by $x = y = t$, $t^2 = w^2$. From Equation (9.26) we read two toric $U(1)$ isometries of the orbifold:

$$\begin{array}{lllll} U(1)_\alpha : & x \to e^{i\alpha} x\,, & y \to e^{-i\alpha} y\,, & w \to w\,, \\ U(1)_\beta : & x \to e^{i\beta} x\,, & y \to e^{i\beta} y\,, & w \to e^{i\beta} w\,. \end{array} \tag{9.28}$$

We can think about these two isometries as generators of two one-cycles, α, β. We can introduce local coordinates parametrizing these cycles, defined whenever they are non-singular,

$$\theta_\alpha \equiv \frac{1}{2}\big(\mathrm{Arg}(x) - \mathrm{Arg}(y)\big) \tag{9.29}$$

$$\theta_\beta \equiv \frac{1}{2}\big(\mathrm{Arg}(x) + \mathrm{Arg}(y)\big) \tag{9.30}$$

We can now identify these two coordinates in terms of the coordinates in Table 9.1: $(\theta_\alpha, \theta_\beta) \sim (x_7, x_5)$. The action of the orientifold on these two cycles, T-dual to the physical torus, are just $\theta_\alpha \to -\theta_\alpha$, $\theta_\beta \to \theta_\beta$. We thus

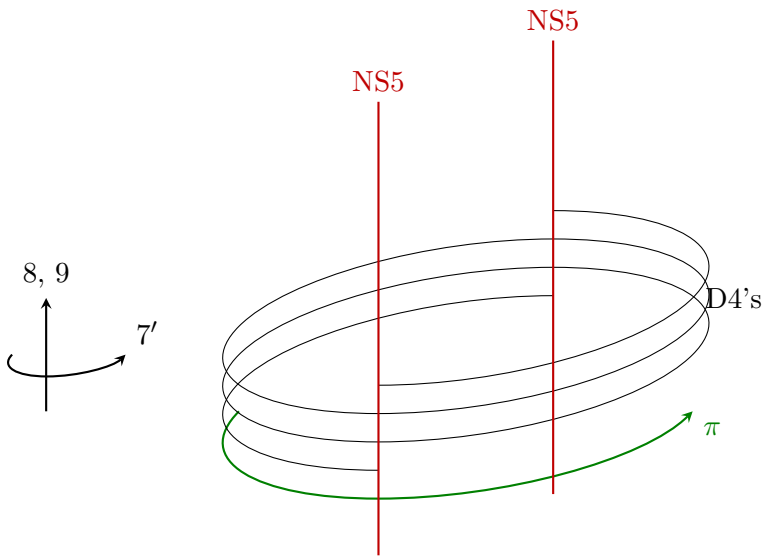

Figure 9.6: Type IIA picture with the orientifold mapping given by a π rotation along x_7' (in green).

learn that the orientifold plane spans x_5 and is located at $x_7 = 0, \pi$. In fact, there are two orientifold planes of opposite charge such that the total flux cancels with no further sources. One may also argue for the signs being opposite by noting the absence of net RR-charges coming from the O-planes in the dimer picture. This can be seen in the absence of SO/USp groups and the corresponding lack of non-homogeneous terms in the ACC, which can be thought of as Gauss law for compact cycles. Quite remarkably, the T-dual of such a cycle with opposite-charge O-planes, is known to be precisely an orientifold acting as a shift on the T-dual cycle. The absence of fixed loci for this action translates into the absence of O-plane in the dual geometry. This is described in [184] where T-duality acts as a sort of Fourier transform: the O-planes of opposite charge are related to delta function whose transforms are constant and opposite, canceling each other. This interpretation nicely matches the Gauss law analogy we presented earlier.

After one T-duality along x_7, the T-dual Type IIA construction is analogous to the ones studied in [185–189]. The relevant information is encoded in a cycle x_7' where D4-branes are suspended between two NS5-branes. As we explained before, the orientifold action acts now as a shift, rotating halfway the configuration, see Figure 9.6. This action is consistent with the mapping of gauge groups and matter fields on the dimer model.

Finally, if we further T-dualize along the direction spanned by NS5-

branes x_9, we get to the tiling picture. After the last T-duality, the orientifold acts on x'_9 as a reflection.[7] Together with the shift on x'_7, these actions reproduce the glide reflection that we see on the tiling.

9.3.2 The mirror picture

One further T-duality on the remaining toric cycle brings us to the mirror setup of our starting point [145] (D3-branes at singularities). The mirror geometry is fully specified by a punctured Riemann surface Σ in which D6-branes, wrapping one-cycles, give rise to the appropriate field theory.[8] Gauge fields are associated with different one-cycles, where D6 are wrapped, matter fields to intersections among these cycles, and superpotential terms arise from open string worldsheet instantons supported at disks in this Riemann surface. In fact, this Riemann surface can be seen as the "thickened" version of the web diagram. Furthermore, one can embed the dimer graph on a planar version of it and read immediately both the geometry and the field theory from it. This diagram has been called the shiver. The shiver and the dimer are related by an untwisting procedure [145]. The physical interpretation is now as follows.

- Faces in the shiver correspond to ZZPs in the dimer and represent punctures in Σ with (p, q) charge given by the winding numbers of the ZZPs.
- ZZPs on the shiver correspond to faces on the dimer and represent the one-cycles (Special Lagrangian three-cycles in the full geometry) where D6-branes wrap. They are hence representing gauge groups.
- ZZP intersections represent brane intersections where open string massless bifundamental fields are located.
- Disks on the surface are euclidean disks in the full geometry where open string worldsheet instantons may arise. These generate the superpotential (albeit non-perturbatively!).

In Figure 9.7 we show the prototypical example, the conifold.

Already in [54], orientifolds were partially understood in this framework. It was noted that the O6-planes should be viewed as stretching between the different punctures. Different pieces of the O-plane would there

[7] This is a standard fact of orientifolds. Upon T-duality along a direction spanned by the O-plane, an Op-plane is mapped to an O$(p-1)$-plane, with action $\theta \to -\theta$ on the dual cycle.

[8] These one-cycles are associated with three-cycles in the full geometry.

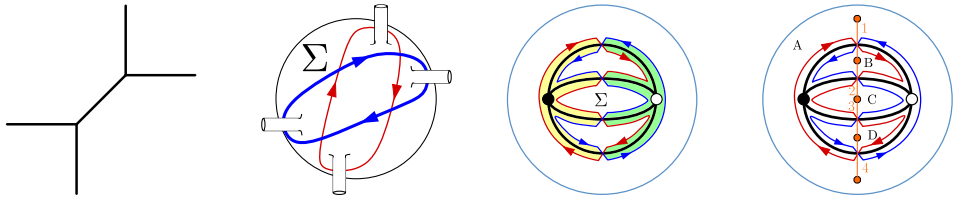

(a) (b) (c) (d)

Figure 9.7: (a) Conifold web diagram. (b) shows the actual surface describing the mirror geometry. The zig-zag paths in blue and red are one-cycles where D6-branes may wrap. (c) Tiling of the mirror Riemann surface Σ giving rise to the conifold gauge theory. (d) Orientifold of the conifold. Orange segments and dots denote O-planes and punctures where they end, respectively.

be assigned different signs. A full understanding of the available sign choices was not achieved and we will not pursue it here. An orientifold of the conifold is shown in Figure 9.7d.

A simple example: $\mathbb{C}^2/\mathbb{Z}_2 \times \mathbb{C}$

In this section, we explicitly map all orientifolds in the dimer with those in the T-dual and mirror picture. While we are not able to derive matter field projections on the T-dual nor the mirror, we hope to convey a unifying picture. We will focus on $\mathbb{C}^2/\mathbb{Z}_2 \times \mathbb{C}$ for several reasons. It admits all kinds of orientifolds (fixed points, lines, and glide reflections), a simple T-dual set-up, and its mirror Σ has genus zero, making it amenable to discussion. Orientifolds in the dimer can be classified into four groups, depending on the fixed loci. There are 2 different fixed point orientifolds, shown in Figures 9.8b and 9.8c and a fixed line orientifold, in Figure 9.8d. These were already discussed in [54]. Different sign assignments, possibly respecting the sign rule, yield different field contents. Finally, as discussed in Section 9.2, a glide orientifold is realized in the dimer as shown in Figure 9.8e.

A complete classification, up to sign permutations and anomaly cancellation, is shown in Table 9.3.

In Section 9.3.1, we have discussed the setup T-dual to the glide orientifold, shown again in Figure 9.9e. The orientifolds in Figures 9.9b to 9.9d have been discussed in the literature [173, 189, 190]. One can easily identify these three orientifolds in the dimer setup as Figures 9.8b to 9.8d, respectively. It is worth mentioning that the fixed lines orientifold with the same sign correspond to the O4-plane in the T-dual, while the case with opposite

O-Type	Figure	Signs	Group	Tensor Content
Fixed Points	Figure 9.8b	$(++++)$	SU	$\text{Adj} + 2\square\square + 2\overline{\square\square}$
		$(++--)$		$\text{Adj} + \square\square + \overline{\square\square} + \square + \overline{\square}$
		$(+--+)$		$\text{Adj} + 2\square + 2\overline{\square\square}$
		$(-++-)$		$\text{Adj} + 2\overline{\square} + 2\square\square$
		$(----)$		$\text{Adj} + 2\square + 2\overline{\square}$
	Figure 9.8c	$(++++)$	$SO \times SO$	$\square\square_1 + \square\square_2$
		$(++--)$	$SO \times USp$	$\square\square_1 + \square_2$
		$(--++)$	$USp \times SO$	$\square_1 + \square\square_2$
		$(+-+-)$	$SO \times SO$	$\square_1 + \square_2$
		$(-+-+)$	$USp \times USp$	$\square\square_1 + \square\square_2$
		$(+--+)$	$SO \times USp$	$\square_1 + \square\square_2$
		$(-++-)$	$USp \times SO$	$\square\square_1 + \square_2$
		$(----)$	$USp \times USp$	$\square_1 + \square_2$
Fixed Lines	Figure 9.8d	$(++)$	$SO \times SO$	$\square\square_1 + \square\square_2$
		$(+-)$	$SO \times USp$	$\square_1 + \square\square_2$
		$(-+)$	$USp \times SO$	$\square\square_1 + \square_2$
		$(--)$	$USp \times USp$	$\square_1 + \square_2$
Glide	Figure 9.8e		SU	$\text{Adj} + \overline{\square\square} + \overline{\square} + \square\square + \square$

Table 9.3: Different orientifold projections on the dimer.

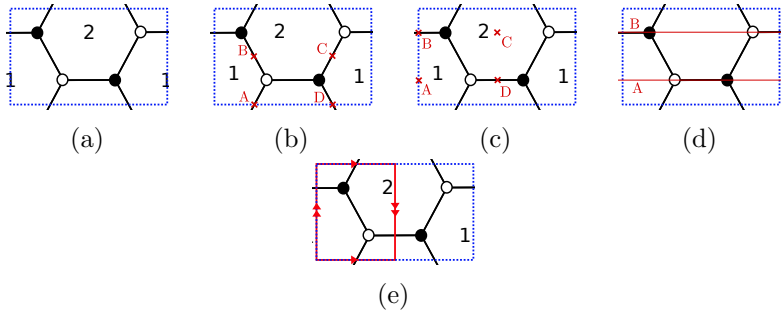

Figure 9.8: (a) Dimer model unit cell of $\mathbb{C}^2/\mathbb{Z}_2\times\mathbb{C}$. Three possible orientifold actions with fixed loci are shown in (b), (c) and (d). (b) and (c) correspond to fixed points, while (d) is a fixed line. (e) is a glide orientifold with no fixed loci.

signs is mapped to an O8-plane. Finally, the glide orientifold, Figure 9.8e is identified with Figure 9.9e.

The shiver is shown in Figure 9.10a. It is essentially the same as the T-dual with punctures A and D sitting at the NS5 locations. This was to be expected since the S^1 in the T-dual is kept in Σ. This makes it particularly easy to find the orientifold actions on this surface.[9] The four types are shown in Figure 9.10 with labels matching those of Figures 9.8 and 9.9. Note, in particular, that the glide reflection, in Figure 9.10e consists of a π rotation and a reflection with respect to the dotted orange circle. The total action thus exchanges punctures B and C, for instance. Unlike the other orientifold actions, there are no fixed loci in this case. While the field content can be deduced from the drawings by assigning a sign to every O-plane piece and assigning the matter projection individually (as in the open string computation), it is not clear how to enforce SUSY in this picture. Without further knowledge, it is not obvious which projections are SUSY-preserving.

9.4 Involutions and zig-zag paths

In this section, we first develop, in Section 9.4.1, a condition the toric diagram (or equivalently, the ZZPs) of a singularity must satisfy to be compatible with the glide reflection. This enlarges the dictionary between orientifold projections of a given toric singularity and its ZZPs content, as

[9] Otherwise one would need to think about the field content on the dimer or the alga map [145].

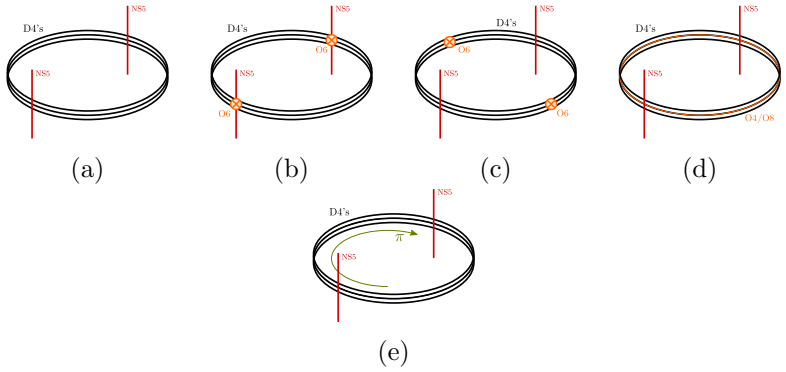

Figure 9.9: (a) T-dual to $\mathbb{C}^2/\mathbb{Z}_2 \times \mathbb{C}$. Three possible orientifold actions with fixed loci are shown in (b), (c) and (d). (b) and (c) correspond to fixed points, while (d) is a fixed line. (e) is a shift (glide reflection) with no fixed loci.

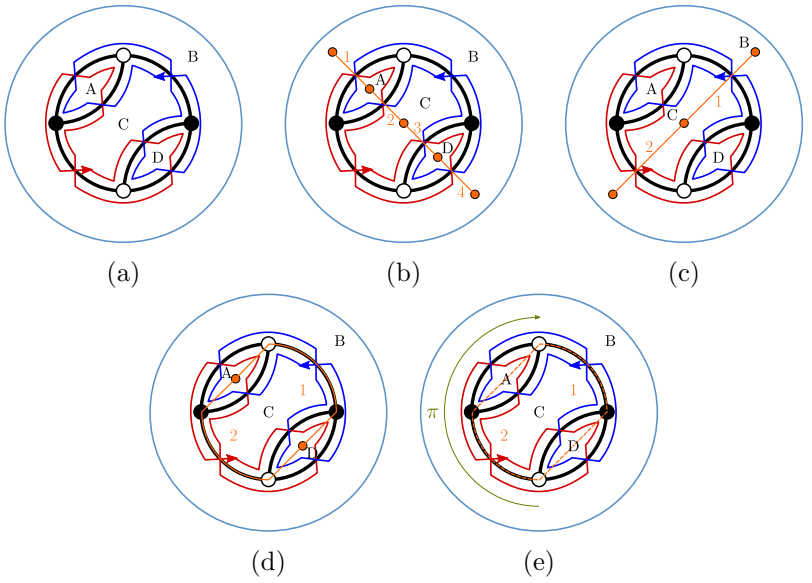

Figure 9.10: (a) Tiling of the mirror Riemann surface Σ of $\mathbb{C}^2/\mathbb{Z}_2 \times \mathbb{C}$. Three possible orientifold planes are shown in (b), (c) and (d). The orientifold plane is shown in orange and its different pieces are labelled using orange numbers. In the dimer (b) and (c) correspond to fixed points, while (d) is a fixed line. (e) is a shift orientifold with no fixed loci.

initiated by [73]. Secondly, and with the help of ZZP techniques [140], we show in Section 9.4.2 how to detect the presence of fractional branes in the orientifolded singularity. Finally, in Section 9.5, we give a general proof that the "would be" shift orientifold projection is incompatible with the requirement to preserve SUSY.

9.4.1 Glide orientifold from the toric diagram

A glide reflection can be seen as a combination of a shift and a reflection in the dimer model, even if each of them is not a symmetry per se. Starting from what we learned in our examples and using this simple observation, we can understand how this involution acts on the ZZP content of the toric diagram.

First of all, we notice that the shift and the reflection are performed along the same axis. Consider, for instance, a horizontal shift and axis of reflection as in Figure 9.11. The action of the glide reflection reverts the horizontal component of each ZZP. Actually, the glide reflection leaves no fixed ZZPs, since even those perpendicular to the axis are mapped among themselves because of the shift part of the glide reflection.

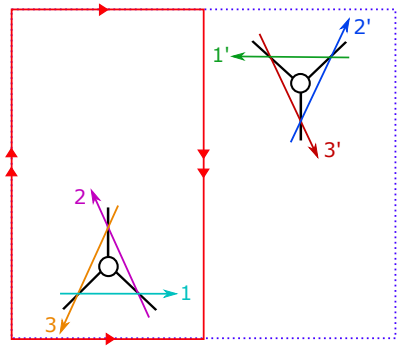

Figure 9.11: The glide orientifold maps together nodes of the same color. The dashed blue line delineates the unit cell of the parent theory, while the red frame represents the orientifold. The ZZPs $1, 2, 3$ are mapped to $1', 2', 3'$ respectively.

Putting the two observations together we can say that: if the glide reflection is composed by a *horizontal shift and a reflection axis*, directed as $(1, 0)$ in the dimer, ZZPs are mapped as follows: (p, q) is sent to $(-p, q)$ when $p \neq 0$, while all other ZZPs of the form $(0, \pm 1)$ are mapped to one another, preserving the orientation, meaning that they come in even numbers. In

our example of Figure 9.12, the orange $(1,1)$ and purple $(-1,1)$ ZZPs are interchanged. The same is true for the blue and green ZZPs of the $(0,-1)$ type.

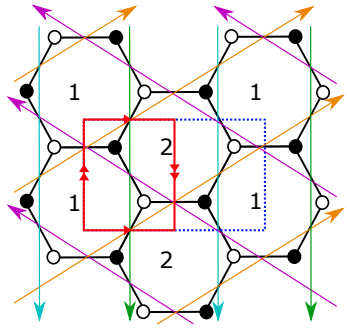

Figure 9.12: The Klein bottle obtained from the dimer of $\mathbb{C}^2/\mathbb{Z}_2 \times \mathbb{C}$ and the corresponding ZZPs.

Similarly, in order to construct a Klein bottle with a *vertical shift and reflection axis*, the toric diagram should have ZZPs $(1,0)$ and $(-1,0)$ in even numbers, possibly different, and ZZPs (p,q) with $q \neq 0$ paired with ZZPs $(p,-q)$.

These statements can be summarized by saying that the toric diagram should be symmetric with respect to a vertical or horizontal axis. Moreover, each ZZP has to be mapped to another one, imposing that each kind of ZZP parallel to the axis of reflection in the toric plane should come in even numbers. We show in Figure 9.13 that our examples of Section 9.2 satisfy this criterion.

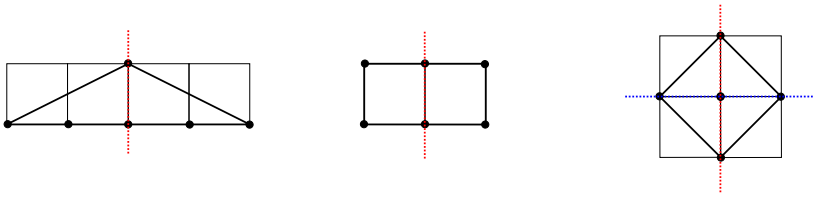

(a) (b) (c)

Figure 9.13: Toric diagrams for singularities that satisfy our necessary criterion to admit one (with an axis of reflection in red) or two (with the second axis of reflection in blue) glide projections: (a) orbifold $\mathbb{C}^2/\mathbb{Z}_4$, (b) conifold-like $\mathcal{C}/\mathbb{Z}_2$, and (c) zeroth Hirzebruch surface F_0.

Lastly, an important remark is that this condition may not be satisfied in some of the $SL(2,\mathbb{Z})$ "frames" of the toric diagram, or equivalently, the unit cell in the dimer model may not be symmetric with respect to the glide reflection. Thus, we should state that a generic toric diagram can admit a glide orientifold if it satisfies the conditions above *up to a* $SL(2,\mathbb{Z})$ *action* that can bring its unit cell to a symmetric form with respect to the glide.

9.4.2 Fractional branes in glide orientifolds

As already mentioned in Section 9.2.4, these orientifolded theories may admit non-trivial rank assignments, *i.e.* fractional branes. Their presence can be deduced from the symmetries of the toric diagram and they can be seen as inherited from the "parent" theory. Following [5, 140], in what we dub "Butti's Algorithm", we can assign a value v_Γ to each of the n ZZPs of the toric diagram. These values give rise to anomaly-free rank assignments, given that they satisfy the following constraints,

$$\begin{cases} \sum_\Gamma v_\Gamma p_\Gamma = 0 \\ \sum_\Gamma v_\Gamma q_\Gamma = 0 \end{cases} , \tag{9.31}$$

where the (p_Γ, q_Γ) are the winding numbers of the ZZP associated with v_Γ.

Since we know how the glide reflection acts on the ZZPs, we may follow the procedure of [5] to see which fractional branes survive the projection. As explained there, only *symmetric* fractional branes survive, in the sense that, given two ZZPs v_α and $v_{\bar{\alpha}}$ mapped to each other under the glide reflection, only rank assignments satisfying the following identification survive,

$$v_\alpha = v_{\bar{\alpha}} \,. \tag{9.32}$$

The orientifold projection thus reduces the number of variables v_Γ to the subset of v_α. Moreover, one can check that Equation (9.31) leaves only one non-trivial relation:

$$\sum_\alpha v_\alpha q_\alpha = 0 \,. \tag{9.33}$$

Butti's algorithm has a redundancy that allows performing a global shift on the v_α without affecting the ranks of the gauge groups. Hence, we end up with

$$\#\text{Fractional branes} = n/2 - 2 \tag{9.34}$$

in the orientifolded theory.

Butti's algorithm also tells how to construct different kind of fractional branes in the parent theory by specifying a set of v_Γ. We now apply this method to theories with a glide reflection orientifold to see when may $\mathcal{N}=2$ and deformation fractional branes arise.

- $\mathcal{N}=2$ fractional branes: The parent theory admits such fractional branes whenever the toric diagram hosts $k>1$ ZZPs with the same winding numbers, say (p_μ, q_μ). They are turned on whenever only some of these v_μ, among the whole set of ZZPs $\{v_\Gamma\}$, are non-vanishing. Following Equation (9.31), one has

$$\sum_{i=1}^{k} v_{\mu_i} = 0\,, \qquad \text{and } v_\nu = 0 \text{ if } (p_\nu, q_\nu) \neq (p_\mu, q_\mu)\,. \tag{9.35}$$

  This condition is compatible with Equation (9.32) only if the k ZZPs are sent to ZZPs with the same winding numbers by the glide reflection, restricting to $(0,1)$ or $(0,-1)$ when (p,q) is mapped to $(-p,q)$. Moreover, k should be a multiple of 4, since for each couple of ZZPs with a symmetric assignment v, we need a second couple with assignment $-v$ in order to satisfy the sum in Equation (9.35). In the examples of Section 9.2, we found that the singularity $\mathbb{C}^2/\mathbb{Z}_4$ satisfies this criterion, see Figure 9.14a.

- Deformation fractional branes: The parent theory will have a deformation fractional brane if there is a subset of m ZZPs in equilibrium $\{v_\sigma\} \subset \{v_\Gamma\}$:

$$\sum_{i=1}^{m} (p_{\sigma_i}, q_{\sigma_i}) = 0\,. \tag{9.36}$$

  The deformation brane is turned on whenever all v_σ have the same non-zero value and all other $v_\tau \notin \{v_\sigma\}$ are vanishing. A glide reflection orientifold theory will have a deformation brane if there is a subset of m ZZPs in equilibrium where each ZZP is accompanied by its image under the glide action, and where m is smaller than n. In the examples of Section 9.2, we found that $\mathcal{C}/\mathbb{Z}_2$ satisfies this criterion while the zeroth Hirzebruch surface F_0 does not, see Figure 9.14b and Figure 9.14c.

9.5 Shift orientifolds

So far we have only considered orientifolds acting as glide reflections on the dimer. Now we address those acting as a simple shift. We have not dis-

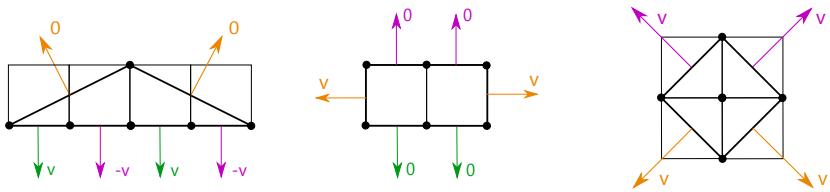

(a) (b) (c)

Figure 9.14: Symmetric fractional branes in the parent theory lead to fractional branes in its glide orientifolded version. Couples of ZZPs paired by the glide action are drawn in the same color. (a) $\mathcal{N} = 2$ fractional brane in $\mathbb{C}^2/\mathbb{Z}_4$, (b) deformation fractional brane in $\mathcal{C}/\mathbb{Z}_2$, and (c) the zeroth Hirzebruch surface F_0 admits only the regular brane as a symmetric fractional brane.

cussed these orientifolds earlier because they always break supersymmetry, as we show in the following. In particular, we will see that the holomorphic three-form Ω_3 is even under such an orientifold action, contradicting the rule of thumb that it should be odd.

As we observed in Section 9.1, the shift involution must identify nodes of opposite colors on the dimer, in order to be consistent with the orientifold identification rules. Under such a shift, each ZZP is mapped to a ZZP of opposite winding numbers, $(p, q) \to (-p, -q)$. This can be easily deduced from Figure 9.15.

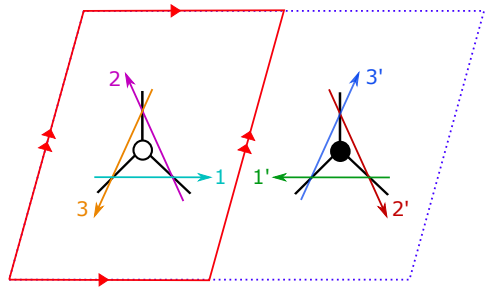

Figure 9.15: The shift orientifold maps white nodes to black nodes, and vice-versa. The dashed blue line delineates the unit cell of the parent theory, while the red frame represents the orientifold. The ZZPs $1, 2, 3$ are mapped to $1', 2', 3'$ respectively.

From the toric diagram, it is possible to obtain the equations defining associated toric variety probed by the D-branes. To do so we need to compute the integer generators of the dual cone to the toric diagram. This procedure is standard in toric geometry and we refer to [126] for all the details. From the lattice vertices on the boundary of the toric diagram (r_i, s_i), we obtain the generators of the cone given by $\mathbf{n}_i = (r_i, s_i, 1)$. Recall that the dual cone is then given by

$$\sigma^\vee = \{a\mathbf{m} \in M_\mathbb{R} \,|\, a \in \mathbb{R}_{>0},\, \mathbf{m}\cdot\mathbf{n}_i \geq 0\, \forall \mathbf{n}_i \in \sigma\}\,, \tag{9.37}$$

where $M_\mathbb{R} \cong \mathbb{R}\times M$ and $M \cong \mathbb{Z}^3$. It is easy to see that the vectors $\mathbf{m}$ are of the form (p, q, a), where (p, q) are the windings of the ZZPs and a is an integer. Indeed, the generators of the dual cone are nothing but the inward-pointing vectors, normal to the faces of the cone generated by the $\mathbf{n}_i$. We now need to add the extra generators to span the dual integer cone, $S^\vee = \sigma^\vee \cap \mathbb{Z}^3$. This is achieved by computing linear combinations of the generators with positive rational coefficients and adding all integer vectors we obtain this way. Finally, the equations defining our singularity are given by associating complex coordinates to the generators of the integer dual cone, and the relations among them are obtained with the following identification,

$$\mathbf{m}_1 + \mathbf{m}_2 + \cdots = \mathbf{m}_4 + \mathbf{m}_5 + \cdots \quad \to \quad x_1x_2\cdots = x_4x_5\cdots\,. \tag{9.38}$$

For example, let us consider the toric diagram of the conifold, which we place in $\mathbb{Z}^2$ as the square with vertices $(0,0), (0,1), (1,1), (0,1)$. The associated cone is

$$\sigma = \left\langle \begin{pmatrix} 0\\0\\1\end{pmatrix}, \begin{pmatrix} 0\\1\\1\end{pmatrix}, \begin{pmatrix} 1\\1\\1\end{pmatrix}, \begin{pmatrix} 1\\0\\1\end{pmatrix} \right\rangle\,, \tag{9.39}$$

and its dual is

$$\sigma^\vee = S^\vee = \left\langle \mathbf{m}_1 = (1,0,0),\, \mathbf{m}_2 = (0,1,0),\, \mathbf{m}_3 = (-1,0,1),\, \mathbf{m}_4 = (0,-1,1)\right\rangle\,, \tag{9.40}$$

from which it is easy to read the equation defining the singularity:

$$\mathbf{m}_1 + \mathbf{m}_3 = \mathbf{m}_2 + \mathbf{m}_4 \quad \to \quad x_1x_3 = x_2x_4\,. \tag{9.41}$$

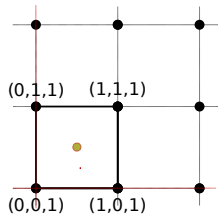

Figure 9.16: The toric diagram of the conifold.

As a second example let us consider the toric diagram of dP_3 and the cone it generates:

$$\sigma = \left\langle \begin{pmatrix} 0 \\ -1 \\ 1 \end{pmatrix}, \begin{pmatrix} 1 \\ -1 \\ 1 \end{pmatrix}, \begin{pmatrix} 1 \\ 0 \\ 1 \end{pmatrix}, \begin{pmatrix} 0 \\ 1 \\ 1 \end{pmatrix}, \begin{pmatrix} -1 \\ 1 \\ 1 \end{pmatrix}, \begin{pmatrix} -1 \\ 0 \\ 1 \end{pmatrix} \right\rangle . \tag{9.42}$$

It is dual to $S^\vee$ which is the cone:

$$\big\langle \mathbf{m}_1 = (0,1,1),\, \mathbf{m}_2 = (-1,0,1),\, \mathbf{m}_3 = (-1,-1,1),\, \mathbf{m}_4 = (0,-1,1), \\ \mathbf{m}_5 = (1,0,1),\, \mathbf{m}_6 = (1,1,1),\, \mathbf{m}_0 = (0,0,1) \big\rangle \ , \tag{9.43}$$

where we added the vector $\mathbf{m}_0$ since $\mathbf{m}_1 + \mathbf{m}_4 = 2\mathbf{m}_0$, meaning that we where missing an integer generator. The equations of the variety are

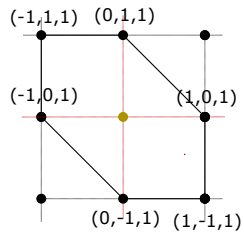

Figure 9.17: The toric diagram of dP_3.

$$\begin{aligned} x_1 x_4 = x_2 x_5 = x_3 x_6 = x_0^2 \\ x_1 x_3 x_5 = x_2 x_4 x_6 \, . \end{aligned} \tag{9.44}$$

We can use the fact that under the shift involution each ZZP is mapped to a ZZP of opposite winding, hence the corresponding toric diagram must

be symmetric under the reflection about its center of mass. Such center of mass has, in general, half-integer coordinates (α, β). Under such a reflection, a generic point in the lattice with coordinates $(r, s) \in \mathbb{Z}^2$ is sent to $(2\alpha - r, 2\beta - s)$. Under this operation, the generators of the cone are mapped according to

$$\mathbf{n}' = \begin{pmatrix} -1 & 0 & 2\alpha \\ 0 & -1 & 2\beta \\ 0 & 0 & 1 \end{pmatrix} \cdot \mathbf{n} \tag{9.45}$$

which maps a generator $m = (a, b, 1)$ to $m' = (2\alpha - r, 2\beta - s, 1)$. The dual cone is in turn invariant under the (right) action of that matrix, which acts as

$$\mathbf{m}' = \begin{pmatrix} -1 & 0 & 0 \\ 0 & -1 & 0 \\ 2\alpha & 2\beta & 1 \end{pmatrix} \cdot \mathbf{m}\,, \tag{9.46}$$

or simply,

$$\mathbf{m} = (p, q, a) \quad \rightarrow \quad \mathbf{m}' = (-p, -q, 2\alpha p + 2\beta q + a)\,. \tag{9.47}$$

From these observations, we deduce the following properties:

1. All generators of the dual cone, obtained via Equation (9.37), $\mathbf{m}_i = (p_i, q_i, a)$, come paired with another generator $\mathbf{m}'_i = (-p_i, -q_i, a')$, for some integer a while a' is obtained via Equation (9.47).

2. Given a generator $\mathbf{m}_i = (p_i, q_i, a)$ and its shift image $\mathbf{m}'_i = (-p_i, -q_i, a')$, we see that a new integer generator that we were missing can be added $\mathbf{m}_0 = (0, 0, 1)$, since

$$\mathbf{m}_i + \mathbf{m}'_i = (a + a')\mathbf{m}_0\,. \tag{9.48}$$

   This generator is invariant under the shift.

3. All other extra generators come in pairs. Given an extra generator n_l such that

$$\mathbf{m}_i + \cdots + \mathbf{m}'_j + \cdots = b\,\mathbf{m}_l\,, \tag{9.49}$$

   with b integer, by a symmetry argument, we also need to add $\mathbf{m}'_l$, since we have[10]

$$\mathbf{m}'_i + \cdots + \mathbf{m}_j + \cdots = b\,\mathbf{m}'_l\,. \tag{9.50}$$

[10]The transformation law in Equation (9.47) acts linearly on Equation (9.49) such that we obtain Equation (9.50).

We now rearrange the generators into two sets: the set of $\mathbf{m}_i$ with $i = 1, ..., k$ and the set $\mathbf{m}_{i+k} = \mathbf{m}'_i$ of their images under the shift. Moreover we have $\mathbf{m}_0$ which is the invariant generator. To each generator $\mathbf{m}_i$ we associate a complex coordinate x_i. We have $2k + 1$ of them, related by $2k - 2$ relations, that define the toric three-fold. We divide these relations in two kinds. The k first kind relations are of the form

$$x_i x_{i+k} - x_0^{a+a'} = 0\,, \tag{9.51}$$

and come from Equation (9.48). We use it to relate every image x_{i+k} to its partner x_i and to x_0. The second kind relations relate all remaining x_i and x_0 together. For example, they may look like

$$x_i x_j x_h^b - x_l x_m x_0^c = 0\,, \tag{9.52}$$

for some integers b and c.

Under the shift, relations of the first kind are invariant, those of the second kind are not. However, we can build more symmetric expressions for the latter. As we did when going from Equation (9.49) to Equation (9.50), Equation (9.52) becomes, under the shift,

$$x_{i+k} x_{j+k} x_{h+k}^b - x_{l+k} x_{m+k} x_0^c = 0\,. \tag{9.53}$$

We can now multiply Equation (9.52) by a term $(x_{i+k} x_{j+k} x_{h+k}^b)$ and use the last equation to find

$$(x_i x_j x_h^b)(x_{l+k} x_{m+k}) x_0^c - (x_l x_m)(x_{i+k} x_{j+k} x_{h+k}^b) x_0^c = 0\,, \tag{9.54}$$

which is now symmetric up to a sign under the shift. We dub these relations the symmetrized second kind relations.

To describe our Calabi-Yau 3-fold, we start with $2k+1$ variables. From the equations of the first kind we can express all the x_{i+k} in terms of the x_i and x_0, fixing k variables. Then we can use the symmetrized second kind relations to fix $k - 2$ equations, leaving us with only 3 independent variables. Now, the non-vanishing holomorphic three-form Ω_3 is obtained as the Poincaré residue along the CY_3 of the meromorphic $(2k + 1)$-form in the ambient space $\mathbb{C}^{2k+1}$:

$$\Omega_3 = \mathrm{Res}\, \frac{\mathrm{d}x_1 \wedge ... \wedge \mathrm{d}x_k \wedge ... \wedge \mathrm{d}x_{2k} \wedge \mathrm{d}x_0}{\left(\prod_{i=1}^{k} P_i \prod_{i=1}^{k-2} Q_i \right)}\,, \tag{9.55}$$

where the P_i are equations of the first kind, while Q_i are of the symmetrized second one.

Under the action of the shift, the numerator of the 3-form is multiplied by $(-1)^k$, since the shift acts on the coordinates exchanging them in pairs. From the denominator we get a factor $(-1)^{k-2}$ coming from the symmetrized second kind equations, canceling the factor at the numerator and leaving the 3-form invariant. This means that such orientifold projection does not preserve the same supersymmetry as the D3-branes.

Let us finish this section working out an explicit example. In the case of dP_3, one has $k = 3$, and the holomorphic 3-form is the residue of the meromorphic 7-form.

$$\Omega_3 = \text{Res}\, \frac{\mathrm{d}x_1 \wedge ... \wedge \mathrm{d}x_6 \wedge \mathrm{d}x_0}{(x_1x_4 - x_0^2)(x_2x_5 - x_0^2)(x_3x_6 - x_0^2)(x_1x_3x_5 - x_2x_4x_6)} \,. \quad (9.56)$$

Under the involution, the numerator is multiplied by $(-1)^3$. The first three relations are invariants while the fourth one takes a minus sign. In the end, Ω_3 is even under the symmetry, and hence there cannot be any supersymmetric shift orientifold of dP_3.

9.6 Conclusions

In this chapter, we have studied orientifolds on D3-branes at toric CY singularities using dimer models. We established a classification in terms of smooth involutions of the dimer torus, which allowed us to find the last supersymmetric possibility, the glide reflection orientifold. This possibility may also be reached by directly performing the orientifold projection on the open string spectrum. A last possibility existed, a shift orientifold, but it breaks all supersymmetries, as explicitly argued by studying its action on the holomorphic three-form. Note that these two cases, not considered before, leave no fixed loci. This exhausts the possible orientifolds acting smoothly on the dimer torus.

Given a toric gauge theory and its associated dimer, one may find the projected theory with the same dictionary as orientifolds with fixed loci. The resulting theories have properties strikingly similar to non-orientifolded theories.

- Unlike orientifold theories with fixed loci, glide reflection orientifolds are guaranteed to satisfy the anomaly cancellation conditions for some rank assignment. In fact, these theories are non-chiral. This fact is non-trivial, see Chapter 8, and granted by the absence of fixed loci in the glide orientifold that would give rise to tensor matter that could spoil the ACC. From the geometric point of view, this boils down to

the absence of net RR fluxes sourced by these orientifolds, as there are no fixed loci that can be interpreted as an O-plane. T-duality sheds further light, since the glide orientifold turns to a pair of oppositely charged O-planes on a circle, in the sense of [166, 184].

- Again contrary to intuition, these theories are conformal, as shown by explicit computation of the β-function, that vanishes identically.

- Some of these theories admit $\mathcal{N} = 2$ or deformation fractional branes. The latter trigger a cascade of dualities à la Klebanov-Strassler, with a constant step that allows for a UV completion purely in terms of field theory. This is unlike some orientifolds with fixed loci in the literature [55] and opens up the possibility of a simple supergravity dual.

- The glide reflection orientifold may be understood in the T-dual and mirror picture, at least for $\mathbb{C}^2/\mathbb{Z}_2$, providing a unifying picture.

This closes the analysis of orientifolds of brane tilings, or at least those acting as smooth involutions on the torus. However, one may consider other kinds of involutions. For example, involutions not respecting the color mapping presented in Section 9.1 or non-smooth involutions, can lead to new projections of the tiling, different from the usual orientifold. One may also look for quotients of higher-order, in the spirit of what has been done with S-folds [191,192], and their connection with dimer models. These directions are yet to be explored.

Orientifolds with fixed loci have found extensive use in phenomenological applications by allowing for non-perturbatively generated superpotentials or opening the door to supersymmetry breaking, as we will see in Part III. We hope that our new results may shed light on these and related issues.

9.A Worldsheet analysis for the Klein bottle projection of $\mathbb{C}^2/\mathbb{Z}_4$

In this appendix, we present the worldsheet computations for the Klein-bottling of $\mathbb{C}^2/\mathbb{Z}_4$ presented in Section 9.2.2.

The open sector of strings on the orbifold before the orientifold projection is obtained as follows:

$$A_\mu = \begin{pmatrix} A_{1\mu} & 0 & 0 & 0 \\ 0 & A_{2\mu} & 0 & 0 \\ 0 & 0 & A_{3\mu} & 0 \\ 0 & 0 & 0 & A_{4\mu} \end{pmatrix}, \quad \Phi_1 = \begin{pmatrix} 0 & X_{12} & 0 & 0 \\ 0 & 0 & X_{23} & 0 \\ 0 & 0 & 0 & X_{34} \\ X_{41} & 0 & 0 & 0 \end{pmatrix},$$
$$\Phi_2 = \begin{pmatrix} 0 & 0 & 0 & Y_{14} \\ Y_{21} & 0 & 0 & 0 \\ 0 & Y_{32} & 0 & 0 \\ 0 & 0 & Y_{43} & 0 \end{pmatrix}, \qquad \Phi_3 = \begin{pmatrix} Z_{11} & 0 & 0 & 0 \\ 0 & Z_{22} & 0 & 0 \\ 0 & 0 & Z_{33} & 0 \\ 0 & 0 & 0 & Z_{44} \end{pmatrix}. \tag{9.57}$$

The appropriate orientifold projection, defined as in Equations (9.8) and (9.9), is given by

$$\gamma_\Omega = \begin{pmatrix} 0 & 0 & \mathbb{1}_N & 0 \\ 0 & 0 & 0 & \mathbb{1}_N \\ \mathbb{1}_N & 0 & 0 & 0 \\ 0 & \mathbb{1}_N & 0 & 0 \end{pmatrix}, \quad \text{and} \quad R = \begin{pmatrix} 0 & 1 & 0 \\ 1 & 0 & 0 \\ 0 & 0 & 1 \end{pmatrix}. \tag{9.58}$$

It gives the following identification of gauge bosons

$$A_{1\,\mu} = -A_{3\,\mu}^T \quad \text{and} \quad A_{2\,\mu} = -A_{4\,\mu}^T\,, \tag{9.59}$$

the resulting gauge group is $SU(N)_1 \times SU(N)_2$. The matter content follows from

$$\begin{array}{rcccl} X_{12} & = & Y_{43}^T & \equiv & \mathcal{X}_{12} \in (\overline{\square}_1, \square_2)\,, \\ X_{23} & = & Y_{14}^T & \equiv & \mathcal{X}_{21} \in (\overline{\square}_2, \overline{\square}_1)\,, \\ Y_{21} & = & X_{34}^T & \equiv & \mathcal{Y}_{21} \in (\overline{\square}_2, \square_1)\,, \\ Y_{32} & = & X_{41}^T & \equiv & \mathcal{Y}_{12} \in (\square_1, \square_2)\,, \\ Z_{11} & = & Z_{33}^T & \equiv & \mathcal{Z}_{11} \in \mathrm{Adj}_1\,, \\ Z_{22} & = & Z_{44}^T & \equiv & \mathcal{Z}_{22} \in \mathrm{Adj}_2\,. \end{array} \tag{9.60}$$

One can check that the superpotential is the one advertised in Equation (9.14).

9.B Computations for the orbifolds of the conifold

9.B.1 Orbifold of the conifold $\mathcal{C}/\mathbb{Z}_2$

Let be a non-chiral orbifold of the conifold, $\mathcal{C}/(\mathbb{Z}_l \times \mathbb{Z}_m)$. The general action is given by

$$\begin{aligned} &\gamma_g V_{1,2} \gamma_g^{-1} = V_{1,2} \\ &\gamma_g A_1 \gamma_g^{-1} = e^{2\pi i/l} A_1 \,, \quad \gamma_g A_2 \gamma_g^{-1} = A_2 \\ &\gamma_g B_1 \gamma_g^{-1} = e^{-2\pi i/l} B_1 \,, \quad \gamma_g B_2 \gamma_g^{-1} = B_2 \,, \end{aligned} \tag{9.61}$$

and

$$\begin{aligned} &\gamma_g V_{1,2} \gamma_g^{-1} = V_{1,2} \\ &\gamma_g A_1 \gamma_g^{-1} = e^{2\pi i/m} A_1 \,, \quad \gamma_g A_2 \gamma_g^{-1} = A_2 \\ &\gamma_g B_1 \gamma_g^{-1} = B_1 \,, \quad \gamma_g B_2 \gamma_g^{-1} = e^{-2\pi i/m} B_2 \,, \end{aligned} \tag{9.62}$$

where $V_{1,2}$ are the two adjoint vectors related to the gauge groups. In the case of our first example, $\mathcal{C}/\mathbb{Z}_2$, the action gives the following fields

$$\begin{aligned} &V_1 = \begin{pmatrix} V_1 & 0 \\ 0 & V_3 \end{pmatrix}, \qquad V_2 = \begin{pmatrix} V_2 & 0 \\ 0 & V_4 \end{pmatrix}, \qquad A_1 = \begin{pmatrix} 0 & A_{14} \\ A_{32} & 0 \end{pmatrix}, \\ &A_2 = \begin{pmatrix} A_{12} & 0 \\ 0 & A_{34} \end{pmatrix}, \quad B_1 = \begin{pmatrix} B_{21} & 0 \\ 0 & B_{43} \end{pmatrix}, \quad B_2 = \begin{pmatrix} 0 & B_{23} \\ B_{41} & 0 \end{pmatrix}, \end{aligned} \tag{9.63}$$

with a superpotential given by

$$W = A_1 B_1 A_2 B_2 - A_1 B_2 A_2 B_1 \,. \tag{9.64}$$

We consider the following orientifold projection in order to reproduce the glide projection.

$$\begin{aligned} V_{1,2} &= -\gamma_\Omega V_{1,2}^T \gamma_\Omega^{-1} \,, \\ A_{1,2} &= \gamma_\Omega B_{1,2}^T \gamma_\Omega^{-1} \,, \end{aligned} \tag{9.65}$$

with

$$\gamma_\Omega = \begin{pmatrix} 0 & \mathbb{1}_N \\ \mathbb{1}_N & 0 \end{pmatrix} . \tag{9.66}$$

The action on mesons, $x = (A_1B_1)^2$ $y = (A_2B_2)^2$, $z = A_1B_2$ and $w = A_2B_1$, is

$$\begin{aligned} & x \leftrightarrow y\,, \qquad z \to z\,, \qquad w \to w\,, \\ & \Omega_3 = \frac{\mathrm{d}x \wedge \mathrm{d}y \wedge \mathrm{d}z}{2wz^2} \to \Omega_3' = \frac{\mathrm{d}y \wedge \mathrm{d}x \wedge \mathrm{d}z}{2wz^2} = -\Omega_3 \end{aligned} \tag{9.67}$$

which means that the action preserves supersymmetry on the branes.

The gauge group is $SU(N_1)_1 \times SU(N_2)_2$ and matter content given by

$$\begin{array}{rcl} A_{14} = B_{23}^T \equiv A & = & (\overline{\square}_1, \overline{\square}_2)\,, \\ B_{41} = A_{32}^T \equiv B & = & (\square_1, \square_2)\,, \\ A_{12} = B_{43}^T \equiv C & = & (\overline{\square}_1, \square_2)\,, \\ B_{21} = A_{34}^T \equiv D & = & (\square_1, \overline{\square}_2)\,, \end{array} \tag{9.68}$$

with superpotential

$$W = ABCD - BAC^TD^T\,. \tag{9.69}$$

9.B.2 Zeroth Hirzebruch surface $\mathbf{F}_0$

In this case we take the following actions on the fields

$$\begin{aligned} \gamma_g V_{1,2} \gamma_g^{-1} &= V_{1,2}\,, \\ \gamma_g A_1 \gamma_g^{-1} &= -A_1\,, \\ \gamma_g A_2 \gamma_g^{-1} &= -A_2\,, \\ \gamma_g B_1 \gamma_g^{-1} &= B_1\,, \\ \gamma_g B_2 \gamma_g^{-1} &= B_2\,, \end{aligned} \tag{9.70}$$

leading to

$$V_1 = \begin{pmatrix} V_1 & 0 \\ 0 & V_3 \end{pmatrix}, \qquad V_2 = \begin{pmatrix} V_2 & 0 \\ 0 & V_4 \end{pmatrix}, \qquad A_1 = \begin{pmatrix} 0 & A_{14}^1 \\ A_{32}^1 & 0 \end{pmatrix},$$
$$A_2 = \begin{pmatrix} 0 & A_{14}^2 \\ A_{32}^2 & 0 \end{pmatrix}, \qquad B_1 = \begin{pmatrix} B_{21}^1 & 0 \\ 0 & B_{43}^1 \end{pmatrix}, \qquad B_2 = \begin{pmatrix} B_{21}^2 & 0 \\ 0 & B_{43}^2 \end{pmatrix}.$$

The orientifold action maps $1 \to 4$ and $2 \to 3$, it can be summarized as

$$\begin{aligned} V_{1,2} &= -\gamma_\Omega V_{1,2}^T \gamma_\Omega^{-1}\,, \\ A_1 &= \gamma_\Omega A_2^T \gamma_\Omega^{-1}\,, \\ B_1 &= \gamma_\Omega B_2^T \gamma_\Omega^{-1}\,, \end{aligned} \tag{9.71}$$

with

$$\gamma_\Omega = \begin{pmatrix} \mathbb{1}_N & 0 \\ 0 & \mathbb{1}_N \end{pmatrix} . \tag{9.72}$$

The resulting gauge group is $SU(N)_1 \times SU(N)_2$ and the matter content is given by

$$\begin{array}{rcccl} A^1_{14} = A^{2T}_{14} & \equiv & U_{S,A} & = & \overline{\square\square}_1, \overline{\square}_1 , \\ A^2_{32} = A^{2T}_{32} & \equiv & Z_{S,A} & = & \square\square_2, \overline{\square}_2 , \\ B^1_{21} = B^2_{43} & \equiv & X & = & (\square_1, \overline{\square}_2) , \\ B^2_{21} = B^1_{43} & \equiv & Y & = & (\square_1, \overline{\square}_2) , \end{array} \tag{9.73}$$

with the following superpotential,

$$W = XU_S Y^T Z_A - X^T Z_S Y U_A . \tag{9.74}$$

In order to compute the action the 3-form, we compute the equations defining the singularity using the geometrical approach described in Section 9.5. The singularity is described by the following equations in $\mathbb{C}^9$

$$\begin{array}{ccc} & z_1 z_3 = z_2 z_4 = z_0^2 , & \\ z_1 z_2 = z_5^2 , & & z_2 z_3 = z_7^2 , \\ z_1 z_4 = z_6^2 , & & z_3 z_4 = z_8^2 . \end{array} \tag{9.75}$$

The action on mesons is

$$z_1 \leftrightarrow z_2 , \qquad z_3 \leftrightarrow z_4 , \qquad z_6 \leftrightarrow z_7 \tag{9.76}$$

while all other coordinates are invariant. The action on the 3-form is

$$\Omega_3 = \mathrm{Res} \frac{\mathrm{d}z_1 \wedge \mathrm{d}z_2 \wedge \mathrm{d}z_3 \wedge \mathrm{d}z_4 \wedge \mathrm{d}z_5 \wedge \mathrm{d}z_6 \wedge \mathrm{d}z_7 \wedge \mathrm{d}z_8 \wedge \mathrm{d}z_0}{\prod_i P_i} \to -\Omega_3 , \tag{9.77}$$

since the polynomials are invariant and in the numerator we are exchanging three pairs of coordinates, resulting in an overall minus sign.

9.B.3 A cascade in the glide projection of $\mathcal{C}/\mathbb{Z}_2$

For a generic choice of ranks, $SU(N+M)_1 \times SU(N)_2$, one finds that the gauge theory has a non-trivial RG-flow and $SU(N+M)_1$ goes more rapidly to strong coupling as we approach the infrared regime of the theory:

$$\beta_1 = 3M , \quad \beta_2 = -3M . \tag{9.78}$$

The mesons of the first gauge group are

$$M_1 = BA \quad M_2 = BC\,, \quad M_3 = C^T D^T \quad \text{and} \quad M_4 = DA\,, \tag{9.79}$$

and one thus finds that this gauge theory is Seiberg dual [91] to $SU(N-M)_1 \times SU(N)_2$ with a matter content given by the mesons M_1, M_2, M_3 and M_4 in addition to the following list of bifundamental fields:

$$a = (\square_1, \square_2)\,, \quad b = (\overline{\square}_1, \overline{\square}_2)\,, \quad c = (\square_1, \overline{\square}_2) \quad \text{and} \quad d = (\overline{\square}_1, \square_2)\,. \tag{9.80}$$

The superpotential is given by

$$\begin{aligned} W &= M_2 M_4 - M_1 M_3 + M_1 ab + M_2 cb + M_3 d^T c^T + M_4 ad \\ &= abd^T c^T - badc \end{aligned} \tag{9.81}$$

where the mesons have been integrated out using F-term relations.

The new gauge theory $SU(N-M)_1 \times SU(N)_2$ ends up with the same matter content and superpotential (up to an overall sign) as the initial $SU(N+M)_1 \times SU(N)_2$. This can be seen easily with the following mapping:

$$A \to b\,, \quad B \to a\,, \quad C \to d \quad \text{and} \quad D \to c\,. \tag{9.82}$$

The M deformation branes thus trigger a cascade of Seiberg dualities à la Klebanov-Strassler [27]. In particular, for N being an integer multiple of M, we expect the cascade flow down to $SU(2M) \times SU(M)$ where the physics should the same as for the deformed conifold. Indeed, we can schematically define baryonic operators $\bar{\mathcal{B}} = [AC^T]^M$, $\mathcal{B} = [BD^T]^M$, and a $2M \times 2M$ squared matrix $\mathcal{M}$ in terms of the mesonic operators of Equation (9.79) that should obey a relation of the form

$$\det \mathcal{M} - \bar{\mathcal{B}}\mathcal{B} = \Lambda_{2M}^{4M}\,, \tag{9.83}$$

where Λ_{2M} is the strong coupling scale of $SU(2M)$. Going on the baryonic branch $\bar{\mathcal{B}} = \mathcal{B} = i\Lambda_{2M}^{2M}$, one finds that the mesons decouple, leaving a SYM $SU(M)$ dynamics displaying confinement and chiral symmetry breaking.

Part III

Dynamical Supersymmetry Breaking in Dimer Models

Chapter 10

Supersymmetry Breaking Vacua and their Coulomb Branch Instability

We present in this chapter a large class of models of D-branes at orientifolded Calabi-Yau singularities which enjoy dynamical supersymmetry breaking at low energy, by means of either the $SU(5)$ or $3-2$ supersymmetry breaking models. Once embedded in a warped throat or, equivalently, in a large N theory, all models display an instability along a Coulomb branch direction towards supersymmetry preserving vacua. Interestingly, the nature of the runaway mechanism is model-independent and has a precise geometrical interpretation. This naturally suggests the properties a Calabi-Yau singularity should have in order for such instability not to occur. These results were originally presented in [2].

The chapter is structured as follows. In Section 10.1 we present a summary of our main results, to provide the reader with a simple illustration of the physical picture that emerges from the examples we have explored. We then proceed to discuss in detail several cases. In Section 10.2 we review the orientifold of the $\mathbb{C}^3/\mathbb{Z}_{6'}$ singularity, already analyzed in [74], finding not only the $SU(5)$ model but also a $3-2$ model, and their instability. In Section 10.3 we consider the orientifold of a pseudo del Pezzo singularity, PdP_4, where we also recover both an $SU(5)$ and a $3-2$ model. The instability is also present, though the presence of anomalous dimensions makes the analysis slightly more subtle. In Section 10.4, we present a large number of new orientifold set-ups, generalizing previous ones, based on orbifolds or blow-ups of del Pezzo CY singularities, where $SU(5)$ and possibly $3-2$ models are found. In all such set-ups, we identify, again, a runaway Coulomb

branch instability. In Section 10.5, we provide a no-go theorem showing that whenever $\mathcal{N} = 2$ fractional branes are allowed, they inevitably destabilize the otherwise stable DSB vacua. We then look at singularities that do not allow for $\mathcal{N} = 2$ fractional branes, in order to avoid from the start the mechanism of instability. A brief and partial scan yielding negative results hints that in such cases an $SU(5)$ or a $3-2$ model cannot be easily found.

10.1 Overview of the problematic

Supersymmetry breaking models in dimer models

Recently, a series of papers renewed the interest in models of D-branes at CY singularities leading to dynamical supersymmetry breaking. This originated from [54] where an existence proof for a possibly stable DSB model obtained by considering fractional branes at orientifold singularities was given. It is then natural to ask first which DSB models we have a chance of being able to engineer. Known DSB models are rather specific gauge theories, and we have to match their properties to the ones of the gauge theories one can engineer with branes.

D-branes at singularities yield quiver gauge theories. In particular, since all matter fields can be related to open strings, they all have two gauge theory indices, corresponding to the two ends of the open strings. Without orientifold projection we have only two possibilities: matter fields are either in the adjoint representation (if both ends are on the same D-brane) or in the bifundamental representation (if they join two different D-branes). In the presence of an orientifold, there is the additional possibility of having fields in the symmetric or antisymmetric representations or their conjugates.

A generic property of DSB models is that they have a rather contrived matter content so that there cannot be mass terms and in addition, classical flat directions should be lifted by the superpotential. In particular, known DSB models, with only a few notable exceptions, are chiral gauge theories. We will focus on the following two well-known models since they involve matter in at most two-index representations of the gauge groups. See Chapter 2 for a more detailed reminder on their properties.

SU(5) model. This model [71] has an $SU(5)$ gauge group and one GUT-like chiral family:

$$\tilde{Q} = \overline{\square}, \quad A = \begin{array}{|c|}\hline \\ \hline \end{array}. \tag{10.1}$$

No chiral gauge-invariant can be written, hence it has no superpo-

tential and no classical flat directions. With arguments based on 't Hooft anomaly matching, its vacuum is believed to break supersymmetry in a purely strongly coupled fashion. The supersymmetry breaking vacuum energy density is given in terms of its dynamical scale, $E_{\text{vac}} \propto \Lambda^4_{SU(5)}$. The $SU(5)$ model has a matter field in the antisymmetric representation, hence to recover it an orientifold projection is necessary.

$3-2$ model. This other model [94] involves two gauge groups, $SU(3)$ and $SU(2)$ respectively, and one chiral family, resembling the ones of the Standard Model:

$$Q = (\square_3, \overline{\square}_2)\,, \quad \bar{U} = \overline{\square}_3\,, \quad \bar{D} = \overline{\square}_3\,, \quad L = \square_2\,. \tag{10.2}$$

This model has a number of flat directions, but a cubic superpotential lifts them all:

$$W = \bar{D}QL\,. \tag{10.3}$$

After taking into account non-perturbatively generated contributions to the superpotential, it turns out there is a conflict between F-terms and D-terms so that no supersymmetric vacuum can be found. The actual minimum breaks supersymmetry dynamically, where now $E_{\text{vac}} \propto \Lambda^4_{SU(3)}$ or $\Lambda^4_{SU(2)}$, depending on which group confines first. In principle, the above field content (SU gauge groups, (bi)fundamental matter, together with a cubic superpotential) does not seem to require an orientifold projection. As it will become clear in Chapter 11, such a projection is nevertheless necessary in order to allow for a fractional brane (*i.e.* an anomaly-free configuration) with the desired ranks for the gauge groups.

It turns out that fixed loci in the orientifold projections will be necessary to recover these DSB models, either for introducing (anti)symmetric matter or $SO(N)/USp(N)$ gauge groups. Hence, we will focus in this part of the thesis on the projections introduced in [54] and leave aside the glide projections of Chapter 9 from now on.

Other known DSB models cannot be engineered with brane constructions, such as the $SO(10)$ model [193] (because of the spinor representation) and the $4-1$ model [194, 195] (because of the $U(1)$ charges). Further models would deserve a closer look, but doing this is beyond the scope of the present work.

As we explained at length in Chapter 8, it turns out that, generically, the anomaly cancellation conditions result in constraints on the various

ranks of the form[1]

$$\sum_i N_i = \sum_{j'} N_{j'} + 4 \ , \tag{10.4}$$

where the two sums run on two different sets of gauge theory nodes, and strictly speaking the N_i and $N_{j'}$ are not the ranks but the dimensions of the fundamental representation of $SU(N)$, $SO(N)$ or $USp(N)$ groups. The imbalance of 4 units in Equation (10.4) is due to the orientifold charge, which contributes to tadpole cancellations.

Two simple ways to satisfy Equation (10.4) are the following. We can take one $N_i = 5$, one $N_{j'} = 1$ and all other ranks to vanish, so that the remaining gauge group is $SU(5) \times SU(1)$ or $SU(5) \times SO(1)$. The trivial factor actually allows for a bifundamental between the two nodes to be interpreted as a (anti)fundamental of $SU(5)$. If the latter also has an antisymmetric matter field, then the field content is exactly the one of the $SU(5)$ DSB model.

The other simple solution to Equation (10.4) is to take one $N_i = 3$, another one $N_{j\neq i} = 2$, one $N_{j'} = 1$, and again all other factors to vanish, leading to the gauge group $SU(3) \times SU(2)/USp(2) \times SU(1)/SO(1)$. The $3-2$ model is recovered if bifundamentals are linking the three gauge groups, together with a cubic superpotential term, and in addition to an antisymmetric of $SU(3)$ which provides for the remaining (anti)triplet, necessary for anomaly cancellation.

In some of the examples that we will review below, some additional decoupled gauge singlets will be present, or even additional decoupled gauge sectors, which themselves do not break supersymmetry. We will even encounter an example with two decoupled $SU(5)$ models.

The first conclusion we will draw is that there is a sizeable number of orientifold singularities that allow for configurations of branes realizing either the $SU(5)$ or $3-2$ models at low energy. They can be engineered by bound states of fractional D3-branes which arise at the end of complicated RG-flows (often described by a duality cascade [27]) or on the $\mathcal{N} = 4$ Coulomb branch of regular D3-branes, depending on the singularity structure.

The Coulomb branch instability

A common feature of *all* CY singularities in which the above DSB models will be found in this chapter is that they admit $\mathcal{N} = 2$ fractional branes.

[1] As explained in [54], we can have a multiple of +4 in the equation.

The latter are related to a partial resolution of the singularity displaying a non-isolated $\mathbb{C}^2/\mathbb{Z}_n$ singularity and a $\mathcal{N}=2$ Coulomb branch associated with it (further details on this class of fractional branes are provided in Chapter 6). Hence, the supersymmetry breaking vacuum is destabilized and ceases to exist. This novel decay mechanism, which remarkably has an elegant geometric origin, was originally uncovered in [74].

The basic dynamical mechanism describing such instability goes as follows. In the decoupling limit [21], the DSB model emerges as a vacuum configuration of a (possibly intricate) system of regular and fractional D-branes, with the vacuum energy depending on the VEVs of the scalar fields. The $\mathcal{N}=4$ Coulomb branch is parameterized by regular branes. If an $\mathcal{N}=2$ fractional brane direction exists, there is, in addition, an $\mathcal{N}=2$ Coulomb branch. One can show that the energy of the supersymmetry breaking vacuum is related to the strong coupling scale Λ of the $SU(5)$ or $SU(3)\times SU(2)$ gauge groups[2] and, by scale matching, to the strong coupling scale Λ_{UV} of the UV-complete model with regular branes as follows

$$E_{vac} = \Lambda^4 = \left(\frac{v'}{v}\right)^{\alpha} \Lambda_{UV}^4 \,, \quad \alpha \in \mathbb{R} \,, \tag{10.5}$$

where the exponent α is model-dependent and given by a ratio of beta functions and v and v' are the VEVs on the Coulomb branches associated with the $\mathcal{N}=2$ fractional brane and its complement, respectively. Fractional branes are defined modulo regular branes so that a fractional brane and its complement combine into a regular brane. The case $v=v'$ then corresponds to the $\mathcal{N}=4$ Coulomb branch.

From Equation (10.5), it follows that on the $\mathcal{N}=4$ Coulomb branch the vacuum energy equals Λ and the supersymmetry breaking vacuum is hence preserved. On the $\mathcal{N}=2$ Coulomb branch, instead, where $v \neq v'$, the vacuum energy relaxes to 0, with a moduli space parameterized by v at $v'=0$ or vice-versa, depending on the sign of α. Geometrically, this corresponds to a supersymmetric configuration described by the $\mathcal{N}=2$ fractional branes associated with v located at a finite distance along the non-isolated $\mathbb{C}^2/\mathbb{Z}_n$ singularity describing its Coulomb branch, and their complement sitting at the origin.

The only possibility for evading this decay mechanism of the supersymmetry breaking vacuum is that $\alpha=0$. Using some basic properties of Calabi-Yau varieties and the fact that fractional branes are described by a non-conformal field theory at low energy, we will show in Section 10.5 that

[2] In the $3-2$ model, Λ refers to the scale of the gauge group factor, either $SU(3)$ or $SU(2)$, that dominates the dynamics.

$\alpha \neq 0$. The upshot is that whenever such $\mathcal{N} = 2$ classical flat directions exist at a singularity which admits the aforementioned DSB models, and so for the models constructed in [74] and the present chapter, the quantum behavior of the latter tilts the flat directions towards supersymmetry preserving vacuum. The models are hence unstable, or at most metastable.

Let us schematically discuss what occurs to the gauge theory in this process. We denote $G_{\not{SUSY}}$ the SUSY breaking model, namely its gauge group (and possibly flavor group), matter fields, and interactions. When N regular D3-branes are added, the SUSY breaking sector extends to

$$G_{\not{SUSY}} \quad \xrightarrow[\text{branes}]{+\ N \text{ regular}} \quad G_{\not{SUSY}+N} \times G'_N \ , \tag{10.6}$$

where $G_{\not{SUSY}+N}$ indicates that the ranks of the gauge and flavor groups are increased by N. G'_N denotes the theory associated with the complement. The subindex indicates that all gauge groups in this sector have rank N. In addition, there is matter connecting the $G_{\not{SUSY}+N}$ and G'_N sectors. Along the $\mathcal{N} = 2$ Coulomb branch, the theory is higgsed down to

$$G_{\not{SUSY}+N} \times G'_N \quad \xrightarrow{v \neq v'} \quad G_{\not{SUSY}} \times G'_N \ , \tag{10.7}$$

We are left precisely with the original SUSY breaking theory of interest, but now coupled to G'_N. This extension of the theory spoils supersymmetry breaking.

The only way to avoid this decay mechanism is to look for singularities that admit supersymmetry breaking D-brane configurations *and* are free of local $\mathbb{C}^2/\mathbb{Z}_n$ singularities. Whether such geometries exist or not is a question that will be investigated in Chapters 11 and 12.

Note that we do not investigate here the existence of stable DSB models in brane constructions that include flavors, engineered by non-compact D7-branes, for which it is already known that metastable DSB vacua can be found [63].

We now turn to the analysis of a series of singularities, showing how the general pattern described above emerges.

10.2 The $\mathbb{C}^3/\mathbb{Z}_{6'}$ singularity

As a warm-up, let us start considering the (fixed point) orientifold of the orbifold $\mathbb{C}^3/\mathbb{Z}_{6'}$, already analysed in [74]. The orbifold action is defined by the $\mathbb{Z}_{6'}$ acting on the complex coordinates of $\mathbb{C}^3$ as

$$g \ : \quad z_i \to e^{i2\pi v_i} z_i \ , \tag{10.8}$$

with $i = 1, 2, 3$ and $v = (1, 2, 3)/6$. The dimer associated with the $\mathbb{C}^3/\mathbb{Z}_{6'}$ orbifold singularity is reported in Figure 10.1, including the fixed points with respect to which we will eventually take the orientifold projection.

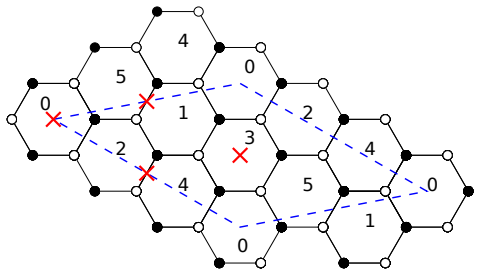

Figure 10.1: The $\mathbb{C}^3/\mathbb{Z}_{6'}$ dimer. The theory is chiral, with 6 gauge factors and 18 bifundamental chiral superfields X_{ij}. The parallelogram is a possible choice of unit cell. Red crosses represent fixed points under the orientifold action.

From the dimer, one can read the field content of the theory as well as the superpotential which is

$$\begin{aligned} W &= X_{152} + X_{143} + X_{032} + X_{053} + X_{254} + X_{104} \\ &\quad - X_{052} - X_{031} - X_{142} - X_{043} - X_{253} - X_{154} \,, \end{aligned} \tag{10.9}$$

where, for the ease of notation, we have defined $X_{lmn} \equiv X_{lm} X_{mn} X_{nl}$, and X_{lm} is in the $(\overline{\square}_l, \square_m)$ representation, where $l, m, n = 0, 1, ..., 5$. Following the general rules summarized in Chapter 7, one can see that there do not exist deformation fractional branes but $\mathcal{N} = 2$ fractional branes. For instance, the strip $0-2-4$ and its complement $1-3-5$, are $\mathcal{N} = 2$ fractional branes.

We now perform an orientifold projection via point reflection. The unit cell has an even number of white nodes hence, following Chapter 7, we have to choose orientifold charges with an even number of $+$ signs. A convenient choice is $(++--)$ starting from the fixed point on face 0 and going clockwise. The orientifold projection gives the following identifications between faces

$$0 \leftrightarrow 0 \qquad 1 \leftrightarrow 5 \qquad 2 \leftrightarrow 4 \qquad 3 \leftrightarrow 3. \tag{10.10}$$

The daughter theory has hence gauge group

$$SO(N_0) \times SU(N_1) \times SU(N_2) \times USp(N_3) \,, \tag{10.11}$$

and matter in the following representations

$$X_1 = (\square_0, \overline{\square}_1) \quad , \quad X_2 = (\square_0, \overline{\square}_2) \quad , \quad X_3 = (\square_0, \square_3),$$
$$Y_1 = (\square_1, \square_3) \quad , \quad Y_2 = (\square_2, \square_3) \quad , \quad Z_1 = (\square_1, \square_2)$$
$$Z_2 = (\overline{\square}_1, \overline{\square}_2) \quad , \quad W = (\square_1, \overline{\square}_2) \quad , \quad A = \begin{smallmatrix}\square\\\square\end{smallmatrix}_2 \quad , \quad S = \overline{\square\square}_1 \tag{10.12}$$

Imposing anomaly cancellation condition on the two SU factors we get

$$\begin{cases} N_0 + N_1 - N_2 - N_3 + 4 = 0 & SU(N_1) \\ N_0 + N_1 - N_2 - N_3 + 4 = 0 & SU(N_2) \end{cases} \tag{10.13}$$

which is one and the same condition, that is

$$N_0 + N_1 - N_2 - N_3 + 4 = 0 \ . \tag{10.14}$$

SU(5) model

An interesting choice of ranks compatible with the constraint in Section 10.2 is $N_0 = 1, N_1 = 0, N_2 = 5, N_3 = 0$. With this choice, the theory becomes exactly the one describing the non-calculable $SU(5)$ DSB model (the $SO(1)$ becomes a flavor index), which breaks supersymmetry dynamically in a stable vacuum. The corresponding quiver is reported in Figure 10.2.

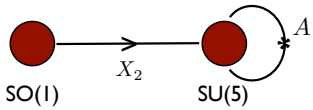

Figure 10.2: The quiver of the $SU(5)$ model at the $\mathbb{C}^3/\mathbb{Z}_{6'}$ orbifold singularity. Matter fields follow the definitions in Section 10.2. The asterisk refers to the antisymmetric representation.

As recently argued in [74], in the decoupling limit this DSB vacuum becomes actually unstable. In such limit the effective matter-coupled gauge theory becomes

$$SO(N+1) \times SU(N) \times SU(N+5) \times USp(N) \ , \tag{10.15}$$

which actually corresponds to adding N regular D3-branes at the singularity. This is a much richer theory than $SO(1) \times SU(5)$ and it might have, possibly, many vacua. One should then ask whether in the larger moduli space of Equation (10.15) there are instabilities that make the supersymmetry breaking vacuum unstable. This can be easily understood by scale matching.

The vacuum energy of the putative supersymmetry breaking vacuum will be $\sim \Lambda^4$, with Λ the intrinsic scale of the $SU(5)$ model. The higgsing of the N regular branes can be obtained giving a VEV of scale v to the gauge-invariant operator[3]

$$\Phi = \mathrm{Tr}(X_1 W Y_2 X_3^T) \ . \tag{10.16}$$

This makes the theory of Equation (10.15) flow to $SO(1) \times SU(5)$, namely the DSB $SU(5)$ model.

We can match the UV and IR scales evaluating the β functions of the relevant SU factor above and below the scale v.[4] Note that because the orbifold theory is a projection of $\mathcal{N} = 4$ SYM, fundamental fields do not acquire anomalous dimensions (equivalently, all superpotential terms are cubic). With obvious notation, we have (here, and in similar formulas thereafter, we omit a factor of $8\pi^2$ for clarity of exposition)

$$\begin{aligned} g_{SU(5+N)}^{-2} &= \left[3(N+5) - \tfrac{1}{2}(6N+4)\right] \ln\left(\tfrac{\mu}{\Lambda_{UV}}\right) = 13 \ln\left(\tfrac{\mu}{\Lambda_{UV}}\right) \ , \\ g_{SU(5)}^{-2} &= \left[15 - \left(\tfrac{1}{2} + \tfrac{3}{2}\right)\right] \ln\left(\tfrac{\mu}{\Lambda}\right) = 13 \ln\left(\tfrac{\mu}{\Lambda}\right) \ . \end{aligned} \tag{10.17}$$

Matching the gauge coupling at $\mu = v$ we get

$$\Lambda = \Lambda_{UV} \ . \tag{10.18}$$

This shows that the effective potential does not depend on the VEV of Φ, meaning that regular brane dynamics does not change the nature of the supersymmetry breaking vacuum and its stability (there is no force acting on the N regular branes).

In fact, it turns out that there exists a different instability channel. This has to do with moduli associated with $\mathcal{N} = 2$ fractional branes, which are massless classically, but become runaway once non-perturbative corrections are taken into account. From the dimer in Figure 10.1 we see that a regular brane can be seen as a bound state of two $\mathcal{N} = 2$ fractional branes corresponding to the strips $0-2-4$ and $1-3-5$, respectively. The classical flat directions correspond to the z_2 fixed line that is left invariant by g^3, see

[3] Hereafter, we assume that all fields appearing in the gauge-invariants have a rank N piece in the upper left part, to ensure the correct higgsing pattern. If the rank N pieces are all proportional to the identity, then an $SU(N)$ diagonal gauge group is preserved. It can be checked to have $\mathcal{N} = 4$ SUSY to a good approximation, and to decouple from the rest of the quiver. We will not consider it further.

[4] The absence of the denominator with respect to the usual NSVZ expression is due to a choice of normalization for the vector superfield which differs from the canonical one by a factor of $1/g^2$, as usual in the framework of the gauge/gravity correspondence.

Equation (10.8). Locally, this is a $\mathbb{C}^2/\mathbb{Z}_2$ singularity. Both these fractional branes survive the orientifold projection, becoming $0-2$ and $1-3$ strips. Note that (135) and (024) are closed loops which represent operators not present in the superpotential. Hence, their VEVs represent motion along classical flat directions. In the daughter theory these directions are given by the operators[5]

$$\tilde{\Phi} = \mathrm{Tr}(X_2 A X_2^T)^2 \quad , \quad \tilde{\Phi}' = \mathrm{Tr}(\mathbb{J} Y_1 S Y_1^T)^2 \ , \tag{10.19}$$

and we will denote the scale of their VEVs as v and v', respectively. The higgsing pattern is then[6]

$$\begin{aligned} & SO(N+1) \times SU(N) \times SU(N+5) \times USp(N) \\ & \quad \xrightarrow{v} \quad SO(1) \times SU(N) \times SU(5) \times USp(N) \quad \xrightarrow{v'} \quad SO(1) \times SU(5) \ . \end{aligned} \tag{10.20}$$

Above and below the scale v the gauge couplings run as

$$\begin{aligned} g^{-2}_{SU(5+N)} &= \left[3(N+5) - \tfrac{1}{2}(6N+4)\right] \ln\left(\tfrac{\mu}{\Lambda_{UV}}\right) = 13 \ln\left(\tfrac{\mu}{\Lambda_{UV}}\right) \ , \\ g^{-2}_{SU(5)_N} &= \left[15 - \tfrac{1}{2}(4N+4)\right] \ln\left(\tfrac{\mu}{\Lambda_N}\right) = (13-2N) \ln\left(\tfrac{\mu}{\Lambda_N}\right) \ . \end{aligned} \tag{10.21}$$

Matching them at $\mu = v$ we get

$$\Lambda_N^{13-2N} = v^{-2N} \Lambda_{UV}^{13} \ . \tag{10.22}$$

Repeating the same computation above and below the scale v' we have

$$\begin{aligned} g^{-2}_{SU(5)_N} &= \left[15 - \tfrac{1}{2}(4N+4)\right] \ln\left(\tfrac{\mu}{\Lambda_N}\right) = (13-2N) \ln\left(\tfrac{\mu}{\Lambda_N}\right) \ , \\ g^{-2}_{SU(5)} &= \left[15 - \left(\tfrac{1}{2} + \tfrac{3}{2}\right)\right] \ln\left(\tfrac{\mu}{\Lambda}\right) = 13 \ln\left(\tfrac{\mu}{\Lambda}\right) \ . \end{aligned} \tag{10.23}$$

and in turn $\Lambda_N^{13-2N} = v'^{-2N} \Lambda^{13}$. The end result is then

$$\Lambda^{13} = \left(\frac{v'}{v}\right)^{2N} \Lambda_{UV}^{13} \ . \tag{10.24}$$

This shows that the DSB vacuum is unstable. There exists a one-dimensional supersymmetric moduli space sitting at $v' = 0$ and parameterized by v. Indeed, one can estimate the minima of the potential in a (v, v') plane and check that any point at $v, v' \neq 0$ is driven to the $v' = 0$ axis. The gradient flow is reported in Figure 10.3.

[5] As before, we assume that the fields in the gauge-invariants have a rank N upper left piece, and we do not consider the decoupled effective $\mathcal{N} = 2$ diagonal gauge group. Note that the traces involve squares since $\mathrm{Tr}(X_2 A X_2^T) = 0$ because of antisymmetry of A, while $\mathrm{Tr}(\mathbb{J} Y_1 S Y_1^T) = 0$ because of antisymmetry of the USp-invariant $\mathbb{J}$.

[6] This pattern occurs for $v \gg v'$. One can check that the end result does not change when inverting the order of the two scales.

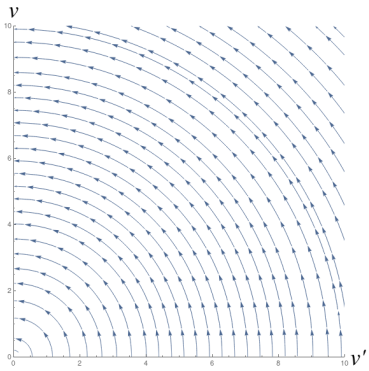

Figure 10.3: Plot of $-\mathrm{Grad}(V)$ as a function of v and v'. The flow goes towards $v' = 0$, suggesting that the system, eventually, relaxes to a supersymmetry preserving vacuum at finite distance in field space.

In principle, one might try to obtain the $SU(5)$ by a different UV completion. For instance, one can add to the DSB configuration M fractional branes populating the second and fourth gauge factors only, corresponding to the strip $1-3-5$ in the mother theory, which becomes $1-3$ after the orientifold projection. The theory, in this case, has gauge group

$$SO(1) \times SU(M) \times SU(5) \times USp(M) \ . \tag{10.25}$$

This configuration does not change much the fate of the DSB vacuum. Previous analysis shows that lacking one modulus, v in our conventions, the one-dimensional moduli space of supersymmetry preserving vacua becomes an isolated vacuum. This agrees with known field theory results [195]: the $SU(5)$ factor has extra vector-like matter and the theory does not lead to a supersymmetry breaking vacuum to start with.

If one instead populates nodes 0 and 2, $N_0 = M, N_1 = 0, N_2 = M + 4, N_3 = 0$ which in the mother theory corresponds to adding M $\mathcal{N} = 2$ fractional branes associated with the strip $0-2-4$, the theory has a runaway direction associated with v. Note that this last system has the same gauge and matter content of a known, stable, DSB model [71, 195], but it lacks a crucial cubic term in the superpotential whose effect is indeed to stop the runaway associated with v. The special case $M = 1$ is the only stable DSB model (our original brane construction, in fact).

To sum up, the $\mathbb{C}^3/\mathbb{Z}_{6'}$ singularity does admit fractional brane configurations whose low energy open string dynamics enjoys stable DSB vacua. However, once coupled to regular branes, the supersymmetry breaking vacuum becomes unstable towards supersymmetry preserving ones. The $\mathbb{C}^3/\mathbb{Z}_{6'}$

singularity can be embedded into a larger singularity which admits deformation branes [72] and, as such, a cascade (dual to a warped throat [196–198]). So the above analysis suggests that, at least within this construction, it is not possible to embed the $SU(5)$ DSB model into a warped throat keeping it stable [74].

$3-2$ model

Looking at Section 10.2, one can see that another possible anomaly-free rank assignment is given by $N_0 = 1, N_1 = 0, N_2 = 3, N_3 = 2$ which corresponds to the following gauge theory

$$SO(1) \times SU(3) \times USp(2) \ . \tag{10.26}$$

Using the fact that $USp(2) = SU(2)$ (for which the fundamental and antifundamental are equivalent representations) and that for $SU(3)$ $\square = \overline{\square}$, from Section 10.2 we see that the matter content is

$$\begin{aligned} X_2 &= (\square_0, \overline{\square}_2) = \overline{D}, \qquad & X_3 &= (\square_0, \square_3) = L, \\ Y_2 &= (\square_2, \square_3) = Q, \qquad & A &= \begin{smallmatrix}\square\\\square\end{smallmatrix}_2 = \overline{U} \ , \end{aligned} \tag{10.27}$$

with tree level superpotential

$$W = \overline{D} Q L \ . \tag{10.28}$$

This reproduces exactly the DSB $3-2$ model [94]! The corresponding quiver is reported in Figure 10.4.

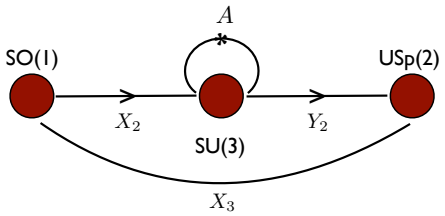

Figure 10.4: The quiver of the $3-2$ model at the $\mathbb{C}^3/\mathbb{Z}_{6'}$ orbifold singularity. Matter fields follow the definitions in Section 10.2. Arrows are indicated only when needed. The asterisk refers to the antisymmetric representation, as in Figure 10.2.

Again, one could ask what is the fate of this DSB vacuum in the full theory. In the present model, we have to perform the scale matchings on the

gauge group that is most strongly coupled, since the DSB vacuum energy will be expressed in terms of its dynamical scale. We start by considering a regime where supersymmetry breaking is driven by the non-perturbative contributions in the $SU(3)$ gauge group [165].

As in the $SU(5)$ model, upon adding regular branes and higgsing them, the vacuum shows no instability. Indeed, giving a VEV to $\Phi = \mathrm{Tr}(X_1 W Y_2 X_3^T)$, the gauge coupling running above and below the matching scale is

$$\begin{aligned} g^{-2}_{SU(3+N)} &= \left[3(N+3) - \tfrac{1}{2}(6N+4)\right] \ln\left(\tfrac{\mu}{\Lambda_{UV}}\right) = 7\ln\left(\tfrac{\mu}{\Lambda_{UV}}\right) , \\ g^{-2}_{SU(3)} &= \left[9 - \left(\tfrac{1}{2}+\tfrac{1}{2}+1\right)\right] \ln\left(\tfrac{\mu}{\Lambda_3}\right) = 7\ln\left(\tfrac{\mu}{\Lambda_3}\right) , \end{aligned} \tag{10.29}$$

and hence $\Lambda = \Lambda_{UV}$.

However, the theory has $\mathcal{N} = 2$ fractional branes, and following the same two-steps higgsing pattern as before, namely

$$\begin{aligned} & SO(N+1) \times SU(N) \times SU(N+3) \times USp(N+2) \\ \xrightarrow{v} \quad & SO(1) \times SU(N) \times SU(3) \times USp(N+2) \\ \xrightarrow{v'} \quad & SO(1) \times SU(3) \times USp(2) \ . \end{aligned} \tag{10.30}$$

we get, above and below the scale v

$$\begin{aligned} g^{-2}_{SU(3+N)} &= \left[3(N+3) - \tfrac{1}{2}(6N+4)\right] \ln\left(\tfrac{\mu}{\Lambda_{UV}}\right) = 7\ln\left(\tfrac{\mu}{\Lambda_{UV}}\right) , \\ g^{-2}_{SU(3)_N} &= \left[9 - \tfrac{1}{2}(4N+4)\right] \ln\left(\tfrac{\mu}{\Lambda_N}\right) = (7-2N)\ln\left(\tfrac{\mu}{\Lambda_N}\right) , \end{aligned} \tag{10.31}$$

and, at scale v'

$$\begin{aligned} g^{-2}_{SU(3)_N} &= \left[9 - \tfrac{1}{2}(4N+4)\right] \ln\left(\tfrac{\mu}{\Lambda_N}\right) = (7-2N)\ln\left(\tfrac{\mu}{\Lambda_N}\right) , \\ g^{-2}_{SU(3)} &= \left[9 - \left(\tfrac{1}{2}+\tfrac{1}{2}+1\right)\right] \ln\left(\tfrac{\mu}{\Lambda_3}\right) = 7\ln\left(\tfrac{\mu}{\Lambda_3}\right) , \end{aligned} \tag{10.32}$$

which gives in the end

$$\Lambda_3^7 = \left(\frac{v'}{v}\right)^{2N} \Lambda_{UV}^7 \ . \tag{10.33}$$

We can now repeat the analysis when the supersymmetry breaking dynamics is driven by the strong coupling scale of $SU(2)$. We have

$$\begin{aligned} g^{-2}_{USp(N+2)} &= \left[3\tfrac{(N+4)}{2} - \tfrac{1}{2}(3N+4)\right] \ln\left(\tfrac{\mu}{\Lambda_{UV}}\right) = 4\ln\left(\tfrac{\mu}{\Lambda_{UV}}\right) , \\ g^{-2}_{USp(2)} &= \left[6 - \left(\tfrac{1}{2}+\tfrac{3}{2}\right)\right] \ln\left(\tfrac{\mu}{\Lambda_2}\right) = 4\ln\left(\tfrac{\mu}{\Lambda_2}\right) , \end{aligned} \tag{10.34}$$

and hence $\Lambda_2 = \Lambda_{UV}$ by higgsing the N regular branes. Along the $\mathcal{N} = 2$ directions we get instead the matching

$$\begin{aligned} g^{-2}_{USp(2+N)} &= \left[3\tfrac{(N+4)}{2} - \tfrac{1}{2}(3N+4)\right] \ln\left(\tfrac{\mu}{\Lambda_{UV}}\right) = 4\ln\left(\tfrac{\mu}{\Lambda_{UV}}\right) , \\ g^{-2}_{USp(2+N)_N} &= \left[3\tfrac{(N+4)}{2} - \tfrac{1}{2}(N+4)\right] \ln\left(\tfrac{\mu}{\Lambda_N}\right) = (4+N)\ln\left(\tfrac{\mu}{\Lambda_N}\right) , \end{aligned} \tag{10.35}$$

at scale v and

$$\begin{aligned} g^{-2}_{USp(2+N)_N} &= \left[3\tfrac{(N+4)}{2} - \tfrac{1}{2}(N+4)\right] \ln\left(\tfrac{\mu}{\Lambda_N}\right) = (4+N)\ln\left(\tfrac{\mu}{\Lambda_N}\right) , \\ g^{-2}_{USp(2)} &= \left[6 - \left(\tfrac{1}{2}+\tfrac{3}{2}\right)\right] \ln\left(\tfrac{\mu}{\Lambda_2}\right) = 4\ln\left(\tfrac{\mu}{\Lambda_2}\right) , \end{aligned} \tag{10.36}$$

at scale v'. The final relation one gets between the UV and IR scale is now

$$\Lambda_2^4 = \left(\frac{v}{v'}\right)^N \Lambda_{UV}^4 . \tag{10.37}$$

This result is analogous to the one obtained before (even though the roles of v and v' are exchanged). We conclude that the Coulomb branch is unstable and it is so independently of the regime in which the $3-2$ model finds itself.

10.3 The PdP_4 singularity

We now want to consider a different model, based on the pseudo del Pezzo 4 singularity, PdP_4 for short. We choose, for definiteness, the phase I, following the conventions of [129], where pseudo del Pezzo singularities were introduced. The dimer is depicted in Figure 10.5.

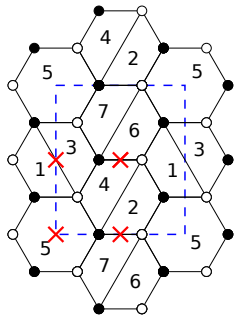

Figure 10.5: $PdP4$ dimer. Red crosses represent fixed points under the orientifold action.

As for the orbifold model, from the dimer, one can extract the field theory content and the corresponding superpotential, which now reads

$$W = X_{1543} + X_{375} + X_{1642} + X_{5276} - X_{152} - X_{7643} - X_{5427} - X_{5316} \ , \quad (10.38)$$

with by now familiar index conventions. Note that the superpotential admits also quartic terms now, implying that (some) fundamental fields have large anomalous dimensions. This is related to an important qualitative difference with respect to the previous example. In this model there exist deformation fractional branes, together with $\mathcal{N} = 2$ ones. For instance, the strip $1-3-5$ is a $\mathcal{N} = 2$ brane, while $2-6$ and $1-2-5$ are two different kinds of deformation branes.

Upon point reflection with charges $(+-+-)$ starting on the fixed point on face 5 and going clockwise, we get the following identifications between faces

$$1 \leftrightarrow 3 \qquad 2 \leftrightarrow 7 \qquad 4 \leftrightarrow 6 \qquad 5 \leftrightarrow 5 \ . \quad (10.39)$$

The daughter theory has hence gauge group

$$SO(N_5) \times SU(N_1) \times SU(N_2) \times SU(N_4) \ , \quad (10.40)$$

and matter in the following representations

$$\begin{array}{lll} X_1 = (\overline{\square}_1, \square_5) \, , & X_2 = (\square_5, \square_2) \, , & X_4 = (\square_5, \square_4) \, , \\ Y_1 = (\overline{\square}_4, \overline{\square}_1) \, , & Y_2 = (\overline{\square}_4, \square_2) \, , & Z = (\overline{\square}_2, \square_1) \, , \\ A_1 = \begin{smallmatrix}\square\\\square\end{smallmatrix}_1 \, , & A_2 = \overline{\begin{smallmatrix}\square\\\square\end{smallmatrix}}_2 \, , & S_4 = \square\square_4 \, . \end{array} \quad (10.41)$$

The anomaly cancellation conditions for the three SU factors are

$$\begin{cases} N_2 + N_1 - N_5 - N_4 - 4 = 0 & SU(N_1) \\ N_5 + N_4 - N_2 - N_1 + 4 = 0 & SU(N_2) \\ N_5 - N_1 - N_2 + N_4 + 4 = 0 & SU(N_4) \end{cases} \ , \quad (10.42)$$

which is the unique condition

$$N_1 + N_2 - N_4 - N_5 - 4 = 0 \ . \quad (10.43)$$

SU(5) model

The constraint in Equation (10.43) allows to obtain an effective $SU(5)$ DSB model, as for the theory studied in the previous section, by choosing $N_5 = 1, N_1 = 5, N_2 = N_4 = 0$.[7]

[7] We note that there is also the configuration $N_4 = 1, N_1 = 5, N_2 = N_5 = 0$ that leads to a $SU(5)$ DSB model, with the extra decoupled singlet S_4. The analysis goes through

We can now proceed as for the orbifold $\mathbb{C}^3/\mathbb{Z}_{6'}$ and add to the aforementioned DSB brane configuration N regular D3-branes, which change the theory to $SO(N+1)\times SU(N+5)\times SU(N)\times SU(N)$ (with the corresponding matter and superpotential terms).

As already noticed, differently from the orbifold case, where the tree-level potential of the parent theory contains only cubic terms, and hence the anomalous dimensions of all fields are zero, in this model, we have both cubic and quartic terms, and so we have to take into account non-trivial anomalous dimensions. We can compute such anomalous dimensions in the parent theory. They are fixed by populating the dimer with regular branes and imposing vanishing β functions and R-charge equal 2 to all superpotential terms (in the present case this corresponds to $7+8=15$ equations).

The symmetries of the dimer help in simplifying the system one has to solve. In particular there exist three $\mathbb{Z}_2$ symmetries acting on faces as $2\leftrightarrow 3$, $1\leftrightarrow 7$ and $(4,1,2)\leftrightarrow(6,3,7)$, respectively. Using these symmetries the number of independent anomalous dimensions is just 5 which gives back only 4 independent equations one has to solve, implying in the end a solution with one unfixed modulus. This can be fixed by a-maximization [88] giving finally, for the fields in Equation (10.41), the following result

$$\begin{aligned}
&\gamma_{X_1}=2/5\,, \quad \gamma_{X_2}=2/5\,, \quad \gamma_{X_4}=-4/5\,,\\
&\gamma_{Y_1}=-4/5\,, \quad \gamma_{Y_2}=-4/5\,, \quad \gamma_{Z}=-4/5\,,\\
&\gamma_{A_1}=-4/5\,, \quad \gamma_{A_2}=-4/5\,, \quad \gamma_{S_4}=2/5\,.
\end{aligned} \tag{10.44}$$

The orientifold projection may provide $1/N$ corrections to these anomalous dimensions, as fractional branes similarly do. Here and in the following, we will consistently neglect both of them.

We can now proceed as in the previous example by adding N regular branes to the DSB system, higgsing and doing scale matching. The gauge coupling associated with face 1 above and below the scale v of the VEV of

very similarly. Further interchanging the roles of nodes 1 and 2 provides two more trivially equal examples.

the gauge-invariant operator $\Phi = \mathrm{Tr}(X_4 Y_2 Z X_1)$ runs as

$$\begin{aligned} g^{-2}_{SU(5+N)} &= \left[3(N+5) - \left(\tfrac{N+1}{2}\left(1-\tfrac{2}{5}\right) + \tfrac{N}{2}\left(1+\tfrac{4}{5}\right) + \tfrac{N}{2}\left(1+\tfrac{4}{5}\right) + \right.\right. \\ &\quad \left.\left. \tfrac{N+3}{2}\left(1+\tfrac{4}{5}\right)\right)\right] \ln\left(\tfrac{\mu}{\Lambda_{UV}}\right) = 12\ln\left(\tfrac{\mu}{\Lambda_{UV}}\right) , \\ g^{-2}_{SU(5)} &= \left[15 - \left(\tfrac{3}{10} + \tfrac{27}{10}\right)\right] \ln\left(\tfrac{\mu}{\Lambda}\right) = 12\ln\left(\tfrac{\mu}{\Lambda}\right) \ . \end{aligned} \tag{10.45}$$

Matching the scale at $\mu = v$ we get

$$\Lambda = \Lambda_{UV} \ . \tag{10.46}$$

Again, the matching of the two scales is exact, *i.e.* Λ does not depend on v.

Let us now investigate other possible decay channels. In the parent theory, a regular brane can be seen as a bound state of a $\mathcal{N} = 2$ brane associated with the strip $1-3-5$ and its complement, $2-4-6-7$. Upon orientifolding these two fractional branes become $1-5$ and $2-4$ strips, respectively. We can see that also in this theory, after the orientifold projection, the two types of $\mathcal{N} = 2$ fractional branes behave differently, one leading to a supersymmetric vacuum and the other triggering supersymmetry breaking into a runaway. The details are similar to the orbifold case, and we refrain to repeat the analysis here. The end result, after scale matching, is

$$\Lambda^{12} = \left(\frac{v'}{v}\right)^{\frac{9}{5}N} \Lambda^{12}_{UV} \ . \tag{10.47}$$

The dynamics is qualitatively the same as for the $\mathbb{C}^3/\mathbb{Z}_{6'}$ case. The theory enjoys a one-dimensional moduli space of supersymmetry preserving vacua at $v' = 0$, parameterized by v.

$3-2$ model

Also this orientifold admits a $3-2$ DSB model. Indeed, a different rank assignment which satisfies the anomaly cancellation condition is $N_5 = 1, N_1 = 3, N_2 = 2, N_4 = 0$ which gives a $SU(3) \times SU(2) \times SO(1)$ gauge theory with matter content

$$\begin{aligned} &X_1 = (\overline{\square}_1, \square_5) = \overline{D} \quad X_2 = (\square_5, \square_2) = L\,, \quad Z = (\overline{\square}_2, \square_1) = Q\,, \\ &A_1 = \begin{smallmatrix}\square\\\square\end{smallmatrix}_1 = \overline{U}\,, \qquad\qquad A_2 = \overline{\begin{smallmatrix}\square\\\square\end{smallmatrix}}_2 = S\,, \end{aligned} \tag{10.48}$$

where we used again that the two index antisymmetric representation of $SU(3)$ is equal to the antifundamental, and that the two index antisymmetric of $SU(2)$ is actually the singlet representation. The matter content is precisely the one of the $3-2$ model (up to a decoupled singlet S) and, from Equation (10.38), one can also see that the only term surviving in the superpotential is precisely

$$W = \overline{D}QL \ . \tag{10.49}$$

As for the $SU(5)$ model, the addition of regular branes does not destabilize the DSB vacuum. As before, however, the theory has $\mathcal{N} = 2$ fractional branes, which eventually do destabilize the vacuum, as in the orbifold case. In particular, it is possible to show, by scale matching, that the strong coupling scale which controls the DSB vacuum energy (Λ_3 of the $SU(3)$ factor or Λ_2 of the $SU(2)$ factor) is affected by the higgsing procedure and the vacuum energy relaxes to zero. The scale matchings give, in the two cases,

$$\Lambda_3^6 = \left(\frac{v'}{v}\right)^{\frac{9}{5}N} \Lambda_{UV}^6 \ , \qquad \Lambda_2^3 = \left(\frac{v}{v'}\right)^{\frac{6}{5}N} \Lambda_{UV}^3 \ , \tag{10.50}$$

which, again, shows that the vacuum is unstable, eventually.

The PdP_4 case is different from the previous orbifold case in that it has a natural warped throat UV completion. Indeed, it contains deformation fractional branes, so that the parent theory admits a cascade of Seiberg dualities. For instance, in the conformal case, $N_i = N$ for any i, it is straightforward to show that starting from node 1 and following the sequence $1 \to 2 \to 4 \to 5 \to 6 \to 7 \to 3$ we get back to the starting point. Then, if we add M (deformation) fractional branes on nodes $1-2-5$, we trigger a cascade. Performing the previous sequence six times, we find that the number of regular branes is diminished by seven times the number of fractional ones

$$\begin{array}{c} SU_1(N'+M) \times SU_2(N'+M) \times SU_3(N') \times SU_4(N') \\ \times SU_5(N'+M) \times SU_6(N') \times SU_7(N') \end{array} \tag{10.51}$$

where $N' = N - 7M$. Upon orientifolding,[8] the fractional brane configuration that could give rise to the one containing the $3-2$ model discussed above should in fact be

$$N_5 = 1 + 2M \quad N_1 = 3 + M \quad N_2 = 2 + M \quad N_4 = 0 \ , \tag{10.52}$$

which is indeed compatible with the anomaly condition in Equation (10.43). This can be seen in the parent theory as a bound state of M fractional branes

[8] See Chapter 7 for the subtleties of performing a duality cascade in an orientifolded theory.

$1-2-5$ and M fractional branes $3-5-7$, both of deformation type, one mirror of the other through the orientifold projection. Now, however, this superposition of deformation branes can be alternatively seen as being composed of two sets of $\mathcal{N}=2$ fractional branes, $1-3-5$ and $2-5-7$, whose Coulomb branch survives the orientifold projection. A straightforward repetition of the scale matchings previously discussed shows that even this different UV completion has a Coulomb branch instability, eventually.

10.4 Other supersymmetry breaking set-ups

In this section, we want to generalize the previous analysis and show that the DSB $SU(5)$ and $3-2$ models arise in a large class of CY orientifold singularities, either $\mathbb{C}^3$ orbifolds or Pseudo del Pezzo's, of which previous examples are prototypes. As we will see, in all these models the same instability channel displayed above emerges.

10.4.1 del Pezzo singularities

We start focusing on non-orbifold singularities, like the one discussed in Section 10.3 and limit ourselves to toric CYs whose dual gauge theories admit at most eight gauge factors. The complete list of corresponding toric diagrams and dimers can be found in [149], to which we refer for details.

Most of these singularities are obtained as blow-ups of del Pezzo singularities. Toric CY del Pezzo singularities are complex cones over del Pezzo surfaces dP_n with $n=0,\ldots,3$ [46]. By blowing up at smooth points of the del Pezzo one obtains larger CY singularities, dubbed Pseudo del Pezzo's, following the terminology of [129]. The blow-up corresponds to unhiggsing in the dual field theory.

Within this class, we list below those singularities which, after suitable orientifold projection, admit an anomaly-free rank assignment giving a $SU(5)$ or $3-2$ dynamical supersymmetry breaking model. The general procedure to obtain a consistent orientifold projection from a dimer is summarized in Chapter 7, whose conventions we follow.

For each singularity, we present the dimer, including the unit cell and the orientifold action. Orientifold charges are reported as a string of plus and minus signs with the following conventions. For point reflection, by starting from the bottom left corner of the unit cell and going clockwise. For lines, the first sign is for the central line and the second for the one on the edge of the fundamental cell. We also present the gauge group and the

	$SU(5)$ model	$3-2$ model
PdP_{3c}	○	○
PdP_{3b} (lines)	○	×
PdP_{3b}(points)	○	×
PdP_{4b}	○	○
PdP_5	○	×
PdP_{5b}	○	×
$PdP_{5'a}$	○	×
$PdP_{5'b}$	○	×

Table 10.1: DSB models in del Pezzo singularities.

matter content of the orientifolded theory, the anomaly cancellation conditions (ACC) for the SU gauge factors, and the rank assignment leading to interesting DSB configurations (as far as the $3-2$ model, it is understood that also the correct cubic superpotential term is reproduced). Finally, for each singularity, we indicate the Coulomb branch directions whose quantum dynamics we have analyzed, following the two-steps higgsing pattern discussed in previous sections. For the sake of clarity, these are indicated in terms of the faces of the dimer after the orientifold action has been taken into account. Our results are summarized in Table 10.1.

- PdP_{3c} $(+-+-)$

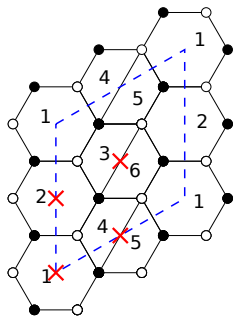

Figure 10.6: PdP_{3c} dimer with orientifold points.

– Gauge group:

$$SO(N_1) \times USp(N_2) \times SU(N_3) \times SU(N_4) \tag{10.53}$$

– Matter content:

$$\begin{aligned} &X_1 = (\square_1\ ,\overline{\square}_3)\ , \quad X_2 = (\square_3,\square_2)\ , \quad Z = (\square_3,\square_4)\,, \\ &Y_1 = (\square_4,\square_1)\ , \quad Y_2 = (\square_2,\overline{\square}_4)\ , \quad V = (\square_2,\square_1)\ , \\ &\overline{A}_4 = \begin{array}{|c|}\hline\square\\\hline\square\\\hline\end{array}_4\ , \qquad \overline{S}_3 = \overline{\square\square}_3\ . \end{aligned} \tag{10.54}$$

– ACC:

$$\begin{cases} N_4 - N_1 + N_2 - N_3 - 4 = 0 & SU(N_3) \text{ and } SU(N_4) \end{cases} \tag{10.55}$$

– DSB configurations:

* $SU(5)$ model: $N_1 = 1$, $N_4 = 5$; $N_3 = 1$, $N_4 = 5$ gives an additional singlet, $\overline{S}_3$.
* $3-2$ model: $N_1 = 1$, $N_2 = 2$ and $N_4 = 3$.

– Coulomb branch directions:

$$1-4\ , \quad 2-3\,. \tag{10.56}$$

- PdP_{3b} $(+-)$

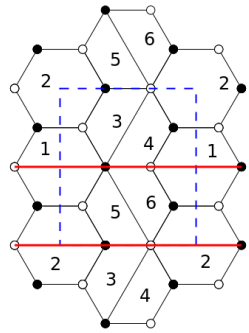

Figure 10.7: PdP_{3b} dimer with orientifold lines.

– Gauge group:

$$SO(N_1) \times USp(N_2) \times SU(N_3) \times SU(N_4) \tag{10.57}$$

– Matter content:

$$\begin{aligned} &Z = (\square_1,\square_2)\,, \quad X_1 = (\square_1,\square_3)\,, \quad X_2 = (\overline{\square}_3,\square_2)\,, \\ &V = (\overline{\square}_3,\square_4)\,, \quad Y_2 = (\overline{\square}_4,\square_2)\,, \quad Y_1 = (\square_1,\square_4)\,, \\ &\overline{S}_4 = \overline{\square\square}_4\,, \qquad A_3 = \begin{array}{|c|}\hline\square\\\hline\square\\\hline\end{array}_3\,. \end{aligned} \tag{10.58}$$

– ACC:

$$\Big\{ N_1 - N_2 + N_3 - N_4 - 4 = 0 \qquad SU(N_3)\ , SU(N_4) \tag{10.59}$$

– DSB configurations:

∗ $SU(5)$ model: $N_3 = 5$ and $N_4 = 1$. This model has an extra singlet due to the symmetric tensor of $SU(N_4)$, $\overline{S}_4$.[9]

– Coulomb branch directions:

$$3 - 4\ , \quad 1 - 2\,. \tag{10.60}$$

Note that this is the only example we found of a *line* orientifold admitting an anomaly-free rank assignment leading to a DSB configuration.

- PdP_{3b} $(+-+-)$

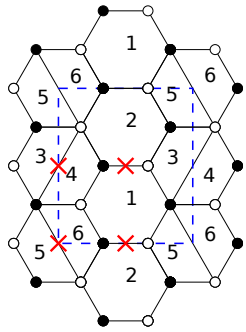

Figure 10.8: PdP_{3b} dimer with orientifold points.

– Gauge group:

$$SU(N_1) \times SU(N_3) \times SU(N_5) \tag{10.61}$$

– Matter content:

$$\begin{array}{lll} Z = (\overline{\square}_5, \square_3), & X_1 = (\overline{\square}_1, \square_3), & X_2 = (\square_1, \square_5) \\ Y_1 = (\overline{\square}_3, \overline{\square}_1), & Y_2 = (\overline{\square}_5, \square_1), & \\ \overline{S}_1 = \overline{\square\square}_1, & A_1 = \begin{smallmatrix}\square\\\square\end{smallmatrix}_1, & \\ S_5 = \square\square_5, & \overline{A}_3 = \begin{smallmatrix}\overline{\square}\\\overline{\square}\end{smallmatrix}_3. & \end{array} \tag{10.62}$$

[9] $N_3 = 5$ and $N_2 = 1$ is not a valid configuration since N_2, being related to a USp group, has to be even.

– ACC:

$$\Big\{ N_3 - N_5 - 4 = 0 \qquad SU(N_1),\, SU(N_3),\, SU(N_5) \tag{10.63}$$

– DSB configurations:

∗ $SU(5)$ model: $N_3 = 5$ and $N_5 = 1$. This model has an extra singlet due to the symmetric tensor of $SU(N_5)$, S_5.

– Coulomb branch directions:

$$3 - 5\,, \quad 1\,. \tag{10.64}$$

- PdP_{4b} $(--++)$

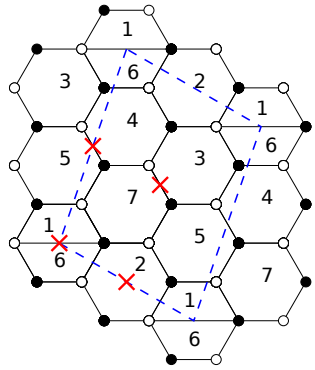

Figure 10.9: PdP_{4b} dimer with orientifold points.

– Gauge group:

$$SU(N_1) \times SO(N_2) \times SU(N_3) \times SU(N_4) \tag{10.65}$$

– Matter content:

$$\begin{array}{lll} X_1 = (\square_2, \square_1)\,, & X_3 = (\square_2, \square_3)\,, & X_4 = (\overline{\square}_4, \square_2)\,, \\ Y_1 = (\overline{\square}_3, \square_1)\,, & Y_2 = (\overline{\square}_1, \square_4)\,, & Z_1 = (\overline{\square}_3, \square_4)\,, \\ Z_2 = (\overline{\square}_4, \square_3)\,, & Z_3 = (\overline{\square}_4, \overline{\square}_3) & \\ \overline{A}_1 = \overline{\square\!\square}_1\,, & S_3 = \square\!\square_3\,, & A_4 = \square\!\square_4\,. \end{array} \tag{10.66}$$

– ACC:

$$\Big\{ N_1 - N_2 - N_3 + N_4 - 4 = 0 \qquad SU(N_1),\, SU(N_3),\, SU(N_4) \tag{10.67}$$

– DSB configurations:

* $SU(5)$ model I: $N_1 = 5$ and $N_2 = 1$; equivalently $N_4 = 5$ and $N_2 = 1$.
* $SU(5)$ model II: $N_1 = 5$ and $N_3 = 1$. This model has an extra singlet due to the symmetric tensor of $SU(N_3)$, S_3.
* $3-2$ model: $N_1 = 3$, $N_2 = 1$ and $N_4 = 2$. There is again an extra singlet due to the antisymmetric tensor of $SU(N_4)$, A_4. The roles of nodes 1 and 4 can be interchanged, providing another equivalent model.

– Coulomb branch directions:

$$1-2\,,\quad 3-4\,. \tag{10.68}$$

- PdP_5 $(-,+,+,-)$

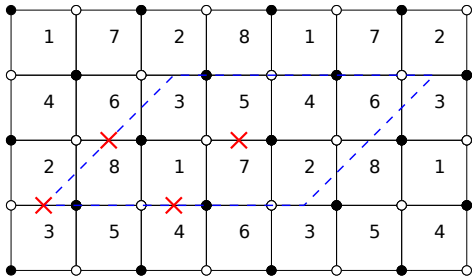

Figure 10.10: $PdP5$ dimer with orientifold points.

– Gauge group:

$$SU(N_1) \times SU(N_2) \times SU(N_5) \times SU(N_6) \tag{10.69}$$

– Matter content:

$$\begin{array}{lll} X_1 = (\overline{\square}_1, \overline{\square}_5)\,, & X_2 = (\square_5, \square_6)\,, & X_3 = (\overline{\square}_1, \overline{\square}_6)\,, \\ X_4 = (\square_2, \square_1)\,, & X_5 = (\overline{\square}_2, \overline{\square}_5)\,, & X_6 = (\overline{\square}_2, \overline{\square}_6)\,, \\ A_2 = \begin{smallmatrix}\square\\\square\end{smallmatrix}_2\,, & S_6 = \square\square_6\,, & S_5 = \square\square_5\,, \\ & A_1 = \begin{smallmatrix}\square\\\square\end{smallmatrix}_1\,. & \end{array} \tag{10.70}$$

– ACC:

$$\begin{cases} N_1 + N_2 - N_5 - N_6 - 4 = 0 & SU(N_1),\ SU(N_2), \\ & SU(N_5),\ SU(N_6) \end{cases} \tag{10.71}$$

– DSB configurations:

* $SU(5)$ models: $N_1 = 5$ or $N_2 = 5$ and $N_5 = 1$ or $N_6 = 1$. In all configurations there is an additional singlet arising from the symmetric representation at nodes 5 or 6.

Note that in this model it is straightforward to exclude the existence of a $3-2$ model, since the superpotential is purely quartic.

– Coulomb branch directions:

$$1-5\,,\quad 2-6\,. \tag{10.72}$$

As a side remark, note that $PdP5$ is actually an orbifold of the conifold, hence it inherits some of its features, such as all anomalous dimensions being equal to $\gamma = -1/2$. This makes the scale matching simpler to check.

- PdP_{5b} $(+--+)$

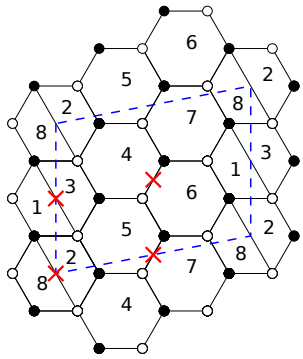

Figure 10.11: $PdP5_b$ dimer with orientifold points.

– Gauge group:

$$SU(N_1) \times SU(N_2) \times SU(N_4) \times SU(N_5) \tag{10.73}$$

– Matter content:

$$\begin{array}{lll} X_1 = (\overline{\square}_1, \square_2)\,, & X_2 = (\square_1, \square_4)\,, & X_3 = (\overline{\square}_1, \overline{\square}_5)\,, \\ Y_1 = (\overline{\square}_4, \square_2)\,, & Y_2 = (\overline{\square}_2, \square_5)\,, & Z_1 = (\overline{\square}_4, \square_5)\,, \\ Z_2 = (\overline{\square}_5, \square_4)\,, & Z_3 = (\overline{\square}_4, \overline{\square}_5)\,, & A_1 = \begin{smallmatrix}\square\\\square\end{smallmatrix}_1\,, \\ S_5 = \square\square_5\,, & \overline{S}_2 = \overline{\square\square}_2\,, & A_4 = \begin{smallmatrix}\square\\\square\end{smallmatrix}_4\,. \end{array} \tag{10.74}$$

– ACC:

$$\begin{cases} N_1 - N_2 - N_5 + N_4 - 4 = 0 & SU(N_1),\ SU(N_2), \\ & SU(N_4),\ SU(N_5) \end{cases} \tag{10.75}$$

– DSB configurations:
  * $SU(5)$ models: $N_1 = 5$ and $N_2 = 1$, or $N_1 = 5$ and $N_5 = 1$, or $N_4 = 5$ and $N_2 = 1$. They all include a singlet related to the symmetric of the $SU(1)$ node.
– Coulomb branch directions:

$$1 - 2\,, \quad 4 - 5\,. \tag{10.76}$$

This exhausts Pseudo del Pezzo's properly defined. Below we consider two more models in the list reported in [149] (corresponding to the toric diagrams 15 and 16 of their table 6, respectively).

- $PdP_{5'a}$ $(-++-)$

  This singularity can be obtained by unhiggsing PdP_{3c}.

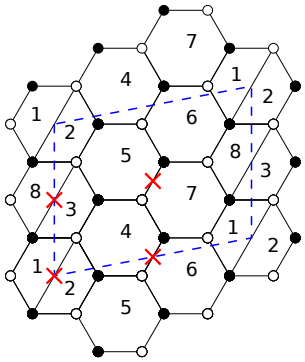

Figure 10.12: $PdP5'_a$ dimer with orientifold points.

– Gauge group:

$$SU(N_1) \times SU(N_3) \times SU(N_4) \times SU(N_5) \tag{10.77}$$

– Matter content:

$$\begin{array}{lll} X_1 = (\overline{\square}_3, \square_1)\,, & X_2 = (\square_4, \square_1)\,, & X_3 = (\overline{\square}_5, \overline{\square}_1)\,, \\ Y_1 = (\overline{\square}_3, \square_5)\,, & Y_2 = (\overline{\square}_4, \square_3)\,, & Z_1 = (\overline{\square}_5, \square_4)\,, \\ Z_2 = (\overline{\square}_4, \overline{\square}_5)\,, & Z_3 = (\overline{\square}_4, \square_5)\,, & \overline{A}_1 = \overline{\square\!\square}_1\,, \\ S_5 = \square\!\square_5\,, & S_3 = \square\!\square_3\,, & A_4 = \square\!\square_4\,. \end{array} \tag{10.78}$$

– ACC:

$$\begin{cases} N_1 - N_3 - N_4 + N_5 - 4 = 0 & SU(N_1),\, SU(N_3) \\ N_1 - N_3 + N_4 - N_5 - 4 = 0 & SU(N_4),\, SU(N_5) \end{cases} \tag{10.79}$$

leading to $N_1 = N_3 + 4$, $N_4 = N_5$.

– DSB configurations:

  * $SU(5)$ model: $N_1 = 5$ and $N_3 = 1$. There is an additional singlet given by S_3.

– Coulomb branch directions:

$$1-3\,,\quad 4-5\,. \tag{10.80}$$

- $PdP_{5'b}$ $(-+-+)$

  This singularity is again an unhiggsing of PdP_{3c}.

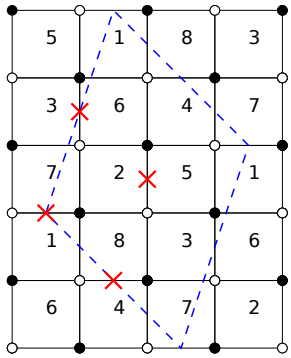

Figure 10.13: $PdP5'_b$ dimer with orientifold points.

– Gauge group:

$$SU(N_1)\times SU(N_2)\times SU(N_3)\times SU(N_4) \tag{10.81}$$

– Matter content:

$$\begin{array}{lll} X_1=(\square_1,\square_2)\,, & X_2=(\square_4,\square_1)\,, & X_3=(\overline{\square}_1,\overline{\square}_3)\,,\\ Y_1=(\overline{\square}_2,\overline{\square}_3)\,, & Y_2=(\overline{\square}_4,\overline{\square}_2)\,, & Z=(\square_4,\square_3)\,,\\ \overline{A}_1=\overline{\square\!\square}_1\,, & A_2=\square\!\square_2\,, & S_3=\square\!\square_3\,,\\ & \overline{S}_4=\overline{\square\!\square}_4\,. & \end{array} \tag{10.82}$$

– ACC:

$$\begin{cases} N_1-N_2+N_3-N_4-4=0 & SU(N_1),\,SU(N_4)\\ N_1+N_2-N_3-N_4-4=0 & SU(N_2),\,SU(N_3) \end{cases} \tag{10.83}$$

leading to $N_1 = N_4 + 4$, $N_2 = N_3$.

– DSB configurations:

* $SU(5)$ model: $N_1 = 5$ and $N_4 = 1$. We have again the additional singlet $\overline{S}_4$.

– Coulomb branch directions:

$$1 - 4\,, \quad 2 - 3\,. \tag{10.84}$$

One can continue the unhiggsing process and look for more and more singularities admitting fractional brane configurations described by $SU(5)$ or $3-2$ DSB models at low energy. The procedure is easy to understand from the point of view of toric diagrams and we refer the interested reader to [149].

The above analysis shows that the DSB $SU(5)$ and the $3-2$ models are not specific to the PdP_4 example discussed in section 10.3 but actually arise in a large (in principle infinite, see above comment) class of (blown up) del Pezzo singularities, sensibly enlarging the landscape of D-brane configurations enjoying a stable DSB vacuum at low energy.

Similarly to the PdP_4 case, one can then ask what is the fate of these vacua in a large N completion. As anticipated, one can show that the Coulomb branch directions we have indicated and that all these singularities possess, become runaway at the quantum level, and the true vacua are in fact supersymmetric.

10.4.2 Orbifolds of flat space

In this subsection, we want to generalize the analysis of Section 10.2 and present other instances of (orientifolds of) $\mathbb{C}^3$ orbifold singularities displaying DSB models. The corresponding dimers can be obtained from the hexagonal tiling of $\mathbb{C}^3$ with algorithms that can be found in [199]. We report below a scan of both $\mathbb{C}^3/\mathbb{Z}_n$ and $\mathbb{C}^3/\mathbb{Z}_p \times \mathbb{Z}_q$ orbifolds.

Orbifolds $\mathbb{C}^3/\mathbb{Z}_n$

Following the same logic of the $\mathbb{C}^3/\mathbb{Z}_{6'}$ case, we extended our analysis to higher orders of the cyclic group $\mathbb{Z}_n$. DSB models can again be found for some orientifold projections. Interestingly, no DSB models were found for n odd. We summarize our scan for n as large as 30 in Table 10.2.

In the above table, a triplet (a, b, c) refers to an orbifold action defined as

$$g \;:\; z_i \to e^{2\pi i w_i} z_i \tag{10.85}$$

	Action on $\mathbb{C}_3$	$SU(5)$ model	$3-2$ model
$\mathbb{Z}_8$	(1,2,5)	$\circ$	$\times$
$\mathbb{Z}_{12}$	(1,4,7)	$\circ$	$\times$
$\mathbb{Z}_{30}$	(1,10,19)	$\circ$	$\times$

Table 10.2: DSB models in orbifolds of flat space $\mathbb{C}^3/\mathbb{Z}_n$.

with $w = (a, b, c)/n$, where $a+b+c = 0 \bmod n$. It turns out that a necessary condition for allowing interesting DSB models is to focus on orientifold point reflection with two points on top a face. This has the effect of giving an orientifoled theory with two SO/USp gauge factors and $(n-2)/2$ SU factors as

$$SO/USp \times SU \times \cdots \times SU \times SO/USp \ . \tag{10.86}$$

Let us summarize the specific features of each case.

- $\mathbb{C}^3/\mathbb{Z}_8$ $(+\,-\,+-)$

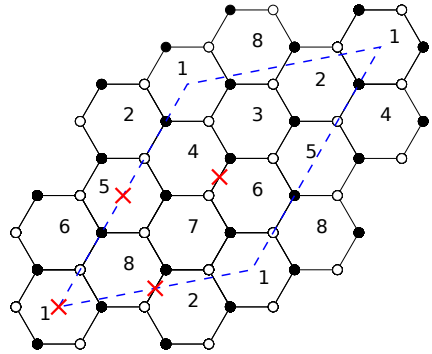

Figure 10.14: $\mathbb{C}^3/\mathbb{Z}_8$ dimer with orientifold points.

  - Gauge group:

$$SO(N_1) \times SU(N_2) \times SU(N_3) \times SU(N_4) \times USp(N_5) \tag{10.87}$$

  - Matter content:

$$\begin{array}{lll} (\Box_1, \overline{\Box}_2)\,, & (\Box_1, \overline{\Box}_3)\,, & (\Box_1, \Box_4)\,, \\ (\Box_2, \overline{\Box}_3)\,, & (\Box_2, \overline{\Box}_4)\,, & (\overline{\Box}_2, \Box_5)\,, \\ (\Box_2, \Box_3)\,, & (\Box_3, \overline{\Box}_4)\,, & (\Box_3, \Box_5)\,, \\ (\overline{\Box}_3, \overline{\Box}_4)\,, & (\Box_4, \Box_5)\,, & \overline{\Box}\\ & \Box\Box_4\,. & \Box_2\,, \end{array} \tag{10.88}$$

– ACC:

$$\begin{cases} N_1 + N_2 - 2N_3 - N_4 + N_5 - 4 = 0 & SU(N_2) \\ N_1 - N_5 = 0 & SU(N_3) \\ N_1 - N_2 - 2N_3 + N_4 + N_5 + 4 = 0 & SU(N_4) \end{cases} \tag{10.89}$$

leading to $N_2 = N_4 + 4$, $N_1 = N_3 = N_5$.

– DSB configurations:

∗ $SU(5)$ model: $N_2 = 5$ and $N_4 = 1$, with an additional singlet at node 4.

– Coulomb branch directions:

$$2 - 4\,, \quad 1 - 3 - 5\,. \tag{10.90}$$

- $\mathbb{C}^3/\mathbb{Z}_{12}$ $(-+-+)$

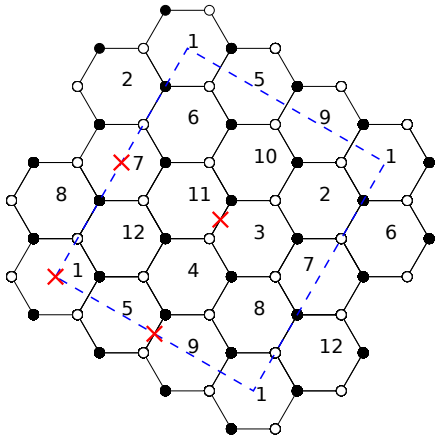

Figure 10.15: $\mathbb{C}^3/\mathbb{Z}_{12}$ dimer with orientifold points.

– Gauge group:

$$\begin{aligned} &USp(N_1) \times SU(N_2) \times SU(N_3) \times SU(N_4) \\ &\times SU(N_5) \times SU(N_6) \times SO(N_7) \end{aligned} \tag{10.91}$$

– Matter content:

$$\begin{array}{llll} (\square_1, \square_2), & (\square_1, \square_5), & (\square_1, \overline{\square}_6), & (\square_2, \square_4) \\ (\overline{\square}_2, \overline{\square}_5), & (\square_2, \square_7), & (\overline{\square}_2, \square_6), & (\overline{\square}_2, \square_3) \\ (\overline{\square}_3, \overline{\square}_4), & (\square_3, \square_6), & (\overline{\square}_3, \square_7), & (\overline{\square}_3, \square_4) \\ (\square_4, \square_5), & (\overline{\square}_4, \overline{\square}_6), & (\overline{\square}_4, \square_5), & (\overline{\square}_5, \square_6) \\ (\overline{\square}_6, \square_7), & \begin{array}{l}\square\\\square\end{array}_3, & \overline{\square\square}_5. & \end{array} \tag{10.92}$$

– ACC:

$$\begin{cases} N_1 + N_4 - N_5 + N_7 - N_6 - N_3 = 0 & SU(N_2) \\ N_2 - 2N_4 + N_6 - N_7 + N_3 - 4 = 0 & SU(N_3) \\ N_2 - N_6 = 0 & SU(N_4) \\ N_1 - N_2 + 2N_4 - N_6 - N_5 - 4 = 0 & SU(N_5) \\ N_1 - N_2 - N_3 + N_4 - N_5 + N_7 = 0 & SU(N_6) \end{cases} \tag{10.93}$$

leading to $N_2 = N_4 = N_6$, $N_1 = N_5 + 4$, $N_3 = N_7 + 4$.

– DSB configurations:

∗ $SU(5)$ model: $N_3 = 5$, $N_7 = 1$ and $N_1 = 4$. This is actually an anomaly-free $SU(5) \times USp(4)$ gauge theory, with matter charged under the $SU(5)$ factor only. The $USp(4)$ pure SYM condenses leaving exactly the non-calculable $SU(5)$ DSB model at low energy.

– Coulomb branch directions:

$$3 - 7\ , \quad 1 - 5\ , \quad 2 - 4 - 6\,. \tag{10.94}$$

- $\mathbb{C}^3/\mathbb{Z}_{30}$

Due to the large order of this orbifold, we will refrain from listing all its characteristics (and displaying the dimer) but just comment on the outcome.

Upon orientifolding, the gauge group reduces to sixteen gauge groups and the ACC allows for the following choice of non-vanishing ranks

$$SO(1)_1 \times SU(5)_2 \times SU(4)_3 \times SU(4)_4 \times SU(4)_5 \times USp(4)_6\ , \tag{10.95}$$

with matter content

$$\begin{aligned} &Q = (\square_1, \overline{\square}_2), \qquad X = (\overline{\square}_4, \square_3), \qquad Y = (\square_5, \square_4), \\ &Z = (\overline{\square}_3, \overline{\square}_5), \qquad A = \begin{smallmatrix}\square\\\square\end{smallmatrix}_2\ , \end{aligned} \tag{10.96}$$

and tree level superpotential

$$W = YXZ\ . \tag{10.97}$$

Each $SU(4)$ factor has four flavors and they all condense on the baryonic branch. Supposing that, say, $SU(4)_3$ condenses first, the superpotential becomes a mass term for the meson $M = XZ$ and the field Y, which can then be integrated out. The remaining two $SU(4)$s become pure SYM at low energy and condense, too, leaving again a DSB $SU(5)$ model at low energy.

	Action on $\mathbb{C}_3$	$SU(5)$ model	3-2 model
$\mathbb{Z}_2 \times \mathbb{Z}_4$	[(0,1,1),(1,0,3)]	$\circ$	$\times$
$\mathbb{Z}_3 \times \mathbb{Z}_3$	[(0,1,2),(1,0,2)]	$\circ$	$\circ$
$\mathbb{Z}_2 \times \mathbb{Z}_6$	[(0,1,1),(1,0,5)]	$\circ\circ$	$\times$

Table 10.3: DSB models in orbifolds of flat space $\mathbb{C}^3/\mathbb{Z}_p \times \mathbb{Z}_q$.

The analysis for orbifolds of orders higher than 30 is more complicated, hence we stop our scan at this level. We just mention that, for instance, a $\mathbb{Z}_{40}$ orbifold seems to possess an $SU(5)$ DSB model configuration, though it comes together with a decoupled sector involving 6 more gauge groups. A preliminary analysis suggests that the extra sector eventually confines in a supersymmetric vacuum, but a detailed analysis is clearly beyond the scope of the present scan.

All the above examples have also the usual Coulomb branch instability that destabilizes the DSB vacua. Being orientifolds of orbifolds, all anomalous dimensions vanish and it is a simple exercise to check that the scale matchings lead to a dependency on the VEVs in the DSB vacuum energy.

Orbifolds $\mathbb{C}^3/\mathbb{Z}_p \times \mathbb{Z}_q$

One may also consider the product of cyclic groups, *i.e.* the $\mathbb{Z}_p \times \mathbb{Z}_q$ orbifold action. Also within this class, at least within our scan, one can find DSB $SU(5)$ models as well as $3-2$ models. The end results, for some of the cases we have analysed, are summarized in Table 10.3.

Starting from $\mathbb{C}^3$, the orbifold action is now defined by two triplets, corresponding to $\mathbb{Z}_p$ and $\mathbb{Z}_q$ actions, respectively, both defined as (10.85). Similarly, following the conventions of [199], to which we refer for details, faces in the dimer have a double-index notation associated with the two independent orbifold actions.

From the dimer, one can look for suitable orientifold projections and DSB anomaly-free rank assignments. Again, in all cases, a Coulomb branch runaway direction is present as soon as one tries to embed the D-brane configurations in a large N theory.

In the following, we list the properties of each case.

- $\mathbb{C}^3/\mathbb{Z}_2 \times \mathbb{Z}_4$ $(-+-+)$

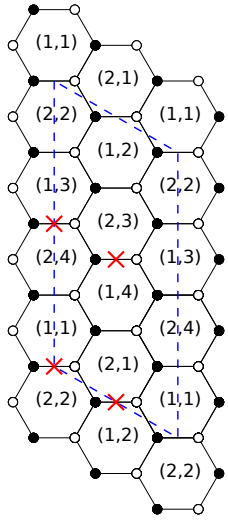

Figure 10.16: $\mathbb{C}^3/\mathbb{Z}_2 \times \mathbb{Z}_4$ dimer with orientifold points.

We denote the surviving faces by $i \equiv (1, i)$ with $i = 1 \ldots 4$.

– Gauge group:

$$SU(N_1) \times SU(N_2) \times SU(N_3) \times SU(N_4) \tag{10.98}$$

– Matter content:

$$\begin{array}{cccc} (\square_1, \overline{\square}_2)\,, & (\square_1, \square_3)\,, & (\overline{\square}_1, \square_4)\,, & (\square_1, \square_2)\,, \\ (\overline{\square}_1, \overline{\square}_2)\,, & (\square_2, \overline{\square}_3)\,, & (\overline{\square}_2, \overline{\square}_4)\,, & (\square_3, \overline{\square}_4)\,, \\ & (\square_3, \square_4)\,, & (\overline{\square}_3, \overline{\square}_4)\,, & \\ \begin{array}{|c|}\hline \\ \hline \end{array}_1\,, & \square\square_2\,, & \overline{\square\square}_3\,, & \begin{array}{|c|}\hline \\ \hline \end{array}_4\,. \end{array} \tag{10.99}$$

– ACC:

$$\begin{cases} N_1 + N_4 - N_2 - N_3 - 4 = 0 \end{cases} \qquad \begin{array}{l} SU(N_1),\, SU(N_2), \\ SU(N_3),\, SU(N_4) \end{array} \tag{10.100}$$

– DSB configurations:

  * $SU(5)$ model: $N_1 = 5$ and $N_3 = 1$, or $N_4 = 5$ and $N_2 = 1$. Both models have an additional singlet at nodes 3 or 2, respectively.

– Coulomb branch directions:

$$1 - 3\,, \quad 2 - 4\,. \tag{10.101}$$

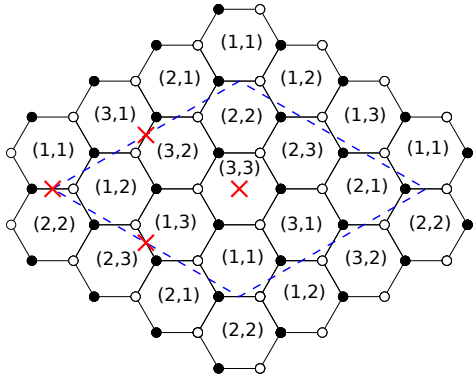

Figure 10.17: $\mathbb{C}^3/\mathbb{Z}_3 \times \mathbb{Z}_3$ dimer with orientifold points.

- $\mathbb{C}^3/\mathbb{Z}_3 \times \mathbb{Z}_3$ $(--+-)$

  We denote the surviving faces as follows

$$\begin{aligned} &1 \equiv (1,1) \leftrightarrow (2,2) && 2 \equiv (1,2) \leftrightarrow (2,1) \\ &3 \equiv (1,3) \leftrightarrow (2,3) && 4 \equiv (3,1) \leftrightarrow (3,2) \\ &&& 5 \equiv (3,3) \end{aligned} \tag{10.102}$$

  – Gauge group:

$$SU(N_1) \times SU(N_2) \times SU(N_3) \times SU(N_4) \times SO(N_5) \tag{10.103}$$

  – Matter content:

$$\begin{array}{llll} (\square_1, \square_2)\,, & (\square_1, \overline{\square}_5)\,, & (\overline{\square}_1, \square_4)\,, & (\overline{\square}_1, \square_3)\,, \\ (\square_1, \overline{\square}_2)\,, & (\overline{\square}_2, \overline{\square}_3)\,, & (\overline{\square}_2, \overline{\square}_4)\,, & (\square_2, \overline{\square}_4)\,, \\ (\square_2, \overline{\square}_3)\,, & (\square_3, \square_4)\,, & (\overline{\square}_3, \square_5)\,, & (\overline{\square}_4, \square_5)\,, \\ \overline{\begin{array}{c}\square\\\square\end{array}}_1\,, & \begin{array}{c}\square\\\square\end{array}_3\,, & \begin{array}{c}\square\\\square\end{array}_4\,. & \end{array} \tag{10.104}$$

  – ACC:

$$\begin{cases} N_1 - 2N_2 + N_3 + N_4 - N_5 - 4 = 0 \end{cases} \qquad \begin{array}{c} SU(N_1),\, SU(N_3), \\ SU(N_4) \end{array} \tag{10.105}$$

  while the ACC on $SU(N_2)$ is trivially satisfied.

  – DSB configurations:

    * $SU(5)$ models: $N_5 = 1$ and either $N_1 = 5$, $N_3 = 5$ or $N_4 = 5$.
    * 3-2 models: $N_1 = 3$, $N_3 = 2$ and $N_5 = 1$, and any other permutation of nodes 1, 3 and 4. There is an additional decoupled singlet related to the antisymmetric at the $SU(2)$ node.

– Coulomb branch directions:

$$1-5\,,\quad 2-3-4\,. \tag{10.106}$$

- $\mathbb{C}^3/\mathbb{Z}_2\times\mathbb{Z}_6$ $(--++)$

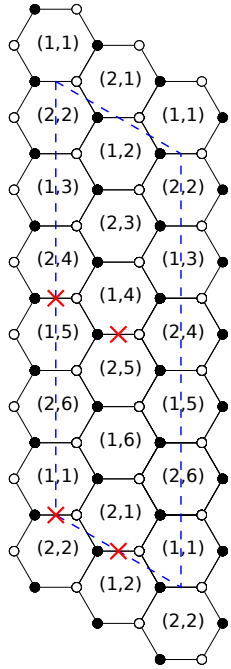

Figure 10.18: The dimer of the orbifold $\mathbb{C}^3/\mathbb{Z}_2\times\mathbb{Z}_6$ with orientifold points.

Upon the following face identifications

$$\begin{aligned} &1\equiv(1,1)\leftrightarrow(2,2) && 2\equiv(1,3)\leftrightarrow(2,6)\\ &3\equiv(1,5)\leftrightarrow(2,4) && 4\equiv(1,2)\leftrightarrow(2,1)\\ &5\equiv(1,6)\leftrightarrow(2,3) && 6\equiv(1,4)\leftrightarrow(2,5) \end{aligned} \tag{10.107}$$

the gauge group is $\prod_i^6 SU(N_i)$ with matter in the following representations

$$\begin{array}{llll} (\Box_1,\Box_2)\,, & (\overline{\Box}_2,\overline{\Box}_3)\,, & (\overline{\Box}_4,\overline{\Box}_5)\,, & (\Box_6,\Box_5)\,,\\ (\overline{\Box}_1,\Box_5)\,, & (\overline{\Box}_5,\Box_3)\,, & (\overline{\Box}_3,\Box_6)\,, & (\overline{\Box}_6,\Box_2)\,,\\ (\overline{\Box}_2,\Box_4)\,, & (\overline{\Box}_4,\Box_1)\,, & (\Box_1,\Box_4)\,, & (\overline{\Box}_1,\overline{\Box}_4)\,,\\ (\Box_2,\Box_5)\,, & (\overline{\Box}_2,\overline{\Box}_5)\,, & (\Box_3,\Box_6)\,, & (\overline{\Box}_3,\overline{\Box}_6)\,,\\ \begin{array}{c}\overline{\Box}\\ \overline{\Box}\end{array}_1\,, & \begin{array}{c}\Box\\ \Box\end{array}_3\,, & \Box\Box_4\,, & \overline{\Box\Box}_6\,. \end{array} \tag{10.108}$$

The ACC read

$$\begin{cases} N_2 - N_5 + N_4 - N_1 + 4 = 0 & SU(N_1) \text{ and } SU(N_4) \\ N_2 - N_5 + N_6 - N_3 + 4 = 0 & SU(N_3) \text{ and } SU(N_6) \\ N_1 - N_3 - N_4 + N_6 = 0 & SU(N_2) \text{ and } SU(N_5) \end{cases} \quad (10.109)$$

The solution to the ACC allows for a choice of ranks leaving a non-anomalous theory with gauge group

$$SU(5)_1 \times SU(1)_2 \times SU(5)_3 \quad (10.110)$$

and matter content given by

$$X = (\square_1, \square_3)\,, \quad A_1 = \overline{\square}_1\,, \quad Y = (\overline{\square}_2, \overline{\square}_3)\,, \quad A_2 = \square_2\,. \quad (10.111)$$

We then end up with two decoupled $SU(5)$ DSB models. Since we now have two independent contributions to the vacuum energy, one could think that the different higgsing scales can conspire in a non-trivial way, possibly leading to a non-zero minimum.

Again, higgsing by regular branes does not destabilize the supersymmetry breaking vacua. Performing the following (three steps, now) $\mathcal{N} = 2$ brane higgsing pattern

$$\begin{aligned} SU(5+N)_1 \times SU(1+N)_2 \times SU(5+N)_3 & \\ \times SU(N)_4 \times SU(N)_5 \times SU(N)_6 & \\ \xrightarrow{v} SU(5)_1 \times SU(1+N)_2 \times SU(5+N)_3 \times SU(N)_5 \times SU(N)_6 & \\ \xrightarrow{v'} SU(5)_1 \times SU(1+N)_2 \times SU(5)_3 \times SU(N)_5 & \\ \xrightarrow{v''} SU(5)_1 \times SU(1)_2 \times SU(5)_3 & \end{aligned} \quad , \quad (10.112)$$

we get instead the following scale matching

$$\Lambda^{13}_{1,\mathrm{IR}} = \left(\frac{v''}{v}\right)^N \Lambda^{13}_{1,\mathrm{UV}} \quad \text{and} \quad \Lambda^{13}_{3,\mathrm{IR}} = \left(\frac{v''}{v'}\right)^N \Lambda^{13}_{3,\mathrm{UV}}\,, \quad (10.113)$$

for the two $SU(5)$ factors, respectively. The potential hence scales as

$$V \sim \left|\left(\frac{v''}{v}\right)^{N/13} \Lambda_{1,\mathrm{UV}}\right|^4 + \left|\left(\frac{v''}{v'}\right)^{N/13} \Lambda_{3,\mathrm{UV}}\right|^4\,. \quad (10.114)$$

When trying to minimize the potential with respect to v, v' and v'', the minimum is reached at $v'' = 0$, and it is a supersymmetry preserving one. In other words, there is no compensation between the two factors in the potential, as one could have in principle hoped for.

This ends the list of examples we wanted to present. As anticipated, in all orbifold models we have discussed, similarly to the models of Section 10.4.1, the supersymmetry breaking vacua are destabilized once one tries to embed the DSB configurations in a large N theory. As one can easily check, the mechanism is again the same: while regular branes correspond to exact flat directions, $\mathcal{N} = 2$ fractional brane directions become runaway once the dependence of the vacuum energy on the Coulomb branch modulus is taken into account.

10.5 A no-go theorem and how to avoid it

In previous sections, we presented several models which allow for brane configurations giving DSB vacua, both at orbifold and del Pezzo-like singularities. However, when properly UV-complete, all models include runaway directions, associated with $\mathcal{N} = 2$ fractional branes, which destabilize the non-supersymmetric minima. One might wonder whether it is possible to get rid of such a ubiquitous instability channel.

The first question one could ask is under which conditions the dangerous Coulomb branch direction can remain flat at the quantum level. For this to hold it suffices that the coefficient α in Equation (10.5) vanishes,

$$\alpha = 0 \ . \tag{10.115}$$

Let us then see if this can happen.

We start by considering the gauge theory prior to the orientifold projection. Generically, N regular D3-branes at the singularity the theory reproduce a SCFT and all β functions vanish, that is for each gauge factor the following holds

$$\beta_{SU(N)} = 3N - \frac{N}{2}\sum_{i=1}^{n}(1-\gamma_i) = 0 \ , \tag{10.116}$$

where γ_i are the anomalous dimensions of the bi-fundamental fields charged under the given gauge group (recall that in the unorientifolded theory all matter fields are in bifundamental representations).

Let us now add M fractional branes to the N regular ones and focus on those gauge groups to which the fractional branes couple to. The corresponding β function changes as

$$\beta_{SU(N+M)} = 3(N+M) - \frac{N}{2}\sum_{i=1}^{j}(1-\gamma_i^{(0)}) - \frac{N+M}{2}\sum_{i=1}^{k}(1-\gamma_i^{(1)}) \ , \tag{10.117}$$

where $\gamma_i^{(0)}$ are the anomalous dimensions of bifundamental fields charged under groups not coupling to the fractional branes while $\gamma_i^{(1)}$ are those of fields charged under groups coupling to the fractional branes. Using Equation (10.116) and the following identity:

$$\sum_i^n (1-\gamma_i) = \sum_i^k (1-\gamma_i^{(1)}) + \sum_i^j (1-\gamma_i^{(0)}) \,, \tag{10.118}$$

Equation (10.117) can be re-written as

$$\beta_{SU(N+M)} = \frac{M}{2} \sum_{i=1}^{j} (1-\gamma_i^{(0)}) \ , \tag{10.119}$$

which does not vanish since fractional branes do not support a SCFT. Hence we conclude that

$$\sum_{i=1}^{j} (1-\gamma_i^{(0)}) \neq 0 \ . \tag{10.120}$$

Let us now consider the orientifold action and start with a configuration with regular D3-branes, only. One important point is that β functions are now affected by the fact that some ranks are finitely shifted to balance the O-plane charge. For example, in the PdP_4 model discussed in Section 10.3, the orientifolded theory with N regular branes has gauge group $SO(N+1) \times SU(N+5) \times SU(N) \times SU(N)$.

Compared to Equation (10.116), the expression for the β function becomes

$$3(N+c) - \sum_{i=1}^{n} (1-\gamma_i) \frac{N+b_i}{2} = 3c - \sum_{i=1}^{n} (1-\gamma_i) \frac{b_i}{2} \ , \tag{10.121}$$

where c is the extra coefficient of the gauge group we are considering and b_i those of the gauge groups under which bifundamental matter is charged (in our PdP_4 example $c = 5$ for the $SU(N+5)$ group, and bifundamental matter charged also under the $SO(N+1)$ group has $b = 1$). Note that the β function is no longer vanishing, due to the O-plane charge, and its coefficient does not depend on N.

Let us now perform the two-steps Higgsing which $\mathcal{N} = 2$ fractional branes make possible, as in all models previously considered. Using the same conventions as in previous sections, the gauge coupling running at different scales is

- UV (above scale v)

$$\begin{aligned}\frac{1}{g^2_{SU(N+c)}} &= \left(3(N+c) - \sum_{i=1}^{n}(1-\gamma_i)\frac{N+b_i}{2}\right)\ln\left(\frac{\mu}{\Lambda_{UV}}\right) \\ &= \left(3c - \sum_{i=1}^{n}(1-\gamma_i)\frac{b_i}{2}\right)\ln\left(\frac{\mu}{\Lambda_{UV}}\right) .\end{aligned} \tag{10.122}$$

- Intermediate scale (below scale v and above scale v')

$$\begin{aligned}\frac{1}{g^2_{SU(c)_N}} &= \left(3c - \sum_{i=1}^{k}(1-\gamma_i^{(1)})\frac{b_i}{2} - \sum_{i=1}^{j}(1-\gamma_i^{(0)})\frac{N+b_i}{2}\right)\ln\left(\frac{\mu}{\Lambda_N}\right) \\ &= \left(3c - \sum_{i=1}^{n}(1-\gamma_i)\frac{b_i}{2} - \sum_{i=1}^{j}(1-\gamma_i^{(0)})\frac{N}{2}\right)\ln\left(\frac{\mu}{\Lambda_N}\right) .\end{aligned} \tag{10.123}$$

- IR (below scale v')

$$\frac{1}{g^2_{SU(c)}} = \left(3c - \sum_{i=1}^{n}(1-\gamma_i)\frac{b_i}{2}\right)\ln\left(\frac{\mu}{\Lambda}\right) . \tag{10.124}$$

Note that this pattern holds for all groups and all kinds of matter. Indeed, the presence of (anti)symmetric representations gives factors of the form $(N+b)/2$ in the β function, the same as having fundamental matter charged under a $SU(N+b)$ flavor group.

Matching the scale at $\mu = v$ and $\mu = v'$ gives

$$\Lambda^{3c-\sum_{i=1}^{n}(1-\gamma_i)\frac{b_i}{2}} = \left(\frac{v'}{v}\right)^{\sum_{i=1}^{j}(1-\gamma_i^{(0)})\frac{N}{2}} \Lambda_{UV}^{3c-\sum_{i=1}^{n}(1-\gamma_i)\frac{b_i}{2}} , \tag{10.125}$$

which implies that

$$\alpha \propto \sum_{i=1}^{j}(1-\gamma_i^{(0)})\frac{N}{2} . \tag{10.126}$$

In order for α to vanish we need that

$$\sum_{i}^{j}(1-\gamma_i^{(0)}) = 0 , \tag{10.127}$$

which is in contradiction with Equation (10.120). This shows that whenever $\mathcal{N} = 2$ fractional branes couple to the DSB nodes, they inevitably become runaway and destabilize the otherwise stable DSB vacuum.

10.6 Outlook

Our no-go theorem suggests that in order to avoid this instability channel one could try to look at singularities which, unlike those we have analyzed, admit deformations or DSB branes and no $\mathcal{N} = 2$ ones, and see whether there could be room for DSB models there.

A comprehensive survey of toric singularities up to eight gauge groups is provided in [149] and we have analyzed, in this finite class, all singularities having deformation and/or DSB fractional branes only (note that $\mathbb{C}^3$ orbifolds do not belong to this class, since at these singularities a basis of fractional branes, if there are any, always includes $\mathcal{N} = 2$ ones).

More specifically, following the list provided in [149], the singularities not admitting $\mathcal{N} = 2$ fractional branes are the following ones: for toric diagrams of area 2 (Table 1) singularity number 2; for toric diagrams of area 4 (Table 2) singularities number 6 and 7; for area 5 (Table 3) number 5, for area 6 (Table 4), number 8, 9, 10, 12 and 13; for area 7 (Table 5), number 7, 8 and 9; for area 8 (Table 6), number 1, 3, 4, 5, 7, 8, 13 and 17. In order to obtain the dimer, we used the techniques of [146].

Starting from these singularities, one has to see which do admit orientifold point or line projections. This can be done using the criteria spelled out in [73]. If an orientifold projection is admitted, one performs it and then checks the anomaly cancellation conditions. The latter often do not have any solutions (barring the addition of flavors). If they do have solutions, instead, one has then to see if the corresponding orientifold admits a configuration reproducing a DSB model.

The upshot of our scan is that there exist several possible points and lines reflections and in some cases, one can also satisfy anomaly cancellation conditions without the addition of extra flavors. When this is the case, however, it turns out that there do not exist configurations leading to any known DSB model and in fact, all solutions lead to supersymmetric vacua. This result seems to suggest that the presence of line singularities (*i.e.* $\mathcal{N} = 2$ fractional branes) is a key property a CY singularity should have to allow for DSB low energy dynamics but, at the same time, the one that eventually makes the vacua unstable. In the next chapter, we will elaborate further on this point.

Chapter 11

Stability of Supersymmetry Breaking Vacua in Dimer Models

In the previous chapter, by generalizing previous results of [74], it was shown that in the decoupling limit [21], in which the DSB fractional D-brane bound state becomes part of a UV complete large N D-brane model and gravity is decoupled, all models display an instability. This instability turned out to have a common, model-independent geometric origin in terms of $\mathcal{N} = 2$ fractional branes probing the singularity. More drastically, a no-go theorem was proven which implies that whenever $\mathcal{N} = 2$ classical flat directions exist at a singularity that admits such DSB models, the quantum behavior of the latter is such that the flat directions are tilted and supersymmetry preserving vacua exist.

An obvious way to circumvent this no-go theorem and avoid the unwanted slide towards supersymmetric vacua is to look at singularities free of $\mathcal{N} = 2$ fractional branes to start with and see whether stable DSB models of the type above can be engineered there. Or, alternatively, a stronger no-go theorem should exist which excludes such a possibility altogether.

This is what we will be concerned about in the two next chapters. More precisely, our main goal will be to answer the following question: *Is it possible to get a DSB model, more specifically the* $SU(5)$ *or the* $3-2$ *models, from D-branes at a Calabi-Yau singularity that is free of any (known) instability?*

In the present chapter, we aim at determining whether DSB models at orientifolds can be embedded on singularities which, locally in the dimer, do not display any non-isolated $\mathbb{C}^2/\mathbb{Z}_n$ singularity. Usual dimer techniques, see Chapter 6, will of course play an important role.

Quite surprisingly, we will find a variant of the $SU(5)$ model, dubbed the *twin* $SU(5)$, as a candidate for a fully stable DSB model, and that can a priori appear in a consistent dimer model. The realization of this particular DSB model on a given singularity is left for Chapter 12.

This chapter is organized as follows. In Section 11.1 and Section 11.2, we discuss the possibility to embed the $SU(5)$ and the $3-2$ models in the absence of $\mathcal{N}=2$ fractional branes. This will single out the twin $SU(5)$. We also address a left open question by explaining in Section 11.2 why orientifold projections are needed for recovering the $3-2$ model in dimers. In Appendix 11.A, we give precisions on the shape of the fractional brane hosting a twin $SU(5)$ model. Finally, in Appendix 11.B some details are given on anomaly cancellation conditions for the models discussed in Section 11.2. These results were originally presented in [4].

11.1 SU(5) models

Let us first consider the $SU(5)$ model. This theory has an $SU(5)$ gauge group and one GUT-like chiral family $\square \oplus \overline{\square}$. The presence of the antisymmetric representation implies that if one wants to engineer such a model by D-branes at a CY singularity, an orientifold projection is necessary. Moreover, one has to consider two gauge groups in order to get the antifundamental representation $\overline{\square}$, which can be generated by either an $SU(1)$ or an $SO(1)$ flavor group, see Chapter 10 for examples. Using the dimer formalism, there are two classes of orientifolds, depending on whether they have *fixed points* or *fixed lines* [54] (see Chapter 7 for a short review). We will analyze them in turn.

11.1.1 Fixed points orientifolds

Let us remind that fixed point orientifolds are associated with dimers that enjoy a point reflection. It is always possible to choose the unit cell of the dimer in such a way that its corners coincide with a fixed point. Additionally, due to the dimer's toroidal periodicity, there will also be fixed points at the center of the boundaries of the unit cell, and in the center of the unit cell itself, see Figure 11.1.

As we now review, we not only need a fixed point on one edge of the $SU(5)$ face but a second fixed point is needed to avoid anomalies in the face providing the (anti)fundamental matter field.

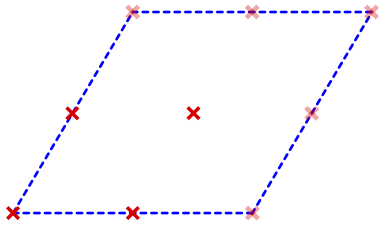

Figure 11.1: A schematic representation of a dimer unit cell with orientifold fixed points. The shaded points are the periodic images of the four basic ones.

The first possibility is to directly avoid the anomaly in the flavor group by having it SO or USp. USp is ruled out since it would give always an even number of antifundamentals, hence more than one. We are then left with $SO(1)$.

- SO flavor group

  Figure 11.2 shows the generic structure of a local configuration of a dimer leading to the $SU(5)$ model, including the signs for the two relevant fixed points. The dotted lines and nodes represent a completely general configuration for the rest of the dimer, only constrained by its compatibility with the point reflections. The blue dotted line indicates that it is possible to choose the unit cell such that the two fixed points live on one of the four segments that form its boundary. This comment will be relevant later.

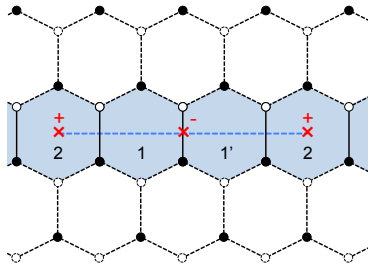

Figure 11.2: Fixed point orientifold realizing the $SU(5)$ model with $SO(1)$ flavor group. The dotted part of the graph indicates the rest of the dimer, which is completely general and not necessarily hexagonal as shown.

Assigning arbitrary ranks to the gauge groups, N_i for face i in the dimer, the anomaly cancellation conditions (ACC) have a solution in

which $N_1 = N_{1'} = 5$, $N_2 = 1$ and the rest of the faces are empty.[1] This choice leads exactly to the $SU(5)$ model. Face 1 becomes the $SU(5)_1$ gauge group. Since face 2 has a fixed point with a positive sign on top of it, becomes the $SO(1)_2$ flavor group.

A second possibility is that the flavor group is of SU type, with its anomaly (when regular branes are added) being canceled by the presence of symmetric matter on a different edge of the face.

- SU flavor group with symmetric

  Figure 11.3 shows the local configuration of a dimer leading to another realization of the $SU(5)$ model in a fixed point orientifold. Once again, the ACC have a solution in which $N_1 = N_{1'} = 5$, $N_2 = N_{2'} = 1$ and the rest of the faces are empty. The resulting theory is the $SU(5)$ model, plus a decoupled singlet corresponding to the symmetric associated with the edge between face 2 and its image.

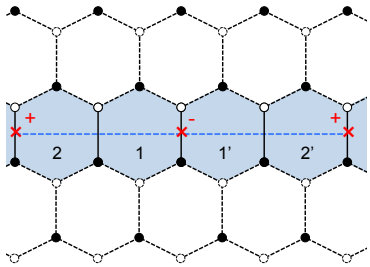

Figure 11.3: Fixed point orientifold realizing the $SU(5)$ model with $SU(1)$ flavor group.

Note that the $SU(1)$ group has no anomaly, but the symmetric is necessary to cancel the anomaly when all the ranks are increased by N (corresponding to the addition of N regular D3-branes which populate the dimer democratically). By construction, the additional (white) faces with rank N will not contribute to the anomaly. In order to cancel the $N + 5$ antifundamentals coming from face 1, we need to have a symmetric of $SU(N + 1)$ at face 2. It reduces to a decoupled singlet when $N = 0$.

A third possibility is that the flavor group is of SU type, and its anomaly (when regular branes are added) is canceled by 5 fundamentals

[1] Of course whether the ACC of the empty nodes are also satisfied depends on the details of the boundary of the cluster of faces under consideration. This observation also applies to the examples that follow.

attached to an $SO(5)$ group. This configuration is shown in Figure 11.4. The low energy theory of this configuration is an $SU(5)$ model together with a decoupled $SO(5)$ SQCD with one flavor. The latter theory develops an ADS superpotential [94], so that we have a runaway behavior (on top of the DSB of the $SU(5)$ model), and hence no true vacuum. We thus discard this possibility since it is already unstable at this low energy field theory level.

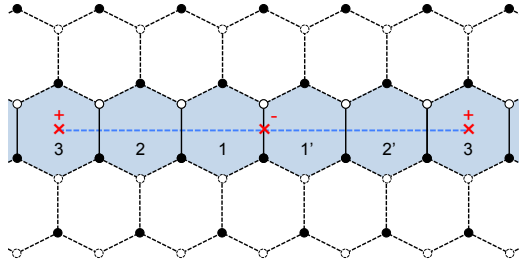

Figure 11.4: Fixed point orientifold realizing the $SU(5)_1$ model with $SU(1)_2$ flavor group and an additional $SO(5)_3$ factor. $SO(5)_3$ develops an ADS superpotential and leads to a runaway behavior.

A fourth possibility is that the flavor group is again of SU type, but now its anomaly is canceled by the presence of a replica of the $SU(5)$ group with its own antisymmetric. We will call this possibility *twin* $SU(5)$ *model*.

- SU flavor group with twin $SU(5)$

  Figure 11.5 shows the local configuration of a dimer leading to yet another realization of the $SU(5)$ model in a fixed point orientifold. The ACC have a solution in which $N_1 = N_{1'} = 5$, $N_2 = N_{2'} = 1$, $N_3 = N_{3'} = 5$ and the rest of the faces are empty. The resulting theory corresponds to two $SU(5)$ models sharing the same $SU(1)$ flavor group which provides their (anti)fundamentals. Since $SU(1)$ is actually empty, and in any case, no chiral gauge-invariants can be written for each $SU(5)$ model, the twins are effectively decoupled and thus their low energy dynamics is completely independent.

In principle, we could go on with further possibilities. Indeed, the anomaly of the second $SU(5)$ gauge group at face 3 can be canceled with a fundamental, instead of an antisymmetric. The simplest possibility is that the fundamental is attached to an $SO(1)$ face. However it could also be an $SU(1)$ with a symmetric, or further an $SU(1)$ with 5 antifundamentals given by an $SO(5)$, or another $SU(5)$. The possibilities already discussed above repeat themselves. What is important to notice is that the gauge theory on

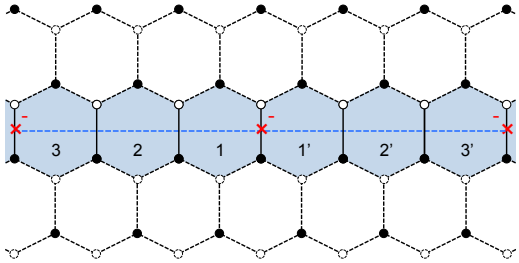

Figure 11.5: Fixed point orientifold realizing the twin $SU(5)$ model.

face 3 would always be an $SU(5)$ with one flavor, hence developing an ADS superpotential and leading to runaway behavior.

We thus conclude that the only possibilities to engineer an $SU(5)$ model, which is stable at low energies, in a dimer with fixed points are the three bullets above: SO flavor group, SU flavor group with a symmetric and SU flavor group with twin $SU(5)$.

An important remark is that in all the examples above the following holds: there can be a long chain of gauge groups to eventually cancel the anomaly of the initial $SU(5)$ gauge group, but it always ends with an orientifold fixed point.[2] As a consequence, we do not have to look far in order to identify an $\mathcal{N} = 2$ fractional brane in these dimers. Remarkably, in all cases, the $SU(5)$ model is fully supported on a set of faces that corresponds to an $\mathcal{N} = 2$ fractional brane in the parent (*i.e.*, non-orientifolded) theory. From Figure 11.2, Figure 11.3 and Figure 11.5 we see that in all cases the $SU(5)$ model indeed lives on a stripe that gives rise to a gauge-invariant not contained in the superpotential. The VEV of such an operator parametrizes the corresponding Coulomb branch.

We conclude that an $SU(5)$ model cannot be obtained for this class of orientifolds if the parent theory does not contain line singularities, *i.e.* $\mathcal{N} = 2$ fractional branes.[3] The previous discussion implies that the no-go theorem in Chapter 10 cannot be avoided for this class of orientifolds.

Let us discuss how the instability explained in Section 10.1 is realized in these models in more detail. We start with the model with SO flavor,

[2]We are ignoring more ramified possibilities. For instance, for an $SU(1)$ flavor at face 2, we could imagine providing the 5 fundamentals from more than one SO gauge group. That would lead to the need for more than one extra fixed point. The other cases can be treated similarly. Thus a more precise statement is that we always need *at least* another fixed point to cancel the anomaly of the $SU(5)$ at face 1.

[3]This result is consistent with an observation made in [73], namely that singularities with deformation branes are incompatible with point projections.

Figure 11.2. After adding N regular D3-branes, the relevant gauge group becomes

$$SU(N+5)_1 \times SO(N+1)_2 \ . \tag{11.1}$$

Let us denote

$$A = \begin{array}{|c|}\hline \\ \hline \end{array}_1 \quad , \quad \overline{Q} = (\overline{\square}_1, \square_2) \tag{11.2}$$

where A corresponds to the edge in the dimer between face 1 and its orientifold image and $\overline{Q}$ corresponds to the edge between faces 1 and 2. The Coulomb branch is parameterized by the expectation value of the gauge-invariant going around the stripe. In principle we can build an $SU(N+5)_1$ gauge-invariant as

$$\phi^{SO}_{ab} = \overline{Q}^i_a \overline{Q}^j_b A_{ij} \ , \tag{11.3}$$

where i, j are fundamental indices of $SU(N+5)_1$ and a, b are fundamental indices of $SO(N+1)_2$. Note that it is in the antisymmetric representation of $SO(N+1)_2$, hence it does not exist for $N = 0$, and it has vanishing trace for $N \geq 1$.

As discussed in the previous chapter, we actually need to go twice around the stripe in order to have a non-vanishing gauge-invariant given by

$$\langle \delta^{ac} \delta^{bd} \phi^{SO}_{ab} \phi^{SO}_{cd} \rangle \ , \tag{11.4}$$

parametrizing the Coulomb branch. That the gauge-invariant still vanishes automatically for $N = 0$, is consistent with the fact that the $SU(5)$ model does not have a moduli space and that the additional regular branes are necessary for the instability.

We now consider the case with SU flavor and a symmetric, Figure 11.3. After adding N regular D3-branes, the gauge group becomes

$$SU(N+5)_1 \times SU(N+1)_2 \ . \tag{11.5}$$

We denote

$$A = \begin{array}{|c|}\hline \\ \hline \end{array}_1 \quad , \quad \overline{Q} = (\overline{\square}_1, \square_2) \quad , \quad \overline{S} = \overline{\square\square}_2 \tag{11.6}$$

where now $\overline{S}$ corresponds to the edge between face 2 and its image under the second fixed point. The $SU(N+5)_1$ gauge-invariant is

$$\phi^{SU}_{ab} = \overline{Q}^i_a \overline{Q}^j_b A_{ij} \ , \tag{11.7}$$

where now a, b are fundamental indices of $SU(N+1)_2$. It is in the anti-symmetric representation of $SU(N+1)_2$, hence again it does not exist for $N = 0$, and for $N \geq 1$ it cannot be contracted with $\overline{S}^{ab}$ which is symmetric. A non-vanishing gauge-invariant is given by

$$\langle \overline{S}^{ac} \overline{S}^{bd} \phi^{SU}_{ab} \phi^{SU}_{cd} \rangle \ , \tag{11.8}$$

which now parametrizes the Coulomb branch. The same remarks as in the previous case apply.

Finally, let us discuss the last case of the twin $SU(5)$, where the gauge group becomes

$$SU(N+5)_1 \times SU(N+1)_2 \times SU(N+5)_3 \ . \tag{11.9}$$

We denote

$$A = \begin{smallmatrix}\square\\ \square\end{smallmatrix}_1 \quad , \quad \overline{Q} = (\overline{\square}_1, \square_2) \quad , \quad \overline{P} = (\overline{\square}_2, \square_3) \quad , \quad \overline{A} = \begin{smallmatrix}\overline{\square}\\ \overline{\square}\end{smallmatrix}_3 \tag{11.10}$$

where now $\overline{P}$ corresponds to the edge between faces 2 and 3, and $\overline{A}$ to the edge between face 3 and its image under the second fixed point. The $SU(N+5)_1$ and $SU(N+5)_3$ gauge-invariants are

$$\phi_{ab} = \overline{Q}^i_a \overline{Q}^j_b A_{ij} \quad , \quad \overline{\phi}^{ab} = \overline{P}^a_\alpha \overline{P}^b_\beta \overline{A}^{\alpha\beta} \ , \tag{11.11}$$

where α, β are fundamental indices of $SU(N+5)_3$. They are in the antisymmetric and conjugate antisymmetric representation of $SU(N+1)_2$, respectively. They do not exist for $N = 0$, but for $N \geq 1$ the simplest gauge-invariant is given by

$$\langle \phi_{ab} \overline{\phi}^{ab} \rangle \ , \tag{11.12}$$

which parametrizes the Coulomb branch in this case. The same remarks as in the previous cases apply. Further, note that this last case allows for a simpler gauge-invariant parametrization of the Coulomb branch because it is the only one where the two fixed points (giving rise to A and $\overline{A}$) have the same sign, see Figure 11.5. In the two previous cases, the fixed points have opposite signs, and we have to take the loop twice.

Double $SU(5)$ models

In some cases, the structure of the dimer is such that it could be possible to use all four fixed points to generate a pair of $SU(5)$ models. Figure 11.6 shows the general structure for a dimer giving rise to two $SU(5)$ models with $SO(1)$ flavor nodes. Other possibilities, for instance, two models with $SU(1)$ flavor nodes, an $SU(1)/SO(1)$ combination, or two twin $SU(5)$ models, are also feasible. The same logic of previous examples applies to each of the two stripes of blue faces, so we conclude that each of these models contains $\mathcal{N} = 2$ fractional branes and hence is not stable.

The different cases considered so far illustrate the general strategy that we will apply to most of the other models we will be considering. While the

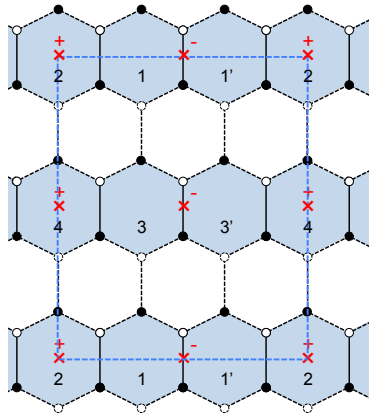

Figure 11.6: General structure of a fixed point orientifold realizing a double $SU(5)$ with $SO(1)$ flavor group model.

DSB models under consideration are relatively simple, we are considering here their embedding into arbitrarily complicated toric singularities. Therefore, establishing the existence of $\mathcal{N} = 2$ fractional branes (which implies the instability of the DSB model) might naively seem an intractable problem since, generically, the majority of the dimer model will be unknown. However, as it occurred in the previous examples, the necessary interplay between the region of the dimer that makes up the DSB model and the orientifold fixed points (or fixed lines, as we will see shortly), implies that we fully know the dimer model along a "short direction" of the unit cell. This is sufficient to identify an $\mathcal{N} = 2$ fractional brane. In even simpler terms, in these cases, the DSB models are actually supported on faces of the dimer that define an $\mathcal{N} = 2$ fractional brane. We will see that there is only one specific way to circumvent this argument.

11.1.2 Fixed line(s) orientifolds

A second possibility is that dimers admit line reflection orientifolds with either two independent fixed lines or a single diagonal fixed line.

An orientifold with two fixed lines is such that the unit cell of the dimer can be taken to be rectangular, and the dimer is further invariant under a reflection leaving fixed the lines going along one of the boundaries of the unit cell. By the periodicity of the dimer, there must be a second fixed line parallel to the first one and going through the middle of the unit cell. Vertical and horizontal fixed lines will be considered on the same footing here.

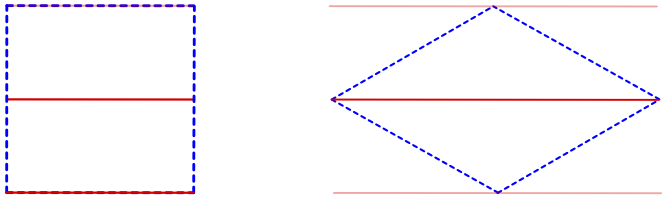

Figure 11.7: A schematic representation of orientifold fixed lines going through the dimer unit cell: two fixed lines on the left, a single fixed line on the right.

Orientifolds with a single fixed line are such that the unit cell can be taken to have the shape of a rhombus, and the dimer is invariant under reflections about a fixed line that goes along one of the diagonals of the rhombus. The periodicity of the dimer does not imply the presence of other fixed lines in the unit cell. Again, we will not make the distinction between the two diagonals. Both situations are depicted in Figure 11.7. In the following, we will use the two nomenclatures "double and single" or "horizontal/vertical and diagonal fixed lines" interchangeably.

DSB models between two fixed lines

The cases with two fixed lines are basically identical to the orientifolds considered in the previous section, with the exchange of fixed points for fixed lines. Therefore, we present them succinctly.

- *SO* flavor group

  Figure 11.8 shows the local configuration realizing the $SU(5)$ model with $SO(1)$ flavor group, including the signs of the fixed lines. This is achieved by setting $N_1 = N_{1'} = 5$, $N_2 = 1$ and vanishing ranks for all other faces. Since the two lines have opposite signs, this configuration is only possible in orientifolds with two independent fixed lines.

- *SU* flavor group with symmetric

  Figure 11.9 shows the local configuration realizing the $SU(5)$ model with $SU(1)$ flavor group and a symmetric. This corresponds to $N_1 = N_{1'} = 5$, $N_2 = N_{2'} = 1$ and vanishing ranks for all other faces. Since the two lines have opposite signs, this configuration is only possible in orientifolds with two independent fixed lines.

- *SU* flavor group with twin $SU(5)$

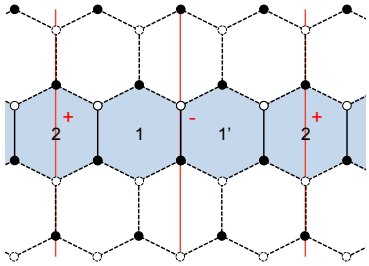

Figure 11.8: Two fixed lines orientifold realizing the $SU(5)$ model with $SO(1)$ flavor group.

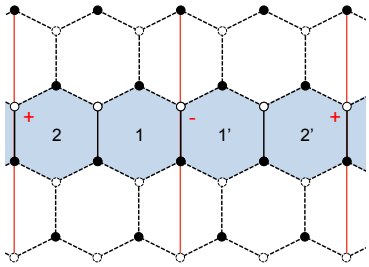

Figure 11.9: Two fixed lines orientifold realizing the $SU(5)$ model with $SU(1)$ flavor group.

Figure 11.10 shows the local configuration realizing the $SU(5)$ model with $SU(1)$ flavor group and a twin $SU(5)$ model. This corresponds to $N_1 = N_{1'} = 5$, $N_2 = N_{2'} = 1$, $N_3 = N_{3'} = 5$ and vanishing ranks for all other faces. In this case, the two lines have the same sign, hence it is possible to find this configuration both in orientifolds with two independent fixed lines or with a single diagonal fixed line. Note that in the latter case, we have to consider the situation in which the strip goes from one line to a second one, in a contiguous unit cell.

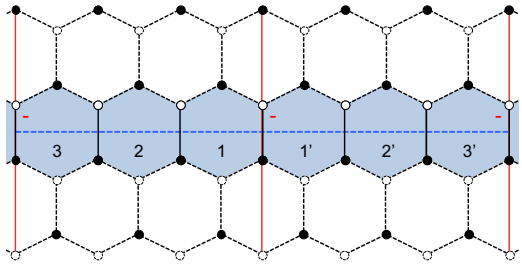

Figure 11.10: Two fixed lines orientifold realizing the twin $SU(5)$ model.

Using the same arguments as for the fixed point orientifolds in Sec-

tion 11.1.1, we conclude that in all these cases the models are supported on a stripe of faces of the dimer that define an $\mathcal{N} = 2$ fractional brane.

Multiple $SU(5)$ models

We previously saw that fixed point orientifolds can give rise to double $SU(5)$ models. Similarly, orientifolds with fixed lines can produce multiple $SU(5)$ models, as shown in Figure 11.11. In this case, the number of models is not restricted to two. It is important to note that, unlike in the example shown in the Figure, it is possible for different stripes to use the two fixed lines in different ways, for instance simultaneously leading to models with both $SO(1)$ and $SU(1)$ flavor groups, when the two lines have opposite signs. Once again, our general discussion applies to each individual stripe of blue faces, so we conclude that $\mathcal{N} = 2$ fractional branes exist for each individual stripe and hence the models are not stable.

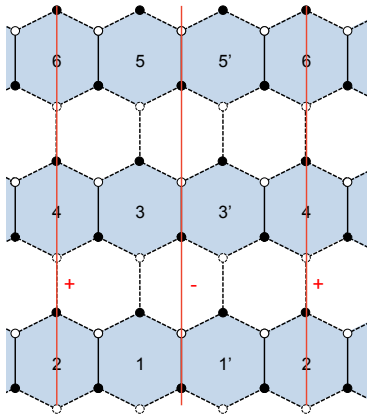

Figure 11.11: An example of the general structure of a portion of a dimer with two fixed lines giving rise to multiple $SU(5)$ models.

DSB Models on a single fixed line: the twin $SU(5)$

There is one additional way in which an $SU(5)$ model could be engineered. This is when both the projection needed for the antisymmetric of $SU(5)$ and the one for canceling the anomaly due to the antifundamental, are provided by the same fixed line. This could be realized both in orientifolds with a diagonal fixed line, and in orientifolds with two fixed lines. What is important is that only one line is needed to define the relevant cluster of faces.

Importantly, since the orientifold line cannot change sign along the dimer, this possibility is effective only when the two projections have the same sign. Then the only case that fits the bill is the twin $SU(5)$ model, as the one in Figure 11.10.

Basically, the chain of gauge groups represented by faces 1, 2, and 3 has to bend and end on the same line. There are now two possibilities. Either all the black nodes at the bottom of the edges between faces 1, 2 and 3 are one and the same, or the chain $1-2-3$ and their images enclose some (unoccupied) faces of the dimer. The latter case is inconsistent from the dimer point of view, as shown in Appendix 11.A: such a chain cannot be a fractional brane in the parent theory. We are thus left with the former case, which in the dimer corresponds to a hexagonal cluster of faces around a node, as depicted in Figure 11.12.

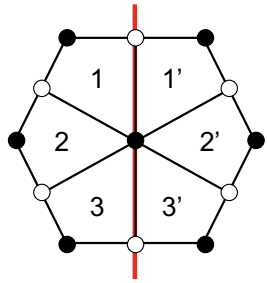

Figure 11.12: The hexagonal cluster with six faces on an orientifold line. All faces are here depicted with four edges, but some of them could have more.

Interestingly, such a collection of faces surrounding a node corresponds to a deformation fractional brane in the classification of [67]. It is reassuring that unlike in the cases with fixed points, deformation branes are compatible with line orientifolds [73].

The analysis of this case is similar to what we carried out for the twin $SU(5)$ model previously, leading to a gauge group

$$SU(N+5)_1 \times SU(N+1)_2 \times SU(N+5)_3 \ . \tag{11.13}$$

The difference is that now the node at the center of the hexagonal cluster corresponds to a sextic superpotential term. Using the same notation as in Equation (11.10), we have

$$W = \mathrm{Tr} A\overline{QPAP}^T\overline{Q}^T = \mathrm{Tr}\phi\overline{\phi} \ . \tag{11.14}$$

For $N = 0$, the superpotential vanishes and we are left with two $SU(5)$ models sharing an $SU(1)$ flavor node, in which both surviving $SU(5)$ fac-

tors break supersymmetry dynamically into a stable vacuum. Unlike the other realizations of the twin $SU(5)$ model, in the present one there is no indication that the dimer must contain an $\mathcal{N}=2$ fractional brane.

Combining the analysis in Sections 11.1.1 and 11.1.2, we conclude that engineering a single $SU(5)$ DSB model without instabilities at an orientifold of a toric singularity is impossible. Conversely, our analysis implies that engineering a minimal $SU(5)$ model requires non-isolated singularities with curves of $\mathbb{C}^2/\mathbb{Z}_n$ singularities passing through the origin, which in turn result in the instability. This means that, as explained in Chapter 6, the toric diagram must contain internal points on its boundary edges. On the other hand, our analysis shows that an instance of a DSB model, the twin $SU(5)$ model, actually exists which is compatible with an orientifold projection with fixed line(s). We should now understand whether such sub-dimer can actually be embedded into a consistent dimer and, if so, whether such dimer can be free of $\mathcal{N}=2$ fractional branes. We investigate these questions in Chapter 12.

11.2 3−2 Models

Let us now turn to the $3-2$ model, another prominent example of DSB that was recovered within brane setups at orientifold singularities in Chapter 10. The model has a gauge group $SU(3)\times SU(2)$. Its matter content is reminiscent of one SM generation

$$Q=(\square_3,\overline{\square}_2)\ ,\ \overline{U}=\overline{\square}_3\ ,\ \overline{D}=\overline{\square}_3\ ,\ L=\square_2\ , \tag{11.15}$$

where the subindices indicate the corresponding gauge group in an obvious way. In addition, the theory has the following superpotential

$$W=\overline{D}QL\ . \tag{11.16}$$

In principle, the above field content (SU gauge groups, (bi)fundamental matter, together with a cubic superpotential) does not seem to require an orientifold projection. As it will become clear in the following, such a projection is nevertheless necessary in order to allow for a fractional brane (*i.e.* an anomaly-free configuration) with the desired ranks for the gauge groups.

11.2.1 General features

Let us think more carefully about the basic features of the D-brane realization of this model. In this subsection, we enumerate all different

ways to recover the $3-2$ model from fractional branes at an orientifold singularity. The structure of these models is more intricate than that of the $SU(5)$ model, so it is convenient to draw the corresponding quivers.

The candidate models are presented in Figure 11.13. In the figure, we have kept the ranks of the gauge group general by introducing N_i, $i = 1, \ldots, 4$. These additional integers account for more general configurations of D-branes at the singularity, *e.g.* the addition of regular or fractional D3-branes, and we posit that anomaly cancellation must hold even in those cases. The $3-2$ model arises when all N_i and the ranks of additional gauge groups, which depend on the specific singularity and are not shown in these quivers, vanish.

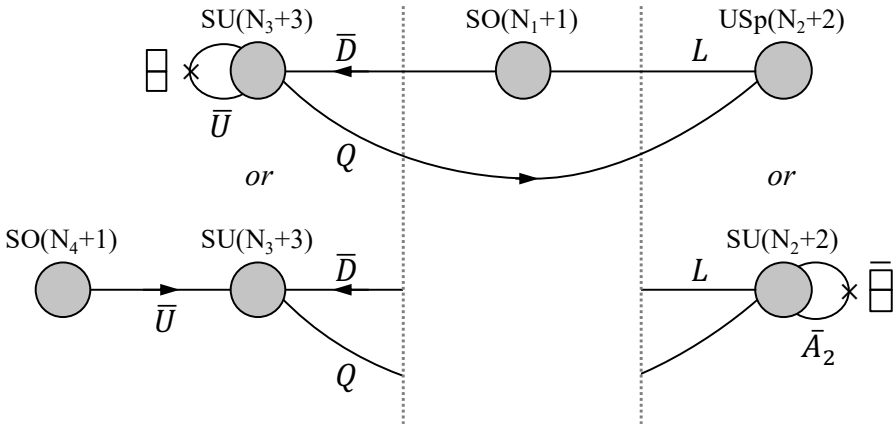

Figure 11.13: Four quivers giving rise to the $3-2$ model when all $N_i = 0$. All these models use three orientifold fixed loci.

For similar reasons as in the case of the $SU(5)$ model, we need at least an additional gauge group factor, which we will call node 1, to serve as a flavor group providing the $\overline{D}$ and L fields. Both $\overline{D}$ and L should be connected to the same node for the superpotential Equation (11.16) to be possible. In dimer terminology, we identify the smallest building block of a $3-2$ model as three faces connected by a trivalent vertex. In this sense, $3-2$ model realizations are necessarily more involved than $SU(5)$ model realizations since the latter only required a building block of two faces.

The quivers in Figure 11.13 should be interpreted as follows. For each of the two endpoints of the quiver, we have presented two possibilities. The two options on the left correspond to realizing $\overline{U}$ as an antisymmetric of node $SU(3)$ or via a fourth gauge group acting as a flavor node. The two options on the right correspond to the fact that node 2 can be either $USp(2)$

or $SU(2)$. All possible combinations of these endpoints realize the desired $3-2$ model, therefore Figure 11.13 accounts for four models.

In principle, the flavor nodes 1 and 4 in Figure 11.13 could be SU or SO. However, if these nodes were of SU type, their ACC in the case of general ranks would require additional nodes, that come to life when regular D-branes are added. Generically, these gauge groups will give rise to new matter fields charged under the nodes of the original quiver. Such fields would contribute to and potentially help in the cancellation of anomalies. However, for N regular D3-branes, it is easy to show that for neither node the anomaly would cancel, as there would still be an imbalance of one or three units for nodes 1 and 4, respectively. In order to cancel the anomalies, there are then only two options. The first is to introduce an orientifold projection. It turns out that setting both nodes to be SO is the simplest such option, and without loss of generality we will stick to it in the following. The second option is to compensate for the anomaly by a mirror construction. We defer the treatment of the latter possibility to the last subsection.

It is worth noting that in two of the four models described by Figure 11.13, those for which the second gauge group is $SU(N_2+2)$, we have also introduced an antisymmetric tensor $\bar{A}_2$. This field is necessary for satisfying the ACC for the more general ranks that arise when regular D3-branes are added (see Appendix 11.B). It becomes a singlet when $N_2=0$, so it decouples and does not affect the IR physics.

A final option is to get the two antifundamentals of the $SU(3)$, $\overline{U}$ and $\overline{D}$ from the same flavor $SO(1)$ group. However, in order to realize the $3-2$ model, the structure of the dimer model should be such that a $\overline{U}QL$ term is not present in the superpotential. This possibility is then obtained by simply identifying nodes 1 and 4 in Figure 11.13.

We thus reach the conclusion that we need no less than three orientifold projections to realize a $3-2$ model: one for the $SO(1)$ flavor group (thus with a + sign), one for node 2 which is either $USp(2)$ or $SU(2)$ with an antisymmetric (in both cases, with a $-$ sign), and one for node 3, either with an antisymmetric ($-$ sign) or with the $SO(1)$ flavor node 4 (+ sign). Of course, some of these projections can be given by the same object, in the case of an orientifold line, provided they require the same sign.[4]

All quivers described by Figure 11.13 are viable as stand-alone gauge theories. However, as for the $SU(5)$ model, we need to verify whether the

[4]It is worth noting that in all the realizations of the $3-2$ model found in Chapter 10, node 3 has an antisymmetric, node 1 is of SO type, while node 2 is $USp(2)$ in the $\mathbb{Z}_6'$ orbifold and in PdP_4, and $SU(2)$ with an antisymmetric in PdP_{3c}, PdP_{4b} and the $\mathbb{Z}_3\times\mathbb{Z}_3$ orbifold.

theories remain anomaly-free upon the addition of regular and/or fractional D3-branes. It turns out that the $SO(N_1+1) \times SU(N_2+2) \times SU(N_3+3) \times SO(N_4+1)$ model does not pass this test, as shown in Appendix 11.B.

Below we investigate the realization of these models in terms of fixed points and fixed line(s) orientifolds.

11.2.2 Fixed points orientifolds

Interestingly, for the purpose of establishing the existence of an $\mathcal{N}=2$ fractional brane, and hence the instability of the supersymmetry breaking vacuum, it is sufficient to focus on a very small part of all these theories. In particular, all of them contain one of the following two subsectors:

- $SO(N_1+1) \times USp(N_2+2)$.
- $SO(N_1+1) \times SU(N_2+2)$ with the tensor $\overline{A}_2$.

Knowledge of the dimer around gauge groups 1 and 2 will be enough for our purposes. Let us consider the general structure of the dimers associated with these two possibilities.

- $SO(N_1+1) \times USp(N_2+2) \subset 3-2$ model

  Figure 11.14 shows the general structure of the relevant part of the dimer model. The edge between faces 1 and 2 represents the L field. Clearly, faces 1 and 2 define a stripe that winds around the unit cell of the parent dimer, giving rise to a gauge-invariant that is not in the superpotential. Therefore, they correspond to an $\mathcal{N}=2$ fractional brane.

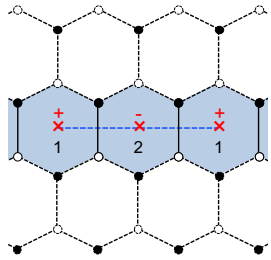

Figure 11.14: A piece of the dimer for a fixed point orientifold realizing the $3-2$ model with an $SO(N_1+1) \times USp(N_2+2)$ subsector.

- $SO(N_1+1) \times SU(N_2+2)$ with $\overline{A}_2 \subset 3-2$ model

  Figure 11.15 shows the part of the dimer that we are interested in. The edge between faces 1 and 2 corresponds to L, while the one between face 2 and its image gives rise to $\overline{A}_2$. Once again, we see that faces 1, 2, and 2' define an $\mathcal{N}=2$ fractional brane in the parent dimer. It is interesting to note that this picture is identical to Figure 11.2 for the $SU(5)$ model.

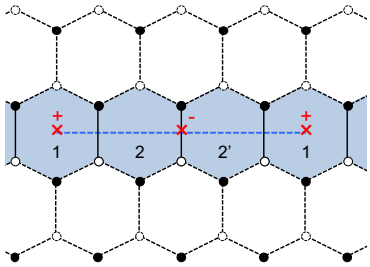

Figure 11.15: A piece of the dimer for a fixed point orientifold realizing the $3-2$ model with an $SO(N_1+1) \times SU(N_2+2)$ with $\overline{A}_2$ subsector.

From the previous discussion, we conclude that all realizations of the $3-2$ model at fixed point orientifolds suffer from an $\mathcal{N}=2$ fractional brane instability.

Models with more than one type of $\mathcal{N}=2$ fractional branes

Before moving on, let us consider the models in Figures 11.14 and 11.15 in further detail. As we have already mentioned, in all these cases the portion of the dimer realizing the $3-2$ model involves three fixed points. For concreteness, let us focus on the case in which $\overline{U}$ is an antisymmetric of node 3 and node 2 if of USp type. All other combinations are analogous and lead to the same conclusions. Figure 11.16 shows the general structure of the dimer model. Interestingly, in this case, we can identify yet another $\mathcal{N}=2$ fractional brane, in addition to the one covered by our previous analysis. This new fractional brane corresponds to faces 1, 3, and 3' in the parent dimer and is shown in pink in Figure 11.16. We conclude that when sub-dimers as in Figures 11.14 and 11.15 are embedded in a complete dimer model, the corresponding toric singularity has at least two different types of $\mathcal{N}=2$ fractional branes. Explicit models illustrating this phenomenon were constructed in [2].

Another interesting fact we would like to notice has to do with the intertwining between $SU(5)$ and $3-2$ models realizations. Figure 11.16

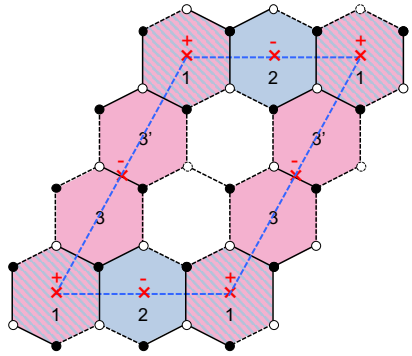

Figure 11.16: General structure of the dimer model for one of the models in Figure 11.13. This model contains two different $\mathcal{N} = 2$ fractional branes. They are shown in blue and pink, with the striped face belonging to both of them.

shows that in any such configuration realizing a $3-2$ model, an $SU(5)$ model can also be realized, by simply turning off the rank of node 2, while pumping up the rank of node 3 to $SU(5)$. Even more, $3-2$ model realizations like the one of Figure 11.15 allow for two alternative $SU(5)$ model realizations, the other one being by turning off node 3 and setting node 2 to $SU(5)$, as already noticed when commenting the figure. Multiple explicit examples of this connection can be found in [2]. The only realization of a $3-2$ model that does not lead directly to a realization of the $SU(5)$ model would be one with $USp(2)$ at node 2 and a node 4 to compensate the anomaly of node 3. Unfortunately, no examples of this exist in the literature, and it is beyond our scope to find one here, as we have in any case shown that it would be afflicted by an $\mathcal{N} = 2$ fractional brane instability.

Double 3−2 models

It is natural to ask whether fixed point orientifolds can lead to a pair of $3-2$ models. In this case, each of the models should use two of the four fixed points. However, all the models of Figure 11.13 need three different projections, and thus three different fixed points. One could still think about the case where nodes 1 and 4 are identified, where only two identifications are actually required. However, in order for node 3 to have two different connections with node 1, the faces corresponding to this $3-2$ model realization end up being spread across all the unit cell, so that again

two such models cannot coexist.[5]

11.2.3 Fixed line(s) orientifolds

We now consider the realization of the $3-2$ models in orientifolds with fixed lines.

The analysis in the case in which the $3-2$ model uses two different orientifold fixed lines is identical to the one for fixed points. In particular, it is sufficient to focus on faces 1 and 2. We simply need to replace fixed points with fixed lines in the previous discussion.

- $SO(N_1+1) \times USp(N_2+2) \subset 3-2$ model

  Figure 11.17 shows the relevant part of the dimer. We immediately identify an $\mathcal{N}=2$ fractional brane in the parent dimer consisting of faces 1 and 2.

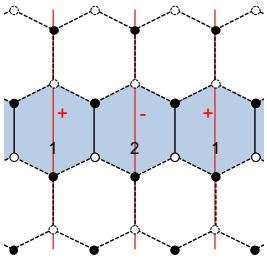

Figure 11.17: A piece of the dimer for an orientifold with two fixed lines realizing the $3-2$ model with an $SO(N_1+1) \times USp(N_2+2)$ subsector.

- $SO(N_1+1) \times SU(N_2+2)$ with $\overline{A}_2 \subset 3-2$ model

  Figure 11.18 shows the part of the dimer that we focus on. Faces 1, 2, and 2' form an $\mathcal{N}=2$ fractional brane in the parent dimer.

Multiple 3−2 models

Orientifolds with fixed lines can in principle give rise to multiple $3-2$ models, stacking them as we did in Figure 11.11 for $SU(5)$. In this case, the projection needed for node 3 can be provided either by the line with a

[5] It would be interesting to investigate whether such model can actually be engineered in terms of dimers. Again, since we have already proven that all realizations of the $3-2$ models at fixed point orientifolds are unstable, we do not pursue this challenging question any further.

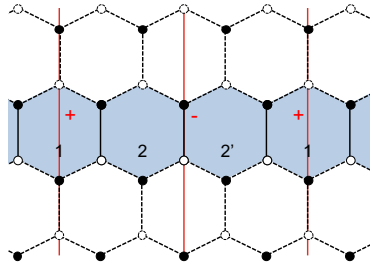

Figure 11.18: A piece of the dimer for an orientifold with two fixed lines realizing the $3-2$ model with an $SO(N_1+1)\times SU(N_2+2)$ with $\overline{A}_2$ subsector.

$-$ sign, in case of an antisymmetric, or by the line with a $+$ sign, in case of a flavor node 4. Our previous arguments show that each of these models contains (at least) an $\mathcal{N}=2$ fractional brane and are hence unstable.

SU(5) - 3−2 mixed models

At this point, it is interesting to point out that our arguments for multiple models, in the case of fixed lines, indicate that we can also have models that realize a combination of $SU(5)$ and $3-2$ models. Once again, our arguments from Section 11.1 and this section show that each DSB sector would be independently unstable.

11.2.4 Twin 3−2 models?

We are now left to investigate the possibility that the anomalies of the $3-2$ model are canceled in a twin realization, along the lines of what was done for the $SU(5)$ model in Figures 11.5 and 11.10. Further, we would like to know if there is a realization similar to the one of Figure 11.12, *i.e.* on a *single* fixed line, which would not automatically imply the presence of $\mathcal{N}=2$ fractional branes.

As already alluded to, we can cancel the anomalies of a node 1 of SU nature, and/or node 4, if in the configuration there is a twin copy of the $3-2$ model sharing the $SU(1)$ node. Note that in compensating the anomaly with a twin, it is important that the two models are decoupled. If we were to use the same mechanism to compensate for the anomaly of node 2, the non-zero coupling of node 2 itself would couple the twins and alter the low energy physics of the models (typically destroying the stable supersymmetry breaking dynamics). Hence whatever we do, node 2 will always require a projection. As a consequence, if such twin model is realized

in a way that it extends between two different fixed points or fixed lines, by the same arguments used around Figures 11.5 and 11.10, there will be $\mathcal{N} = 2$ fractional branes that render the DSB model eventually unstable. We will thus refrain from investigating further the feasibility of such a configuration.

Finally, we would like to see if it is possible to realize a twin $3-2$ model on a single fixed line. Given that node 2 and its twin require a $-$ sign, in principle we have two options. Either both node 3 and its twin have an antisymmetric by ending up on the same fixed line, or they compensate the anomaly by sharing an $SU(1)$ node 4. It is easy to draw the minimal requirements for the portion of the dimer that would translate these properties, see respectively Figures 11.19 and 11.20.

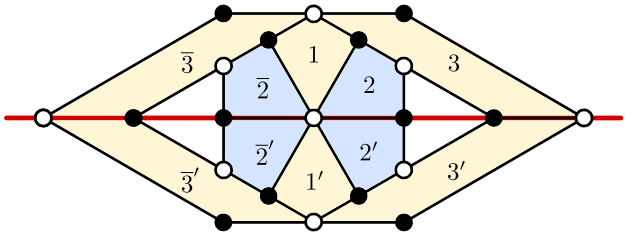

Figure 11.19: A tentative sub-dimer for a twin $3-2$ model where the $SU(3)$ faces have an antisymmetric flavor.

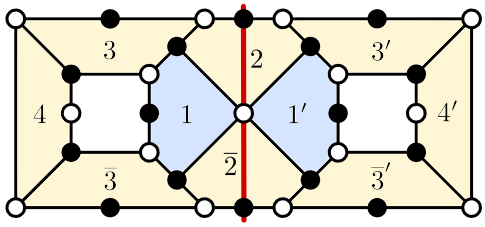

Figure 11.20: A tentative sub-dimer for a twin $3-2$ model where the $SU(3)$ faces share a flavor $SU(1)_4$.

Naively, these configurations look consistent and one can find a choice of ranks satisfying the ACC. These are the following. For Figure 11.19, $N_3 = N_{3'} = N_{\bar{3}} = N_{\bar{3}'} = M_3 + 3$, $N_2 = N_{2'} = N_{\bar{2}} = N_{\bar{2}'} = M_2 + 2$ and $N_1 = N_{1'} = M_2 + M_3 + 1$. For Figure 11.20, $N_3 = N_{3'} = N_{\bar{3}} = N_{\bar{3}'} = M_3 + 3$, $N_1 = N_{1'} = M_1 + 1$, $N_4 = N_{4'} = M_1' + 1$ and $N_2 = N_{\bar{2}} = M_1 + M_1' + 2$.

Assuming that in the parent theory every rank parametrizing the solutions above can be taken independently large, we observe that both situations would imply the existence of a fractional brane described by a ring of faces with equal ranks (up to the usual $\mathcal{O}(1)$ corrections) surrounding a

hole. These are obtained by setting $M_2 = 0$ in Figure 11.19, and $M_1 = 0$, $M_1' = M_3$ in Figure 11.20. The ring-shaped would-be fractional brane is depicted in both figures by the yellow-shaded faces. As shown in the Appendix 11.A, this is an inconsistent dimer. We conclude that unlike the $SU(5)$ model, there is no way to build a stable twin version of the $3-2$ model on a single orientifold line.

11.3 Outlook

We carried out an investigation that shows that in the minimal realizations of the $SU(5)$ and $3-2$ models at orientifolds of singularities, the instability associated with $\mathcal{N}=2$ fractional branes is unavoidable. Remarkably, this result ties the ability to engineer these models to basic geometric features of the underlying singularity: the presence of non-isolated $\mathbb{C}^2/\mathbb{Z}_n$ singularities, and hence it explains the results collected in Chapter 10. This is yet another example of the connection between geometry and features or dynamics of the corresponding quantum field theories, such as *e.g.* confinement and complex deformations [27] or runaway DSB and the absence of complex deformations [66, 67].

These general results will then guide our search for models without instabilities. Indeed, we showed that a simple variant of the $SU(5)$ model, that we dub twin $SU(5)$, can a priori be realized by D-branes at an orientifold of a toric CY, which lacks non-isolated $\mathbb{C}^2/\mathbb{Z}_n$ singularities and, as such, is free of the aforementioned decay channel, and stable. The next chapter is devoted to the search of such a singularity.

11.A Holes in the dimer and zig-zag paths

In the following, we present an argument forbidding the presence of holes of reduced rank inside a specific sub-dimer that appears in different twin models. We rely on ZZP techniques for anomaly cancellation developed in [5, 140]. One associates a value v_i to every ZZP in the dimer and then assigns an arbitrary rank to a given face in the dimer. The remaining ranks are set by requiring that the rank differences between two adjacent faces m, n obey $N_m - N_n = v_i - v_j$ where i, j are the ZZP separating them.

Consider a ring-shaped sub-dimer of rank $N + \mathcal{O}(1)$. We assume that as we go along it, from one of its faces to another, we only cross edges with identical orientation, see Figure 11.21a. We now show that the region inside the ring, the "hole", is inconsistent if of reduced rank.

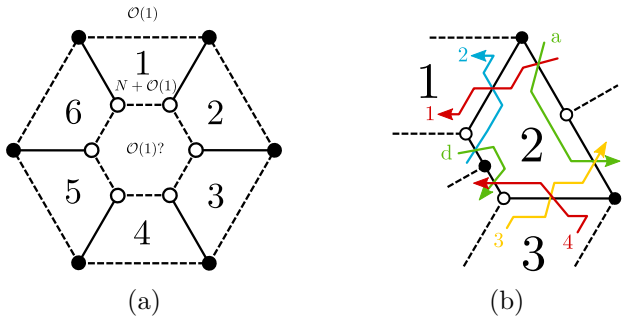

Figure 11.21: (a) Generic ring of rank $N+\mathcal{O}(1)$ surrounded by faces of rank $\mathcal{O}(1)$ with a hole of rank $\mathcal{O}(1)$. (b) Face 2 edges with zig-zag paths.

Consider a face of the ring, as face 2 in Figure 11.21b. The intersections between the ZZP 1, 2, 3, and 4 yield

$$N_1 - N_2 = v_1 - v_2 \sim 0\,, \quad N_2 - N_3 = v_4 - v_3 \sim 0\,, \tag{11.17}$$

where $\sim$ means "equal up to $\mathcal{O}(1)$". Since the hole is supposed to be of rank $\mathcal{O}(1)$, the intersections with Zig-Zags that separate it from the ring give

$$N \sim v_2 - v_d, \quad -N \sim v_d - v_4, \quad \Rightarrow \quad v_2 \sim v_4\,. \tag{11.18}$$

Changing the number of edges between face 2 and the hole can only be done by adding/removing pairs of edges and will not change the fact that

$$v_1 \sim v_2 \sim v_3 \sim v_4 \qquad \text{and} \qquad v_d \sim v_1 - N\,, \tag{11.19}$$

where v_d is understood as any ZZP that comes with the pair of edges added between the hole and face 2. One can repeat the reasoning for every face

of the ring and find that its internal edges will be always produced by ZZP $\sim v_1$. This is in contradiction with the presence of ZZP $v_d \sim v_1 - N$ since there are only ZZP $\sim v_1$ entering the hole. It implies that v_d is circular or not present. The first option is forbidden in dimer models and the second spoils the presence of the hole itself. Hence the presence of an anomaly-free hole inside such a ring is inconsistent.

As a comment, let us notice that to reach this conclusion we did not assume anything about the exterior of the ring. If one does not look at the hole but asks that the exterior has a reduced rank, it implies that ZZP v_a on its border, see Figure 11.21b, will satisfy

$$v_a \sim v_1 + N \sim v_3 + N \,, \tag{11.20}$$

and thus we recover the result of Equation (11.18) using Equation (11.17). Again, it can be shown that this result does not depend on the number of edges in contact with the exterior of the ring. The cluster (hexagonal or otherwise) is now viable only with ranks $N + \mathcal{O}(1)$, because it is made only of ZZP $\sim v_1$.

11.B Anomaly cancellation conditions for 3−2 quivers

Not all of the quivers presented in Figure 11.13 are free of anomalies when $N_i \neq 0$. In this appendix, we check this explicitly. Our calculations also motivate the choice of the antisymmetric tensor $\overline{A}_2$ to satisfy the ACC. Below we summarize the ACC for each of these models. For completeness, we added here as different cases also the two models where nodes 1 and 4 are identified.

- $SO(N_1+1) \times USp(N_2+2) \times SU(N_3+3)$ with $\square_3$:

$$\textbf{Node 3:}\quad (N_3+3-4) - (N_1+1) + (N_2+2) \;=\; 0\,. \tag{11.21}$$

- $SO(N_1+1) \times SU(N_2+2) \times SU(N_3+3)$ with $\overline{\square}_3$:

$$\begin{aligned} \textbf{Node 2:}\quad & -(N_2+2-4) + (N_1+1) - (N_3+3) \;=0\,, \\ \textbf{Node 3:}\quad & (N_3+3-4) - (N_1+1) + (N_2+2) \;=0\,. \end{aligned} \tag{11.22}$$

  Note that the choice of conjugate representation for the antisymmetric tensor of $SU(N_2+2)$ is fixed by the first equation, in order to satisfy it when all $N_i = 0$.

For these two first models, the ACC reduce to

$$N_1 = N_2 + N_3\,. \tag{11.23}$$

- $\underline{SO(N_1+1) \times USp(N_2+2) \times SU(N_3+3) \times SO(N_4+1)}$:

$$\textbf{Node 3:} \quad -(N_1+1) + (N_2+2) - (N_4+1) = 0\,. \tag{11.24}$$

In this case, N_3 is not constrained by the ACC, which can be rewritten as

$$N_2 = N_1 + N_4\,. \tag{11.25}$$

- $\underline{SO(N_1+1) \times SU(N_2+2) \times SU(N_3+3) \times SO(N_4+1)}$:

$$\begin{array}{rr} \textbf{Node 2:} & -(N_2+2-4) + (N_1+1) - (N_3+3) \;\; = 0\;, \\ \textbf{Node 3:} & -(N_1+1) + (N_2+2) - (N_4+1) \;\; = 0\;. \end{array} \tag{11.26}$$

This translates to the two conditions

$$\begin{array}{rl} N_1 = & N_2 + N_3\,, \\ N_2 = & N_1 + N_4\,, \end{array} \tag{11.27}$$

implying $N_3 = -N_4$. This in turn sets $N_3 = N_4 = 0$, since all N_i must be positive and potentially large. In principle this issue does not rule out the possible engineering of these models, since the corresponding dimers might give rise to additional gauge groups and fields when regular D3-branes are added, in a way that anomalies are cancelled. Assuming that at least some fractional branes are needed in order to turn on all the ranks of the $3-2$ model (*i.e.* even for $N_i = 0$), then such models are excluded.

- $\underline{SO(N_1+1) \times USp(N_2+2) \times SU(N_3+3) \text{ with } 2(\overline{\square}_3, \square_1)}$:

$$-2(N_1+1) + (N_2+2) = 0\,, \tag{11.28}$$

which is simply

$$N_2 = 2N_1\,. \tag{11.29}$$

- $\underline{SO(N_1+1) \times SU(N_2+2) \times SU(N_3+3) \text{ with } 2(\overline{\square}_3, \square_1)}$:

$$\begin{array}{rr} \textbf{Node 2:} & -(N_2+2-4) + (N_1+1) - (N_3+3) \;\; = 0\;, \\ \textbf{Node 3:} & -2(N_1+1) + (N_2+2) \;\; = 0\;. \end{array} \tag{11.30}$$

This can be simplified into

$$\begin{array}{rl} N_2 = & 2N_1\;, \\ N_3 = & -N_1\;, \end{array} \tag{11.31}$$

which has no solution beyond $N_i = 0$ in the absence of additional ingredients coming from the full dimer.

The results of this appendix can be summarized in Table 11.1.

Gauge theories	ACC
$SO(N_1+1) \times USp(N_2+2) \times SU(N_3+3)$ with $\square_3$	✓
$SO(N_1+1) \times SU(N_2+2) \times SU(N_3+3)$ with $\square_3$	✓
$SO(N_1+1) \times USp(N_2+2) \times SU(N_3+3) \times SO(N_4+4)$	✓
$SO(N_1+1) \times SU(N_2+2) \times SU(N_3+3) \times SO(N_4+4)$	✗
$SO(N_1+1) \times USp(N_2+2) \times SU(N_3+3)$ with $2(\overline{\square}_3, \square_1)$	✓
$SO(N_1+1) \times SU(N_2+2) \times SU(N_3+3)$ with $2(\overline{\square}_3, \square_1)$	✗

Table 11.1: List of $3-2$ model realizations and their ACC.

Chapter 12

The Octagon

In this chapter, we argue that stable DSB is in the landscape of string theory. We produce an orientifold of a toric singularity which allows for a brane configuration displaying a variant of the $SU(5)$ DSB model, dubbed the twin $SU(5)$ in the previous chapter, and that has no instabilities. In particular, those described in Chapter 10 are absent because the singularity does not admit $\mathcal{N} = 2$ fractional branes. This provides a counter-example to what could have been conjectured, namely that DSB models were possible only in singularities admitting $\mathcal{N} = 2$ fractional branes, and hence, following the no-go theorem presented in Chapter 10, unstable towards supersymmetric vacua. Our results were originally presented in [3, 4].

In Section 12.1 we show that such local construction can be embedded in a fully consistent singularity, the Octagon, and present the orientifold that leads to the twin $SU(5)$ model. We review the UV-complete supersymmetry breaking gauge theory associated with it and study its stability in the infrared in Section 12.2. Finally, we comment on the perspectives of our results in Section 12.3. Appendices 12.A and 12.B present an application of the Fast Forward Algorithm for the Octagon and complementary comments on the stability of the supersymmetry breaking vacuum respectively.

12.1 The rise of the Octagon

We have shown previously that the only alternative for an a priori consistent realization of a DSB model which does not automatically imply the presence of an $\mathcal{N} = 2$ fractional brane, and hence is potentially stable in the decoupling limit, is the twin $SU(5)$ living on a single fixed line of an

orientifold. The twin $SU(5)$ model is described by the hexagonal cluster in the dimer, reproduced in Figure 12.1. Now, we want to understand if such cluster can be embedded in a fully consistent dimer and if such dimer can be free of $\mathcal{N} = 2$ fractional branes.

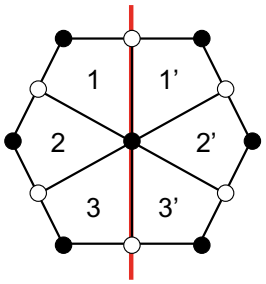

Figure 12.1: The hexagonal cluster with six faces on an orientifold line. All faces are here depicted with four edges, but some of them could have more.

Now we can ask whether this fractional brane is of deformation or runaway DSB type, in the parent theory (we already know we do not want it to be of $\mathcal{N} = 2$ type). If it were a runaway DSB brane some other regions of the dimer, besides the hexagon, would be populated and the corresponding faces would have ranks with different multiples of N [67, 68]. This is the key ingredient to generate an ADS superpotential and hence a runaway behavior, and this will still be true after orientifolding. Thus a runaway DSB brane in the parent theory, if it survives the orientifold, will still be of runaway type. Populating the dimer with regular branes, the runaway sector will communicate with the twin $SU(5)$ sector, destabilizing the vacuum. The other possibility is that the hexagonal cluster corresponds to a deformation brane in the parent theory and that it survives the orientifold projection.

It is known [67, 140] that deformation fractional branes are related to subset of ZZPs in equilibrium, see Chapter 6. We are looking for a dimer containing a six-valent node inside a cluster of faces. The corresponding toric diagram must contain at least 6 edges whose associated ZZPs are ordered around the relevant node [154, 157]. Those ZZPs need to be themselves in equilibrium, and once removed the rest of the (p, q)-web must be in equilibrium too. This implies that we need at least two extra ZZPs in equilibrium, for a total of eight. The absence of $\mathcal{N} = 2$ fractional branes in the dimer further requires that there cannot be more than one ZZP with a given winding (p, q) of the unit cell. This corresponds to toric diagrams with no more than two consecutive points which are aligned on an external edge.

Since we are looking for a singularity admitting line orientifolds, we consider toric diagrams with line symmetry, either vertical/horizontal or diagonal.

- Diagonal line

  From Figure 12.1 we see that we need two antisymmetric fields, in $\overline{\square}_1$ and $\square_3$ representations, respectively. Even if dimer models containing the required deformation can be engineered, it turns out that there is no solution to the ACC of the full dimer, as it happens for all the theories but a very special family, the *trapezoids*, which typically contains $\mathcal{N} = 2$ fractional branes obtained as orientifolds of dimers with a diagonal fixed line, see Chapter 8. Thus, such cases are excluded.

- Vertical/horizontal lines

  As discussed in Section 11.1, the freedom in choosing different charges for the two fixed lines is a crucial difference with respect to diagonal line orientifolds. In fact, it guarantees the existence of solutions to the ACC after orientifolding, exactly balancing the contribution from the different tensor fields. As discussed in Chapter 8, this is ensured by noticing that tensor fields come in pairs in the dimer, one in each of the two lines. Assigning opposite signs to the two lines grants that the two contributions cancel, yielding an anomaly-free theory. If the two signs are chosen the same, the situation is the same as with diagonal lines.

The upshot is that having vertical/horizontal lines, with opposite signs for the two orientifold lines, is the only option that can lead to viable twin $SU(5)$ models and it is what we are going to focus on in the following.

The need for two tensor fields is a stringent constraint on the ZZPs, and therefore on the toric diagram. In particular, it implies that two couples of ZZPs must have the correct intersection number among themselves and with the fixed lines, as computed from the toric diagram, see Chapters 6 and 8.

Remarkably, the aforementioned necessary conditions provide substantial guidance for where to look for a model that works, as we now explain. The simplest example of a toric diagram with the required eight ZZP, with the correct intersection numbers, no $\mathcal{N} = 2$ fractional branes and the necessary horizontal symmetry is the toric diagram depicted in Figure 12.2, that we dub *the Octagon*.

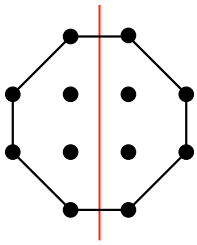

Figure 12.2: The toric diagram of the Octagon singularity.

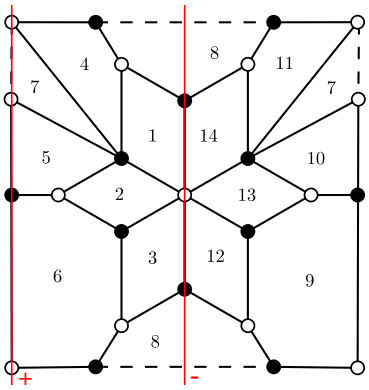

Figure 12.3: The (unit cell of the) dimer describing the symmetric phase of the Octagon. Orientifold lines are in red. Each orientifold line has a sign associated with it, which in this case needs to be opposite one another.

Using standard techniques one can associate a dimer to a toric diagram, one for each different toric phase [32, 46]. A generic toric phase does not display the symmetry required to perform the orientifold projection. In the present case, however, one can find a symmetric toric phase where the vertical fixed lines are manifest and which realizes the twin $SU(5)$ model as described above. The corresponding dimer is depicted in Figure 12.3, where the hexagonal cluster is described by the white dot in the center of the unit cell. A quick and direct way to check that the dimer in Figure 12.3 does correspond to the toric diagram in Figure 12.2 is by the Fast Forward Algorithm [46], as detailed in Appendix 12.A.

Before performing the orientifold projection, it is straightforward to see that the following rank assignment is anomaly-free: faces $1, 2, 3, 7, 12, 13$ and 14 have gauge group $SU(N+M)$, and all the others have gauge group $SU(N)$. Setting $N = 0$, one has only seven $SU(M)$ gauge groups: one isolated Super-Yang-Mills (SYM) on face 7 and the six others forming a loop whose links are bi-fundamentals, together with a sextic superpotential

proportional to the only gauge-invariant (it is represented by the white dot in the center of the unit cell). This rank assignment corresponds to a so-called deformation fractional brane [67], as expected. One can easily see that such a gauge theory eventually leads to a confining behavior just like SYM. This can be naturally UV-complete starting from a system of N regular and M fractional D3-branes which trigger an RG-flow that can be described by a duality cascade, similar to [27] and many other examples that were found since then. The effective number of regular branes diminishes along with the flow and the deep IR dynamics is described by fractional branes only.

In the presence of an orientifold projection, it is no longer granted that an anomaly-free rank assignment exists at all. For instance, in the present case, it can be shown that it is not possible to find one if the signs of the two lines are the same, in agreement with the results of Chapter 8. However, choosing opposite signs as in Figure 12.3, one can see that there is a rank assignment that is anomaly-free: $SU(N+M+4)$ for faces 1 and 3, $SU(N+M)$ for face 2, $SO(N+M+4)$ for face 7, $SU(N)$ for faces 4, 5 and 6, and $USp(N)$ for face 8. Setting $N=0$ we obtain a gauge theory with an isolated $SO(M+4)_7$ SYM together with a quiver gauge theory based on the group $SU(M+4)_1 \times SU(M)_2 \times SU(M+4)_3$ with matter fields and a superpotential that we proceed to analyze in-depth in the next section. See Figure 12.4 to visualize the deformation brane on the dimer model. The twin $SU(5)$ model is given by the rank assignment $SU(5)_1 \times SU(1)_2 \times SU(5)_3$ with all other faces being empty but face 7 which is a decoupled pure SYM with gauge group $SO(5)$ and hence confines on its own.

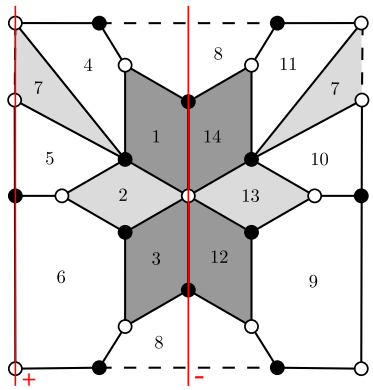

Figure 12.4: Dimer diagram of the Octagon with the deformation brane in grey. Red lines represent the orientifold lines.

12.2 Dynamical supersymmetry breaking on the Octagon

12.2.1 The UV-complete model

The gauge theory

$$SU(M+4)_1 \times SU(M)_2 \times SU(M+4)_3 \tag{12.1}$$

has matter content

$$A_1 = \square_1,\ X_{12} = (\overline{\square}_1, \square_2),\ X_{23} = (\overline{\square}_2, \square_3),\ A_3 = \overline{\square}_3\,, \tag{12.2}$$

and superpotential

$$W = A_1 X_{12} X_{23} A_3 X_{23}^T X_{12}^T\,. \tag{12.3}$$

The superpotential can be interpreted as follows. The gauge-invariant $X_{12}^T A_1 X_{12}$ of group 1 and the gauge-invariant $X_{23} A_3 X_{23}^T$ of group 3 are respectively in the $\square_2$ and $\overline{\square}_2$ of gauge group 2, with the superpotential above providing a bilinear in these two invariants, thus akin to a mass term. It is obvious that the antisymmetrics of $SU(M)_2$ can exist as such only if $M \geq 2$. In this case, one can show that strongly coupled dynamics generates superpotential terms that, together with the tree-level one, eventually lead to supersymmetric vacua. For $M = 0$ one gets instead two decoupled theories at faces 1 and 3 both having gauge group $SU(4)$ and one chiral superfield in the antisymmetric, which have a runaway behavior. The case of interest is of course $M = 1$.

For $M = 1$, we recover the twin $SU(5)$ model. Node 2 becomes trivial ($SU(1)$ is empty) and, more importantly, the superpotential actually vanishes. Indeed, both nodes 1 and 3 are $SU(5)$ gauge theories with matter in the $\square \oplus \overline{\square}$ representations, and there is no chiral gauge-invariant that can be written in this situation [71]. Hence the two gauge theories are effectively decoupled, and their IR behavior can be established independently. Both happen to be the $SU(5)$ model for stable DSB. Since the $SO(5)$ SYM on node 7 just confines, we thus determine that this configuration displays DSB in its vacuum. Quite interestingly, this DSB vacuum may then arise at the bottom of a duality cascade (possibly more complicated with respect to the simpler unorientifolded case, due to the orientifold projection which would modify it, see [55]), hence within a stringy UV-complete theory.

12.2.2 Stability in the infrared

Is this DSB vacuum stable? In principle, there can be different sources of potential instabilities.

First, one could be concerned about stringy instantons, whose presence may affect the low energy dynamics. Indeed, the D-brane configuration giving rise to the twin $SU(5)$ DSB model, $N = 0, M = 1$, contains both a $USp(0)$ and an $SU(1)$ factor coupling to the $SU(5)$ gauge groups. These are the two instances where contributions to the low energy effective superpotential are allowed (see [56] and [200], respectively). However, no such contributions can be generated in our model simply because there are no chiral gauge-invariants that can be written which can contribute to the superpotential. We thus conclude that stringy instantons cannot alter the DSB dynamics.

A second source of instability is the one discussed in [74] and Chapter 10. In fact, as can be readily seen from the toric diagram of Figure 12.2, this singularity does not admit $\mathcal{N} = 2$ fractional branes. The latter arise when the singularity can be partially resolved to display, locally, a non-isolated $\mathbb{C}^2/\mathbb{Z}_n$ singularity and a Coulomb-like branch associated with it. This translates into the presence of points inside some of the edges along the boundary of the toric diagram. The Octagon does not have this property. Hence, without the presence of $\mathcal{N} = 2$ fractional branes, there is no vacuum expectation value on which the energy of the DSB vacuum can depend, or equivalently there is no Coulomb branch along which the energy can slide to zero value.

The attentive reader might note that, given a singularity free of any $\mathcal{N} = 2$ fractional brane directions, there can exist partial resolutions which generate a different singularity which admits non-isolated singularities. The Octagon is no exception. However, the fractional brane configuration we consider and the orientifold projection, both instrumental to our DSB model, obstruct such dangerous resolutions [198]. See Appendix 12.B for more details on this point.

A final source of instability may come from the $\mathcal{N} = 4$ Coulomb branch represented by regular D3-branes. As in the previously analyzed cases of Chapter 10, one can easily show that this is a non-supersymmetric flat direction, essentially because of the conformality of the parent (non-orientifolded, large N) gauge theory. Therefore, there are no supersymmetric vacua along this branch.[1]

[1]Flat directions are usually not expected in a non-supersymmetric vacuum. Subleading $1/N$ corrections to anomalous dimensions of matter fields, which could lift such flat

12.3 Conclusions

In this chapter, we have presented a model, based on the Octagon, which is the first instance, to our knowledge, of a stable DSB configuration of fractional branes. The Octagon emerges as the simplest possible dimer having all required properties to admit, upon orientifolding, stable DSB D-brane configurations. One might ask whether less minimal models exist which share the same properties. Given the remarkable properties of this family of models, we consider it important to study them in further detail. We do not have an answer to this question, yet. Still, dimer techniques have (once again) proven to be a very powerful tool to provide a direct link between geometry and gauge theories dynamics, both in finding no-go theorems, like the one presented in Chapter 10 or the connection between minimal $SU(5)$ and $3-2$ models and the presence of $\mathcal{N}=2$ fractional branes established Chapter 11, as well as in unveiling concrete ways to evade them. Therefore, we cannot exclude that further surprises are possible and generalizations of the Octagon model will eventually be found.

In particular, we would also like to find other types of DSB models from dimers with possibly higher ranks and, as such, a higher number of fractional branes in their string theory realization. They are of interest since the gauge-gravity correspondence may then provide a reliable supergravity solution to study dynamical supersymmetry breaking from another viewpoint than QFT. Indeed, we would access the decoupling limit that ensures a valid description of our model in a supergravity regime all the way down to the infrared, where the interesting dynamical phenomenon occurs.

Finally, we remark that it seems possible to extend the computations shown in Appendix 12.B to any kind of fractional branes living on a toric CY variety. It would be interesting to find geometric criteria for the singularity, along the lines of Chapter 8, to determine whether its fractional branes obstruct certain partial resolutions, in the absence and presence of orientifold plane.

direction, are not easily calculable, particularly in a complicated singularity such as the Octagon. However, they should neither change the number of supersymmetric vacua nor modify the behavior of the potential at infinity, at least for sufficiently large N.

12.A The Octagon and its symmetric phase

As discussed in Chapter 6, to any dimer model one can associate a weighted, signed adjacency matrix, known as the Kasteleyn matrix, whose determinant is the characteristic polynomial of the dimer model from which one can extract the toric data. This procedure is known as the Fast Forward Algorithm.

To obtain the Kasteleyn matrix one assigns a sign to every edge such that for every face in the dimer the product of signs is $+1$ if its number of edges is $2 \bmod 4$ and -1 if its number of edges is $0 \bmod 4$. One then constructs two closed oriented (gauge-invariant) paths γ_w, γ_z with holonomy $(0,1)$ and $(1,0)$. Every edge crossed by these paths is multiplied by w or $1/w$, depending on the relative orientation (respectively by z or $1/z$). The resulting graph for the Octagon is shown in Figure 12.5.

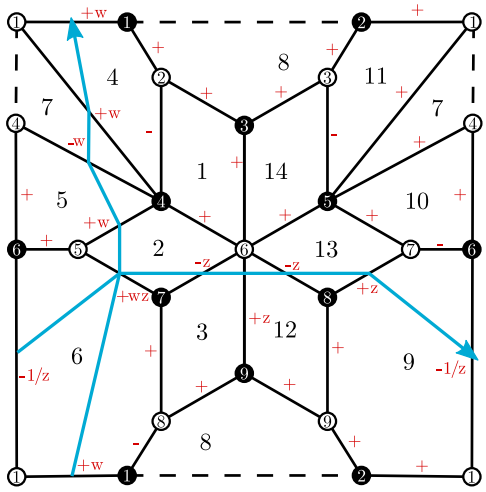

Figure 12.5: Dimer diagram of the Octagon with weights (in red) for building the Kasteleyn matrix. White and black nodes have been numbered. Two fundamental paths are shown in blue.

The adjacency matrix of the graph with such weights is the Kasteleyn Matrix and, for the Octagon, it reads

$$K = \left(\begin{array}{c|ccccccccc} & 1 & 2 & 3 & 4 & 5 & 6 & 7 & 8 & 9 \\ \hline 1 & w & 1 & 0 & w & 1 & -\frac{1}{z} & 0 & 0 & 0 \\ 2 & 1 & 0 & 1 & -1 & 0 & 0 & 0 & 0 & 0 \\ 3 & 0 & 1 & 1 & 0 & -1 & 0 & 0 & 0 & 0 \\ 4 & 0 & 0 & 0 & -w & 1 & 1 & 0 & 0 & 0 \\ 5 & 0 & 0 & 0 & w & 0 & 1 & wz & 0 & 0 \\ 6 & 0 & 0 & 1 & 1 & 1 & 0 & -z & -z & z \\ 7 & 0 & 0 & 0 & 0 & 1 & -1 & 0 & z & 0 \\ 8 & -1 & 0 & 0 & 0 & 0 & 0 & 1 & 0 & 1 \\ 9 & 0 & 1 & 0 & 0 & 0 & 0 & 0 & 1 & 1 \end{array}\right) \tag{12.4}$$

where rows and columns correspond to white and black nodes in the dimer, respectively. Its determinant is

$$\det K = w^3z^2+w^3z+w^2z^3-24w^2z^2+26w^2z-w^2+wz^3+24wz^2+26wz+w-z^2+z\ . \tag{12.5}$$

One may compute the Newton Polygon of the above expression and it should correspond to the toric diagram of the dimer one is dealing with [45]. For every monomial $a\ w^b z^c$ one draws a point in a $2d$ lattice with coordinates (b, c). As expected, one obtains the toric diagram depicted in Figure 12.2. Nicely, there is a single perfect matching for each of its external points, thus ensuring that the dimer meets a necessary condition of minimality.

12.B Partial resolutions of the Octagon

In Figure 12.6 we depict the toric diagram of the Octagon singularity and the corresponding dimer diagram with the fractional brane configuration which gives rise, upon orientifolding, to our DSB model. The rank assignments are as specified in Section 12.2. Neighboring faces with different colors indicate the fact that the gauge groups are different in the considered configuration.

We list in Figure 12.7 the first partial resolutions of the Octagon that preserve the orientifold symmetry (following [73], the resulting toric diagram has to remain symmetric with respect to the orientifold line) and allow for the presence of $\mathcal{N} = 2$ fractional branes. Further partial resolutions consistent with the orientifold projection inexorably lead to orbifolds of the conifold, for which our comments on the case of Figure 12.7c (see below) will remain valid.

The corresponding dimer diagrams are obtained following Gulotta's algorithm [157] and are presented in Figure 12.8. The algorithm operates

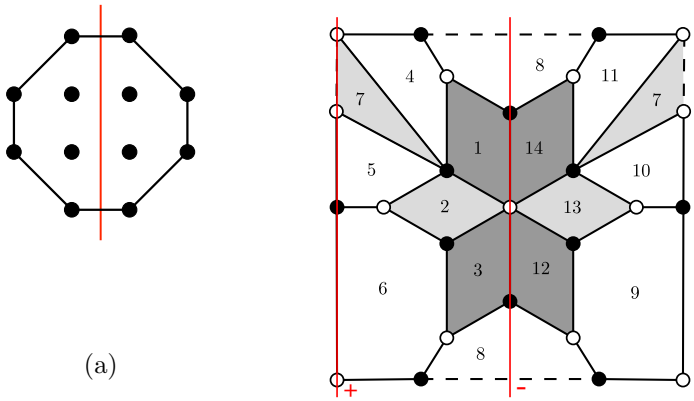

Figure 12.6: The Octagon: (a) Toric diagram. (b) Dimer diagram with the deformation brane in grey. Red lines represent the orientifold lines.

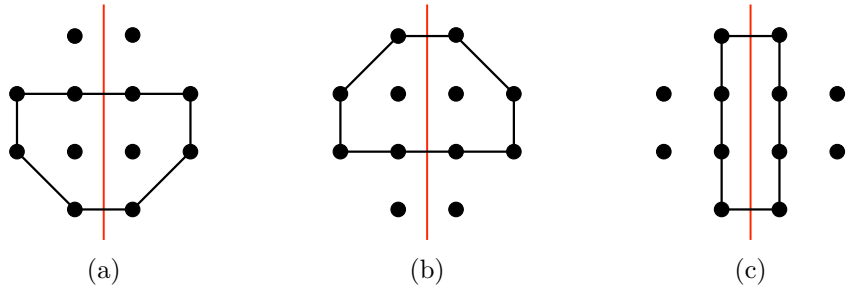

Figure 12.7: First partial resolutions of the orientifolded Octagon admitting $\mathcal{N} = 2$ fractional branes.

the partial resolution by "merging" some zig-zag paths within the dimer diagram of Figure 12.6b. This action is equivalent to assigning a VEV to the edges on which these zig-zag paths cross each other.

In the cases of Figure 12.8a and Figure 12.8b, we see that the partial resolution is in obstruction with the very nature of our deformation brane because it implies the fusion of faces of different ranks already at the level of the non-orientifolded theory. In the case of Figure 12.8c, instead, the partial resolution is obstructed because it is obtained giving a VEV to edges separating faces of ranks that differ by the orientifold charge, for example, the edge separating faces 1 and 2.

Therefore, we conclude that any partial resolution of the Octagon singularity which opens up $\mathcal{N} = 2$ fractional brane directions is indeed obstructed in our model.

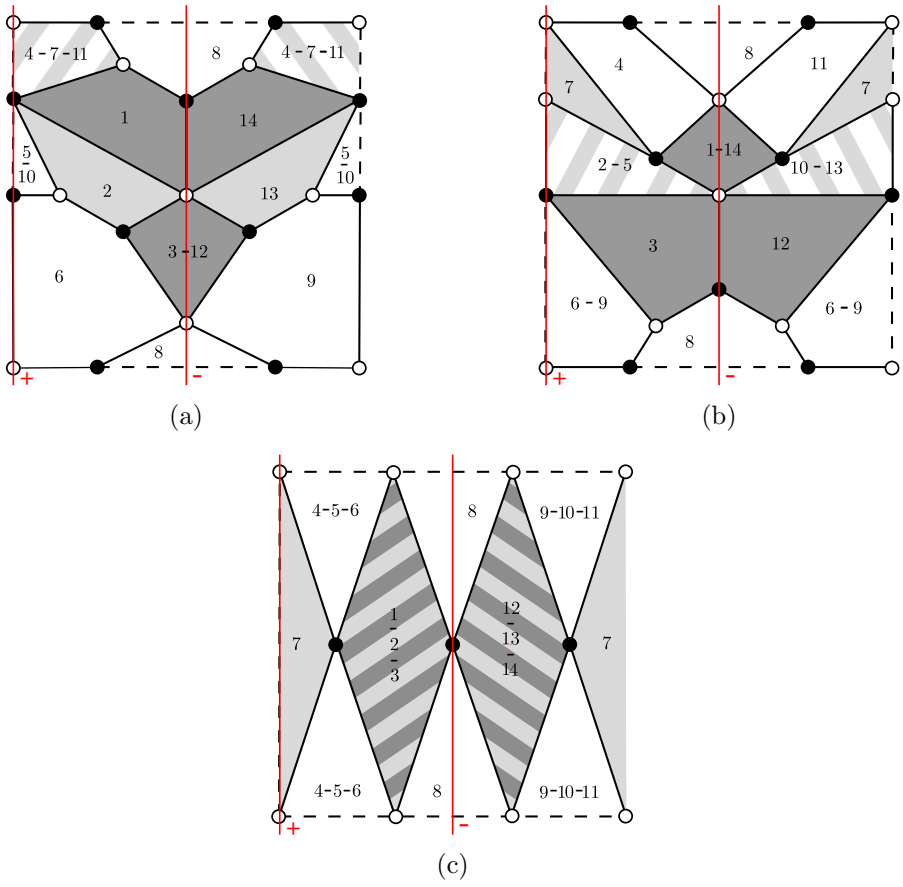

Figure 12.8: Dimer diagrams after partial resolutions.

Bibliography

[1] R. Argurio, D. Naegels, and A. Pasternak, *Are there Goldstone bosons in $d \leq z + 1$?*, *Phys. Rev. D* **100** (2019), no. 6 066002, [arXiv:1903.11417].

[2] R. Argurio, M. Bertolini, S. Meynet, and A. Pasternak, *On supersymmetry breaking vacua from D-branes at orientifold singularities*, *JHEP* **12** (2019) 145, [arXiv:1909.04682].

[3] R. Argurio, M. Bertolini, S. Franco, E. García-Valdecasas, S. Meynet, A. Pasternak, and V. Tatitscheff, *The Octagon and the Non-Supersymmetric String Landscape*, *Phys. Lett. B* **815** (2021) 136153, [arXiv:2005.09671].

[4] R. Argurio, M. Bertolini, S. Franco, E. García-Valdecasas, S. Meynet, A. Pasternak, and V. Tatitscheff, *Dimers, Orientifolds and Stability of Supersymmetry Breaking Vacua*, *JHEP* **01** (2021) 061, [arXiv:2007.13762].

[5] R. Argurio, M. Bertolini, S. Franco, E. García-Valdecasas, S. Meynet, A. Pasternak, and V. Tatitscheff, *Dimers, Orientifolds and Anomalies*, *JHEP* **02** (2021) 153, [arXiv:2009.11291].

[6] E. García-Valdecasas, S. Meynet, A. Pasternak, and V. Tatitscheff, *Dimers in a Bottle*, *JHEP* **04** (2021) 274, [arXiv:2101.02670].

[7] B. Zumino, *Supersymmetry then and now*, *Fortsch. Phys.* **54** (2006) 199–204, [hep-th/0508127].

[8] G. Veneziano, *Construction of a crossing - symmetric, Regge behaved amplitude for linearly rising trajectories*, *Nuovo Cim. A* **57** (1968) 190–197.

[9] D. J. Gross and F. Wilczek, *Ultraviolet Behavior of Nonabelian Gauge Theories*, *Phys. Rev. Lett.* **30** (1973) 1343–1346.

[10] H. D. Politzer, *Reliable Perturbative Results for Strong Interactions?*, *Phys. Rev. Lett.* **30** (1973) 1346–1349.

[11] J. Scherk and J. H. Schwarz, *Dual Models for Nonhadrons*, *Nucl. Phys. B* **81** (1974) 118–144.

[12] T. Yoneya, *Connection of Dual Models to Electrodynamics and Gravidynamics*, *Prog. Theor. Phys.* **51** (1974) 1907–1920.

[13] F. Gliozzi, J. Scherk, and D. I. Olive, *Supersymmetry, Supergravity Theories and the Dual Spinor Model*, *Nucl. Phys. B* **122** (1977) 253–290.

[14] M. B. Green and J. H. Schwarz, *Supersymmetrical string theories*, *Physics Letters B* **109** (1982), no. 6 444–448.

[15] M. B. Green and J. H. Schwarz, *Anomaly Cancellation in Supersymmetric D=10 Gauge Theory and Superstring Theory*, *Phys. Lett. B* **149** (1984) 117–122.

[16] D. J. Gross, J. A. Harvey, E. Martinec, and R. Rohm, *Heterotic string*, *Phys. Rev. Lett.* **54** (Feb, 1985) 502–505.

[17] P. Candelas, G. T. Horowitz, A. Strominger, and E. Witten, *Vacuum Configurations for Superstrings*, *Nucl. Phys. B* **258** (1985) 46–74.

[18] E. Witten, *String theory dynamics in various dimensions*, *Nucl. Phys. B* **443** (1995) 85–126, [hep-th/9503124].

[19] J. Dai, R. Leigh, and J. Polchinski, *New Connections Between String Theories*, *Mod. Phys. Lett. A* **4** (1989) 2073–2083.

[20] P. Horava, *Background Duality of Open String Models*, *Phys. Lett. B* **231** (1989) 251–257.

[21] J. M. Maldacena, *The Large N limit of superconformal field theories and supergravity*, *Int. J. Theor. Phys.* **38** (1999) 1113–1133, [hep-th/9711200].

[22] E. Witten, *Anti-de Sitter space and holography*, *Adv. Theor. Math. Phys.* **2** (1998) 253–291, [hep-th/9802150].

[23] S. S. Gubser, I. R. Klebanov, and A. M. Polyakov, *Gauge theory correlators from noncritical string theory*, *Phys. Lett. B* **428** (1998) 105–114, [hep-th/9802109].

[24] I. R. Klebanov and E. Witten, *Superconformal field theory on three-branes at a Calabi-Yau singularity*, *Nucl. Phys. B* **536** (1998) 199–218, [hep-th/9807080].

[25] I. R. Klebanov and N. A. Nekrasov, *Gravity duals of fractional branes and logarithmic RG flow*, *Nucl. Phys. B* **574** (2000) 263–274, [hep-th/9911096].

[26] I. R. Klebanov and A. A. Tseytlin, *Gravity duals of supersymmetric SU(N) x SU(N+M) gauge theories*, *Nucl. Phys. B* **578** (2000) 123–138, [hep-th/0002159].

[27] I. R. Klebanov and M. J. Strassler, *Supergravity and a confining gauge theory: Duality cascades and chi SB resolution of naked singularities*, *JHEP* **08** (2000) 052, [hep-th/0007191].

[28] J. P. Gauntlett, D. Martelli, J. Sparks, and D. Waldram, *Sasaki-Einstein metrics on S**2 x S**3*, *Adv. Theor. Math. Phys.* **8** (2004), no. 4 711–734, [hep-th/0403002].

[29] M. Bertolini, F. Bigazzi, and A. Cotrone, *New checks and subtleties for AdS/CFT and a-maximization*, *JHEP* **12** (2004) 024, [hep-th/0411249].

[30] S. Benvenuti, S. Franco, A. Hanany, D. Martelli, and J. Sparks, *An Infinite family of superconformal quiver gauge theories with Sasaki-Einstein duals*, *JHEP* **06** (2005) 064, [hep-th/0411264].

[31] M. Cvetic, H. Lu, D. N. Page, and C. Pope, *New Einstein-Sasaki spaces in five and higher dimensions*, *Phys. Rev. Lett.* **95** (2005) 071101, [hep-th/0504225].

[32] S. Franco, A. Hanany, D. Martelli, J. Sparks, D. Vegh, and B. Wecht, *Gauge theories from toric geometry and brane tilings*, *JHEP* **01** (2006) 128, [hep-th/0505211].

[33] A. Butti, D. Forcella, and A. Zaffaroni, *The Dual superconformal theory for L**pqr manifolds*, *JHEP* **09** (2005) 018, [hep-th/0505220].

[34] G. Aldazabal, L. E. Ibanez, F. Quevedo, and A. Uranga, *D-branes at singularities: A Bottom up approach to the string embedding of the standard model*, *JHEP* **08** (2000) 002, [hep-th/0005067].

[35] D. Berenstein, V. Jejjala, and R. G. Leigh, *The Standard model on a D-brane*, *Phys. Rev. Lett.* **88** (2002) 071602, [hep-ph/0105042].

[36] H. Verlinde and M. Wijnholt, *Building the standard model on a D3-brane*, *JHEP* **01** (2007) 106, [hep-th/0508089].

[37] M. Buican, D. Malyshev, D. R. Morrison, H. Verlinde, and M. Wijnholt, *D-branes at Singularities, Compactification, and Hypercharge*, *JHEP* **01** (2007) 107, [hep-th/0610007].

[38] D. Malyshev and H. Verlinde, *D-branes at singularities and string phenomenology*, *Nucl. Phys. B Proc. Suppl.* **171** (2007) 139–163, [arXiv:0711.2451].

[39] B. Feng, A. Hanany, and Y.-H. He, *D-brane gauge theories from toric singularities and toric duality*, *Nucl. Phys. B* **595** (2001) 165–200, [hep-th/0003085].

[40] B. Feng, A. Hanany, and Y.-H. He, *Phase structure of D-brane gauge theories and toric duality*, *JHEP* **08** (2001) 040, [hep-th/0104259].

[41] C. E. Beasley and M. Plesser, *Toric duality is Seiberg duality*, *JHEP* **12** (2001) 001, [hep-th/0109053].

[42] B. Feng, A. Hanany, Y.-H. He, and A. M. Uranga, *Toric duality as Seiberg duality and brane diamonds*, *JHEP* **12** (2001) 035, [hep-th/0109063].

[43] B. Feng, S. Franco, A. Hanany, and Y.-H. He, *Symmetries of toric duality*, *JHEP* **12** (2002) 076, [hep-th/0205144].

[44] D. Berenstein and M. R. Douglas, *Seiberg duality for quiver gauge theories*, hep-th/0207027.

[45] A. Hanany and K. D. Kennaway, *Dimer models and toric diagrams*, hep-th/0503149.

[46] S. Franco, A. Hanany, K. D. Kennaway, D. Vegh, and B. Wecht, *Brane dimers and quiver gauge theories*, *JHEP* **01** (2006) 096, [hep-th/0504110].

[47] A. Sagnotti, *Open Strings and their Symmetry Groups*, in *NATO Advanced Summer Institute on Nonperturbative Quantum Field Theory (Cargese Summer Institute)*, pp. 0521–528, 9, 1987. hep-th/0208020.

[48] G. Pradisi and A. Sagnotti, *Open String Orbifolds*, *Phys. Lett. B* **216** (1989) 59–67.

[49] P. Horava, *Strings on World Sheet Orbifolds*, *Nucl. Phys. B* **327** (1989) 461–484.

[50] M. Bianchi and A. Sagnotti, *On the systematics of open string theories*, *Phys. Lett. B* **247** (1990) 517–524.

[51] M. Bianchi and A. Sagnotti, *Twist symmetry and open string Wilson lines*, *Nucl. Phys. B* **361** (1991) 519–538.

[52] E. G. Gimon and J. Polchinski, *Consistency conditions for orientifolds and d manifolds*, *Phys. Rev. D* **54** (1996) 1667–1676, [hep-th/9601038].

[53] M. R. Douglas and G. W. Moore, *D-branes, quivers, and ALE instantons*, hep-th/9603167.

[54] S. Franco, A. Hanany, D. Krefl, J. Park, A. M. Uranga, and D. Vegh, *Dimers and orientifolds*, *JHEP* **09** (2007) 075, [arXiv:0707.0298].

[55] R. Argurio and M. Bertolini, *Orientifolds and duality cascades: confinement before the wall*, *JHEP* **02** (2018) 149, [arXiv:1711.08983].

[56] R. Argurio, M. Bertolini, G. Ferretti, A. Lerda, and C. Petersson, *Stringy instantons at orbifold singularities*, *JHEP* **06** (2007) 067, [arXiv:0704.0262].

[57] M. Bianchi, F. Fucito, and J. F. Morales, *D-brane instantons on the T**6 / Z(3) orientifold*, *JHEP* **07** (2007) 038, [arXiv:0704.0784].

[58] R. Blumenhagen, M. Cvetic, S. Kachru, and T. Weigand, *D-Brane Instantons in Type II Orientifolds*, *Ann. Rev. Nucl. Part. Sci.* **59** (2009) 269–296, [arXiv:0902.3251].

[59] M. Bertolini, P. Di Vecchia, M. Frau, A. Lerda, R. Marotta, and I. Pesando, *Fractional D-branes and their gauge duals*, *JHEP* **02** (2001) 014, [hep-th/0011077].

[60] J. Polchinski, *N=2 Gauge / gravity duals*, *Int. J. Mod. Phys. A* **16** (2001) 707–718, [hep-th/0011193].

[61] M. Bertolini, P. Di Vecchia, G. Ferretti, and R. Marotta, *Fractional branes and N=1 gauge theories*, *Nucl. Phys. B* **630** (2002) 222–240, [hep-th/0112187].

[62] S. Kachru, J. Pearson, and H. L. Verlinde, *Brane / flux annihilation and the string dual of a nonsupersymmetric field theory*, *JHEP* **06** (2002) 021, [hep-th/0112197].

[63] S. Franco and A. M. . Uranga, *Dynamical SUSY breaking at meta-stable minima from D-branes at obstructed geometries*, *JHEP* **06** (2006) 031, [hep-th/0604136].

[64] R. Argurio, M. Bertolini, S. Franco, and S. Kachru, *Gauge/gravity duality and meta-stable dynamical supersymmetry breaking*, *JHEP* **01** (2007) 083, [hep-th/0610212].

[65] R. Argurio, M. Bertolini, S. Franco, and S. Kachru, *Meta-stable vacua and D-branes at the conifold*, *JHEP* **06** (2007) 017, [hep-th/0703236].

[66] D. Berenstein, C. Herzog, P. Ouyang, and S. Pinansky, *Supersymmetry breaking from a Calabi-Yau singularity*, *JHEP* **09** (2005) 084, [hep-th/0505029].

[67] S. Franco, A. Hanany, F. Saad, and A. M. Uranga, *Fractional branes and dynamical supersymmetry breaking*, *JHEP* **01** (2006) 011, [hep-th/0505040].

[68] M. Bertolini, F. Bigazzi, and A. Cotrone, *Supersymmetry breaking at the end of a cascade of Seiberg dualities*, *Phys. Rev. D* **72** (2005) 061902, [hep-th/0505055].

[69] K. A. Intriligator and N. Seiberg, *The Runaway quiver*, *JHEP* **02** (2006) 031, [hep-th/0512347].

[70] R. Argurio, M. Bertolini, C. Closset, and S. Cremonesi, *On Stable non-supersymmetric vacua at the bottom of cascading theories*, *JHEP* **09** (2006) 030, [hep-th/0606175].

[71] I. Affleck, M. Dine, and N. Seiberg, *Dynamical Supersymmetry Breaking in Chiral Theories*, *Phys. Lett. B* **137** (1984) 187.

[72] A. Retolaza and A. Uranga, *De Sitter Uplift with Dynamical Susy Breaking*, *JHEP* **04** (2016) 137, [arXiv:1512.06363].

[73] A. Retolaza and A. Uranga, *Orientifolds of Warped Throats from Toric Calabi-Yau Singularities*, *JHEP* **07** (2016) 135, [arXiv:1605.01732].

[74] G. Buratti, E. Garcia-Valdecasas, and A. M. Uranga, *Supersymmetry Breaking Warped Throats and the Weak Gravity Conjecture*, *JHEP* **04** (2019) 111, [arXiv:1810.07673].

[75] S. B. Giddings, S. Kachru, and J. Polchinski, *Hierarchies from fluxes in string compactifications*, *Phys. Rev. D* **66** (2002) 106006, [hep-th/0105097].

[76] C. Vafa, *The String landscape and the swampland*, hep-th/0509212.

[77] T. D. Brennan, F. Carta, and C. Vafa, *The String Landscape, the Swampland, and the Missing Corner*, *PoS* **TASI2017** (2017) 015, [arXiv:1711.00864].

[78] E. Palti, *The Swampland: Introduction and Review*, *Fortsch. Phys.* **67** (2019), no. 6 1900037, [arXiv:1903.06239].

[79] K. A. Intriligator and N. Seiberg, *Lectures on supersymmetric gauge theories and electric-magnetic duality*, *Subnucl. Ser.* **34** (1997) 237–299, [hep-th/9509066].

[80] E. Poppitz and S. P. Trivedi, *Dynamical supersymmetry breaking*, *Ann. Rev. Nucl. Part. Sci.* **48** (1998) 307–350, [hep-th/9803107].

[81] Y. Shadmi and Y. Shirman, *Dynamical supersymmetry breaking*, *Rev. Mod. Phys.* **72** (2000) 25–64, [hep-th/9907225].

[82] J. Terning, *TASI 2002 lectures: Nonperturbative supersymmetry*, in *Theoretical Advanced Study Institute in Elementary Particle Physics (TASI 2002): Particle Physics and Cosmology: The Quest for Physics Beyond the Standard Model(s)*, 6, 2003. hep-th/0306119.

[83] Y. Shadmi, *Supersymmetry breaking*, in *Les Houches Summer School on Theoretical Physics: Session 84: Particle Physics Beyond the Standard Model*, 1, 2006. hep-th/0601076.

[84] K. A. Intriligator and N. Seiberg, *Lectures on Supersymmetry Breaking*, *Class. Quant. Grav.* **24** (2007) S741–S772, [hep-ph/0702069].

[85] V. A. Novikov, M. A. Shifman, A. I. Vainshtein, and V. I. Zakharov, *Exact Gell-Mann-Low Function of Supersymmetric Yang-Mills Theories from Instanton Calculus*, *Nucl. Phys. B* **229** (1983) 381–393.

[86] V. A. Novikov, M. A. Shifman, A. I. Vainshtein, and V. I. Zakharov, *The beta function in supersymmetric gauge theories. Instantons versus traditional approach*, *Phys. Lett. B* **166** (1986) 329–333.

[87] C. P. Herzog, I. R. Klebanov, and P. Ouyang, *Remarks on the warped deformed conifold*, in *Modern Trends in String Theory: 2nd Lisbon School on g Theory Superstrings*, 8, 2001. `hep-th/0108101`.

[88] K. A. Intriligator and B. Wecht, *The Exact superconformal R symmetry maximizes a*, *Nucl. Phys. B* **667** (2003) 183–200, [`hep-th/0304128`].

[89] N. Seiberg, *The Power of holomorphy: Exact results in 4-D SUSY field theories*, in *Particles, Strings, and Cosmology (PASCOS 94)*, 5, 1994. `hep-th/9408013`.

[90] G. 't Hooft, *Naturalness, Chiral Symmetry, and Spontaneous Chiral Symmetry Breaking*, in *Recent Developments in Gauge Theories*, vol. 59 of *NATO Advanced Study Institutes Series (Series B. Physics)*, pp. 135–157. Springer, Boston, MA, 1980.

[91] N. Seiberg, *Electric - magnetic duality in supersymmetric nonAbelian gauge theories*, *Nucl. Phys. B* **435** (1995) 129–146, [`hep-th/9411149`].

[92] Y. Meurice and G. Veneziano, *SUSY VACUA VERSUS CHIRAL FERMIONS*, *Phys. Lett. B* **141** (1984) 69–72.

[93] H. Murayama, *Studying noncalculable models of dynamical supersymmetry breaking*, *Phys. Lett. B* **355** (1995) 187–192, [`hep-th/9505082`].

[94] I. Affleck, M. Dine, and N. Seiberg, *Dynamical Supersymmetry Breaking in Four-Dimensions and Its Phenomenological Implications*, *Nucl. Phys. B* **256** (1985) 557–599.

[95] M. B. Green, J. H. Schwarz, and E. Witten, *SUPERSTRING THEORY. VOL. 1: INTRODUCTION*. Cambridge Monographs on Mathematical Physics. 7, 1988.

[96] M. B. Green, J. H. Schwarz, and E. Witten, *Superstring Theory Vol. 2: 25th Anniversary Edition*. Cambridge Monographs on Mathematical Physics. Cambridge University Press, 11, 2012.

[97] J. Polchinski, *String theory. Vol. 1: An introduction to the bosonic string*. Cambridge Monographs on Mathematical Physics. Cambridge University Press, 12, 2007.

[98] J. Polchinski, *String theory. Vol. 2: Superstring theory and beyond.* Cambridge Monographs on Mathematical Physics. Cambridge University Press, 12, 2007.

[99] B. Zwiebach, *A first course in string theory.* Cambridge University Press, 7, 2006.

[100] K. Becker, M. Becker, and J. H. Schwarz, *String theory and M-theory: A modern introduction.* Cambridge University Press, 12, 2006.

[101] L. E. Ibanez and A. M. Uranga, *String theory and particle physics: An introduction to string phenomenology.* Cambridge University Press, 2, 2012.

[102] R. Szabo, *An Introduction to String Theory and D-Brane Dynamics.* Advanced Textbooks in Physics. WSP, 2, 2020.

[103] J. Polchinski, S. Chaudhuri, and C. V. Johnson, *Notes on D-branes*, `hep-th/9602052`.

[104] J. Polchinski, *Tasi lectures on D-branes*, in *Theoretical Advanced Study Institute in Elementary Particle Physics (TASI 96): Fields, Strings, and Duality*, 11, 1996. `hep-th/9611050`.

[105] C. V. Johnson, *D-branes.* Cambridge Monographs on Mathematical Physics. Cambridge University Press, 2005.

[106] P. Ramond, *Dual Theory for Free Fermions*, *Phys. Rev. D* **3** (1971) 2415–2418.

[107] A. Neveu and J. H. Schwarz, *Factorizable dual model of pions*, *Nucl. Phys. B* **31** (1971) 86–112.

[108] M. B. Green and J. H. Schwarz, *Supersymmetrical Dual String Theory*, *Nucl. Phys. B* **181** (1981) 502–530.

[109] M. B. Green and J. H. Schwarz, *Supersymmetrical Dual String Theory. 2. Vertices and Trees*, *Nucl. Phys. B* **198** (1982) 252–268.

[110] M. B. Green and J. H. Schwarz, *Supersymmetrical Dual String Theory. 3. Loops and Renormalization*, *Nucl. Phys. B* **198** (1982) 441–460.

[111] L. Alvarez-Gaume and E. Witten, *Gravitational Anomalies*, *Nucl. Phys. B* **234** (1984) 269.

[112] J. Polchinski, *Dirichlet Branes and Ramond-Ramond charges*, *Phys. Rev. Lett.* **75** (1995) 4724–4727, [hep-th/9510017].

[113] J. E. Paton and H.-M. Chan, *Generalized veneziano model with isospin*, *Nucl. Phys. B* **10** (1969) 516–520.

[114] T. H. Buscher, *A Symmetry of the String Background Field Equations*, *Phys. Lett. B* **194** (1987) 59–62.

[115] H. Ooguri and C. Vafa, *Two-dimensional black hole and singularities of CY manifolds*, *Nucl. Phys. B* **463** (1996) 55–72, [hep-th/9511164].

[116] D. Tong, *NS5-branes, T duality and world sheet instantons*, *JHEP* **07** (2002) 013, [hep-th/0204186].

[117] O. Aharony, S. S. Gubser, J. M. Maldacena, H. Ooguri, and Y. Oz, *Large N field theories, string theory and gravity*, *Phys. Rept.* **323** (2000) 183–386, [hep-th/9905111].

[118] B. R. Greene, *String theory on Calabi-Yau manifolds*, in *Theoretical Advanced Study Institute in Elementary Particle Physics (TASI 96): Fields, Strings, and Duality*, 6, 1996. hep-th/9702155.

[119] D. R. Morrison and M. R. Plesser, *Nonspherical horizons. 1.*, *Adv. Theor. Math. Phys.* **3** (1999) 1–81, [hep-th/9810201].

[120] M. Nakahara, *Geometry, topology and physics*. 2003.

[121] V. Bouchard, *Lectures on complex geometry, Calabi-Yau manifolds and toric geometry*, hep-th/0702063.

[122] J. Sparks, *Sasaki-Einstein Manifolds*, *Surveys Diff. Geom.* **16** (2011) 265–324, [arXiv:1004.2461].

[123] N. C. Leung and C. Vafa, *Branes and toric geometry*, *Adv. Theor. Math. Phys.* **2** (1998) 91–118, [hep-th/9711013].

[124] H. Skarke, *String dualities and toric geometry: An Introduction*, *Chaos Solitons Fractals* **10** (1999) 543, [hep-th/9806059].

[125] K. Hori, S. Katz, A. Klemm, R. Pandharipande, R. Thomas, C. Vafa, R. Vakil, and E. Zaslow, *Mirror symmetry*, vol. 1 of *Clay mathematics monographs*. AMS, Providence, USA, 2003.

[126] D. Cox, J. Little, and H. Schenck, *Toric Varieties*. Graduate studies in mathematics. American Mathematical Soc., 2011.

[127] C. Closset, *Toric geometry and local Calabi-Yau varieties: An Introduction to toric geometry (for physicists)*, arXiv:0901.3695.

[128] C. Bar, *Real Killing Spinors and Holonomy*, *Commun. Math. Phys.* **154** (1993), no. 3 509–521.

[129] B. Feng, S. Franco, A. Hanany, and Y.-H. He, *UnHiggsing the del Pezzo*, *JHEP* **08** (2003) 058, [hep-th/0209228].

[130] M. R. Douglas, B. R. Greene, and D. R. Morrison, *Orbifold resolution by D-branes*, *Nucl. Phys. B* **506** (1997) 84–106, [hep-th/9704151].

[131] A. Kehagias, *New type IIB vacua and their F theory interpretation*, *Phys. Lett. B* **435** (1998) 337–342, [hep-th/9805131].

[132] B. S. Acharya, J. M. Figueroa-O'Farrill, C. M. Hull, and B. J. Spence, *Branes at conical singularities and holography*, *Adv. Theor. Math. Phys.* **2** (1999) 1249–1286, [hep-th/9808014].

[133] D. Martelli and J. Sparks, *Toric geometry, Sasaki-Einstein manifolds and a new infinite class of AdS/CFT duals*, *Commun. Math. Phys.* **262** (2006) 51–89, [hep-th/0411238].

[134] S. Benvenuti, A. Hanany, and P. Kazakopoulos, *The Toric phases of the Y**p,q quivers*, *JHEP* **07** (2005) 021, [hep-th/0412279].

[135] S. S. Gubser and I. R. Klebanov, *Baryons and domain walls in an N=1 superconformal gauge theory*, *Phys. Rev. D* **58** (1998) 125025, [hep-th/9808075].

[136] S. Kachru and E. Silverstein, *4-D conformal theories and strings on orbifolds*, *Phys. Rev. Lett.* **80** (1998) 4855–4858, [hep-th/9802183].

[137] M. Bertolini, *Four lectures on the gauge / gravity correspondence*, *Int. J. Mod. Phys. A* **18** (2003) 5647–5712, [hep-th/0303160].

[138] M. J. Strassler, *The Duality cascade*, in *Theoretical Advanced Study Institute in Elementary Particle Physics (TASI 2003): Recent Trends in String Theory*, 5, 2005. hep-th/0505153.

[139] D.-E. Diaconescu, M. R. Douglas, and J. Gomis, *Fractional branes and wrapped branes*, *JHEP* **02** (1998) 013, [hep-th/9712230].

[140] A. Butti, *Deformations of Toric Singularities and Fractional Branes*, *JHEP* **10** (2006) 080, [hep-th/0603253].

[141] Y. Imamura, *Anomaly cancellations in brane tilings*, *JHEP* **06** (2006) 011, [hep-th/0605097].

[142] J. McKay, *Graphs, singularities, and finite groups*, *Proc. Symp. Pure Math.* **37** (1980) 183.

[143] A. M. Uranga, *D-brane probes, RR tadpole cancellation and K theory charge*, *Nucl. Phys. B* **598** (2001) 225–246, [hep-th/0011048].

[144] L. E. Ibanez, R. Rabadan, and A. Uranga, *Anomalous U(1)'s in type I and type IIB D = 4, N=1 string vacua*, *Nucl. Phys. B* **542** (1999) 112–138, [hep-th/9808139].

[145] B. Feng, Y.-H. He, K. D. Kennaway, and C. Vafa, *Dimer models from mirror symmetry and quivering amoebae*, *Adv. Theor. Math. Phys.* **12** (2008), no. 3 489–545, [hep-th/0511287].

[146] A. Hanany and D. Vegh, *Quivers, tilings, branes and rhombi*, *JHEP* **10** (2007) 029, [hep-th/0511063].

[147] K. D. Kennaway, *Brane Tilings*, *Int. J. Mod. Phys. A* **22** (2007) 2977–3038, [arXiv:0706.1660].

[148] M. Yamazaki, *Brane tilings and their applications*, *Fortschritte der Physik* **56** (Jun, 2008) 555–686.

[149] S. Franco, Y.-H. He, C. Sun, and Y. Xiao, *A Comprehensive Survey of Brane Tilings*, *Int. J. Mod. Phys. A* **32** (2017), no. 23n24 1750142, [arXiv:1702.03958].

[150] Y. Imamura, *Global symmetries and 't Hooft anomalies in brane tilings*, *JHEP* **12** (2006) 041, [hep-th/0609163].

[151] S. Franco and D. Vegh, *Moduli spaces of gauge theories from dimer models: Proof of the correspondence*, *JHEP* **11** (2006) 054, [hep-th/0601063].

[152] R. Kenyon, *An introduction to the dimer model*, *arXiv preprint math/0310326* (2003).

[153] R. Kenyon, A. Okounkov, and S. Sheffield, *Dimers and amoebae*, math-ph/0311005.

[154] A. Ishii and K. Ueda, *A note on consistency conditions on dimer models*, 2010.

[155] D. P. Thurston *et al.*, *From dominoes to hexagons*, in *Proceedings of the 2014 Maui and 2015 Qinhuangdao Conferences in Honour of Vaughan FR Jones' 60th Birthday*, pp. 399–414, Centre for Mathematics and its Applications, Mathematical Sciences Institute ..., 2017.

[156] A. B. Goncharov and R. Kenyon, *Dimers and cluster integrable systems*, 2012.

[157] D. R. Gulotta, *Properly ordered dimers, R-charges, and an efficient inverse algorithm*, *JHEP* **10** (2008) 014, [arXiv:0807.3012].

[158] A. Butti and A. Zaffaroni, *From toric geometry to quiver gauge theory: The Equivalence of a-maximization and Z-minimization*, *Fortsch. Phys.* **54** (2006) 309–316, [hep-th/0512240].

[159] J. S. Scott, *Grassmannians and cluster algebras*, *Proc. London Math. Soc. (3)* **92** (2006), no. 2 345–380.

[160] A. B. Goncharov and R. Kenyon, *Dimers and cluster integrable systems*, in *Annales scientifiques de l'École Normale Supérieure*, vol. 46, pp. 747–813, 2013.

[161] V. V. Fock, *Inverse spectral problem for GK integrable system*, 2015.

[162] K. Altmann, *The versal deformation of an isolated toric gorenstein singularity*, *arXiv preprint alg-geom/9403004* (1994).

[163] O. Aharony and A. Hanany, *Branes, superpotentials and superconformal fixed points*, *Nucl. Phys. B* **504** (1997) 239–271, [hep-th/9704170].

[164] O. Aharony, A. Hanany, and B. Kol, *Webs of (p,q) five-branes, five-dimensional field theories and grid diagrams*, *JHEP* **01** (1998) 002, [hep-th/9710116].

[165] I. Affleck, M. Dine, and N. Seiberg, *Dynamical Supersymmetry Breaking in Supersymmetric QCD*, *Nucl. Phys. B* **241** (1984) 493–534.

[166] A. Dabholkar and J. Park, *Strings on orientifolds*, *Nucl. Phys. B* **477** (1996) 701–714, [hep-th/9604178].

[167] A. Dabholkar, *Lectures on orientifolds and duality*, in *ICTP Summer School in High-Energy Physics and Cosmology*, 6, 1997. hep-th/9804208.

[168] A. Giveon and D. Kutasov, *Brane Dynamics and Gauge Theory*, *Rev. Mod. Phys.* **71** (1999) 983–1084, [hep-th/9802067].

[169] R. Blumenhagen, B. Kors, D. Lust, and S. Stieberger, *Four-dimensional String Compactifications with D-Branes, Orientifolds and Fluxes*, *Phys. Rept.* **445** (2007) 1–193, [hep-th/0610327].

[170] R. Blumenhagen, D. Lüst, and S. Theisen, *Basic concepts of string theory*. Theoretical and Mathematical Physics. Springer, Heidelberg, Germany, 2013.

[171] B. S. Acharya, M. Aganagic, K. Hori, and C. Vafa, *Orientifolds, mirror symmetry and superpotentials*, hep-th/0202208.

[172] A. Hanany and B. Kol, *On orientifolds, discrete torsion, branes and M theory*, *JHEP* **06** (2000) 013, [hep-th/0003025].

[173] S. Imai and T. Yokono, *Comments on orientifold projection in the conifold and SO x USp duality cascade*, *Phys. Rev. D* **65** (2002) 066007, [hep-th/0110209].

[174] F. Benini, F. Canoura, S. Cremonesi, C. Nunez, and A. V. Ramallo, *Backreacting flavors in the Klebanov-Strassler background*, *JHEP* **09** (2007) 109, [arXiv:0706.1238].

[175] S. G. Naculich, H. J. Schnitzer, and N. Wyllard, *A Cascading N = 1 Sp(2N + 2M) x Sp(2N) gauge theory*, *Nucl. Phys. B* **638** (2002) 41–61, [hep-th/0204023].

[176] Y. Imamura, K. Kimura, and M. Yamazaki, *Anomalies and O-plane charges in orientifolded brane tilings*, *JHEP* **03** (2008) 058, [arXiv:0801.3528].

[177] I. n. García-Etxebarria and B. Heidenreich, *Strongly coupled phases of $\mathcal{N} = 1$ S-duality*, *JHEP* **09** (2015) 032, [arXiv:1506.03090].

[178] I. n. García-Etxebarria and B. Heidenreich, *S-duality in $\mathcal{N} = 1$ orientifold SCFTs*, *Fortsch. Phys.* **65** (2017), no. 3-4 1700013, [arXiv:1612.00853].

[179] M. Bianchi, S. Cremonesi, A. Hanany, J. F. Morales, D. Ricci Pacifici, and R.-K. Seong, *Mass-deformed Brane Tilings*, *JHEP* **10** (2014) 027, [arXiv:1408.1957].

[180] M. Bianchi, D. Bufalini, S. Mancani, and F. Riccioni, *Mass deformations of unoriented quiver theories*, *JHEP* **07** (2020) 015, [arXiv:2003.09620].

[181] D. Dugger, *Involutions on surfaces*, *Journal of Homotopy and Related Structures* **14** (2019), no. 4 919–992.

[182] W. Thurston, "The geometry and topology of three-manifolds." Notes http://library.msri.org/books/gt3m/, 2002.

[183] A. Antinucci, S. Mancani, and F. Riccioni, *Infrared duality in unoriented Pseudo del Pezzo*, *Phys. Lett. B* **811** (2020) 135902, [arXiv:2007.14749].

[184] E. Witten, *Toroidal compactification without vector structure*, *JHEP* **02** (1998) 006, [hep-th/9712028].

[185] J. Park and A. M. Uranga, *A Note on superconformal N=2 theories and orientifolds*, *Nucl. Phys. B* **542** (1999) 139–156, [hep-th/9808161].

[186] J. Park, R. Rabadan, and A. Uranga, *N=1 type IIA brane configurations, chirality and T duality*, *Nucl. Phys. B* **570** (2000) 3–37, [hep-th/9907074].

[187] A. M. Uranga, *A New orientifold of C**2 / Z(N) and six-dimensional RG fixed points*, *Nucl. Phys. B* **577** (2000) 73–87, [hep-th/9910155].

[188] I. P. Ennes, C. Lozano, S. G. Naculich, and H. J. Schnitzer, *Elliptic models, type IIB orientifolds and the AdS / CFT correspondence*, *Nucl. Phys. B* **591** (2000) 195–226, [hep-th/0006140].

[189] B. Feng, Y.-H. He, A. Karch, and A. M. Uranga, *Orientifold dual for stuck NS5-branes*, *JHEP* **06** (2001) 065, [hep-th/0103177].

[190] N. J. Evans, C. V. Johnson, and A. D. Shapere, *Orientifolds, branes, and duality of 4-D gauge theories*, *Nucl. Phys. B* **505** (1997) 251–271, [hep-th/9703210].

[191] I. García-Etxebarria and D. Regalado, $\mathcal{N} = 3$ *four dimensional field theories*, *JHEP* **03** (2016) 083, [arXiv:1512.06434].

[192] O. Aharony and Y. Tachikawa, *S-folds and 4d N=3 superconformal field theories*, *JHEP* **06** (2016) 044, [arXiv:1602.08638].

[193] I. Affleck, M. Dine, and N. Seiberg, *Exponential Hierarchy From Dynamical Supersymmetry Breaking*, *Phys. Lett. B* **140** (1984) 59–62.

[194] M. Dine, A. E. Nelson, Y. Nir, and Y. Shirman, *New tools for low-energy dynamical supersymmetry breaking*, *Phys. Rev. D* **53** (1996) 2658–2669, [hep-ph/9507378].

[195] E. Poppitz and S. P. Trivedi, *Some examples of chiral moduli spaces and dynamical supersymmetry breaking*, *Phys. Lett. B* **365** (1996) 125–131, [hep-th/9507169].

[196] S. Franco, Y.-H. He, C. Herzog, and J. Walcher, *Chaotic duality in string theory*, *Phys. Rev. D* **70** (2004) 046006, [hep-th/0402120].

[197] S. Franco, A. Hanany, and A. M. Uranga, *Multi-flux warped throats and cascading gauge theories*, *JHEP* **09** (2005) 028, [hep-th/0502113].

[198] I. Garcia-Etxebarria, F. Saad, and A. M. Uranga, *Quiver gauge theories at resolved and deformed singularities using dimers*, *JHEP* **06** (2006) 055, [hep-th/0603108].

[199] J. Davey, A. Hanany, and R.-K. Seong, *Counting Orbifolds*, *JHEP* **06** (2010) 010, [arXiv:1002.3609].

[200] C. Petersson, *Superpotentials From Stringy Instantons Without Orientifolds*, *JHEP* **05** (2008) 078, [arXiv:0711.1837].

Université Libre de Bruxelles

2017 - 2021